UNIVERSIDADE FEDERAL DO CEARÁ
CENTRO DE TECNOLOGIA
DEPARTAMENTO DE ENGENHARIA DE TELEINFORMÁTICA
PROGRAMA DE PÓS-GRADUAÇÃO EM ENGENHARIA DE TELEINFORMÁTICA

TESE DE DOUTORADO

TENSOR MODELING AND SIGNAL PROCESSING FOR WIRELESS COMMUNICATION SYSTEMS

Autor:

André Lima Férrer de Almeida

Orientadores:

Gérard Favier
e
João Cesar M. Mota

Composição da banca:

Sr. Gérard FAVIER	Diretor de Pesquisa do CNRS, I3S
Sr. Pierre COMON	Diretor de Pesquisa do CNRS, I3S
Sr. Philippe LOUBATON	Professor titular, Université de Marne la Vallée
Sr. Dirk SLOCK	Professeur titular, Institut Eurecom
Sr. João Cesar M. MOTA	Professor titular, Universidade Federal do Ceará
Sr. João M. T. ROMANO	Professor titular, Universidade Estadual de Campinas
Sr. Charles C. CAVALCANTE	Professor visitante, Universidade Federal do Ceará
Sr. Francisco R. P. CAVALCANTI	Professor associado, Universidade Federal do Ceará
Sr. Guilherme BARRETO	Professor associado, Universidade Federal do Ceará

Tese apresentada à Coordenação do Programa de Pós-Graduação em Engenharia de Teleinformática da Universidade Federal do Ceará como parte dos requisitos exigidos para obtenção do grau de Doutor em Engenharia de Teleinformática.

Fortaleza–Ceará
Novembro–2007

A mon épouse Julliana.

Remerciements

Cette thèse a été préparée dans le cadre d'une convention de co-tutelle entre l'Université de Nice Sophia Antipolis (UNSA) et l'Universidade Federal do Ceará (UFC) au Brésil. Elle a été financée par le gouvernement brésilien au travers d'une bourse CAPES, organisme du Ministère de l'Education Nationale du Brésil à qui j'adresse mes premiers remerciements.

Je tiens à remercier aussi M. Philippe LOUBATON et M. João Marcos ROMANO d'avoir accepté d'être rapporteurs de ma thèse et pour leurs remarques constructives. Je remercie également M. Pierre COMON et M. Dirk SLOCK pour avoir accepté de participer à mon jury de thèse. Je souhaite remercier aux collègues Rodrigo CAVALCANTI et Charles CAVALCANTE, membres brésiliens de mon jury de thèse, pour m'avoir accueilli chaleureusement au sein de leur équipe pendant mes stages doctoraux au Laboratoire GTEL.

J'exprime une profonde reconnaissance envers Gérard FAVIER, directeur de thèse modèle, pour sa rigueur scientifique, sa grande disponibilité, sa patience et sa vision en matière de recherche. Je lui remercie également pour son grand soutien lors de mon installation à Nice. Merci Gérard, pour tes précieuses remarques et ton efficacité lors des révisions de nos plusieurs articles ainsi que de mon mémoire. Enfin, merci pour m'avoir donné l'opportunité unique de travailler avec toi dans ce magnifique environnement.

Je suis également très reconnaissant à João Cesar MOTA, mon directeur de thèse brésilien, avec qui j'ai pris goût pour la recherche. Merci João, pour les nombreuses discussions fructueuses, et pour m'avoir toujours guidé avec patience et rigueur depuis presque dix ans. Sans ton soutien, mes projets de recherche ne seraient pas arrivés à terme. Je te suis redevable pour tout cela.

Je souligne le soutien amical et chaleureux de tous les doctorants du Laboratoire I3S, qui ont croisé ma route durant ce parcours doctoral et, plus particulièrement, à tous ceux qui m'ont soutenu et encouragé. Un merci très spécial aux amis et co-bureaux Carlos Estêvão Rolim FERNANDES, Sofiane BOUDAOUD, Thu NGUYEN, et Le PHAM pour les échanges divers, scientifiques et culturels, ainsi que pour tous les bons moments vécus. Je ne pourrais pas oublier ceux qui étaient là au tout début de mon doctorat: un grand merci à Vicente ZARZOSO, Alain KIBANGOU, Myriam RAJIH, Anis KHOUAJA, Ludwig ROTA, etc. pour leur gentillesse et leur amitié. D'une manière plus générale, je remercie tous les membres de l'I3S qui, directement ou non, ont contribué à la réalisation de ce travail.

Finalement, mais pas pour autant moins important à mes yeux, je voudrais témoigner tout mon amour et ma reconnaissance à mon épouse Julliana, à qui je dédie cette thèse. Je te remercie pour ta présence dans ma vie, pour tes conseils, tes encouragements, ton réconfort, ta patience, et ton soutien plein et inconditionnel, même dans les moments les plus difficiles. Sans toi je n'aurais pas réussi. Je ne pourrai jamais t'en remercier assez.

Abstract

In several signal processing applications for wireless communications, the received signal is multidimensional in nature and may exhibit a multilinear algebraic structure. In this context, the PARAFAC tensor decomposition has been the subject of several works in the past six years. However, generalized tensor decompositions are necessary for covering a wider class of wireless communication systems with more complex transmission structures, more realistic channel models and more efficient receiver signal processing. This thesis investigates tensor modeling approaches for multiple-antenna systems, channel equalization, signal separation and parametric channel estimation. New tensor decompositions, namely, the block-constrained PARAFAC and CONFAC decompositions, are developed and studied in terms of identifiability. First, the block-constrained PARAFAC decomposition is applied for a unified tensor modeling of oversampled, DS-CDMA and OFDM systems with application to blind multiuser equalization. This decomposition is also used for modeling multiple-antenna (MIMO) transmission systems with block space-time spreading and blind detection, which generalizes previous tensor-based MIMO transmission models. The CONFAC decomposition is then exploited for designing new MIMO-CDMA transmission schemes combining spatial diversity and multiplexing. Blind symbol/code/channel recovery is discussed from the uniqueness properties of this decomposition. This thesis also studies new applications of third-order PARAFAC decomposition. A new space-time-frequency spreading system is proposed for multicarrier multiple-access systems, where this decomposition is used as a joint spreading and multiplexing tool at the transmitter using tridimensional spreading code with trilinear structure. Finally, we present a PARAFAC modeling approach for the parametric estimation of SIMO and MIMO multipath wireless channels with time-varying structure.

Keywords : Tensor modeling, wireless communication systems, blind detection, multiple-antenna transmission, multiuser equalization, signal separation, channel estimation, PARAFAC, CONFAC, MIMO, CDMA, OFDM.

Résumé

Dans plusieurs applications de traitement du signal pour les systèmes de communication sans fil, le signal reçu est de nature multidimensionnelle et possède une structure algébrique multilinéaire. Dans ce contexte, la décomposition tensorielle de type PARAFAC a fait l'objet de plusieurs travaux au cours des six dernières années. Il s'avère que des décompositions tensorielles plus générales sont nécessaires pour couvrir des classes plus larges de systèmes de communication faisant intervenir à la fois des modèles de transmission et de canal plus complexes et des méthodes de traitement plus efficaces. Cette thèse traite les problèmes de modélisation des systèmes multi-antennes, d'égalisation de canal, de séparation de signaux et d'estimation paramétrique de canal à l'aide d'approches tensorielles. Dans un premier temps, de nouvelles décompositions tensorielles (bloc-PARAFAC avec contraintes et CONFAC) ont été développées et étudiées en termes d'identifiabilité. Dans un deuxième temps, la décomposition bloc-PARAFAC avec contraintes a été appliquée tout d'abord pour mettre en évidence une modélisation tensorielle unifiée des systèmes suréchantillonnés, DS-CDMA et OFDM, avec application à l'égalisation multiutilisateur. Puis, cette décomposition a été utilisée pour modéliser des systèmes de transmission MIMO avec étalement spatio-temporel et détection aveugle. La décomposition CONFAC a ensuite été exploitée pour concevoir un nouveau schéma de transmission MIMO/CDMA combinant diversité et multiplexage spatial. Les propriétés d'unicité de cette décomposition ont permis de réaliser un traitement aveugle au niveau du récepteur pour la reconstruction du canal et des symboles transmis. Un troisième volet du travail concerne l'application de la décomposition PARAFAC pour la conception de nouveaux schéma de transmission spatio-temporel-fréquentiel pour des systèmes MIMO multiporteuses, et pour l'estimation paramétrique de canaux multitrajets.

Mots clés: Modélisation tensorielle, systèmes de communication sans fil, détection aveugle, transmission multi-antenne, égalisation multiutilisateur, séparation de signaux, estimation de canal, PARAFAC, CONFAC, MIMO, CDMA, OFDM.

Resumo

Em diversas aplicações do processamento de sinais em sistemas de comunicação sem-fio, o sinal recebido é de natureza multidimensional, possuindo uma estrutura algébrica multilinear. Neste contexto, a decomposição tensorial PARAFAC tem sido utilizada em vários trabalhos ao longo dos últimos seis anos. Observa-se, entretanto, que decomposições tensoriais generalizadas são necessárias para modelar uma classe mais ampla de sistemas de comunicação, caracterizada pela presença de estruturas de transmissão mais complexas, por modelos de canal mais realistas, e por técnicas de processamento de sinais mais eficientes no receptor. Esta tese investiga novas abordagens tensorias e suas aplicações em modelagem de sistemas MIMO, equalização, separação de sinais e estimação paramétrica de canal. Inicialmente, duas novas decomposições tensoriais (PARAFAC em blocos com restrições e CONFAC) são desenvolvidas e estudadas em termos de identificabilidade. Em uma segunda parte do trabalho, novas aplicações destas decomposições tensoriais são propostas. A decomposição PARAFAC em blocos com restrições é aplicada, primeiramente, à modelagem unificada de sistemas superamostrados, DS-CDMA e OFDM, com aplicação em equalização multiusuária. Em seguida, esta decomposição é utilizada na modelagem de sistemas de transmissão MIMO com espalhamento espaço-temporal e detecção conjunta. Em seguida, a decomposição CONFAC é explorada na concepção de uma nova arquitetura generalizada de transmissão MIMO/CDMA que combina diversidade e multiplexagem. As propriedades de unicidade desta decomposição permitem o uso do processamento não-supervisionado no receptor, visando a reconstrução dos sinais transmitidos e a estimação do canal. Na terceira e última parte deste trabalho, explora-se a decomposição PARAFAC no contexto de duas aplicações diferentes. Na primeira, uma nova estrutura de transmissão espaço-temporal-frequêncial é proposta para sistemas MIMO multiportadora. A segunda aplicação consiste em um novo estimador paramétrico para canais multipercursos.

Palavras-chave: Modelagem tensorial, sistemas de communicação sem-fio, detecção não-supervisionada, transmissão multi-antena, equalização multiusuária, separação de sinais, estimação de canal, PARAFAC, CONFAC, MIMO, CDMA, OFDM.

Acronyms

2D	Two-Dimensional
3D	Three-Dimensional
m-PSK	m-symbol Phase Shift Keying
m-QAM	m-symbol Quadrature Amplitude Modulation
ALS	Alternating Least Squares
BER	Bit-Error-Rate
CDMA	Code-Division Multiple-Access
CONFAC	CONstrained FACtors
CP	Cyclic Prefix
DOA	Direction-Of-Arrival
DOD	Direction-Of-Departure
DFT	Discrete Fourier Transform
ELS	Enhanced Line Search
FFT	Fast Fourier Transform
FIR	Finite Impulse Response
ICI	Inter-Chip Interference
IFFT	Inverse Fast Fourier Transform
ISI	Inter-Symbol Interference
LS	Least Squares
MC	Multi-Carrier

MIMO	Multiple-Input Multiple-Output
ML	Maximum Likelihood
MMSE	Minimum Mean Square Error
MSE	Mean Square Error
MU	Multi-User
MUI	Multi-User Interference
OFDM	Orthogonal Frequency Division Multiplexing
PARAFAC	PARAllel FACtors
PARALIND	PARAllel profiles with LINear Dependencies
RMSE	Root Mean Square Error
SIMO	Single-Input Multiple-Output
SF	Space-Frequency
SM	Spatial Multiplexing
SNR	Signal-to-Noise Ratio
ST	Space-Time
STF	Space-Time-Frequency
STS	Space-Time Spreading
T-STFS	Trilinear Space-Time-Frequency Spreading
TDMA	Time-Division Multiple-Access
ZF	Zero Forcing

Notation

In this thesis the following conventions are used. Scalar variables are denoted by lower-case letters ($a, b, \ldots, \alpha, \beta, \ldots$), vectors are written as boldface lower-case letters ($\mathbf{a}, \mathbf{b}, \ldots, \boldsymbol{\alpha}, \boldsymbol{\beta}, \ldots$), matrices correspond to boldface capitals ($\mathbf{A}, \mathbf{B}, \ldots$), and tensors are written as calligraphic letters ($\mathcal{A}, \mathcal{B}, \ldots$). The meaning of the following symbols are, if nothing else is explicitly stated:

$\mathbb{C}$	set of complex-valued numbers
$\mathbb{C}^I$	set of complex-valued I-dimensional vectors
$\mathbb{C}^{I \times J}$	set of complex-valued $(I \times J)$-matrices
$\mathbb{C}^{I_1 \times \cdots \times I_N}$	set of complex-valued $(I_1 \times \cdots \times I_N)$-tensors
a^*	complex conjugate of $a \in \mathbb{C}$
$\lvert\mathbf{a}\rvert$	modulus of $\mathbf{a}$
$\lVert\mathbf{a}\rVert_1$	l-1 norm of $\mathbf{a}$
$\lVert\mathbf{a}\rVert$	l-2 norm of $\mathbf{a}$
$\mathbf{A}^T$	transpose of $\mathbf{A}$
$\mathbf{A}^H$	Hermitian transpose of $\mathbf{A}$
$\mathbf{A}^{-1}$	inverse of $\mathbf{A}$
$\mathbf{A}^\dagger$	Moore-Penrose pseudo-inverse of $\mathbf{A}$
$\lVert\mathbf{A}\rVert_F$ ($\lVert\mathcal{A}\rVert_F$)	Frobenius norm of $\mathbf{A}(\mathcal{A})$
$\mathbf{1}_N$	"All-ones" vector of dimension N.
$\mathbf{I}_N$	Identity matrix of dimension N.

$\mathbf{e}_n^{(N)}$	n-th canonical vector in $\mathbb{R}^N$, i.e. a unitary vector containing an element equal to 1 in its n-th position and 0's elsewhere.
$E^{(N)} = \{\mathbf{e}_1^{(N)}, \ldots, \mathbf{e}_N^{(N)}\}$	Canonical basis in $\mathbb{R}^N$.
$[\mathbf{A}]_{i_1,i_2} = a_{i_1,i_2}$	(i_1, i_2)-th element of matrix $\mathbf{A} \in \mathbb{C}^{I_1 \times I_2}$.
$[\mathbf{A}]_{i_1 \cdot}$ ($[\mathbf{A}]_{\cdot i_2}$)	i_1-th row (i_2-th column) of $\mathbf{A}$.
$[\mathcal{A}]_{i_1,i_2,i_3} = a_{i_1,i_2,i_3}$	(i_1, i_2, i_3)-th element of tensor $\mathcal{A}$.
$\mathbf{A}_{i_1 \cdot \cdot} \in \mathbb{C}^{I_2 \times I_3}$	i_1-th first-mode matrix-slice of tensor $\mathcal{A}$.
$\mathbf{A}_{\cdot i_2 \cdot} \in \mathbb{C}^{I_3 \times I_1}$	i_2-th second-mode matrix-slice of tensor $\mathcal{A}$.
$\mathbf{A}_{\cdot \cdot i_3} \in \mathbb{C}^{I_1 \times I_2}$	i_3-th third-mode matrix-slice of tensor $\mathcal{A}$.
$\mathbf{a} \circ \mathbf{b}$	Outer product between $\mathbf{a} \in \mathbb{C}^{I_1}$ and $\mathbf{b} \in \mathbb{C}^{I_2}$. $\mathbf{a} \circ \mathbf{b} = \begin{bmatrix} a_1 b_1 & \cdots & a_1 b_{I_2} \\ \vdots & & \vdots \\ a_{I_1} b_1 & \cdots & a_{I_1} b_{I_2} \end{bmatrix} \in \mathbb{C}^{I_1 \times I_2}$.
$\mathbf{A} \otimes \mathbf{B}$	The Kronecker product of $\mathbf{A} \in \mathbb{C}^{I \times J}$ with $\mathbf{B} \in \mathbb{C}^{K \times L}$, $\mathbf{A} \otimes \mathbf{B} = \begin{bmatrix} a_{1,1}\mathbf{B} & a_{1,2}\mathbf{B} & \cdots & a_{1,J}\mathbf{B} \\ a_{2,1}\mathbf{B} & a_{2,2}\mathbf{B} & \cdots & a_{2,J}\mathbf{B} \\ \vdots & \vdots & & \vdots \\ a_{I,1}\mathbf{B} & a_{I,2}\mathbf{B} & \cdots & a_{I,J}\mathbf{B} \end{bmatrix} \in \mathbb{C}^{IK \times JL}$.
$\mathbf{A} \,\vert\otimes\vert\, \mathbf{B}$	The "block-wise" Kronecker product. For $\mathbf{A} = [\mathbf{A}^{(1)} \cdots \mathbf{A}^{(Q)}] \in \mathbb{C}^{I \times J}$, $\mathbf{B} = [\mathbf{B}^{(1)} \cdots \mathbf{B}^{(Q)}] \in \mathbb{C}^{K \times L}$, $\mathbf{A} \,\vert\otimes\vert\, \mathbf{B} = [\mathbf{A}^{(1)} \otimes \mathbf{B}^{(1)} \cdots \mathbf{A}^{(Q)} \otimes \mathbf{B}^{(Q)}] \in \mathbb{C}^{IK \times R}$, with $\mathbf{A}^{(q)} \in \mathbb{C}^{I \times J_q}$, $\mathbf{B}^{(q)} \in \mathbb{C}^{K \times L_q}$, and $J = \sum_{q=1}^{Q} J_q, \quad L = \sum_{q=1}^{Q} L_q, \quad R = \sum_{q=1}^{Q} J_q L_q$.
$\mathbf{A} \diamond \mathbf{B}$	The Khatri-Rao (column-wise Kronecker) product. For $\mathbf{A} \in \mathbb{C}^{I \times K}$ and $\mathbf{B} \in \mathbb{C}^{J \times K}$, $\mathbf{A} \diamond \mathbf{B} = [\mathbf{A}_{\cdot 1} \otimes \mathbf{B}_{\cdot 1}, \ \ldots, \ \mathbf{A}_{\cdot K} \otimes \mathbf{B}_{\cdot K}] \in \mathbb{C}^{IJ \times K}$.
$\mathrm{vec}(\mathbf{A})$	The vectorization operator. For $\mathbf{A} \in \mathbb{C}^{I \times J}$: $\mathrm{vec}(\mathbf{A}) = \begin{bmatrix} \mathbf{A}_{\cdot 1} \\ \vdots \\ \mathbf{A}_{\cdot J} \end{bmatrix} \in \mathbb{C}^{IJ}$.
$\mathrm{diag}(\mathbf{a})$	Diagonal matrix with diagonal entries given by the elements of $\mathbf{a}$.
$\mathrm{blockdiag}(\mathbf{A}_1, \ldots, \mathbf{A}_N)$	Forms a block-diagonal matrix out of the N matrix blocks $\mathbf{A}_1, \ldots, \mathbf{A}_N$.

Contents

List of Figures

List of Tables

Introduction

Several existing signal processing problems in wireless communication systems with multiple transmit and/or receive antennas are modeled by means of matrix (2-D) decompositions that represent the transformations on the transmitted signal from the transmitter to the receiver. At the receiver, signal processing is generally used to combat multipath fading effects, inter-symbol interference and multiuser (co-channel) interference by means of multiple receive antennas. Usually considered signal processing dimensions are *space* and *time* dimensions [114]. This area has progressed over the past twenty years and has resulted in several powerful solutions. In order to allow for a higher spectral efficiency, numerous works have proposed blind signal processing techniques, which aim at avoiding the loss of bandwidth due to the use of training sequences. Blind receiver algorithms generally take special (problem-specific) structural properties of the transmitted signals into account such as constant-modulus, finite-alphabet, cyclostationarity or statistical independence for performing multiuser signal separation, equalization and channel estimation [114, 141, 149, 11, 153, 151, 154].

On the other hand, signal processing solutions based on the use of multiple transmit and receive antennas have come latter, and date back to ten years ago. Intensive research has been carried out, and the literature is abundant. Wireless communication systems employing multiple antennas at both ends of the link, commonly known as Multiple-Input Multiple-Output (MIMO) systems, are being considered as one of the key technologies to be deployed in current and upcoming wireless communications standards [113]. MIMO systems have shown to potentially provide high spectral efficiencies by capitalizing on spatial multiplexing

[66, 67, 143, 70], while considerably improving the link reliability by means of space-time coding [2, 142, 112, 76, 59]. The integration of multiple-antenna and Code-Division Multiple-Access (CDMA) technologies has also been subject of several studies [78, 79, 56, 123, 97, 57]. The combination of MIMO and multicarrier modulation by means of Orthogonal Frequency Division Multiplexing (OFDM) has also been the focus of a large number of recent works [137]. In MIMO-OFDM systems, multiple transmit antennas and orthogonal subcarrriers are jointly employed to achieve high data rates and to combat fading effects by means of Space-Time-Frequency (STF) coding [1, 6, 139, 138, 124].

The use of tensor decompositions has gained increased attention in several signal processing applications for wireless communication systems. In wireless communications, the fact that the received signal is a third-order tensor, means that each received signal sample is associated with a three-dimensional space, and is represented by three indices, each one associated with a particular type of systematic variation of the received signal. In such a three-dimensional space, each dimension of the *received signal tensor* can be interpreted as a particular form of signal "diversity". In most of cases, two of these three axes account for *space* and *time* dimensions. The *space* dimension generally corresponds to the number of receive antennas while the *time* dimension corresponds to the length of the data block to be processed at the receiver. The third dimension of the third-order tensor depends on the particular wireless communication system. This dimension is generally linked to the type of processing that is done at the transmitter and/or at the receiver.

In the context of wireless communications, the practical motivation for a tensor modeling in signal processing comes from the fact that one can simultaneously benefit from multiple (more than two) forms of diversity to perform multiuser signal separation/equalization and channel estimation under model uniqueness conditions/requirements more relaxed than with conventional matrix-based approaches. One of the most popular tensor decomposition is the Parallel Factor (PARAFAC) decomposition, independently proposed by Harshman [73] and Caroll & Chang [12]. This tensor decomposition has been used as a data analysis tool in psychometrics, phonetics, exploratory data analysis, statistics, arithmetic complexity, and other fields and disciplines. Intensive research on PARAFAC analysis has been conducted in the context of chemometrics in the food industry, where it is used for spectrophotometric, chromatographic, and flow injection analyses [7, 8, 135]. The attractive feature of the PARAFAC decomposition is its intrinsic uniqueness. In contrast to matrix (bilinear) decompositions, where there is the well-known problem of rotational freedom, the PARARAC decomposition of higher-order tensors is essentially unique, up to scaling and permutation

indeterminacies [90, 136]. Aside from its powerful uniqueness properties, tensor models are mathematically elegant and allow a new algebraic interpretation of the transmitter-channel-receiver transformations over the transmitted signals.

Tensor modeling appears in several existing wireless communication systems where the received signal has a multidimensional nature. For instance, in addition to common *space* and *time* dimensions, in a Direct-Sequence Code-Division Multiple-Access (DS-CDMA) system [116], the third dimension is the *spreading* dimension which appears due to the use of a direct sequence spreading at the transmitter. The use of temporal oversampling at each receive antenna and the use of multicarrier modulation at the transmitter also create a third dimension to the received signal, which is called here *oversampling* and *frequency* dimensions, respectively. This interpretation is illustrated in Fig. 1.

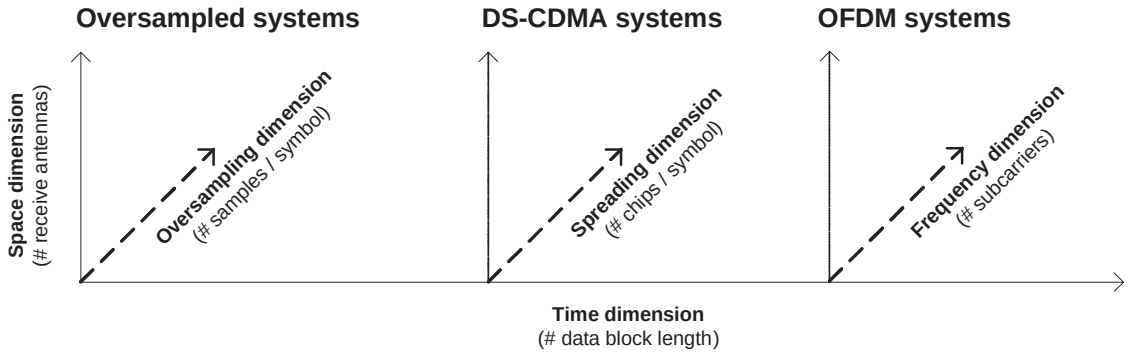

Figure 1: Tridimensional visualization of the received signal in oversampled, DS-CDMA and OFDM systems.

The seminal works using tensor decompositions in wireless communications are due to Sidiropoulos *et al.*. In [131], the authors show that a mixture of DS-CDMA signals received at an uniform linear array of antennas can be interpreted as a third-order tensor admitting a Parallel Factor (PARAFAC) decomposition. In [128], the same authors established an interesting conceptual link between the PARAFAC decomposition and the problem of multiple invariance sensor array processing. Following these works, the authors have proposed applications of PARAFAC to blind multiuser detection in Wideband Code Division Multiple Access (W-CDMA) systems [130], Orthogonal Frequency Division Multiplexing (OFDM) systems, [81], blind beamforming [133], multiple-antenna space-time coding [129], and blind spatial signature estimation [119] (see the reference list of [126] for further related works). This decomposition has also been exploited for the blind identification of undetermined mixtures [17, 118] and for the blind separation of DS-CDMA signals [53] using higher-order statistics. Generalized tensor decompositions have

been proposed in [28, 40, 47, 109] to handle frequency-selective channels under different assumptions concerning the multipath propagation structure. Tensor decompositions have also been exploited recently for the blind identification of linear and nonlinear channels [63, 64, 65, 85, 86] and for kernel complexity reduction of third-order Volterra models [83, 84].

In the context of MIMO antenna systems, the use of tensor modeling has first appeared in [129], where a space-time coding model with blind detection has been proposed. This multiple-antenna scheme allows to build a third-order PARAFAC model for the received signal thanks to a temporal spreading of the data streams at each transmit antenna as in a conventional CDMA system. In [48], a tensor model is proposed for a MIMO-CDMA system with multiuser spatial multiplexing, but no spreading across the transmit antennas is permitted. In our recent works [32, 33, 39], we have proposed a generalization of [129] and [48], by covering multiple-antenna transmission systems with partial or full spatial spreading of each data stream across sets of transmit antennas. This idea was further generalized by the authors in subsequent works [35, 36, 37, 42] using the CONstrained FACtor (CONFAC) decomposition. They provide extension of [32, 33, 39] by allowing to use multiple transmit antennas and spreading codes per data stream. In [43, 45], the PARAFAC decomposition was exploited to design a new signaling technique for multi-carrier multiple-access MIMO systems. These works proposed a space-time-frequency transmission model based on a PARAFAC decomposition of the 3-D spreading code into space-, time- and frequency-domain spreading codes.

For the applications mentioned above, the key characteristics of signal processing based on tensor decompositions, not covered by matrix based signal processing, are the following. It does not require the use of training sequences, nor the knowledge of channel impulse responses and antenna array responses. Moreover, it does not rely on statistical independence between the transmitted signals. Instead, the proposed receiver algorithms are *deterministic*, and exploit the multilinear algebraic structure of the received signal, treated as a higher-order tensor. The proposed receiver algorithms act on blocks of data (instead of using a sample-by-sample processing approach) and are generally based on a joint detection of the transmitted signals (either from different users or from multiple transmit antennas).

This thesis lies in a research field that connects tensor decompositions and signal processing for wireless communications. New (generalized) tensor decompositions are developed and exploited as a modeling and signal processing tool for wireless communication problems, such as multiuser signal separation/equalization/detection, multiple-antenna transmission systems, and channel modeling/estimation. We will show that several wireless communication systems can be modeled by means of generalized tensor decompositions other than the

standard PARAFAC one. For instance, this is the case of i) oversampled, DS-CDMA and OFDM systems under frequency-selective propagation and multiple paths per user and ii) multiple-input multiple-output (MIMO) antenna systems under different space-time spreading/multiplexing strategies.

Contributions

The contributions of this thesis will address the three following main research axes:

- Multiuser signal separation/equalization/detection;
- Multiple-antenna transmission structures;
- Channel modeling and estimation;

Multiuser signal separation/equalization/detection: Several works have focused on the use of the PARAFAC decomposition. Despite its simplicity and powerful uniqueness properties, the PARAFAC decomposition has its own modeling limitations and does not cover certain wireless communication systems. Little attention has been given to the study of other tensor decompositions, with the aim of covering a wider class of systems where the received signal has a more complicated algebraic structure. This is generally the case when frequency-selective fading and specular multipath propagation are jointly present. In this context, we have proposed a generalized tensor decomposition for an unified tensor modeling of oversampled, DS-CDMA and OFDM systems, with application to blind multiuser separation/equalization/detection. We have studied this issue in several works [28, 29, 27, 40]. These works can be viewed as generalizations of the ideas originally presented in [131] under different channel models and working assumptions.

In the context of MIMO antenna systems, we propose a new modeling approach for multiuser downlink transmission. A block space-time spreading scheme is formulated using the tensor formalism. The proposed model allows multiuser space-time transmission with different spatial spreading factors (diversity gains) as well as different multiplexing factors (code rates) for the users. This approach can be viewed as a generalization of [129, 48] due to the fact that i) it is designed to cope with multiuser MIMO transmission and ii) it jointly performs space-time spreading and multiuser spatial multiplexing. In contrast to [129, 48] where no spatial spreading is allowed and the number of data streams is restricted to be equal to the number of transmit antennas, the proposed MIMO system allows a variable number of data streams to access all the transmit spatial channels. We have addressed this subject in [32, 33, 39, 24].

Multiple-antenna transmission structures: Few applications of tensor decompositions to multiple-antenna (MIMO) systems have been developed. In this thesis, we give special attention to the application of tensor decompositions to MIMO systems by showing that they are useful in the design of different transmission structures with blind detection. As will be shown, transmission schemes combining transmit diversity, spatial multiplexing and spatial reuse of the spreading codes can be formulated by explicitly exploiting the multilinear algebraic structure of tensor decompositions. We have addressed this subject in several recent works [32, 33, 35, 36, 37, 43, 45]. The originality of the proposed tensor-based multiple-antenna transmission structures is on the following aspects.

First, the tensor-based models of [35, 36, 37] allow the association of multiple spreading codes and data streams per transmit antenna, in contrast to [129, 48], where each transmit antenna is necessarily associated with only one spreading code and data stream. Secondly, a different way of exploiting the trilinear structure of the PARAFAC decomposition is originally studied in this thesis. In this case, tensor decomposition is exploited also at the transmitter for designing a new signaling technique. We propose an STF multiple-access transmission model based on a 3-D spreading code tensor decomposed into the outer product of the space-, time- and frequency-domain spreading codes. These codes allow the data streams to simultaneously access the same set of transmit antennas, chips and subcarriers/tones. Compared to competing multiple-antenna multiple-access models such as [157, 58, 105, 106], the trilinear STF spreading model has the flexibility for controlling both the spreading and the multiplexing pattern over space, time and frequency dimensions while allowing a blind joint detection and channel estimation thanks to the PARAFAC modeling. We have addressed this subject in [43, 45].

Channel modeling and estimation: Another problem of interest in this thesis is that of modeling/estimation of SIMO and MIMO wireless communication channels by means of a PARAFAC modeling approach. We benefit from the fact that paths amplitudes are fast-varying, while angles and delays are slowly-varying over multiple transmission blocks or data-blocks to build a third-order PARAFAC model for the wireless channel and for the received signal. We have treated this problem in [31, 25]. Contrarily to other parametric channel estimation approaches such as [153, 151, 154], in which multipath parameters are extracted from a previous unstructured channel estimate, the proposed PARAFAC-based estimator directly works on the received signal, avoiding error propagation in cases where the unstructured channel estimate may not be accurate. The proposed estimator also works with fewer receiver antennas than multipaths thanks to the uniqueness properties of the PARAFAC decomposition.

The different contributions of this thesis are associated with both transmitter and receiver processing. Some of them focus primarily on receiver signal processing (multiuser signal separation/equalization/decoding and channel estimation). Others emphasize the transmitter signal processing (e.g. space-time multiplexing/spreading, space-time-frequency multiple-access), although these also affect the receiver processing. Figures 2 and 3 link the use of tensor modeling to the signal processing purpose at both ends of the communication chain and highlight the three signal dimensions that generally appear in each case. Figure 4 links the chapters to the three main research axes of the thesis.

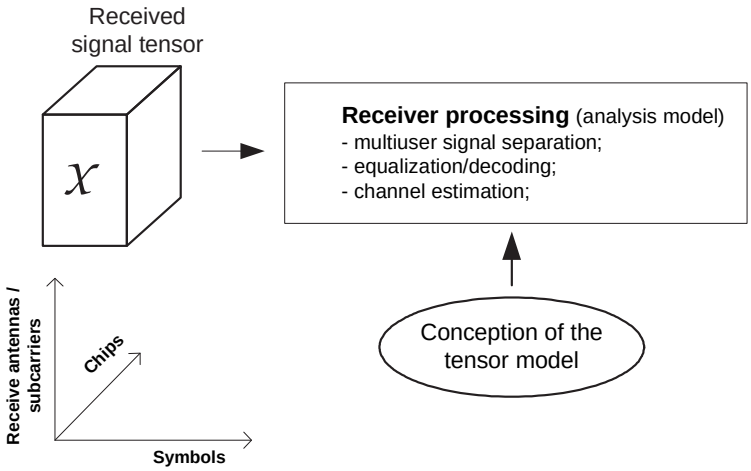

Figure 2: Link of tensor modeling to receiver signal processing.

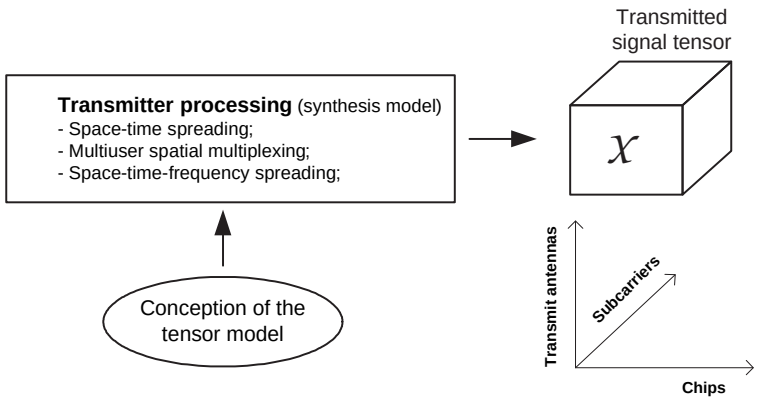

Figure 3: Link of tensor modeling to transmitter signal processing.

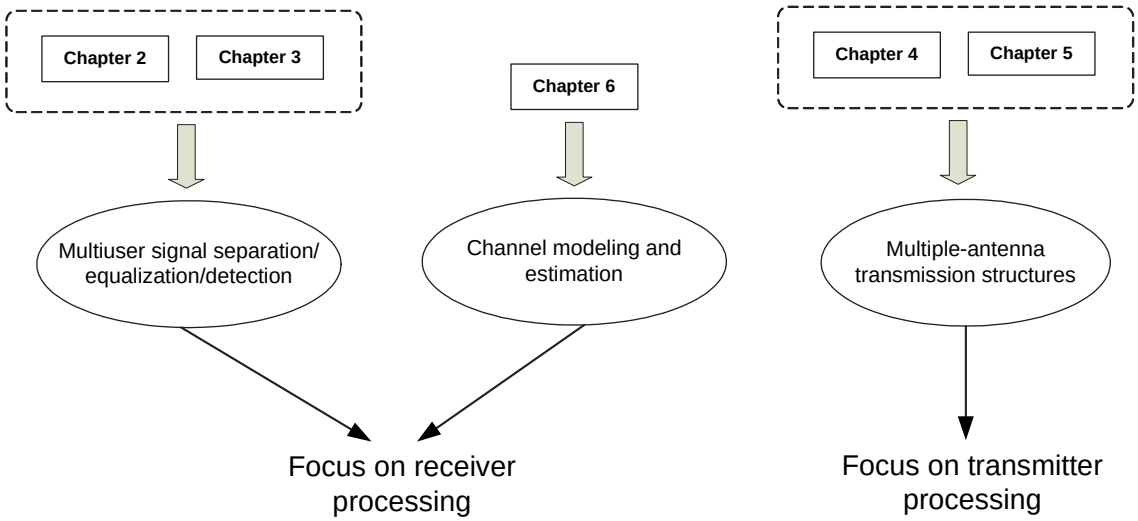

Figure 4: Link between the chapters and the research axes of the thesis.

To summarize, the major contributions of this thesis are the following:

- Development of new generalized tensor decompositions (block-constrained PARAFAC and CONstrained FACtors (CONFAC));
- Study of the uniqueness property of the CONFAC decomposition;
- Unified tensor modeling of oversampled, DS-CDMA and OFDM systems under frequency-selective channels with specular multipath propagation;
- Proposal of a new blind multiuser separation/equalization receiver based on the block-constrained PARAFAC model and combining a subspace method with finite-alphabet projection;
- Development of new tensor-based transceivers for multiple-antenna systems using space-time spreading/multiplexing based on the block-constrained PARAFAC decomposition;
- Tensor modeling of MIMO-CDMA transmit schemes with blind detection exploiting the CONFAC decomposition;
- Proposal of a new space-time-frequency spreading model for MIMO multicarrier system with trilinear decomposition structure of the spreading code;
- Development of a PARAFAC-based estimator of time-varying multipath SIMO channels and generalization to MIMO channels.

Organization

The different contributions of this thesis are divided into six chapters. In the following, we briefly describe the content of each chapter.

Chapter 1: *Tensor Decompositions: Background and New Contributions.* This chapter provides an overview of multilinear algebra and tensor decompositions. It contains the basic material to be exploited throughout the thesis. We first introduce the mathematical formalism, representations and most important operations involving tensors. In the second part, we provide a survey of tensor decompositions and also present original contributions. We begin by presenting the Tucker-3 decomposition and its special cases. Then, the PARAFAC decomposition is introduced and its uniqueness properties are discussed. An overview on block tensor decompositions is given. We present two new tensor decompositions, which are the block-constrained PARAFAC and the CONstrained FACtor (CONFAC) decompositions, and their uniqueness properties are studied.

Chapter 2: *Tensor Modeling for Wireless Communication Systems with Application to Blind Multiuser Equalization.* This chapter presents a new tensor modeling approach for the received signal in wireless communication systems with a receive antenna array. Assuming a frequency-selective channel model with specular multipath propagation and multiple paths per source, we formulate the received signal in temporally-oversampled, DS-CDMA and OFDM systems using a block-constrained PARAFAC decomposition. A unified tensor modeling for these three systems is proposed. A generalization of this unified model based on a constrained Tucker-3 decomposition is presented by considering that the number of multipaths of each user can be different. A new blind receiver is presented as an application of the proposed tensor model to multiuser separation/equalization.

Chapter 3: *Multiuser MIMO Systems Using Block Space-Time Spreading.* In this chapter, a new block space-time spreading model is proposed for the downlink of a multiuser MIMO system based on tensor modeling. The core of the proposed transmitter model is a 3-D *spreading tensor* that jointly spreads and combines independent data streams across multiple transmit antennas. The received signal is formulated as a block-constrained PARAFAC model, where the two fixed constraint matrices reveal the overall space-time spreading pattern at the transmitter. We present a receiver algorithm based on a deterministic elimination of multiuser interference by each user, followed by a blind joint channel and symbol recovery stage.

Chapter 4: *Constrained Tensor Modeling Approaches to MIMO-CDMA Systems.* This chapter presents new modeling approaches to MIMO-CDMA trans-

mit schemes based on the CONstrained FACtor (CONFAC) decomposition. We show that this generalized decomposition can be exploited to design space-time spreading/precoding schemes for MIMO-CDMA systems with a meaningful physical interpretation for the constraint matrices of this tensor decomposition. We begin by considering a MIMO-CDMA transmission model based on the type-3 CONFAC decomposition with two constraint matrices only. A systematic design procedure for the canonical precoding matrices leading to unique blind symbol recovery is presented. Then, generalized transmission model is proposed which fully exploits all the three constraint matrices of the CONFAC decomposition. Blind symbol/code/channel recovery are discussed from the identifiability properties of this decomposition.

Chapter 5: *Trilinear Space-Time-Frequency Spreading for MIMO Wireless Systems.* This chapter presents a new space-time-frequency spreading model for MIMO multicarrier multiple-access wireless communication system using tridimensional (3-D) spreading code with trilinear decomposition (PARAFAC) structure. The proposed transmission model, called Trilinear Space-Time-Frequency Spreading (T-STFS), is based on a joint multiplexing and spreading of multiple data streams across space (transmit antennas), time (chips) and frequency (tones). The diversity performance of the proposed T-STFS model is analyzed and a necessary condition for maximum diversity gain is derived. A PARAFAC model for the received signal is developed and exploited for a blind joint detection and channel estimation, and identifiability issues are discussed.

Chapter 6: *PARAFAC Methods for Modeling/Estimation of Time-Varying Multipath Channels.* In this chapter, we address the problem of multipath parameter estimation of time-varying space-time wireless channels using PARAFAC modeling. We use the fact that the variation of multipath amplitudes over multiple data-blocks is faster than that of angles and delays for showing that the received signal can be modeled as a third-order (3D) tensor. A PARAFAC-based estimator using a training sequence is proposed for jointly recovering the directions of arrival, the time delays and the complex amplitudes of the multipaths. We also extend this joint modeling/estimation approach to MIMO channels.

The organization of this thesis is illustrated in Fig. 5, where the links between the different chapters are given.

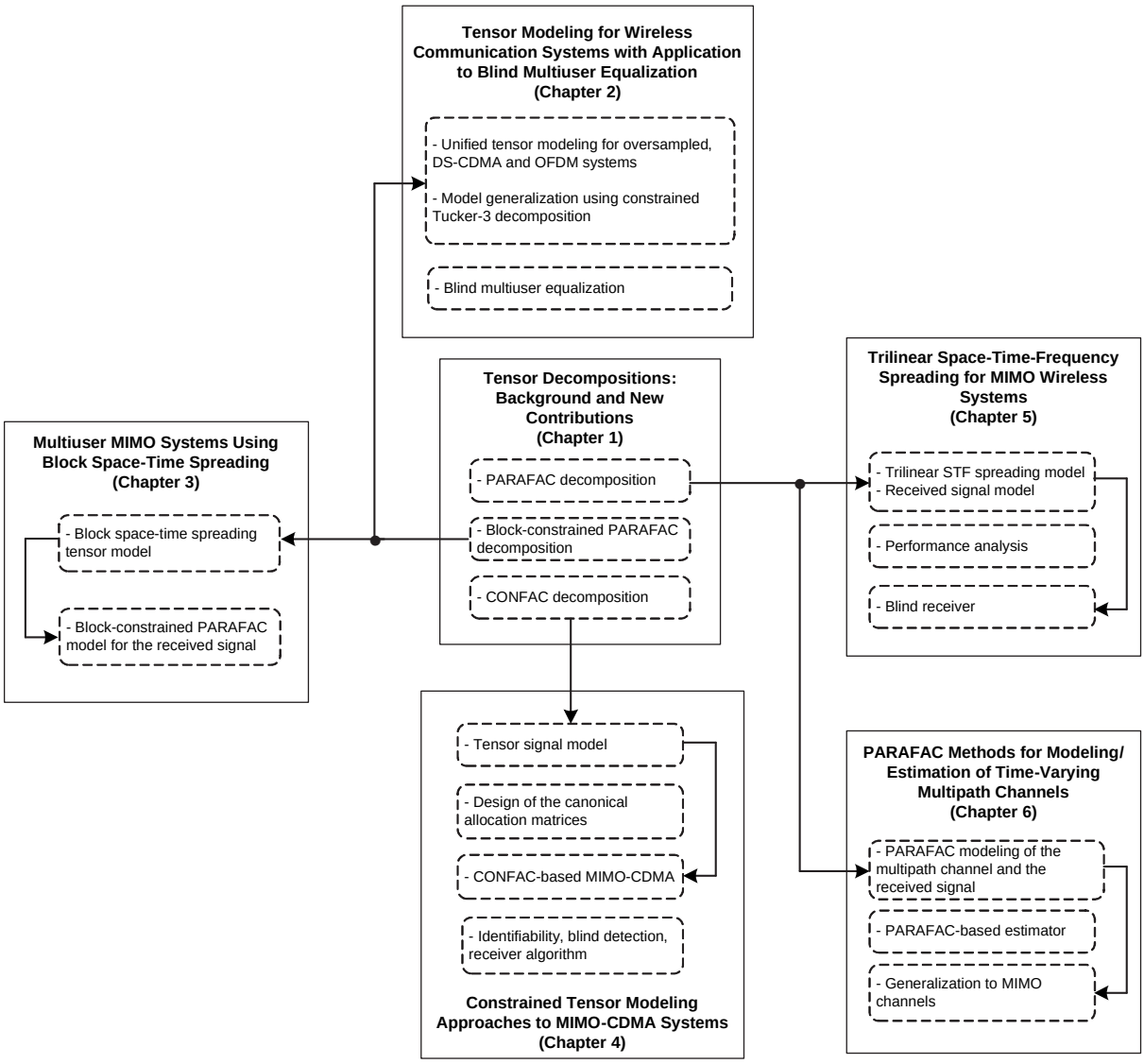

Figure 5: Organization of the thesis in block-diagram.

This thesis work has originated several publications in conferences and journals. In the following, a list of publications is presented:

Journal papers:

1. A. L. F. de Almeida, G. Favier, and J. C. M. Mota, "PARAFAC-based unified tensor modeling for wireless communication systems with application to blind multiuser equalization", *Elsevier Signal Processing*, vol. 87, n. 2, pp. 337–351, 2007.

2. A. L. F. de Almeida, G. Favier, and J. C. M. Mota, "Constrained Tensor Modeling Approach to Blind Multiple-Antenna CDMA Schemes", *IEEE Transactions on Signal Processing*, accepted for publication, 2007.

3. A. L. F. de Almeida, G. Favier, and J. C. M. Mota, "A Constrained Factor Decomposition with Application to MIMO Antenna Systems", *IEEE Transactions on Signal Processing*, accepted for publication, 2007.

4. A. L. F. de Almeida, G. Favier, and J. C. M. Mota, "Multiuser MIMO System Using Block Space-Time Spreading and Tensor Modeling", *Elsevier Signal Processing*, accepted for publication, 2007.

5. A. L. F. de Almeida, G. Favier, and J. C. M. Mota, "Trilinear Space-Time-Frequency Spreading for MIMO Wireless Systems With Blind Detection", *IEEE Transactions on Signal Processing*, submitted, 2007.

6. A. L. F. de Almeida, G. Favier, and J. C. M. Mota, "Space-Time Spreading MIMO-CDMA Downlink System Using Constrained Tensor Modeling", *Elsevier Signal Processing*, submitted, 2007.

7. A. L. F. de Almeida, G. Favier, and J. C. M. Mota, "Constrained Tucker3 Model for Blind Beamforming", *Elsevier Signal Processing*, submitted, 2007.

Conference papers:

1. A. L. F. de Almeida, G. Favier, and J. C. M. Mota, "PARAFAC Models for Wireless Communication Systems", In *Proc. Int. Conf. on Physics in Signal and Image processing (PSIP)*, Toulouse, France, Jan. 31 - Feb. 2, 2005.

2. A. L. F. de Almeida, G. Favier, J. C. M. Mota, "A Generalized PARAFAC Model for Oversampled, DS-CDMA and OFDM Wireless Communication Systems", *2nd Workshop on Tensor Decompositions and Applications (TDA)*, Marseille, France, August 2005.

3. A. L. F. de Almeida, G. Favier, J. C. M. Mota, "An Application of Tensor Modeling to Blind Multiuser Equalization", *2nd Workshop on Tensor Decompositions and Applications (TDA)*, Marseille, France, August 2005.

4. A. L. F. de Almeida, G. Favier, and J. C. M. Mota, "PARAFAC Receiver for Blind Multiuser Equalization in Wireless Communication Systems with Temporal Oversampling", *In Proc. European Signal Processing Conference (EUSIPCO)*, Antalya, Turkey, September 4-8, 2005.

5. A. L. F. de Almeida, G. Favier, J. C. M. Mota, "Blind Multiuser Equalization using a PARAFAC-Subspace Approach", *Proc. of GRETSI*, Louvain-la-Neuve, Belgium, September 6-9, 2005.

6. A. L. F. de Almeida, G. Favier, J. C. M. Mota, "Combined PARAFAC-Subspace Approach to Blind Multiuser Equalization", *Proc. of the Brazilian Telecommunications Symposium (SBT)*, Campinas, Brazil, September 4-8, 2005.

7. A. L. F. de Almeida, G. Favier, and J. C. M. Mota, "Generalized PARAFAC Model for Multidimensional Wireless Communications with Application to Blind Multiuser Equalization", In *Proc. Asilomar Conference Sig. Syst. Comp.*, Pacific Grove, CA, October 31 - November 2, 2005.

8. A. L. F. de Almeida, G. Favier, J. C. M. Mota, "PARAFAC Models for Hybrid MIMO: Joint Blind Channel Estimation and Detection", *Proc. of Wireless World Research Forum (WWRF)*, Paris, France, December 8-9, 2005.

9. A. L. F. de Almeida, G. Favier, and J. C. M. Mota, "Multipath Parameter Estimation of Time-varying Space-time Communication Channels using Parallel Factor Analysis. In *Proc. IEEE Int. Conf. Acoustics, Speech and Sig. Proc. (ICASSP)*, Toulouse, France, May 14-18, 2006.

10. A. L. F. de Almeida, G. Favier, and J. C. M. Mota, "The Constrained Block-PARAFAC Decomposition", Three-way methods in Chemistry and Psychology (TRICAP), Chania, Crete, Greece, June 4-9, 2006.

11. A. L. F. de Almeida, G. Favier, and J. C. M. Mota, "Space-time Multiplexing Codes: A Tensor Modeling Approach", In *Proc. IEEE 7th Workshop on Sig. Proc. Advances in Wireless Commun. (SPAWC)*, Cannes, France, July 2-5, 2006.

12. A. L. F. de Almeida, G. Favier, J. C. M. Mota, "Trilinear Space-Time-Frequency Codes for Broadband MIMO-OFDM Systems", *Proc. of International Telecommunications Symposium (ITS)*, Fortaleza, Brazil, September 3-6, 2006.

13. A. L. F. de Almeida, G. Favier, and J. C. M. Mota, "Tensor-based Space-time Multiplexing Codes for MIMO-OFDM Systems with Blind Detection", In *Proc. IEEE Symp. Pers. Ind. Mob. Radio Commun. (PIMRC)*, Helsinki, Finland, September 11-14, 2006.

14. A. L. F. de Almeida, G. Favier, J. C. M. Mota, and R. L. de Lacerda, "Estimation of Frequency-Selective Block-fading MIMO Channels using PARAFAC Modeling and Alternating Least Squares", In *Proc. Asilomar Conference Sig. Syst. Comp.*, Pacific Grove, CA, October 29 - November 1, 2006.

15. A. L. F. de Almeida, G. Favier, and J. C. M. Mota, "A Trilinear Decomposition Approach to Space-time-frequency Multiple-access Wireless systems", In *Proc. IEEE Int. Workshop on Sig. Proc. Advances in Wireless Commun. (SPAWC)*, Helsinki, Finland, June, 2007.

16. A. L. F. de Almeida, G. Favier, and J. C. M. Mota, "Constrained Space-time Spreading for MIMO-CDMA Systems: Tensor modeling and Blind Detection", European Signal Processing Conference (EUSIPCO), Poznan, Poland, September 4-7, 2007.

17. A. L. F. de Almeida, G. Favier, and J. C. M. Mota, "The Constrained Trilinear Decomposition with Application to MIMO Wireless Communication Systems", GRETSI, Troyes, France, September 11-14, 2007.

18. A. L. F. de Almeida, G. Favier, and J. C. M. Mota, "Tensor-based Space-time Multiplexing (TSTM) for MIMO-OFDM Systems: Receiver Algorithms and Performance Evaluation", Brazilian Telecommunications Symposium (SBT), Recife, Brazil, September 3-6, 2007.

19. A. L. F. de Almeida, G. Favier, and J. C. M. Mota, "Space-time Spreading MIMO System Using Canonical Precoding Tensor Model", *Proc. Asilomar Conference Sig. Syst. Comp.*, Pacific Grove, CA, November 4-7, 2007.

Book chapter:

– A. L. F. de Almeida, G. Favier, J. C. M. Mota, "Tensor Decompositions and Applications to Wireless Communications Systems", Chapter 3. In *C. C. Cavalcante, R. F. Colares and P. C. Barbosa (Eds.), Telecommunications: Advances and Trends in Transmission, Networking and Applications*, ISBN: 85-98876-18-6, University of Fortaleza Press, 2006.

CHAPTER 1

Tensor Decompositions: Background and New Contributions

Multilinear algebra is the algebra of tensors of order higher than two. The decompositions of higher-order tensors can be viewed as generalizations of matrix decompositions. In the first part of this chapter, we briefly introduce the basic mathematical formalism, the main representations, and operations involving tensors. A background on tensor decompositions is given in the second part. We begin by presenting the Tucker-3 decomposition and its special cases. Then, the PARAFAC decomposition is introduced and its uniqueness issues are discussed. Connections between Tucker-3 and PARAFAC are given. An overview on tensor decompositions in block terms is also given. Then, we present some original contributions of this thesis, which are the block-constrained PARAFAC and the CONstrained FACtor (CONFAC) decompositions. Both decompositions will be exploited in subsequent chapters in the context of the applications we shall treat.

The theory of tensors is a branch of linear algebra, called nowadays *multilinear algebra*. The word "tensor" was first introduced by William R. Hamilton in 1846, to denote what is now called *modulus*. In 1899, Woldemar Voigt was the first who used this word in its current meaning. The first tensor notations and developments were done by Gregorio Ricci-Curbastro around 1890 in the context of differential geometry. A broader acceptance of tensor calculus was achieved with the introduction of Einstein's theory of general relativity, around 1915.

A different way of viewing and treating a tensor was developed between 1960 and 1970, where the attention was given to the analysis, factorization or decomposition of third-order tensors. L. R. Tucker [148], Richard A. Harshman [73], Carroll and Chang [12] and Kruskal [90] are the first "players" in the development of *tensor decompositions*, which can be seen as extensions of matrix decompositions to higher-orders. Among them, two types have been extensively studied in the literature, while being focus of several applications in different domains. These are the Parallel Factor (PARAFAC) analysis/decomposition [73, 74], also known as Canonical Decomposition (CANDECOMP) [12], and the Tucker-3 decomposition, which can be interpreted as a generalization of Principal Component Analysis (PCA) to higher orders [148]. The Tucker-3 decomposition, also known as three-mode PCA, has been successfully applied in different areas such as chromatography [8] and person perception analysis [89].

The attractive feature of the PARAFAC decomposition is its intrinsic uniqueness. In contrast to matrix (bilinear) decompositions, where there is the well-known problem of rotational freedom, the PARARAC decomposition of higher-order tensors is essentially unique, up to scaling and permutation indeterminacies [90, 136]. The first uniqueness proof was provided by Kruskal in [90]. Recently, this proof has been reformulated using basic linear algebra [136]. A concise proof that is valid for complex tensors was given in [131]. A generalization of the uniqueness result of [90] to tensors of arbitrary order was given in [127]. An alternative proof can be found in [82, 136]. Contrarily to the PARAFAC decomposition, the Tucker-3 decomposition possesses no intrinsic uniqueness and is not interesting from a parameter estimation point of view. However, by using constrained versions of the Tucker models one can sometimes overcome this problem [87, 144].

Tensor decompositions implicitly appear in the context of Higher-Order Statistics (HOS) [98, 15, 16, 19]. This is due to the fact that the PARAFAC decomposition describes the basic structure of high-order cumulants of multivariate data. HOS-based Independent Component Analysis (ICA) of non-Gaussian source mixtures intrinsically involves manipulation of tensor objects [14, 49, 54, 18]. A solid contribution to the area of multilinear algebra and tensor decompositions was given by De Lathauwer in [49], who generalized the concept of matrix Singular Value

Decomposition (SVD) to tensors, with applications to blind source separation problems using ICA.

Tensor decompositions fall within an inter-disciplinary research field. Although important progress has been obtained, this research field has several open issues. On-going research ranges from fundamental studies such as uniqueness, degeneracy and rank [20], to more practical aspects, where tensors decompositions are used to model physical phenomena.

1.1 Basics of tensor algebra

Several approaches exist in the literature for the definition of the term *tensor*. They generally depend on the scientific domain in which they are used. In a general case, a tensor is defined in generalized coordinate systems where the coordinate axes are general curves and not necessarily orthogonal. In this context, a tensor is treated as a mathematical entity that enjoys the *multilinearity property* after a change of coordinate system [15]. A N-th order tensor is interpreted here as an *array* that exhibits a linear dependency with respect to N vector spaces, and the elements of which are accessed via N indices [49]. *Tensors* are also used as a synonym of *multidimensional arrays*, also known as *multi-way arrays*.

As special cases, a tensor of order 2 is a matrix, a tensor of order 1 is a vector and a tensor of order 0 is a scalar. Provided that a tensor is a multilinear form and has its own associated linear vector space, common linear operations that are valid for matrices can be extended to higher orders.

Definition 1.1 (scalar notation) *Let $\mathcal{X} \in \mathbb{C}^{I_1 \times I_2 \times \cdots \times I_N}$ be a N-th order tensor. A scalar component of $\mathcal{X}$ is specified as*

$$x_{i_1,i_2,\ldots,i_N} = [\mathcal{X}]_{i_1,i_2,\ldots,i_N}, \tag{1.1}$$

where i_n is the n-th dimension of $\mathcal{X}$, also called the mode-n of $\mathcal{X}$.

Definition 1.2 (inner product) *The inner product of two tensors $\mathcal{X}$ and $\mathcal{Y}$ of the same order N is given by:*

$$\langle \mathcal{X}, \mathcal{Y} \rangle = \sum_{i_1=1}^{I_1} \sum_{i_2=1}^{I_2} \cdots \sum_{i_N=1}^{I_N} x_{i_1,i_2,\ldots,i_N} y_{i_1,i_2,\ldots,i_N}. \tag{1.2}$$

Similar to the case of matrices, the notion of orthogonality between two tensors is linked to the inner product, i.e., $\mathcal{X}$ and $\mathcal{Y}$ are said to be mutually orthogonal tensors if (1.2) equals 0.

Definition 1.3 (outer product) *Let $\mathcal{X} \in \mathbb{C}^{I_1 \times I_2 \times \cdots \times I_N}$ and $\mathcal{Y} \in \mathbb{C}^{J_1 \times J_2 \times \cdots \times J_M}$ be two tensors of orders N and M respectively. The outer product between $\mathcal{X}$ and $\mathcal{Y}$ is given by:*

$$[\mathcal{X} \circ \mathcal{Y}]_{i_1,i_2,\ldots,i_N,j_1,j_2,\ldots,j_M} = x_{i_1,i_2,\ldots,i_N} y_{j_1,j_2,\ldots,i_M}. \tag{1.3}$$

The outer product of two tensors is another tensor, the order of which is given by the sum of the orders of the two former tensors. Equation (1.3) is a generalization of the concept of outer product of two vectors, which is itself a matrix (second-order tensor). It also gives the notion of *rank-1 tensor* [88], as a special case.

Definition 1.4 (rank-1 tensor) *A rank-1 tensor $\mathcal{X} \in \mathbb{C}^{I_1 \times I_2 \times \cdots \times I_N}$ is a tensor that can be written as the outer product of N vectors $\mathbf{u}^{(1)} \in \mathbb{C}^{I_1}, \mathbf{u}^{(2)} \in \mathbb{C}^{I_2}, \ldots, \mathbf{u}^{(N)} \in \mathbb{C}^{I_N}$, i.e.:*

$$x_{i_1,i_2,\ldots,i_N} = u^{(1)}_{i_1} u^{(2)}_{i_2} \cdots u^{(N)}_{i_N}. \tag{1.4}$$

The vectors $u^{(n)}$ are called the components of $\mathcal{X}$. As a special case, a rank-1 matrix is given by the outer product of two vectors. As will be clear later, tensor decompositions are in general linear combinations of rank-1 tensors.

Definition 1.5 (Rank) *The rank of an arbitrary tensor $\mathcal{X} \in \mathbb{C}^{I_1 \times I_2 \times \cdots \times I_N}$, denoted by $R = r(\mathcal{X})$, is the minimal number of rank-1 tensors that yield $\mathcal{X}$ in a linear combination.*

Definition 1.6 (Frobenius norm) *The Frobenius norm of a tensor $\mathcal{X} \in \mathbb{C}^{I_1 \times I_2 \times \cdots \times I_N}$ is defined as:*

$$\|\mathcal{X}\|_F = \sqrt{\langle \mathcal{X}, \mathcal{X} \rangle} = \left(\sum_{i_1=1}^{I_1} \sum_{i_2=1}^{I_2} \cdots \sum_{i_N=1}^{I_N} |x|^2_{i_1,i_2,\ldots,i_N} \right)^{1/2}. \tag{1.5}$$

The Frobenius norm can be interpreted as a measure of "energy" in the tensor.

Definition 1.7 (Unfolded matrices) *The n-th mode unfolded matrix $\mathbf{X}_n$ of a tensor $\mathcal{X} \in \mathbb{C}^{I_1 \times I_2 \times \cdots \times I_N}$ is defined as the $I_n \times I_1 I_2 \cdots I_{n-1} I_{n+1} I_N$ matrix, the columns of which are the I_n-dimensional vectors (mode-n vectors) obtained by varying index i_n and keeping the other indices fixed.*

The order of appearance of the mode-n vectors in $\mathbf{X}_n$ may vary from one definition to another. A visualization of the three unfolded representations $\mathbf{X}_1$, $\mathbf{X}_2$ and $\mathbf{X}_3$ for a third-order tensor $\mathcal{X} \in \mathbb{C}^{I_1 \times I_2 \times I_3}$ is depicted in Fig. 1.1.

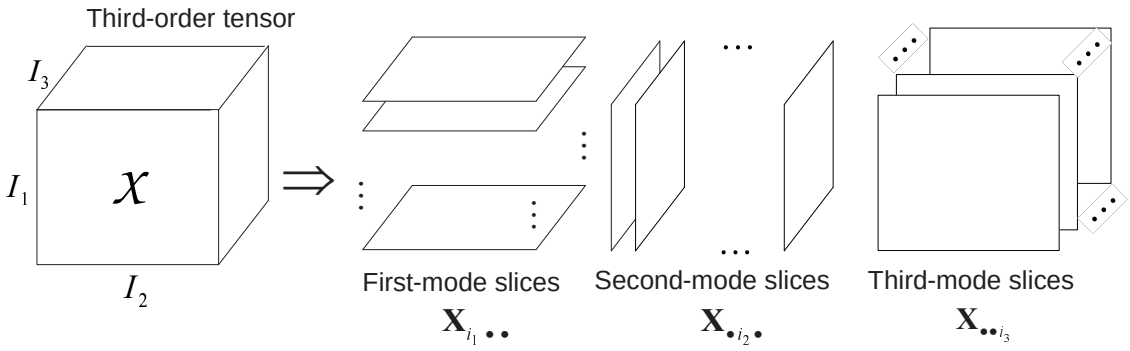

Figure 1.1: Visualization of the unfolded representations of a third-order tensor.

Definition 1.8 (mode-n rank) *Let $\mathbf{X}_n$ be the n-th mode unfolded matrix of $\mathcal{X} \in \mathbb{C}^{I_1 \times I_2 \times \cdots \times I_N}$. The mode-$n$ rank of $\mathcal{X}$ is the dimension of the vector space generated by the n-th mode vectors (i.e., the columns of $\mathbf{X}_n$).*

The definition of mode-n rank is a generalization of the classical concept of rank for matrices. Contrarily to the matrix case, where $R_1 = R_2 = R$ (i.e. row rank equal to column rank), mode-n ranks of a higher-order tensor are not necessarily the same. Furthermore, when the mode-n ranks are equal, they can still be different from the rank of the tensor. The mode-n rank is always inferior or equal to the rank, i.e., $R_n \leq R$.

Definition 1.9 (mode-n product) *The mode-n product of a tensor $\mathcal{X} \in \mathbb{C}^{I_1 \times I_2 \times \cdots \times I_N}$ and a matrix $\mathbf{A} \in \mathbb{C}^{J_n \times I_n}$, denoted by $\mathcal{X} \bullet_n \mathbf{A}$ is specified as:*

$$[\mathcal{X} \bullet_n \mathbf{A}]_{i_1, i_2, \ldots, i_{n-1}, j_n, i_{n+1}, \ldots, i_N} = \sum_{i_n=1}^{I_n} x_{i_1, i_2, \ldots, i_{n-1}, i_n, i_{n+1}, \ldots, i_N} a_{j_n, i_n} \tag{1.6}$$

The result of a mode-n product is a tensor of the same order, but with a new n-th dimension J_n.

The mode-n product is a compact way of representing linear transformations involving tensors. It is an alternative to the so-called Einstein summation convention

[98]. As pointed out in [49], this notation makes clear the analogy between matrix and tensor decompositions, as well as it gives an intuitive understanding of tensor decompositions.

1.2 Background on tensor decompositions

This section is focused on the decomposition of higher-order tensors (multi-way arrays). Tensor decompositions, also referred to as *multi-way factor analysis*, is an area of the multilinear algebra that characterizes a tensor as a linear combination of *outer product factors*. Depending on the approach considered, tensor decompositions can be viewed as generalizations of Principal Component Analysis (PCA) or Singular Value Decomposition (SVD) to orders higher than two. The analysis of a tensor in terms of its *decomposed tensor factors* is useful in problems where a *multilinear mixture* of different factors or contributions must be identified from measured data. In the context of this thesis, the computation of a tensor decomposition of an observed data tensor separates the signals transmitted by different sources. This is exactly the goal of several signal processing problems that will be addressed in this thesis. In the following, some tensor decompositions are presented. More attention is given to decompositions of third-order tensors or *three-way arrays*, since this will be the case in most of the applications encountered in this thesis. In some cases, the generalization to the N-th order is also given.

1.2.1 Tucker-3 decomposition

The Tucker-3 decomposition was proposed by L. Tucker in the sixties [148]. It can be seen as an extension of bilinear factor analysis to third-order tensors. The Tucker-3 decomposition is also a common name to denote the Higher-Order Singular Value Decomposition (HOSVD) of a third-order tensor [49]. The Tucker-3 decomposition is general in the sense that it incorporates most of the other third-order tensor decompositions as special cases.

The Tucker-3 decomposition of a tensor $\mathcal{X} \in \mathbb{C}^{I_1 \times I_2 \times I_3}$ can be written in scalar form as:

$$x_{i_1,i_2,i_3} = \sum_{p=1}^{P} \sum_{q=1}^{Q} \sum_{r=1}^{R} a_{i_1,p} b_{i_2,q} c_{i_3,r} g_{p,q,r}, \tag{1.7}$$

where $a_{i_1,p} = [\mathbf{A}]_{i_1,p}$, $b_{i_2,q} = [\mathbf{B}]_{i_2,q}$ and $c_{i_3,r} = [\mathbf{C}]_{i_3,r}$ are scalar components of *three factor matrices* $\mathbf{A} \in \mathbb{C}^{I_1 \times P}$, $\mathbf{B} \in \mathbb{C}^{I_2 \times Q}$ and $\mathbf{C} \in \mathbb{C}^{I_3 \times R}$ respectively, and

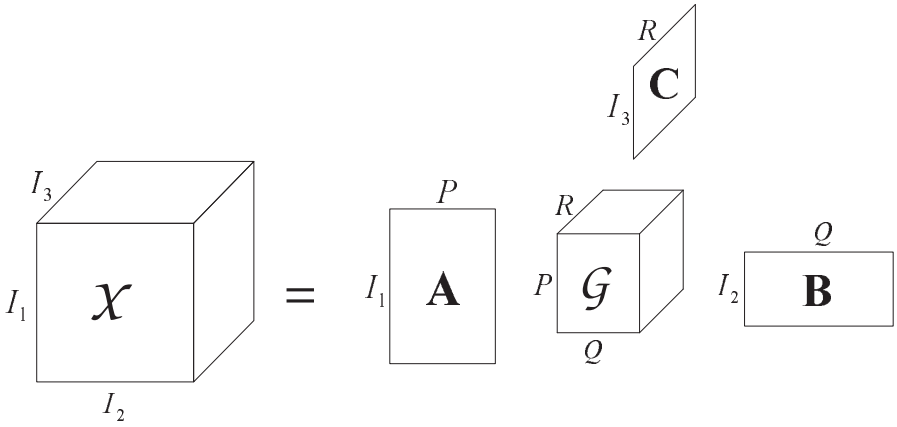

Figure 1.2: Visualization of the Tucker-3 decomposition.

$g_{p,q,r} = [\mathcal{G}]_{p,q,r}$ is a scalar component of the *core tensor* $\mathcal{G} \in \mathbb{C}^{P \times Q \times R}$.

From (1.7), we note that a Tucker-3-decomposed tensor is equal to a linear combination (or weighted sum) of PQR outer products, where the coefficient (or weighting factor) of each outer product term is the corresponding scalar component of the core tensor. We call P as the number of factors in the first mode of the tensor $\mathcal{X}$. Similarly, Q and R denote the number of factors in the second and third modes of $\mathcal{X}$. The Tucker-3 decomposition can be referred to as a tensor decomposition that allows *interactions* among factors across the three modes of the tensor [73]. An illustration of the Tucker-3 decomposition is given in Fig. 1.2.

The Tucker-3 decomposition can also be stated by resorting to the mode-n product (tensor) notation defined in (1.6):

$$\mathcal{X} = \mathcal{G} \bullet_1 \mathbf{A} \bullet_2 \mathbf{B} \bullet_3 \mathbf{C}. \tag{1.8}$$

Alternatively, we can state the Tucker-3 decomposition using a *matrix-slice notation*. This notation characterizes the tensor by a set of parallel matrix-slices that are obtained by "slicing" the tensor in a given "direction". Each matrix-slice is obtained by fixing one index of a given *mode* and varying the two indices of the two other modes. For a third-order tensor, there are three possible slicing directions. We call $\mathbf{X}_{i_1 \cdot \cdot} \in \mathbb{C}^{I_2 \times I_3}$ the i_1-th *first-mode slice*, $\mathbf{X}_{\cdot i_2 \cdot} \in \mathbb{C}^{I_3 \times I_1}$ the i_2-th *second-mode slice* and $\mathbf{X}_{\cdot \cdot i_3} \in \mathbb{C}^{I_1 \times I_2}$ the i_3-th *third-mode slice*. In order to obtain

the matrix-slice notation for the Tucker-3 decomposition, we rewrite (1.7) as:

$$x_{i_1,i_2,i_3} = \sum_{q=1}^{Q}\sum_{r=1}^{R} b_{i_2,q}c_{i_3,r}\left(\sum_{p=1}^{P} a_{i_1,p}g_{p,q,r}\right), \tag{1.9}$$

and define an "equivalent" (first-mode combined) core as:

$$u^{(1)}_{i_1,q,r} = \sum_{p=1}^{P} a_{i_1,p}g_{pqr} = [\mathcal{G} \bullet_1 \mathbf{A}]_{i_1,q,r} \tag{1.10}$$

i.e., $u^{(1)}_{i_1,q,r} = [\mathcal{G} \bullet_1 \mathbf{A}]_{i_1,q,r}$. The i_1-th matrix slice $\mathbf{X}_{i_1\cdot\cdot}$, $i_1 = 1, \ldots, I_1$, is given by:

$$\mathbf{X}_{i_1\cdot\cdot} = \mathbf{B}\mathbf{U}^{(1)}_{i_1}\mathbf{C}^T, \quad i_1 = 1, \ldots I_1, \tag{1.11}$$

where $\mathbf{U}^{(1)}_{i_1}$ is the i_1-th first-mode matrix-slice of the transformed core tensor $\mathcal{U}^{(1)} \in \mathbb{C}^{I_1\times Q\times R}$. The other two matrix-slice notations are obtained in a similar way, by changing the order of the summations in (1.7) and defining

$$u^{(2)}_{p,i_2,r} = \sum_{q=1}^{Q} b_{i_2,q}g_{p,q,r}, \quad u^{(3)}_{p,q,i_3} = \sum_{r=1}^{R} c_{i_3,r}g_{p,q,r}, \tag{1.12}$$

as scalar component of the transformed core tensors $\mathcal{U}^{(2)} = [\mathcal{G} \bullet_2 \mathbf{B}] \in \mathbb{C}^{P\times I_2\times R}$ and $\mathcal{U}^{(3)} = [\mathcal{G} \bullet_3 \mathbf{C}] \in \mathbb{C}^{P\times Q\times I_3}$. This leads to:

$$\mathbf{X}_{\cdot i_2\cdot} = \mathbf{C}\mathbf{U}^{(2)}_{i_2}\mathbf{A}^T, \quad i_2 = 1, \ldots I_2, \tag{1.13}$$

and

$$\mathbf{X}_{\cdot\cdot i_3} = \mathbf{A}\mathbf{U}^{(3)}_{i_3}\mathbf{B}^T, \quad i_3 = 1, \ldots I_3. \tag{1.14}$$

Let $\mathbf{X}_1 \in \mathbb{C}^{I_3I_1\times I_2}$, $\mathbf{X}_2 \in \mathbb{C}^{I_1I_2\times I_3}$ and $\mathbf{X}_3 \in \mathbb{C}^{I_2I_3\times I_1}$ be the first- second- and third-mode unfolded matrices of $\mathcal{X}$. These matrices are defined as:

$$\mathbf{X}_1 = \begin{bmatrix} \mathbf{X}_{\cdot\cdot 1} \\ \vdots \\ \mathbf{X}_{\cdot\cdot I_3} \end{bmatrix}, \quad \mathbf{X}_2 = \begin{bmatrix} \mathbf{X}_{1\cdot\cdot} \\ \vdots \\ \mathbf{X}_{I_1\cdot\cdot} \end{bmatrix}, \quad \mathbf{X}_3 = \begin{bmatrix} \mathbf{X}_{\cdot 1\cdot} \\ \vdots \\ \mathbf{X}_{\cdot I_2\cdot} \end{bmatrix}, \tag{1.15}$$

It can be shown from (1.11), (1.13) and (1.14) that $\mathbf{X}_1$, $\mathbf{X}_2$ and $\mathbf{X}_3$ can be expressed as:

$$\mathbf{X}_1 = (\mathbf{C} \otimes \mathbf{A})\mathbf{G}_1\mathbf{B}^T, \quad \mathbf{X}_2 = (\mathbf{A} \otimes \mathbf{B})\mathbf{G}_2\mathbf{C}^T, \quad \mathbf{X}_3 = (\mathbf{B} \otimes \mathbf{C})\mathbf{G}_3\mathbf{A}^T, \tag{1.16}$$

where $\mathbf{G}_1 \in \mathbb{C}^{RP\times Q}$, $\mathbf{G}_2 \in \mathbb{C}^{PQ\times R}$ and $\mathbf{G}_3 \in \mathbb{C}^{QR\times P}$ are unfolded matrices of the core tensor $\mathcal{G}$, which are constructed in the same fashion as (1.15), i.e.:

$$\mathbf{G}_1 = \begin{bmatrix} \mathbf{G}_{\cdot\cdot 1} \\ \vdots \\ \mathbf{G}_{\cdot\cdot R} \end{bmatrix}, \quad \mathbf{G}_2 = \begin{bmatrix} \mathbf{G}_{1\cdot\cdot} \\ \vdots \\ \mathbf{G}_{P\cdot\cdot} \end{bmatrix}, \quad \mathbf{G}_3 = \begin{bmatrix} \mathbf{G}_{\cdot 1\cdot} \\ \vdots \\ \mathbf{G}_{\cdot Q\cdot} \end{bmatrix}, \tag{1.17}$$

and $\otimes$ denotes the Kronecker product. Each one of the three unfolded matrices in (1.16) are different rearrangements of the same information contained in the tensor $\mathcal{X}$.

N-th order Tucker

The generalization of the Tucker-3 decomposition to the N-th order is straightforward. Let us consider a N-th order tensor $\mathcal{X} \in \mathbb{C}^{I_1\times I_2\times\cdots\times I_N}$. Its N-th order Tucker decomposition can be expressed as:

$$x_{i_1,i_2,\cdots,i_N} = \sum_{r_1=1}^{R_1}\sum_{r_2=1}^{R_2}\cdots\sum_{r_N=1}^{R_N} a^{(1)}_{i_1,r_1}a^{(2)}_{i_2,r_2}\cdots a^{(N)}_{i_N,r_N}g_{r_1,r_2,\cdots,r_N}, \tag{1.18}$$

where $a^{(n)}_{i_n,r_n} = [\mathbf{A}^{(n)}]_{i_n,r_n}$ is a scalar component of the n-th mode factor matrix and $g_{r_1,r_2,\cdots,r_N} = [\mathcal{G}]_{r_1,r_2,\cdots,r_N}$ is a scalar component of the N-th order core tensor. The mode-n product notation for (1.18) is written as:

$$\mathcal{X} = \mathcal{G} \bullet_1 \mathbf{A}^{(1)} \bullet_2 \mathbf{A}^{(2)} \cdots \bullet_N \mathbf{A}^{(N)}. \tag{1.19}$$

Let us go back to the third-order case. The Tucker-3 decomposition is not unique, since there are infinite solutions for the factor matrices and for the core tensor leading to the same tensor $\mathcal{X}$. In other words, the Tucker-3 decomposition allows arbitrary linear transformations on the three factor matrices (provided that the inverse of these transformations is applied to the core tensor) without affecting the reconstructed tensor $\mathcal{X}$. In order to see this, let us define nonsingular matrices $\mathbf{T}_a \in \mathbb{C}^{P\times P}$, $\mathbf{T}_b \in \mathbb{C}^{Q\times Q}$ and $\mathbf{T}_c \in \mathbb{C}^{R\times R}$. Considering the unfolded matrix $\mathbf{X}_1$, we have that:

$$\begin{aligned} \mathbf{X}_1 &= (\mathbf{C}\mathbf{T}_c\mathbf{T}_c^{-1} \otimes \mathbf{A}\mathbf{T}_a\mathbf{T}_a^{-1})\mathbf{G}_1(\mathbf{B}\mathbf{T}_b\mathbf{T}_b^{-1})^T \\ &= [(\mathbf{C}\mathbf{T}_c) \otimes (\mathbf{A}\mathbf{T}_a)]\left[(\mathbf{T}_c^{-1} \otimes \mathbf{T}_a^{-1})\mathbf{G}_1\mathbf{T}_b^{-T}\right](\mathbf{B}\mathbf{T}_b)^T, \end{aligned}$$

i.e.,

$$\mathbf{X}_1 = (\tilde{\mathbf{C}} \otimes \tilde{\mathbf{A}})\tilde{\mathbf{G}}_1\tilde{\mathbf{B}}^T, \tag{1.20}$$

where $\tilde{\mathbf{A}} = \mathbf{A}\mathbf{T}_a$, $\tilde{\mathbf{B}} = \mathbf{B}\mathbf{T}_b$ and $\tilde{\mathbf{C}} = \mathbf{C}\mathbf{T}_c$ are transformed factor matrices and $\tilde{\mathbf{G}}_1 = (\mathbf{T}_c^{-1} \otimes \mathbf{T}_a^{-1})\mathbf{G}_1\mathbf{T}_b^{-T}$ is a transformed Tucker-3 core. In (1.20), we have applied the following property of the Kronecker product:

Property 1.1 : Given $\mathbf{A} \in \mathbb{C}^{I\times R}$, $\mathbf{B} \in \mathbb{C}^{J\times S}$, $\mathbf{C} \in \mathbb{C}^{R\times P}$, and $\mathbf{D} \in \mathbb{C}^{S\times Q}$, we have:

$$\mathbf{AC} \otimes \mathbf{BD} = (\mathbf{A} \otimes \mathbf{B})(\mathbf{C} \otimes \mathbf{D}). \tag{1.21}$$

Equation (1.20) means that we have an infinite number of matrices $\tilde{\mathbf{A}}$, $\tilde{\mathbf{B}}$, $\tilde{\mathbf{C}}$ and $\tilde{\mathbf{G}}_1$ giving rise to the same matrix $\mathbf{X}_1$. This fact clearly states the general nonuniqueness of the Tucker-3 decomposition. Complete uniqueness of the factor matrices and the core tensor of a Tucker-3 decomposition is only possible in some special cases, where at least two factor matrices have some special structure that allows a unique determination of the transformation matrices. It has been shown that partial uniqueness (i.e., uniqueness of at least some factors) may exist in cases where the Tucker-3 core tensor is constrained to have several elements equal to zero [144].

Special cases: Tucker-2 and Tucker-1

Consider a Tucker-3 decomposition and rewrite (1.7) as:

$$x_{i_1,i_2,i_3} = \sum_{p=1}^{P}\sum_{q=1}^{Q} a_{i_1,p}b_{i_2,q}\left(\sum_{r=1}^{R} c_{i_3,r}g_{p,q,r}\right) = \sum_{p=1}^{P}\sum_{q=1}^{Q} a_{i_1,p}b_{i_2,q}h_{p,q,i_3}, \tag{1.22}$$

where $c_{i_3,r}$ has been absorbed in the core $g_{p,q,r}$, giving rise to an equivalent core h_{p,q,i_3} i.e., $h_{p,q,i_3} = [\mathcal{G} \bullet_3 \mathbf{C}]_{p,q,i_3}$. Equation (1.22) is the scalar notation of an equivalent Tucker-2 decomposition. Note that the Tucker-2 decomposition is simpler than its Tucker-3 equivalent, since the number of outer product terms has been reduced to PQ. A Tucker-2 decomposition also arises from a Tucker-3 one when one of the factor matrices, say $\mathbf{C}$, is equal to the identity matrix. The slice and unfolded notations for the Tucker-2 case can be easily obtained from (1.11), (1.13), (1.14) and (1.16) by setting $\mathbf{C} = \mathbf{I}_{I_3}$ and $\mathcal{G} = \mathcal{H} \in \mathbb{C}^{P\times Q\times I_3}$. The Tucker-2 decomposition is illustrated in Fig. 1.3.

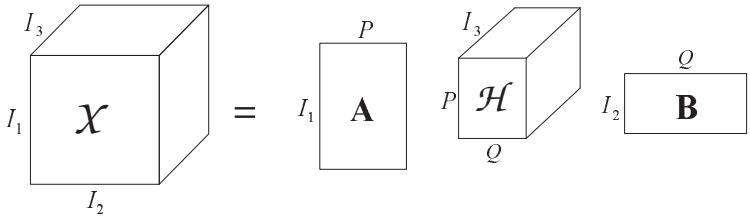

Figure 1.3: Visualization of the Tucker-2 decomposition.

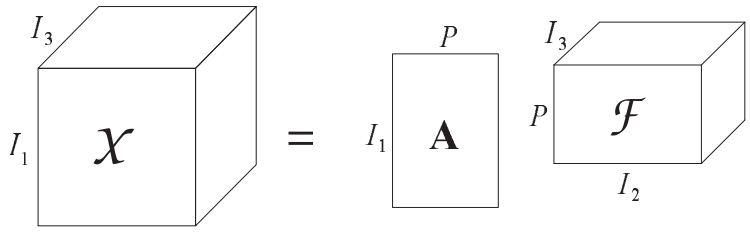

Figure 1.4: Visualization of the Tucker-1 decomposition.

Now, let us rewrite (1.7) as:

$$x_{i_1,i_2,i_3} = \sum_{p=1}^{P} a_{i_1,p} \left(\sum_{q=1}^{Q} \sum_{r=1}^{R} b_{i_2,q} c_{i_3,r} g_{p,q,r} \right) = \sum_{p=1}^{P} a_{i_1,p} f_{p,i_2,i_3}, \tag{1.23}$$

where both $b_{i_2,q}$ and $c_{i_3,r}$ have been absorbed in the core $g_{p,q,r}$, resulting in another core f_{p,i_2,i_3} i.e., $f_{p,i_2,i_3} = [\mathcal{G} \bullet_2 \mathbf{B} \bullet_3 \mathbf{C}]_{p,i_2,i_3}$. Equation (1.23) is the scalar notation of the Tucker-1 decomposition. A Tucker-1 decomposition also arises from a Tucker-3 one when two factor matrices, say $\mathbf{B}$ and $\mathbf{C}$, are equal to the identity matrix. The slice and unfolded notations for the Tucker-1 case are obtained from (1.11), (1.13), (1.14) and (1.16) by setting $\mathbf{B} = \mathbf{I}_{I_2}$, $\mathbf{C} = \mathbf{I}_{I_3}$ and $\mathcal{G} = \mathcal{F} \in \mathbb{C}^{P \times I_2 \times I_3}$. Figure 1.4 illustrates the Tucker-1 decomposition.

1.2.2 Parallel Factor (PARAFAC) decomposition

The PARAllel FACtor (PARAFAC) decomposition, also known as CANonical DECOMPosition (CANDECOMP), was independently developed by Harshman [73] and Carol & Chang [12] in the seventies. It is also known by the acronym CP (Candecomp-Parafac). Recently, this decomposition has found several applications in signal processing. Its has been exploited in wireless communications in a

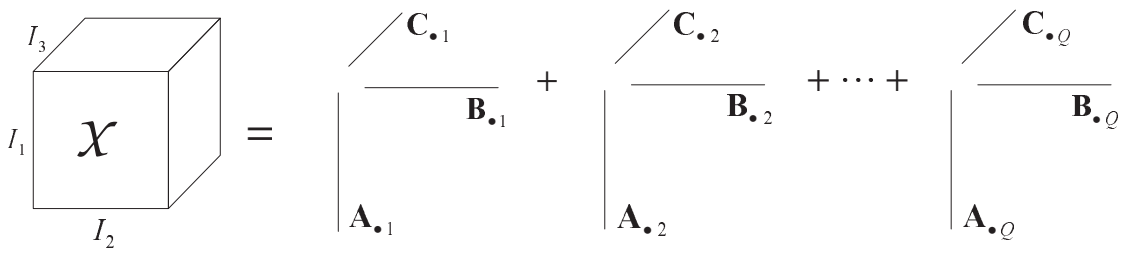

Figure 1.5: Visualization of the third-order PARAFAC decomposition.

number of different applications such [131, 128, 133, 53]. The PARAFAC decomposition also describes the basic structure of higher-order cumulants of multivariate data on which all algebraic methods for Independent Component Analysis (ICA) are based [14, 80, 18].

For a third-order tensor, it is a decomposition of a tensor in a sum of *triple products* or *triads*. PARAFAC can be equivalently stated as a decomposition of a three-way array in a sum of rank-1 tensors (c.f (1.4)). The PARAFAC decomposition of a tensor $\mathcal{X} \in \mathbb{C}^{I_1 \times I_2 \times I_3}$ has the following scalar form:

$$x_{i_1,i_2,i_3} = \sum_{q=1}^{Q} a_{i_1,q} b_{i_2,q} c_{i_3,q}, \tag{1.24}$$

where $a_{i_1,q} = [\mathbf{A}]_{i_1,q}$, $b_{i_2,q} = [\mathbf{B}]_{i_2,q}$ and $c_{i_3,q} = [\mathbf{C}]_{i_3,q}$ are scalar components of factor matrices $\mathbf{A} \in \mathbb{C}^{I_1 \times Q}$, $\mathbf{B} \in \mathbb{C}^{I_2 \times Q}$ and $\mathbf{C} \in \mathbb{C}^{I_3 \times Q}$ respectively. Q is the number of factors, also known as the *rank* of the decomposition. The columns of the first-, second- and third-factor matrices $\mathbf{A}$, $\mathbf{B}$ and $\mathbf{C}$ are respectively called first-, second- and third-mode *factor loadings*. Other synonyms for the columns of $\mathbf{A}$, $\mathbf{B}$ and $\mathbf{C}$ are *loading patterns* or *loading vectors*.

Using outer product notation, the third-order PARAFAC decomposition of $\mathcal{X}$ can be written as:

$$\mathcal{X} = \sum_{q=1}^{Q} \mathbf{A}_{\cdot q} \circ \mathbf{B}_{\cdot q} \circ \mathbf{C}_{\cdot q}.$$

In Fig. 1.5, a third-order PARAFAC decomposition is visualized as a sum of Q rank-1 tensors. A different visualization is depicted in Fig. 1.6, where the PARAFAC decomposition is interpreted as a special Tucker-3 decomposition with an identity core tensor.

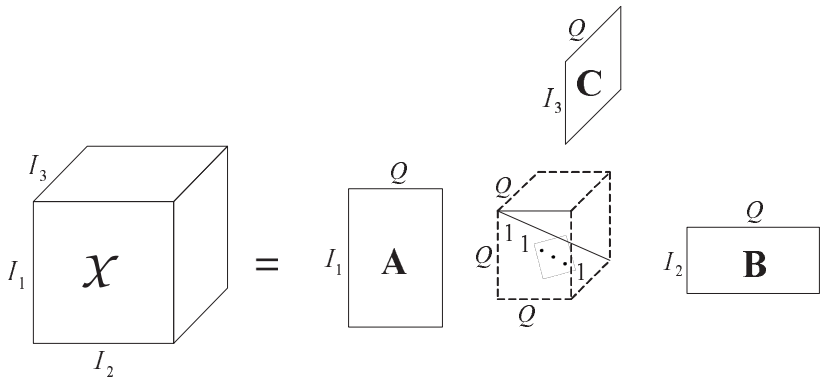

Figure 1.6: Visualization of the third-order PARAFAC decomposition as a special case of the Tucker-3 decomposition.

From the three possible slicing directions of $\mathcal{X}$, we get the following notation for the PARAFAC decomposition:

$$\begin{aligned} \mathbf{X}_{i_1 \cdot \cdot} &= \mathbf{B} D_{i_1}(\mathbf{A}) \mathbf{C}^T, \\ \mathbf{X}_{\cdot i_2 \cdot} &= \mathbf{C} D_{i_2}(\mathbf{B}) \mathbf{A}^T, \\ \mathbf{X}_{\cdot \cdot i_3} &= \mathbf{A} D_{i_3}(\mathbf{C}) \mathbf{B}^T, \end{aligned} \tag{1.25}$$

where $D_{i_1}(\mathbf{A})$ forms a diagonal matrix holding the i_1-th row of $\mathbf{A} \in \mathbb{C}^{I_1 \times Q}$ on its main diagonal.

By stacking row-wise the first-, second- and third-mode slices we have:

$$\begin{aligned} \mathbf{X}_1 &= \begin{bmatrix} \mathbf{X}_{\cdot \cdot 1} \\ \vdots \\ \mathbf{X}_{\cdot \cdot I_3} \end{bmatrix} = \begin{bmatrix} \mathbf{A} D_1(\mathbf{C}) \\ \vdots \\ \mathbf{A} D_{I_3}(\mathbf{C}) \end{bmatrix} \mathbf{B}^T = (\mathbf{C} \diamond \mathbf{A}) \mathbf{B}^T, \\ \mathbf{X}_2 &= \begin{bmatrix} \mathbf{X}_{1 \cdot \cdot} \\ \vdots \\ \mathbf{X}_{I_1 \cdot \cdot} \end{bmatrix} = \begin{bmatrix} \mathbf{B} D_1(\mathbf{A}) \\ \vdots \\ \mathbf{B} D_{I_1}(\mathbf{A}) \end{bmatrix} \mathbf{C}^T = (\mathbf{A} \diamond \mathbf{B}) \mathbf{C}^T, \\ \mathbf{X}_3 &= \begin{bmatrix} \mathbf{X}_{\cdot 1 \cdot} \\ \vdots \\ \mathbf{X}_{\cdot I_2 \cdot} \end{bmatrix} = \begin{bmatrix} \mathbf{C} D_1(\mathbf{B}) \\ \vdots \\ \mathbf{C} D_{I_2}(\mathbf{B}) \end{bmatrix} \mathbf{A}^T = (\mathbf{B} \diamond \mathbf{C}) \mathbf{A}^T, \end{aligned} \tag{1.26}$$

where $\diamond$ denotes the Khatri-Rao (column-wise Kronecker) product.

One of the most interesting properties of PARAFAC is its uniqueness. Contrarily

to bilinear (matrix) decompositions, which are in general not unique for ranks greater than one (rank-one matrices are unique up to a scalar factor), the PARAFAC decomposition of tensors of rank greater than one can be unique up to scaling and permutation of factors.

The first uniqueness studies of the PARAFAC decomposition were done in the seventies by Jennrich and Harshman [73, 74]. The deepest formal uniqueness proof was provided by Kruskal in [90]. Kruskal derived *sufficient* conditions for uniqueness of third-order PARAFAC decompositions of real-valued tensors. Around two decades later, Sidiropoulos *et al* [131] extended Kruskal condition to complex-valued tensors. Sidiropoulos & Bro [127] further generalized Kruskal's uniqueness condition to N-th order tensors. In [147], ten Berge and Sidiropoulos showed that Kruskal's condition is not only sufficient but also *necessary* for $Q \in \{2, 3\}$. Further PARAFAC uniqueness issues were addressed by Jiang & Sidiropoulos in [82], who derived necessary and sufficient conditions for uniqueness of the so-called *restricted* PARAFAC model (i.e., when at least one factor matrix is full column-rank). A more accessible proof of uniqueness is provided in [136] using conventional linear algebra. In [52], a new uniqueness bound that is more relaxed than Kruskal bound, is derived from a link between the PARAFAC decomposition and simultaneous matrix decompositions.

The study of the PARAFAC uniqueness condition is based on a fundamental concept, which is the concept of k-rank (*Kruskal*-rank), which is more restricted than the usual concept of matrix rank. The k-rank concept was proposed by Kruskal in his seminal paper [90], although the term "*Kruskal*-rank" was first used by Harshman and Lundy [75]. The k-rank concept has been extensively used as a key concept for stating PARAFAC uniqueness.

Definition 1.10 (k-rank): *The rank of* $\mathbf{A} \in \mathbb{C}^{I_1 \times Q}$*, denoted by* $r_{\mathbf{A}}$*, is equal to* r iff $\mathbf{A}$ *contains* at least *a set of* r *linearly independent columns but no set of* $r+1$ *linearly independent columns. The* Kruskal*-rank (or* k*-rank) of* $\mathbf{A}$ *is the maximum number* k *such that* every *set of* k *columns of* $\mathbf{A}$ *is linearly independent. Note that the* k*-rank is always less than or equal to the rank, and we have:*

$$k_{\mathbf{A}} \leq r_{\mathbf{A}} \leq min(I_1, Q).$$

Theorem 1.1 (uniqueness) [90]: *Consider the set of* I_1 *matrix-slices* $\mathbf{X}_{i_1 ..} = \mathbf{B} D_{i_1}(\mathbf{A}) \mathbf{C}^T, i_1 = 1, \cdots, I_1$*, defined in (1.25). If*

$$k_{\mathbf{A}} + k_{\mathbf{B}} + k_{\mathbf{C}} \geq 2Q + 2, \tag{1.27}$$

the matrices $\mathbf{A}$*,* $\mathbf{B}$ *and* $\mathbf{C}$ *are unique up to permutation and (complex) scaling of*

its columns [90, 131]. This means that any matrices $\tilde{\mathbf{A}}$, $\tilde{\mathbf{B}}$ *and* $\tilde{\mathbf{C}}$ *satisfying (1.25) are linked to* $\mathbf{A}$, $\mathbf{B}$ *and* $\mathbf{C}$ *by:*

$$\tilde{\mathbf{A}} = \mathbf{A}\mathbf{\Pi}\mathbf{\Delta}_1, \quad \tilde{\mathbf{B}} = \mathbf{B}\mathbf{\Pi}\mathbf{\Delta}_2, \quad \tilde{\mathbf{C}} = \mathbf{C}\mathbf{\Pi}\mathbf{\Delta}_3, \tag{1.28}$$

where $\mathbf{\Pi}$ *is a permutation matrix and* $\mathbf{\Delta}_1$, $\mathbf{\Delta}_2$ *and* $\mathbf{\Delta}_3$ *are diagonal matrices satisfying the condition*

$$\mathbf{\Delta}_1\mathbf{\Delta}_2\mathbf{\Delta}_3 = \mathbf{I}_Q. \tag{1.29}$$

Condition (1.27) is also necessary if $Q \leq 3$. However, ten Berge & Sidiropoulos provided in [147] a simple counter-example to the necessity of (1.27). They also claimed that the uniqueness of PARAFAC depends on the particular joint pattern of zeros in the factor matrices. This was better explained and clarified by Jiang & Sidiropoulos in [82]. They provided both necessary and sufficient uniqueness conditions for PARAFAC, when one factor matrix is full column-rank. This justified the examples shown in [147].

Theorem 1.2 [132, 126]: *For general PARAFAC decompositions with* $Q > 1$, two necessary conditions *for uniqueness are:*

$$min(r_{\mathbf{A}\diamond\mathbf{B}}, r_{\mathbf{B}\diamond\mathbf{C}}, r_{\mathbf{C}\diamond\mathbf{A}}) = Q \quad and \quad min(k_{\mathbf{A}}, k_{\mathbf{B}}, k_{\mathbf{C}}) \geq 2. \tag{1.30}$$

Conditions (1.30) can be interpreted in the following manner. Note that $r_{\mathbf{A}\diamond\mathbf{B}} \leq \min(I_1 I_2, Q)$, $r_{\mathbf{B}\diamond\mathbf{C}} \leq \min(I_2 I_3, Q)$ and $r_{\mathbf{C}\diamond\mathbf{A}} \leq \min(I_1 I_3, Q)$. Note also that the meaning of $k_{\mathbf{A}} \geq 2$ is that matrix $\mathbf{A}$ has no proportional columns (otherwise $k_{\mathbf{A}} = 1$, according to the definition of k-rank). It is thus equivalent to state that, uniqueness arises only if: i) *the product of any two dimensions of the tensor is at least equal to the number of factors* and ii) *none of the three factor matrices is allowed to have a pair of proportional columns.*

It was shown in [82] that (1.30) is a necessary and sufficient condition if one factor matrix is full column-rank. Assuming for instance, that $\mathbf{C}$ is full column-rank i.e., $r_{\mathbf{C}} = Q$, it is easily checked that condition (1.30), can be equivalently stated as:

$$r_{\mathbf{A}\diamond\mathbf{B}} = Q \quad \text{and} \quad \min(k_{\mathbf{A}}, k_{\mathbf{B}}) \geq 2, \tag{1.31}$$

which means that PARAFAC is unique if and only if the Khatri-Rao product $\mathbf{A}\diamond\mathbf{B}$ is full column-rank and ii) neither $\mathbf{A}$ nor $\mathbf{B}$ has a pair of proportional columns. In [82], it was also proposed an equivalent necessary and sufficient condition, which is valid for general PARAFAC decompositions and is also easier to verify than (1.30) and (1.31).

As will be shown later, uniqueness of at least a subset of PARAFAC factors is possible, even in cases where (a maximum of) two factor matrices have proportional columns. Uniqueness of at least a subset of factors in one or more modes is called *partial uniqueness*. It was first observed by Harshman [73, 74], who pointed out that PARAFAC uniqueness can break down in "parts". This concept is useful for studying uniqueness properties of some special PARAFAC models exhibiting proportional factors in one or more modes.

N-th order PARAFAC

The PARAFAC decomposition of a tensor $\mathcal{X} \in \mathbb{C}^{I_1 \times I_2 \times \cdots \times I_N}$ can be stated as:

$$x_{i_1,i_2,\cdots,i_N} = \sum_{q=1}^{Q} a_{i_1,q}^{(1)} a_{i_2,q}^{(2)} \cdots a_{i_N,q}^{(N)} = \sum_{q=1}^{Q} \prod_{n=1}^{N} a_{i_n,q}^{(n)}, \tag{1.32}$$

where $a_{i_n,q}^{(n)} = [\mathbf{A}^{(n)}]_{i_n,q}$, $i_n = 1, \ldots, I_n$, $n = 1, \ldots, N$. Model (1.32) is a Q-factor sum of N-fold products. In [127], Sidiropoulos & Bro provided a sufficient uniqueness condition for N-th order PARAFAC:

$$\sum_{n=1}^{N} k_{\mathbf{A}^{(n)}} \geq 2Q + (N-1). \tag{1.33}$$

For the N-th order case, necessary conditions follow directly from those of the third-order case, given in (1.30). However, the existence of a necessary and sufficient condition for uniqueness is not well established in the literature.

1.2.3 Alternating Least Squares (ALS) algorithm

The estimation of the three factor matrices of the PARAFAC decomposition is generally carried out by minimizing the following nonlinear quadratic cost function:

$$f(\mathbf{A}, \mathbf{B}, \mathbf{C}) = \left\| \mathcal{X} - \sum_{q=1}^{Q} \mathbf{A}_{\cdot q} \circ \mathbf{B}_{\cdot q} \circ \mathbf{C}_{\cdot q} \cdot \right\|_F^2. \tag{1.34}$$

The Alternating Least Squares (ALS) algorithm is the classical solution to minimize this cost function [7, 131, 135]. It is an iterative algorithm that alternates among the estimation of $\mathbf{A}$, $\mathbf{B}$ and $\mathbf{C}$. In other words, the ALS algorithm converts a nonlinear (in fact, trilinear) optimization problem into three independent linear

Least Squares (LS) problems.

Each iteration is composed of three LS estimation steps. At each step, one factor matrix, say, $\mathbf{A}$ is updated while the two others ($\mathbf{B}$ and $\mathbf{C}$) are fixed to their values obtained in previous estimation steps. The algorithm makes use of the Khatri-Rao factorizations of the unfolded matrices $\mathbf{X}_1$, $\mathbf{X}_2$ and $\mathbf{X}_3$ given in (1.26). It can be summarized as follows:

1. Set $i = 0$;
   Randomly initialize $\widehat{\mathbf{B}}_{(i=0)}$ and $\widehat{\mathbf{C}}_{(i=0)}$;
2. $i = i + 1$;
3. From $\mathbf{X}_3$ and using $\widehat{\mathbf{B}}_{(i-1)}$ and $\widehat{\mathbf{C}}_{(i-1)}$, find an estimate of $\mathbf{A}$ by solving the following LS problem:
   $$\widehat{\mathbf{A}}_{(i)} = \underset{\mathbf{A}}{\operatorname{argmin}} \left\| \mathbf{X}_3 - \left(\mathbf{B}_{(i-1)} \diamond \mathbf{C}_{(i-1)}\right)\mathbf{A}^T \right\|_F^2,$$
   the solution of which is given by:
   $$\widehat{\mathbf{A}}_{(i)}^T = \left(\widehat{\mathbf{B}}_{(i-1)} \diamond \widehat{\mathbf{C}}_{(i-1)}\right)^\dagger \mathbf{X}_3;$$
4. From $\mathbf{X}_1$, and using $\widehat{\mathbf{A}}_{(i)}$ and $\widehat{\mathbf{C}}_{(i-1)}$, find an estimate of $\mathbf{B}$ by solving the following LS problem:
   $$\widehat{\mathbf{B}}_{(i)} = \underset{\mathbf{B}}{\operatorname{argmin}} \left\| \mathbf{X}_1 - \left(\mathbf{C}_{(i-1)} \diamond \mathbf{A}_{(i)}\right)\mathbf{B}^T \right\|_F^2,$$
   the solution of which is given by:
   $$\widehat{\mathbf{B}}_{(i)}^T = \left(\widehat{\mathbf{C}}_{(i-1)} \diamond \widehat{\mathbf{A}}_{(i)}\right)^\dagger \mathbf{X}_1;$$
5. From $\mathbf{X}_2$, and using $\widehat{\mathbf{A}}_{(i)}$ and $\widehat{\mathbf{B}}_{(i)}$, find an estimate of $\mathbf{C}$ by solving the following LS problem:
   $$\widehat{\mathbf{C}}_{(i)} = \underset{\mathbf{C}}{\operatorname{argmin}} \left\| \mathbf{X}_2 - \left(\mathbf{A}_{(i)} \diamond \mathbf{B}_{(i)}\right)\mathbf{C}^T \right\|_F^2,$$
   the solution of which is given by:
   $$\widehat{\mathbf{C}}_{(i)}^T = \left(\widehat{\mathbf{A}}_{(i)} \diamond \widehat{\mathbf{B}}_{(i)}\right)^\dagger \mathbf{X}_2;$$
6. Repeat steps 2-5 until convergence.

The convergence at the i-th iteration is declared when the error between the true tensor and its reconstructed version from the estimated factor matrices does not

significantly change between iterations i and $i+1$. An error measure at the i-th iteration can be calculated from the following formula:

$$e_{(i)} = \left\| \mathbf{X}_1 - \left(\mathbf{C}_{(i)} \diamond \mathbf{A}_{(i)} \right) \mathbf{B}_{(i)}^T \right\|_F.$$

The convergence at the i-th iteration can be declared when $\|e_{(i+1)} - e_{(i)}\| < \delta$, where δ is a prescribed threshold value (e.g. $\delta = 10^{-6}$).

The conditional update of any given matrix may either improve or maintain but cannot worsen the current fit. The algorithm always monotonically converges to (at least) a local minimum. However, the ALS algorithm is strongly dependent on the initialization, and convergence to the global minimum can sometimes be slow. Moreover, the convergence of the algorithm can, in some cases, fall in regions of "swamps", during which the convergence speed is very small and the error between two consecutive iterations does not decrease. In this case, for avoiding a premature termination of the algorithm, it is a common practice to impose a minimum acceptable error value $e_{(i)}$, above which the global convergence is not assumed to be reached yet (even when $\|e_{(i+1)} - e_{(i)}\| < \delta$).

Alternative algorithms and methods

Several variants of the ALS algorithm have been proposed in the literature. See [61] for a critical review on some alternative algorithms. In order to alleviate the slow convergence problems caused by a random initialization of the algorithm, an eigenanalysis solution can be used [121, 91, 131]. This solution is also known as the direct trilinear decomposition in [121]. It consists in obtaining an initial estimate of the factor matrices of the decomposition by constructing a generalized eigenvalue problem (or joint diagonalization problem) from two slices of the tensor. The eigenanalysis based initialization, in addition to be limited to tensors with only two slices in one of the modes, requires that both two factor matrices are full column rank and the third one does not contain zero elements. The work [52] proposes a generalization of the eigenanalysis solution to tensors with more than two slices by linking the estimation of the PARAFAC factor matrices to the problem of simultaneous matrix diagonalization.

Another way of improving the speed of the ALS algorithm is based on the Tucker-3 compression method (see [3, 9] for details). This method is useful when the dimensions of the tensor are large. [131] proposes an algorithm to accelerate the ALS convergence This algorithm applies the Tucker-3 compression method followed by an eigenanalysis based initialization. The convergence of the ALS algorithm can also be improved by means of the so called Enhanced Line Search (ELS)

method [117]. The ELS method has shown to be useful when the decomposition of the tensor is affected by factor degeneracies. The ELS method was also used for estimating the factors of block tensor decompositions in [111]. A Levenberg-Marquadt method is proposed in [110].

1.2.4 Connection between PARAFAC and Tucker-3

Although Tucker-3 and PARAFAC are conceptually different tensor decompositions, it is possible to approach them in some sense. In other words, PARAFAC can be interpreted as a special case of Tucker-3 as well as Tucker-3 can be viewed as a *constrained* version of PARAFAC. This indicates that both decompositions could in principle be applied to model the same tensor data, although their computation is different.

Conceptual equivalences between Tucker-3 and PARAFAC were well described and discussed by Harshman in [73]. He also pointed out that not only PARAFAC can be equivalently stated as a special Tucker-3 and vice-versa, but both can be combined in different ways, resulting in hybrid decompositions that simultaneously enjoy properties of Tucker-3 and PARAFAC. This combination can be useful in cases where one is interested in characterizing/modeling tensors with a more complex inherent structure.

Going back to the Tucker-3 model (1.7) and considering that $P = Q = R$, we have:

$$x_{i_1,i_2,i_3} = \sum_{p=1}^{P}\sum_{q=1}^{Q}\sum_{r=1}^{R} a_{i_1,p}b_{i_2,q}c_{i_3,r}g_{p,q,r} = \sum_{q=1}^{Q} a_{i_1,q}b_{i_2,q}c_{i_3,q}g_{q,q,q}. \tag{1.35}$$

Note that we fall into the standard PARAFAC model when $g_{q,q,q} = \delta_{q,q,q}$. In other words, third-order PARAFAC is a special case of Tucker-3 with a "superdiagonal" core tensor $\mathcal{G} = \mathcal{I}_Q$, having zeros in all positions except in the main superdiagonal, which has all elements equal to one. $\mathcal{I}_Q$ is called the *identity tensor*. Note that the elements in the superdiagonal of $g_{q,q,q}$ need not to be restricted to one, since one can always absorb $g_{q,q,q}$ in any of the three factor matrices and still have an equivalent PARAFAC representation as a special case. Uniqueness in this special case is possible, provided that the necessary and sufficient conditions of PARAFAC are satisfied.

Now, let us go in the opposite direction and show how Tucker-3 decomposition can be interpreted as a constrained PARAFAC one. Rewrite (1.7) in its equivalent

Tucker-2 form (1.22):

$$x_{i_1,i_2,i_3} = \sum_{p=1}^{P}\sum_{q=1}^{Q} a_{i_1,p} b_{i_2,q} h_{p,q,i_3}, \tag{1.36}$$

with $h_{p,q,i_3} = [\mathcal{G} \bullet_3 \mathbf{C}]_{p,q,i_3}$. Define $\tilde{\mathbf{C}} \in \mathbb{C}^{I_3 \times PQ}$ as an unfolded matrix of the equivalent core tensor h_{p,q,i_3}, in the following manner:

$$\tilde{c}_{i_3,p,q} = [\tilde{\mathbf{C}}]_{i_3,(q-1)P+p}. \tag{1.37}$$

Define also *augmented* factor matrices $\tilde{\mathbf{A}} \in \mathbb{C}^{I_1 \times PQ}$ and $\tilde{\mathbf{B}} \in \mathbb{C}^{I_2 \times PQ}$ as:

$$\tilde{\mathbf{A}} = [\underbrace{\mathbf{A}, \ldots, \mathbf{A}}_{Q \text{ times}}], \quad \tilde{\mathbf{B}} = [\underbrace{\mathbf{B}_{\cdot 1}, \ldots, \mathbf{B}_{\cdot 1}}_{P \text{ times}}, \ldots, \underbrace{\mathbf{B}_{\cdot Q}, \ldots, \mathbf{B}_{\cdot Q}}_{P \text{ times}}], \tag{1.38}$$

where $\tilde{\mathbf{A}}$ is a concatenation of Q identical matrices $\mathbf{A}$ while $\tilde{\mathbf{B}}$ is a matrix where each column of $\mathbf{B}$, denoted by $\mathbf{B}_{\cdot q}$, $q = 1, \ldots, Q$, is repeated P times. Taking these definitions into account, a Tucker-3 decomposition can be represented by the following third-order PARAFAC decomposition of $F = PQ$ factors:

$$x_{i_1,i_2,i_3} = \sum_{f=1}^{F} \tilde{a}_{i_1,f} \tilde{b}_{i_2,f} \tilde{c}_{i_3,f}, \tag{1.39}$$

where the first- and second-mode factors $\tilde{a}_{i_1,f} = [\tilde{\mathbf{A}}]_{i_1,f}$ and $\tilde{b}_{i_2,f} = [\tilde{\mathbf{B}}]_{i_2,f}$, are constrained in the following form:

$$\begin{aligned} [\tilde{\mathbf{A}}]_{i_1,(q-1)P+p} &= [\mathbf{A}]_{i_1,p}, \\ [\tilde{\mathbf{B}}]_{i_2,(q-1)P+p} &= [\mathbf{B}]_{i_2,q}, \end{aligned} \tag{1.40}$$

where $f = (q-1)P + p$, $p = 1, \ldots, P$, $\quad q = 1, \ldots, Q$. Hence, a Tucker-3 decomposition can always be embedded in an equivalent PARAFAC one, where the first- and second-mode factor matrices have repeated loading vectors while the third-mode factor matrix is an unfolded matrix of an equivalent Tucker-3 core. The repetition patterns on $\tilde{\mathbf{A}}$ and $\tilde{\mathbf{B}}$ are given by (1.40). They produce all possible combinations of outer product factors necessary to completely characterize the Tucker-3 interaction structure.

The equivalent PARAFAC decomposition (1.39) is not unique in general, since uniqueness does not admit a pair of proportional columns in any of the factor matrices. Both $\tilde{\mathbf{A}}$ and $\tilde{\mathbf{B}}$ are such that $k_{\tilde{\mathbf{A}}} = k_{\tilde{\mathbf{B}}} = 1$ and the necessary condition

(1.30) fails to prove uniqueness. Therefore, any PARAFAC representation of a general Tucker-3 structure will show the same indeterminacies as the Tucker-3 representation.

1.2.5 Tensor decomposition in block terms

A tensor decomposition in block terms consists in decomposing a tensor "block" into a sum of "blocks" of smaller mode-n ranks [50, 51]. Block term decompositions cover both PARAFAC and Tucker-type decompositions as particular cases.

In its general formulation, the decomposition of a third-order tensor $\mathcal{X} \in \mathbb{C}^{I_1 \times I_2 \times I_3}$ into a sum of F tensor blocks, where the core tensor of each block has mode-1, mode-2 and mode-3 ranks equal to P, Q and R, respectively, is given by:

$$x_{i_1,i_2,i_3} = \sum_{f=1}^{F} \sum_{p=1}^{P} \sum_{q=1}^{Q} \sum_{r=1}^{R} a_{i_1,p}^{(f)} b_{i_2,q}^{(f)} c_{i_3,r}^{(f)} g_{p,q,r}^{(f)}, \tag{1.41}$$

or, equivalently:

$$\mathcal{X} = \sum_{f=1}^{F} \mathcal{G}^{(f)} \bullet_1 \mathbf{A}^{(f)} \bullet_2 \mathbf{B}^{(f)} \bullet_3 \mathbf{C}^{(f)}, \tag{1.42}$$

where $\mathcal{G}^{(f)} \in \mathbb{C}^{P \times Q \times R}$ is a rank-(P, Q, R) core tensor, and $\mathbf{A}^{(f)} \in \mathbb{C}^{I_1 \times P}$, $\mathbf{B}^{(f)} \in \mathbb{C}^{I_2 \times Q}$ and $\mathbf{C}^{(f)} \in \mathbb{C}^{I_3 \times R}$ are the factor matrices associated with the f-th decomposed tensor block. Note that (1.41) (resp. (1.42)) is a direct generalization of (1.7) (resp. (1.8)) by assuming $F > 1$ blocks. Therefore, block term decompositions of third-order tensors are generalized (block) Tucker-3 decompositions. An illustration of the block term decomposition is provided in Figure 1.7.

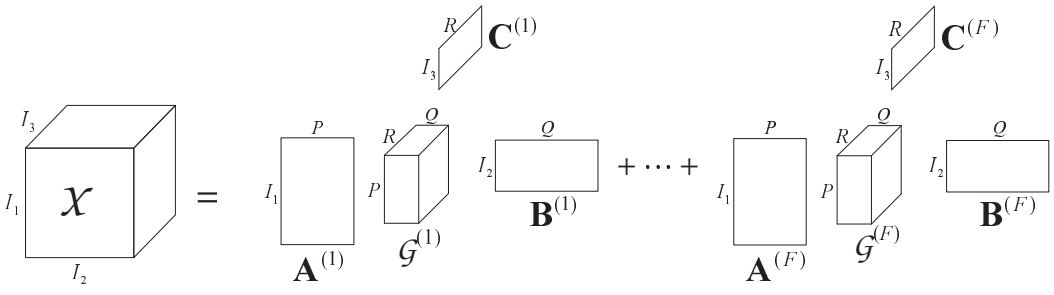

Figure 1.7: Visualization of the tensor decomposition in block terms.

The matrix-slices $\mathbf{X}_{..i_1}$, $i_1 = 1, \ldots, I_1$,$\mathbf{X}_{..i_2}$, $i_2 = 1, \ldots, I_2$, $\mathbf{X}_{..i_3}$, $i_3 = 1, \ldots, I_3$, are

constructed in a similar way as for the Tucker-3 decomposition (c.f. Section 1.2.1):

$$\begin{aligned}
\mathbf{X}_{i_1\cdot\cdot} &= \sum_{f=1}^{F} \mathbf{B}^{(f)} \mathbf{U}_{i_1}^{(1,f)} \mathbf{C}^{(f)T}, \quad i_1 = 1, \dots I_1, \\
\mathbf{X}_{\cdot i_2\cdot} &= \sum_{f=1}^{F} \mathbf{C}^{(f)} \mathbf{U}_{i_2}^{(2,f)} \mathbf{A}^{(f)T}, \quad i_2 = 1, \dots I_2, \\
\mathbf{X}_{\cdot\cdot i_3} &= \sum_{f=1}^{F} \mathbf{A}^{(f)} \mathbf{U}_{i_3}^{(3,f)} \mathbf{B}^{(f)T}, \quad i_3 = 1, \dots I_3,
\end{aligned} \tag{1.43}$$

i.e.

$$\mathbf{X}_{i_1\cdot\cdot} = \mathbf{B}\mathbf{U}_{i_1}^{(1)}\mathbf{C}^T, \quad \mathbf{X}_{\cdot i_2\cdot} = \mathbf{C}\mathbf{U}_{i_2}^{(2)}\mathbf{A}^T, \quad \mathbf{X}_{\cdot\cdot i_3} = \mathbf{A}\mathbf{U}_{i_3}^{(3)}\mathbf{B}^T, \tag{1.44}$$

where

$$\begin{aligned}
[\mathbf{U}_{i_1}^{(1,f)}]_{q,r} &= [\mathcal{G}^{(f)} \bullet_1 \mathbf{A}^{(f)}]_{i_1,q,r}, \\
[\mathbf{U}_{i_2}^{(2,f)}]_{p,r} &= [\mathcal{G}^{(f)} \bullet_2 \mathbf{B}^{(f)}]_{p,i_2,r}, \\
[\mathbf{U}_{i_3}^{(3,f)}]_{p,q} &= [\mathcal{G}^{(f)} \bullet_3 \mathbf{C}^{(f)}]_{p,q,i_3},
\end{aligned} \tag{1.45}$$

are respectively, the first-, second- and third-mode combined/transformed cores, associated with the f-th block, and

$$\begin{aligned}
\mathbf{A} &= \left[\mathbf{A}^{(1)} \cdots \mathbf{A}^{(F)}\right] \in \mathbb{C}^{I_1 \times FP}, \\
\mathbf{B} &= \left[\mathbf{B}^{(1)} \cdots \mathbf{B}^{(F)}\right] \in \mathbb{C}^{I_2 \times FQ}, \\
\mathbf{C} &= \left[\mathbf{C}^{(1)} \cdots \mathbf{C}^{(F)}\right] \in \mathbb{C}^{I_3 \times FR}
\end{aligned} \tag{1.46}$$

are the first-, second, and third-mode block-factor matrices. The unfolded matrices $\mathbf{X}_1$, $\mathbf{X}_2$ and $\mathbf{X}_3$ are given by:

$$\begin{aligned}
\mathbf{X}_1 &= (\mathbf{C} \,|\otimes|\, \mathbf{A})\text{blockdiag}\big(\mathbf{G}_1^{(1)} \cdots \mathbf{G}_1^{(F)}\big)\mathbf{B}^T, \\
\mathbf{X}_2 &= (\mathbf{A} \,|\otimes|\, \mathbf{B})\text{blockdiag}\big(\mathbf{G}_2^{(1)} \cdots \mathbf{G}_2^{(F)}\big)\mathbf{C}^T, \\
\mathbf{X}_3 &= (\mathbf{B} \,|\otimes|\, \mathbf{C})\text{blockdiag}\big(\mathbf{G}_3^{(1)} \cdots \mathbf{G}_3^{(F)}\big)\mathbf{A}^T,
\end{aligned} \tag{1.47}$$

where $|\otimes|$ denotes the block-wise Kronecker product, and $\mathbf{G}_1^{(f)} \in \mathbb{C}^{RP \times Q}$, $\mathbf{G}_2^{(f)} \in \mathbb{C}^{PQ \times R}$ and $\mathbf{G}_3^{(f)} \in \mathbb{C}^{QR \times P}$ are the unfolded matrices of the core tensor $\mathcal{G}^{(f)}$, which are constructed as in (1.17).

Depending on the mode-n ranks of the tensor blocks $\mathcal{G}^{(1)}, \dots, \mathcal{G}^{(F)}$, special block

term decompositions are possible. Among them, the most used are the decomposition in rank-$(P, P, 1)$ terms and the type-2 decomposition in rank-$(P, Q, \cdot)$ terms [50, 51]. These decompositions have found applications in blind deconvolution of DS-CDMA signals [47, 48, 109, 111].

Some uniqueness results for block term decompositions have been obtained recently in [50, 51]. They capitalize on the concept of k'-rank, which is a generalization of the k-rank for block-matrices [47]. The generalization of the uniqueness proof for PARAFAC in [90] for block term decompositions relies on the so-called "generalized equivalence lemma" [50, 51].

1.3 Block-constrained PARAFAC

We now present a new tensor decomposition also mixing some properties of PARAFAC and Tucker-3 decompositions. This decomposition is called block-constrained PARAFAC [30]. It consists in decomposing a third-order tensor into a sum of Q "structured" PARAFAC blocks. Within each block, a constrained pattern of linear combinations or *interactions* involving columns of the three component matrices is permitted. The interaction structure within each block may differ from one block to another, and is characterized by two fixed *constraint matrices*.

For a third-order tensor $\mathcal{X} \in \mathbb{C}^{I_1 \times I_2 \times I_3}$, we consider the following decomposition:

$$x_{i_1,i_2,i_3} = \sum_{q=1}^{Q} \sum_{r_1^{(q)}=1}^{R_1^{(q)}} \sum_{r_2^{(q)}=1}^{R_2^{(q)}} a^{(q)}_{i_1,r_1^{(q)}} \, b^{(q)}_{i_2,r_2^{(q)}} \, c^{(q)}_{r_1^{(q)},r_2^{(q)},i_3}. \tag{1.48}$$

x_{i_1,i_2,i_3} is decomposed into a sum of Q trilinear blocks, every block being itself the sum of $R_1^{(q)} R_2^{(q)}$ triple products. In the composition of the full tensor, $a^{(q)}_{i_1,r_1^{(q)}}$ contributes $R_2^{(q)}$ times, $b^{(q)}_{i_2,r_2^{(q)}}$ contributes $R_1^{(q)}$ times, and $c^{(q)}_{r_1^{(q)},r_2^{(q)},i_3}$ contributes $R_1^{(q)} R_2^{(q)}$ times.

Let us define two sets of matrices:

$$\{\mathbf{A}^{(q)}\} \in \mathbb{C}^{I_1 \times R_1^{(q)}}, \quad \{\mathbf{B}^{(q)}\} \in \mathbb{C}^{I_2 \times R_2^{(q)}}$$

and a set of Q third-order tensors $\{\mathcal{C}^{(q)}\} \in \mathbb{C}^{R_1^{(q)} \times R_2^{(q)} \times I_3}$ with typical elements

given, respectively by:

$$a^{(q)}_{i_1,r_1^{(q)}} = [\mathbf{A}^{(q)}]_{i_1,r_1^{(q)}}, \quad b^{(q)}_{i_2,r_2^{(q)}} = [\mathbf{B}^{(q)}]_{i_2,r_2^{(q)}}, \quad c^{(q)}_{r_1^{(q)},r_2^{(q)},i_3} = [\mathcal{C}^{(q)}]_{r_1^{(q)},r_2^{(q)},i_3}.$$

Define also a set of Q matrices $\{\mathbf{C}^{(1)}, \ldots, \mathbf{C}^{(Q)}\} \in \mathbb{C}^{I_3 \times R_1^{(q)} R_2^{(q)}}$ in the following way:

$$[\mathbf{C}^{(q)}]_{i_3,(r_1^{(q)}-1)R_2^{(q)}+r_2^{(q)}} = c^{(q)}_{r_1^{(q)},r_2^{(q)},i_3}, \quad q = 1, \ldots, Q,$$

where the q-th matrix $\mathbf{C}^{(q)}$ is linked to tensor $\mathcal{C}^{(q)}$ by:

$$\mathbf{C}^{(q)} = \left[\mathrm{vec}(\mathbf{C}^{(q)T}_{\cdot\cdot 1}) \cdots \mathrm{vec}(\mathbf{C}^{(q)T}_{\cdot\cdot I_3})\right]^T,$$

$\mathbf{C}^{(q)}_{\cdot\cdot i_3} \in \mathbb{C}^{R_1^{(q)} \times R_2^{(q)}}$ being the i_3-th matrix slice of $\mathcal{C}^{(q)}$, $i_3 = 1, \ldots, I_3$. The matrix slices $\mathbf{X}_{\cdot\cdot i_3} \in \mathbb{C}^{I_1 \times I_2}$ of $\mathcal{X}$ can be expressed in PARAFAC-based form as [40]:

$$\mathbf{X}_{\cdot\cdot i_3} = \sum_{q=1}^{Q} (\mathbf{A}^{(q)} \otimes \mathbf{1}^T_{R_2^{(q)}}) D_{i_3}(\mathbf{C}^{(q)}) (\mathbf{1}^T_{R_1^{(q)}} \otimes \mathbf{B}^{(q)})^T. \tag{1.49}$$

Using property (1.21), we obtain the following equivalences:

$$\mathbf{A}^{(q)} \otimes \mathbf{1}^T_{R_2^{(q)}} = (\mathbf{A}^{(q)} \otimes 1)(\mathbf{I}_{R_1^{(q)}} \otimes \mathbf{1}^T_{R_2^{(q)}}) = \mathbf{A}^{(q)} \underbrace{(\mathbf{I}_{R_1^{(q)}} \otimes \mathbf{1}^T_{R_2^{(q)}})}_{\mathbf{\Psi}^{(q)}} = \mathbf{A}^{(q)} \mathbf{\Psi}^{(q)},$$

and

$$\mathbf{1}^T_{R_1^{(q)}} \otimes \mathbf{B}^{(q)} = (1 \otimes \mathbf{B}^{(q)})(\mathbf{1}^T_{R_1^{(q)}} \otimes \mathbf{I}_{R_2^{(q)}}) = \mathbf{B}^{(q)} \underbrace{(\mathbf{1}^T_{R_1^{(q)}} \otimes \mathbf{I}_{R_2^{(q)}})}_{\mathbf{\Phi}^{(q)}} = \mathbf{B}^{(q)} \mathbf{\Phi}^{(q)},$$

where

$$\mathbf{\Psi}^{(q)} = \mathbf{I}_{R_1^{(q)}} \otimes \mathbf{1}^T_{R_2^{(q)}}, \qquad \mathbf{\Phi}^{(q)} = \mathbf{1}^T_{R_1^{(q)}} \otimes \mathbf{I}_{R_2^{(q)}} \tag{1.50}$$

are *constraint matrices* that model interactions or linear combinations of factors of different modes within the q-th block. They have dimensions $R_1^{(q)} \times R_1^{(q)} R_2^{(q)}$ and $R_2^{(q)} \times R_1^{(q)} R_2^{(q)}$, respectively. These definitions allow us to rewrite (1.49) as:

$$\mathbf{X}_{\cdot\cdot i_3} = \sum_{q=1}^{Q} \mathbf{A}^{(q)} \mathbf{\Psi}^{(q)} D_{i_3}(\mathbf{C}^{(q)}) (\mathbf{B}^{(q)} \mathbf{\Phi}^{(q)})^T. \tag{1.51}$$

Figure 1.8 illustrates the block-constrained PARAFAC decomposition in slice form.

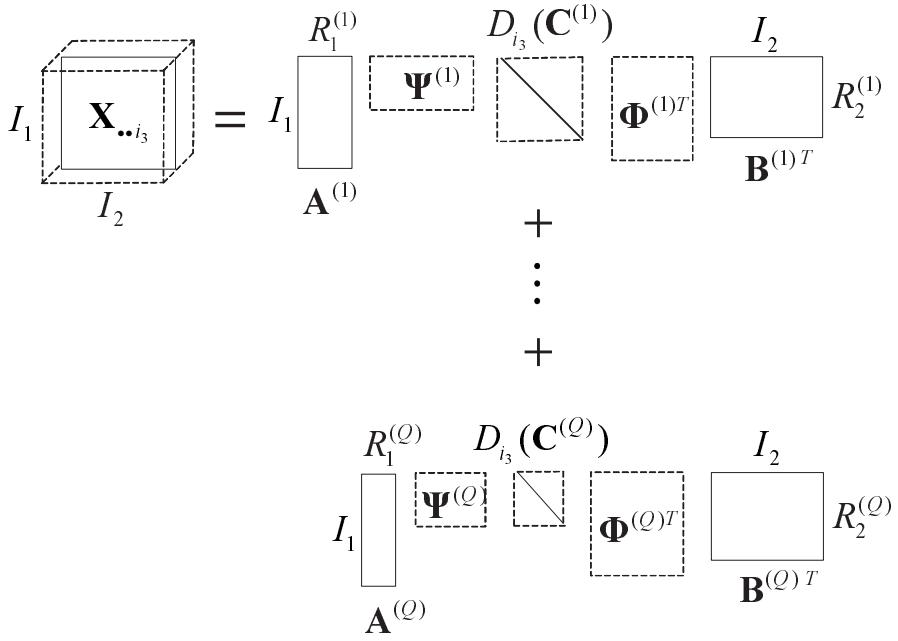

Figure 1.8: Visualization of the block-constrained PARAFAC decomposition.

Now, let us define the following block-matrices:

$$\begin{aligned}\mathbf{A} &= [\mathbf{A}^{(1)}, \ldots, \mathbf{A}^{(Q)}] \in \mathbb{C}^{I_1 \times R_1} \\ \mathbf{B} &= [\mathbf{B}^{(1)}, \ldots, \mathbf{B}^{(Q)}] \in \mathbb{C}^{I_2 \times R_2} \\ \mathbf{C} &= [\mathbf{C}^{(1)}, \ldots, \mathbf{C}^{(Q)}] \in \mathbb{C}^{I_3 \times R_3},\end{aligned}$$

where we have defined

$$R_1 = \sum_{q=1}^{Q} R_1^{(q)}, \quad R_2 = \sum_{q=1}^{Q} R_2^{(q)}, \quad R_3 = \sum_{q=1}^{Q} R_1^{(q)} R_2^{(q)}. \tag{1.52}$$

Define also *block-diagonal constraint matrices* as:

$$\begin{aligned}\mathbf{\Psi} &= \text{blockdiag}(\mathbf{\Psi}^{(1)} \cdots \mathbf{\Psi}^{(Q)}) \quad (R_1 \times R_3) \\ \mathbf{\Phi} &= \text{blockdiag}(\mathbf{\Phi}^{(1)} \cdots \mathbf{\Phi}^{(Q)}) \quad (R_2 \times R_3).\end{aligned} \tag{1.53}$$

Taking these definitions into account, (1.51) can be expressed in a compact matrix-

slice form as:

$$\mathbf{X}_{\cdot\cdot i_3} = \mathbf{A}\mathbf{\Psi} D_{i_3}(\mathbf{C})(\mathbf{B}\mathbf{\Phi})^T. \tag{1.54}$$

By comparing (1.25) and (1.54), we deduce the following correspondences:

$$\mathbf{A} \to \mathbf{A}\mathbf{\Psi}, \quad \mathbf{B} \to \mathbf{B}\mathbf{\Phi}, \quad \mathbf{C} \to \mathbf{C}.$$

Hence, by analogy with (1.26), $\mathbf{X}_{i=1,2,3}$ can be written as:

$$\mathbf{X}_1 = (\mathbf{C} \diamond \mathbf{A}\mathbf{\Psi})(\mathbf{B}\mathbf{\Phi})^T, \quad \mathbf{X}_2 = (\mathbf{A}\mathbf{\Psi} \diamond \mathbf{B}\mathbf{\Phi})\mathbf{C}^T, \quad \mathbf{X}_3 = (\mathbf{B}\mathbf{\Phi} \diamond \mathbf{C})(\mathbf{A}\mathbf{\Psi})^T. \tag{1.55}$$

The demonstration of (1.55) is provided in Appendix A.

From the previous equations and definitions, the following can be said about this tensor decomposition:

- It is the factorization of a third-order tensor into a sum of Q structured/constrained PARAFAC blocks, everyone of them being a function of three *component matrices* $\mathbf{A}^{(q)}, \mathbf{B}^{(q)}$ and $\mathbf{C}^{(q)}$. Each component matrix models the variation of the tensor data along one dimension or *mode*.

- Within the same constrained PARAFAC block, it is permitted that columns of different component matrices are linearly combined to generate the tensor data. The term *interaction* is used to denote such a linear combination.

- The interaction patterns within a block are modeled by the *constraint matrices* $\mathbf{\Psi}^{(q)}$ and $\mathbf{\Phi}^{(q)}$, which may differ from block to block.

- When the computation of the decomposition is performed, the term *between-block resolution* is a synonym of *separability* of the Q blocks, while the term *within-block uniqueness* stands for a unique determination of the three component matrices of the corresponding block (up to permutation and scaling). It depends on the particular interaction structure of each block.

Note that (1.51) can be interpreted as a structured PARAFAC model [73, 12] with augmented component matrices $\mathbf{A}\mathbf{\Psi}$, $\mathbf{B}\mathbf{\Phi}$ and $\mathbf{C}$. It is also worth noting that the within-block structure of block-constrained PARAFAC is similar to that of the PARALIND (PARAllel profiles with LINear Dependencies) model proposed in [10]. The proposed approach is more general, since it considers multiple constrained blocks, each one with its own interaction structure. The block-constrained PARAFAC model can also be linked to Tucker-2 and Tucker-3 analysis [148, 8]. From the scalar notation (1.48), it is easy to conclude that this model naturally

takes the form of a sort of "block-Tucker-2" decomposition with variable within-block interaction structure. It can also be interpreted as a constrained Tucker-3 decomposition [87, 147]. The block-constrained PARAFAC decomposition can be written as a constrained decomposition in block terms (c.f 1.2.5), where each block is constrained to have 1's and 0's, possibly having a different constrained structure.

1.3.1 N-th order generalization

The generalization of the block-constrained PARAFAC decomposition to a N-th order tensor is relatively straightforward. For a tensor $\mathcal{X} \in \mathbb{C}^{I_1 \times I_2 \times \cdots \times I_N}$, it can be stated as:

$$x_{i_1,\ldots,i_N} = \sum_{q=1}^{Q} \sum_{r_1^{(q)}=1}^{R_1^{(q)}} \cdots \sum_{r_{N-1}^{(q)}=1}^{R_{N-1}^{(q)}} \left(\prod_{n=1}^{N-1} a_{i_n, r_n^{(q)}}^{(n,q)} \right) g_{r_1^{(q)},\ldots,r_{N-1}^{(q)},i_N}^{(q)} \tag{1.56}$$

where $a_{i_n, r_n^{(q)}}^{(n,q)} = [\mathbf{A}^{(n,q)}]_{i_n, r_n^{(q)}}$, $i_n = 1, \ldots, I_n$, $n = 1, \ldots, N-1$, $q = 1, \ldots, Q$, is the n-th mode factor matrix of the q-th block, while $g_{r_1^{(q)},\ldots,r_{N-1}^{(q)},i_N}^{(q)}$ is the N-th mode factor matrix of q-th block. Model (1.56) is a sum of Q tensor blocks of N-th order, each one being a sum of $\prod_{n=1}^{N-1} R_n^{(q)}$ outer products. The strength (or weight) of each outer product contribution is given by the corresponding value of $g_{r_1^{(q)},\ldots,r_{N-1}^{(q)},i_N}^{(q)}$.

1.3.2 Block-constrained Tucker-3 writing

Recall the expression for $\mathbf{X}_2$ in (1.55), and consider the following property of the Khatri-Rao product:

Property 1.2 : Given $\mathbf{A} \in \mathbb{C}^{I \times R}$, $\mathbf{B} \in \mathbb{C}^{J \times S}$, $\mathbf{C} \in \mathbb{C}^{R \times P}$, and $\mathbf{D} \in \mathbb{C}^{S \times P}$, we have:

$$\mathbf{AC} \diamond \mathbf{BD} = (\mathbf{A} \otimes \mathbf{B})(\mathbf{C} \diamond \mathbf{D}). \tag{1.57}$$

Property 1.3 : Given block-partitioned matrices:

$$\mathbf{A} = [\mathbf{A}^{(1)} \cdots \mathbf{A}^{(Q)}] \in \mathbb{C}^{I \times R}, \quad \mathbf{B} = [\mathbf{B}^{(1)} \cdots \mathbf{B}^{(Q)}] \in \mathbb{C}^{J \times S},$$

$$\mathbf{C} = [\mathbf{C}^{(1)} \cdots \mathbf{C}^{(Q)}] \in \mathbb{C}^{R \times P}, \quad \mathbf{D} = [\mathbf{D}^{(1)} \cdots \mathbf{D}^{(Q)}] \in \mathbb{C}^{S \times P},$$

where

$$R = \sum_{q=1}^{Q} R_q, \quad S = \sum_{q=1}^{Q} S_q,$$

and $\mathbf{A}^{(q)} \in \mathbb{C}^{I \times R_q}$, $\mathbf{B}^{(q)} \in \mathbb{C}^{J \times S_q}$, $\mathbf{C}^{(q)} \in \mathbb{C}^{R_q \times P}$, $\mathbf{D}^{(q)} \in \mathbb{C}^{S_q \times P}$, we have:

$$\mathbf{AC} \diamond \mathbf{BD} = (\mathbf{A} \mid\otimes\mid \mathbf{B}) \cdot \text{blockdiag}(\mathbf{C}^{(1)} \diamond \mathbf{D}^{(1)} \cdots \mathbf{C}^{(Q)} \diamond \mathbf{D}^{(Q)}). \tag{1.58}$$

Using property (1.58), we can rewrite (1.55) in the following manner:

$$\mathbf{X}_2 = (\mathbf{A}\boldsymbol{\Psi} \diamond \mathbf{B}\boldsymbol{\Phi})\mathbf{C}^T = (\mathbf{A} \mid\otimes\mid \mathbf{B})F(\boldsymbol{\Psi}, \boldsymbol{\Phi})\mathbf{C}^T, \tag{1.59}$$

where $\mathbf{A} \mid\otimes\mid \mathbf{B}$ denotes the block-wise Kronecker product, and $F(\boldsymbol{\Psi}, \boldsymbol{\Phi})$ is given by:

$$F(\boldsymbol{\Psi}, \boldsymbol{\Phi}) = \text{blockdiag}(\boldsymbol{\Psi}^{(1)} \diamond \boldsymbol{\Phi}^{(1)} \cdots \boldsymbol{\Psi}^{(Q)} \diamond \boldsymbol{\Phi}^{(Q)}). \tag{1.60}$$

Note that:

$$\begin{aligned} \boldsymbol{\Psi}^{(q)} \diamond \boldsymbol{\Phi}^{(q)} &= (\mathbf{I}_{R_1^{(q)}} \otimes \mathbf{1}^T_{R_2^{(q)}}) \diamond (\mathbf{1}^T_{R_1^{(q)}} \otimes \mathbf{I}_{R_2^{(q)}}) \\ &= \mathbf{I}_{R_3^{(q)}} \diamond \mathbf{1}^T_{R_3^{(q)}} = \mathbf{I}_{R_3^{(q)}}, \end{aligned} \tag{1.61}$$

where $R_3^{(q)} = R_1^{(q)} R_2^{(q)}$, yielding:

$$F(\boldsymbol{\Psi}, \boldsymbol{\Phi}) = \text{blockdiag}(\mathbf{I}_{R_3^{(1)}}, \cdots, \mathbf{I}_{R_3^{(Q)}}) = \mathbf{I}_{R_3} \tag{1.62}$$

and consequently:

$$\mathbf{X}_2 = (\mathbf{A} \mid\otimes\mid \mathbf{B})\mathbf{G}_2\mathbf{C}^T, \quad \mathbf{G}_2 = \mathbf{I}_{R_3}. \tag{1.63}$$

Equation (1.63) is an unfolded matrix of a special block-Tucker-3 model, where the associated unfolded block-core $\mathbf{G}_2$ is equal to the identity matrix. Working similarly on the other unfolded matrices

$$\mathbf{X}_1 = (\mathbf{C} \diamond \mathbf{A}\boldsymbol{\Psi})\boldsymbol{\Phi}^T\mathbf{B}^T, \qquad \mathbf{X}_3 = (\mathbf{B}\boldsymbol{\Phi} \diamond \mathbf{C})\boldsymbol{\Psi}^T\mathbf{A}^T, \tag{1.64}$$

we arrive at the two other block-Tucker-3 unfolded matrices:

$$\mathbf{X}_1 = (\mathbf{C} \mid\otimes\mid \mathbf{A})\mathbf{G}_1\mathbf{B}^T, \qquad \mathbf{X}_3 = (\mathbf{B} \mid\otimes\mid \mathbf{C})\mathbf{G}_3\mathbf{A}^T, \tag{1.65}$$

where the unfolded block-core representations $\mathbf{G}_1$ and $\mathbf{G}_3$ are given by:

$$\mathbf{G}_1 = \text{blockdiag}(\mathbf{G}_1^{(1)}, \ldots, \mathbf{G}_1^{(Q)}) \in \mathbb{C}^{R' \times R_2}, \quad \mathbf{G}_1^{(q)} = (\mathbf{I}_{R_3^{(q)}} \diamond \mathbf{\Psi}^{(q)})\mathbf{\Phi}^{(q)T} \quad (1.66)$$

$$\mathbf{G}_3 = \text{blockdiag}(\mathbf{G}_3^{(1)}, \ldots, \mathbf{G}_3^{(Q)}) \in \mathbb{C}^{R'' \times R_1}, \quad \mathbf{G}_3^{(q)} = (\mathbf{\Phi}^{(q)} \diamond \mathbf{I}_{R_3^{(q)}})\mathbf{\Psi}^{(q)T} \quad (1.67)$$

where $R' = \sum_{q=1}^{Q} R_1^{(q)} R_3^{(q)}$ and $R'' = \sum_{q=1}^{Q} R_2^{(q)} R_3^{(q)}$. The visualization of the equivalent block-constrained Tucker-3 decomposition is provided in Fig. 1.9.

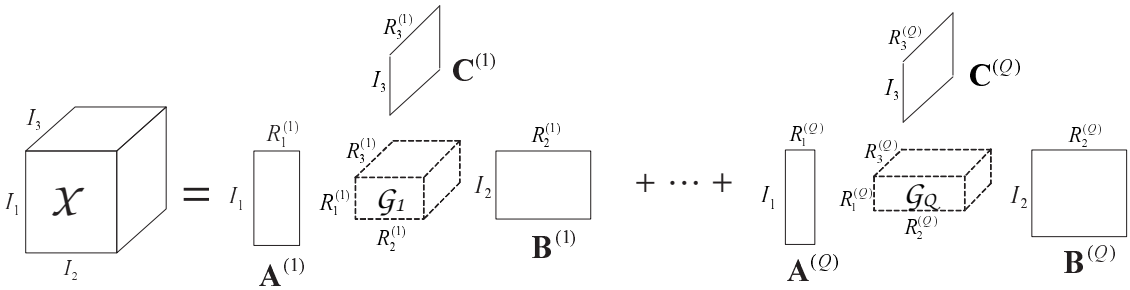

Figure 1.9: Interpretation of the block-constrained PARAFAC decomposition as a block-constrained Tucker-3 decomposition.

1.3.3 Necessary uniqueness condition

Theorem 1.3 (necessary condition for uniqueness): *Consider the set of unfolded representations (1.55) for the block-constrained PARAFAC decomposition. Assume that the matrices* $\mathbf{A} \in \mathbb{C}^{I_1 \times R_1}$, $\mathbf{B} \in \mathbb{C}^{I_2 \times R_2}$ *and* $\mathbf{C} \in \mathbb{C}^{I_3 \times R_3}$ *are full rank. For the uniqueness of the decomposition in the Least Squares (LS) sense, the three following inequalities must hold:*

$$I_1 I_3 \geq R_2, \quad I_1 I_2 \geq R_3, \quad I_2 I_3 \geq R_1. \quad (1.68)$$

In this case, there are nonsingular block-diagonal transformation matrices

$$\begin{aligned} \mathbf{T}_a &= \textit{blockdiag}(\mathbf{T}_a^{(1)}, \ldots, \mathbf{T}_a^{(Q)}), \\ \mathbf{T}_b &= \textit{blockdiag}(\mathbf{T}_b^{(1)}, \ldots, \mathbf{T}_b^{(Q)}), \\ \mathbf{T}_c &= \textit{blockdiag}(\mathbf{T}_c^{(1)}, \ldots, \mathbf{T}_c^{(Q)}), \end{aligned} \quad (1.69)$$

satisfying:

$$\left(\mathbf{T}_a^{(q)} \otimes \mathbf{T}_b^{(q)}\right)^{-1} = \mathbf{T}_c^{(q)T}, \quad q = 1, \ldots, Q, \tag{1.70}$$

such that $\overline{\mathbf{A}} = \mathbf{A}\mathbf{T}_a$, $\overline{\mathbf{B}} = \mathbf{B}\mathbf{T}_b$ *and* $\overline{\mathbf{C}} = \mathbf{C}\mathbf{T}_c$ *give rise to the same matrices* $\{\mathbf{X}\}_{i=1,2,3}$.

Proof: First of all, let us rewrite the three unfolded matrices of the received signal (1.55) in the following equivalent manner:

$$\mathbf{X}_1 = \mathbf{Z}_1\big(\mathbf{C}, \mathbf{A}\big)\mathbf{B}^T, \quad \mathbf{X}_2 = \mathbf{Z}_2\big(\mathbf{A}, \mathbf{B}\big)\mathbf{C}^T, \quad \mathbf{X}_3 = \mathbf{Z}_3\big(\mathbf{B}, \mathbf{C}\big)\mathbf{A}^T. \tag{1.71}$$

where

$$\begin{aligned}
\mathbf{Z}_1\big(\mathbf{C}, \mathbf{A}\big) &= (\mathbf{C} \diamond \mathbf{A}\mathbf{\Psi})\mathbf{\Phi}^T \in \mathbb{C}^{I_1 I_3 \times R_2}, \\
\mathbf{Z}_2\big(\mathbf{A}, \mathbf{B}\big) &= (\mathbf{A}\mathbf{\Psi}) \diamond (\mathbf{B}\mathbf{\Phi}) \in \mathbb{C}^{I_1 I_2 \times R_3}, \\
\mathbf{Z}_3\big(\mathbf{B}, \mathbf{C}\big) &= (\mathbf{B}\mathbf{\Phi} \diamond \mathbf{C})\mathbf{\Psi}^T \in \mathbb{C}^{I_2 I_3 \times R_1}.
\end{aligned} \tag{1.72}$$

From (1.71), $\mathbf{B}$ is identifiable in the LS sense if and only if $\mathbf{Z}_1\big(\mathbf{C}, \mathbf{A}\big)$ admits a unique left pseudo-inverse, i.e. if it does *not* exist $\mathbf{Y}$ belonging to the kernel $K(\mathbf{Z}_1)$ such that $\mathbf{Z}_1(\mathbf{Y} + \mathbf{B}^T) = \mathbf{Z}_1\tilde{\mathbf{B}}^T$. From the rank theorem, we have:

$$\dim\big(K(\mathbf{Z}_1)\big) = 0 \Rightarrow \operatorname{rank}(\mathbf{Z}_1) = R_2,$$

which means that $\mathbf{Z}_1$ is full column-rank. Moreover, as we have $\operatorname{rank}(\mathbf{Z}_1) \leq \min(I_1 I_3, R_2)$, it follows that $I_1 I_3 \geq R_2$, i.e. $\mathbf{Z}_1$ is tall. Applying the same reasoning to $\mathbf{C}$ and $\mathbf{A}$ in $\mathbf{X}_2 = \mathbf{Z}_2\big(\mathbf{A}, \mathbf{B}\big)\mathbf{C}^T$ and $\mathbf{X}_3 = \mathbf{Z}_3\big(\mathbf{B}, \mathbf{C}\big)\mathbf{A}^T$, we obtain the inequalities $I_1 I_2 \geq R_3$ and $I_2 I_3 \geq R_1$, respectively.

Now, we prove the relation (1.70). First, it should be noted that the non-singularity of $\mathbf{T}_a, \mathbf{T}_b$ and $\mathbf{T}_c$ comes from the full-rank assumption for $\mathbf{A}$, $\mathbf{B}$ and $\mathbf{C}$. Inserting the block-diagonal matrices $\mathbf{T}_a\mathbf{T}_a^{-1} = \mathbf{I}_{R_1}$, $\mathbf{T}_b\mathbf{T}_b^{-1} = \mathbf{I}_{R_2}$ and $\mathbf{T}_c\mathbf{T}_c^{-1} = \mathbf{I}_{R_3}$ in the unfolded representation $\mathbf{X}_2$ of (1.59), and then using (1.60)-(1.62), we get:

$$\begin{aligned}
\mathbf{X}_2 &= \big(\mathbf{A}\mathbf{T}_a\mathbf{T}_a^{-1}\mathbf{\Psi} \diamond \mathbf{B}\mathbf{T}_b\mathbf{T}_b^{-1}\mathbf{\Phi}\big)\mathbf{T}_c^{-T}\mathbf{T}_c^T\mathbf{C}^T \\
&= \big(\tilde{\mathbf{A}} \,|\otimes|\, \tilde{\mathbf{B}}\big)\operatorname{blockdiag}\big((\mathbf{T}_a^{-1}\mathbf{\Psi} \diamond \mathbf{T}_b^{-1}\mathbf{\Phi})\mathbf{T}_c^{-T}\big)\tilde{\mathbf{C}}^T \\
&= \big(\tilde{\mathbf{A}} \,|\otimes|\, \tilde{\mathbf{B}}\big)\operatorname{blockdiag}\Big(\big(\mathbf{T}_a^{(1)} \,|\otimes|\, \mathbf{T}_b^{(1)}\big)^{-1}, \ldots, \big(\mathbf{T}_a^{(Q)} \,|\otimes|\, \mathbf{T}_b^{(Q)}\big)^{-1}\Big) \underbrace{F(\mathbf{\Psi}, \mathbf{\Phi})}_{\mathbf{I}_{R_3}} \mathbf{T}_c^{-T}\mathbf{C}^T \\
&= \big(\tilde{\mathbf{A}} \,|\otimes|\, \tilde{\mathbf{B}}\big)\tilde{\mathbf{G}}_2\tilde{\mathbf{C}}^T.
\end{aligned} \tag{1.73}$$

where

$$\tilde{\mathbf{G}}_2 = \text{blockdiag}\Big(\big(\mathbf{T}_a^{(1)}\big)^{-1} \otimes \big(\mathbf{T}_b^{(1)}\big)^{-1}, \ldots, \big(\mathbf{T}_a^{(Q)}\big)^{-1} \otimes \big(\mathbf{T}_b^{(Q)}\big)^{-1}\Big)\mathbf{T}_c^{-T}.$$

Comparing (1.73) with (1.63), we deduce that we must have:

$$\tilde{\mathbf{G}}_2^{(q)} = \big((\mathbf{T}_a^{(q)})^{-1} \otimes (\mathbf{T}_b^{(q)})^{-1}\big)\big(\mathbf{T}_c^{(q)}\big)^{-T} = \mathbf{I}_{R_1^{(q)}R_2^{(q)}}, \quad q = 1, \ldots, Q.$$

which implies that:

$$\big(\mathbf{T}_a^{(q)} \otimes \mathbf{T}_b^{(q)}\big)^{-1} = \big(\mathbf{T}_c^{(q)}\big)^{T}, \quad q = 1, \ldots, Q. \quad \blacksquare \tag{1.74}$$

In the special case $R_1^{(1)} = \cdots R_1^{(Q)} = \overline{R}_1$ and $R_2^{(1)} = \cdots R_2^{(Q)} = \overline{R}_2$, condition (1.68) can be rewritten as:

$$I_1 I_2 \geq Q\overline{R}_1\overline{R}_2, \quad I_1 I_3 \geq Q\overline{R}_2, \quad I_2 I_3 \geq Q\overline{R}_1,$$

which is equivalent to:

$$\min\left(\Big\lfloor \frac{I_1 I_2}{\overline{R}_1\overline{R}_2} \Big\rfloor, \Big\lfloor \frac{I_1 I_3}{\overline{R}_2} \Big\rfloor, \Big\lfloor \frac{I_2 I_3}{\overline{R}_1} \Big\rfloor\right) \geq Q, \tag{1.75}$$

where $\lfloor x \rfloor$ is the "floor" operator that rounds x to the nearest smaller integer. This condition guarantees between-block uniqueness of block-constrained PARAFAC. Note that, for $\overline{R}_1 = \overline{R}_2 = 1$, condition (1.75) reduces to the necessary uniqueness conditions for standard PARAFAC [132].

The block-diagonal structure of $\mathbf{T}_a$, $\mathbf{T}_b$ and $\mathbf{T}_c$ means that rotational freedom is confined within the blocks. In other words, the block-constrained PARAFAC decomposition has *between-block uniqueness*. *Within-block non-uniqueness*, however, remains in the general case $R_1^{(q)} \geq 2$ and $R_2^{(q)} \geq 2$. Note however, that rotational freedom affecting the component matrices of a given block is constrained and obeys $\mathbf{T}_c^{(q)T} = \big(\mathbf{T}_a^{(q)} \otimes \mathbf{T}_b^{(q)}\big)^{-1}$, which imposes some uniqueness constraints on the block-constrained PARAFAC model that are not as strong as those of unconstrained Tucker-3 models. For example, complete within-block uniqueness is restored, e.g., if $\mathbf{C}$ is known. Otherwise, if $\mathbf{C}$ has some special structure (e.g. block-diagonal, Toeplitz, etc) one can enforce the underlying structure during the computation of the model, in order to restrict within-block non-uniqueness.

Example 1.1: Suppose that $R_1^{(1)} = \cdots = R_1^{(Q)} = 1$. This means that interactions involving the columns of the first- and third-mode component matrices no longer

exist, for all the blocks. In this case we have (ignoring scaling ambiguity):

$$\mathbf{T}_b^T = \mathbf{T}_c^{-1}, \quad 1, \ldots, Q, \tag{1.76}$$

i.e. within-block rotational freedom only affects the second- and third-mode component matrices, while $\{\mathbf{A}^{(1)}, \cdots, \mathbf{A}^{(Q)}\}$ can be determined up to common column permutation and scaling. In this case, the within-block structure of this particular block-constrained PARAFAC decomposition exhibits partial uniqueness. It takes on the same partial uniqueness properties of the PARALIND decomposition considered in [130, 10] (see these references for a constructive proof of partial uniqueness).

Discussion: Uniqueness of this decomposition is related in some sense to the "minimum uniqueness conditions" for PARAFAC originally presented in [74]. The implication of this uniqueness study to our case, is that it establishes between-block uniqueness of the block-constrained PARAFAC. On the other hand, within-block uniqueness can be studied by taking special structures of one or more factor matrices into account. Different levels of partial uniqueness within the blocks are possible. By "partial uniqueness", we mean that (at least some columns of) the component matrices of one or more blocks can be uniquely determined (up to permutation and scaling) while the determination of the other ones is affected by a nonsingular matrix multiplication [146]. This means that within-block uniqueness breaks down "in parts", as pointed out by Harshman in [74], but also in "in blocks", since different levels of partial uniqueness (or restricted nonuniqueness) exist and may vary from block to block.

1.4 Constrained Factor decomposition

In this section, we present a new third-order tensor decomposition herein called CONstrained FACtor (CONFAC) decomposition [44, 35]. The tensor is decomposed into a triple sum of rank-one tensor factors, where component combinations, or *interactions*, involving the different tensor factors are allowed. The interaction pattern is captured by three *constraint matrices* the columns of which are canonical vectors. Each constraint matrix is associated with a given dimension or *mode* of the tensor.

Let us consider a third-order tensor $\mathcal{X} \in \mathbb{C}^{I_1 \times I_2 \times I_3}$, three *factor matrices* $\mathbf{A} \in \mathbb{C}^{I_1 \times R_1}$, $\mathbf{B} \in \mathbb{C}^{I_2 \times R_2}$, $\mathbf{C} \in \mathbb{C}^{I_3 \times R_3}$, and three *constraint matrices* $\mathbf{\Psi} \in \mathbb{C}^{R_1 \times F}$, $\mathbf{\Phi} \in \mathbb{C}^{R_2 \times F}$, $\mathbf{\Omega} \in \mathbb{C}^{R_3 \times F}$. The Constrained Factor (CONFAC) decomposition of $\mathcal{X}$

with F factor combinations is defined in scalar form as:

$$x_{i_1,i_2,i_3} = \sum_{f=1}^{F} \sum_{r_1=1}^{R_1} \sum_{r_2=1}^{R_2} \sum_{r_3=1}^{R_3} a_{i_1,r_1} b_{i_2,r_2} c_{i_3,r_3} \psi_{r_1,f} \phi_{r_2,f} \omega_{r_3,f}, \tag{1.77}$$

$$\text{with } F \geq \max(R_1, R_2, R_3).$$

The structure of the constraint matrices are defined by the two following assumptions:

A.1 The columns of $\boldsymbol{\Psi}$ (resp. $\boldsymbol{\Phi}$ and $\boldsymbol{\Omega}$) are canonical vectors belonging to the following canonical bases, respectively:

$$\{\mathbf{e}_1^{(R_1)}, \ldots, \mathbf{e}_F^{(R_1)}\} \in \mathbb{R}^{R_1}, \quad \{\mathbf{e}_1^{(R_2)}, \ldots, \mathbf{e}_F^{(R_2)}\} \in \mathbb{R}^{R_2}, \\ \{\mathbf{e}_1^{(R_3)}, \ldots, \mathbf{e}_F^{(R_3)}\} \in \mathbb{R}^{R_3}. \tag{1.78}$$

A.2 $\boldsymbol{\Psi}$, $\boldsymbol{\Phi}$ and $\boldsymbol{\Omega}$ are full-rank matrices.

Based on these assumptions, the constraint matrices satisfy the following properties:

$$\sum_{r_1=1}^{R_1} D_{r_1}(\boldsymbol{\Psi}) = \sum_{r_2=1}^{R_2} D_{r_2}(\boldsymbol{\Phi}) = \sum_{r_3=1}^{R_3} D_{r_3}(\boldsymbol{\Omega}) = \mathbf{I}_F, \tag{1.79}$$

$$\sum_{f=1}^{F} \psi_{r_1,f}\psi_{r_1',f} = \begin{cases} n_{r_1}^{(a)}, & r_1 = r_1' \\ 0, & r_1 \neq r_1' \end{cases}, \quad \sum_{f=1}^{F} \phi_{r_2,f}\phi_{r_2',f} = \begin{cases} n_{r_2}^{(b)}, & r_2 = r_2' \\ 0, & r_2 \neq r_2' \end{cases}, \\ \sum_{f=1}^{F} \omega_{r_3,f}\omega_{r_3',f} = \begin{cases} n_{r_3}^{(c)}, & r_3 = r_3' \\ 0, & r_3 \neq r_3' \end{cases}, \tag{1.80}$$

where $n_{r_1}^{(a)} \in [1, F - R_1]$ denotes the number of combinations involving the r_1-th column of $\mathbf{A}^{(1)}$ in (1.77), i.e., the number of times that the r_1-th column of $\mathbf{A}^{(1)}$ is reused for composing the tensor $\mathcal{X}$. Similarly, $n_{r_2}^{(b)} \in [1, F - R_2]$ and $n_{r_3}^{(c)} \in [1, F - R_3]$ represent the number of combinations involving the r_2-th column of $\mathbf{A}^{(2)}$ and the r_3-th column of $\mathbf{A}^{(3)}$, respectively. In matrix form, (1.80) yields:

$$\boldsymbol{\Psi}\boldsymbol{\Psi}^T = \mathbf{D}_1, \quad \boldsymbol{\Phi}\boldsymbol{\Phi}^T = \mathbf{D}_2, \quad \boldsymbol{\Omega}\boldsymbol{\Omega}^T = \mathbf{D}_3, \tag{1.81}$$

where $\mathbf{D}_1 = \text{diag}(n_1^{(a)}, \ldots, n_{R_1}^{(a)})$, $\mathbf{D}_2 = \text{diag}(n_1^{(b)}, \ldots, n_{R_2}^{(b)})$, and $\mathbf{D}_3 =$

$\text{diag}(n_1^{(c)}, \ldots, n_{R_3}^{(c)})$. We also have:

$$\sum_{r_1,r_2} \left(\mathbf{\Psi}\mathbf{\Phi}^T\right)_{r_1,r_2} = \sum_{r_2,r_3} \left(\mathbf{\Phi}\mathbf{\Omega}^T\right)_{r_2,r_3} = \sum_{r_3,r_1} \left(\mathbf{\Omega}\mathbf{\Psi}^T\right)_{r_3,r_1} = F. \tag{1.82}$$

This property can be demonstrated by noting that:

$$\sum_{r_1,r_2} \left(\mathbf{\Psi}\mathbf{\Phi}^T\right)_{r_1,r_2} = \sum_{r_1,r_2,f} \psi_{r_1,f}\phi_{r_2,f}.$$

For any $f \in [1, F]$, there is one and only one pair (r_1, r_2) such as $\psi_{r_1,f}\phi_{r_2,f} = 1$, which implies $\sum_{r_1,r_2} \left(\mathbf{\Psi}\mathbf{\Phi}^T\right)_{r_1,r_2} = F$. Reasoning similarly for $\mathbf{\Phi}\mathbf{\Omega}^T$ and $\mathbf{\Omega}\mathbf{\Psi}^T$, we obtain (1.82).

The CONFAC decomposition can be stated in a different manner, which sheds light on a different way of interpreting its constrained structure. By exchanging summations in (1.77), we obtain:

$$x_{i_1,i_2,i_3} = \sum_{r_1=1}^{R_1} \sum_{r_2=1}^{R_2} \sum_{r_3=1}^{R_3} a_{i_1,r_1} b_{i_2,r_2} c_{i_3,r_3} g_{r_1,r_2,r_3}(\mathbf{\Psi}, \mathbf{\Phi}, \mathbf{\Omega}), \tag{1.83}$$

where

$$g_{r_1,r_2,r_3}(\mathbf{\Psi}, \mathbf{\Phi}, \mathbf{\Omega}) = \sum_{f=1}^{F} \psi_{r_1,f}\phi_{r_2,f}\omega_{r_3,f} \tag{1.84}$$

is an element of a tensor $\mathcal{G}(\mathbf{\Psi}, \mathbf{\Phi}, \mathbf{\Omega}) \in \mathbb{C}^{R_1 \times R_2 \times R_3}$ that follows an F-factor PARAFAC decomposition in terms of $\mathbf{\Psi}$, $\mathbf{\Phi}$ and $\mathbf{\Omega}$. We call $\mathcal{G}(\mathbf{\Psi}, \mathbf{\Phi}, \mathbf{\Omega}) \in \mathbb{C}^{R_1 \times R_2 \times R_3}$, or simply $\mathcal{G}$, the *constrained core tensor* of the CONFAC decomposition.

Using the mode-n product notation, the CONFAC decomposition can be written as:

$$\mathcal{X} = \mathcal{G}(\mathbf{\Psi}, \mathbf{\Phi}, \mathbf{\Omega}) \bullet_1 \mathbf{A} \bullet_2 \mathbf{B} \bullet_3 \mathbf{C}.$$

Alternatively, we can use the outer product notation to write the CONFAC decomposition in the following (PARAFAC-like) manner:

$$\mathcal{X} = \sum_{f=1}^{F} \left(\mathbf{A}\mathbf{\Psi}\right)_{\cdot f} \circ \left(\mathbf{B}\mathbf{\Phi}\right)_{\cdot f} \circ \left(\mathbf{C}\mathbf{\Omega}\right)_{\cdot f}.$$

Relation with the Tucker-3 decomposition: It is worth noting that (1.83) takes the form of a constrained Tucker-3 decomposition [8, 87, 144] with the par-

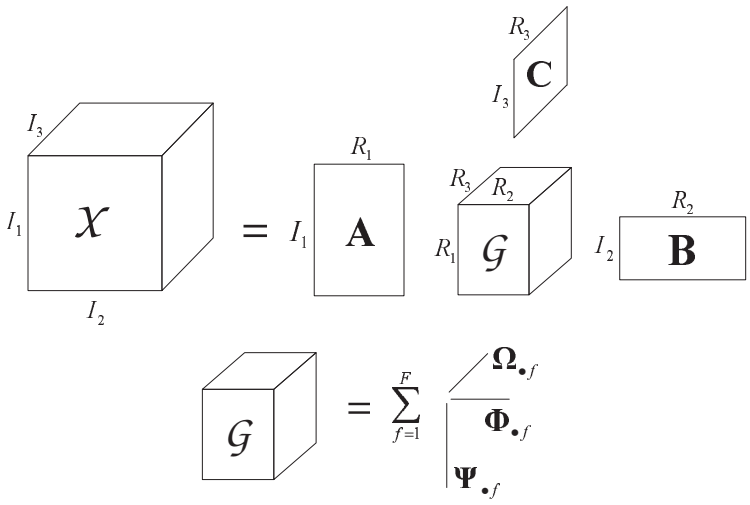

Figure 1.10: Visualization of the CONFAC decomposition of a third-order tensor.

ticular characteristic of having a PARAFAC-decomposed core tensor. The main difference between CONFAC and Tucker-3 decompositions is in the following aspect. In the Tucker-3 decomposition, all the $R_1R_2R_3$ possible factor combinations exist for the composition of the tensor $\mathcal{X}$, where each entry of the Tucker-3 core tensor $\mathcal{G}$ defines the "strength" of each factor combination. Differently, in the CONFAC decomposition, only F *effective* combinations take place for the composition of the tensor $\mathcal{X}$. In this case, the F-factor PARAFAC decomposition of the constrained core tensor $\mathcal{G}$ reveals the pattern of combinations involving the columns of the factor matrices $\mathbf{A}, \mathbf{B}$ and $\mathbf{C}$. Figure 1.10 provides an illustration of the CONFAC decomposition.

Relation with the PARAFAC decomposition: Let us consider the CONFAC decomposition in (1.77) with $R_i = F$, $i = 1, 2, 3$ and $\mathbf{\Psi} = \mathbf{\Phi} = \mathbf{\Omega} = \mathbf{I}_F$. In this case, the CONFAC decomposition coincides with the F-factor PARAFAC decomposition [73]:

$$x_{i_1,i_2,i_3} = \sum_{f=1}^{F} a_{i_1,f} b_{i_2,f} c_{i_3,f}. \tag{1.85}$$

Matrix representations: The CONFAC decomposition can be represented in matrix forms. Two different matrix representations of the tensor $\mathcal{X} \in \mathbb{C}^{I_1 \times I_2 \times I_3}$ are possible, namely the *slice* and *unfolded* representations. Their construction is

similar to that of the standard PARAFAC decomposition [73, 131]. By analogy with (1.25), these matrix-slices can be expressed as a function of $\{\mathbf{A}, \mathbf{B}, \mathbf{C}\}$ and $\{\mathbf{\Psi}, \mathbf{\Phi}, \mathbf{\Omega}\}$, by the following set of equations:

$$\begin{aligned}
\mathbf{X}_{i_1\cdot\cdot} &= \mathbf{B\Phi} D_{i_1}\big(\mathbf{A\Psi}\big)\big(\mathbf{C\Omega}\big)^T \in \mathbb{C}^{I_2\times I_3} \\
\mathbf{X}_{\cdot i_2\cdot} &= \mathbf{C\Omega} D_{i_2}\big(\mathbf{B\Phi}\big)\big(\mathbf{A\Psi}\big)^T \in \mathbb{C}^{I_3\times I_1} \\
\mathbf{X}_{\cdot\cdot i_3} &= \mathbf{A\Psi} D_{i_3}\big(\mathbf{C\Omega}\big)\big(\mathbf{B\Phi}\big)^T, \in \mathbb{C}^{I_1\times I_2}
\end{aligned} \tag{1.86}$$

The full information contained in the tensor $\mathcal{X} \in \mathbb{C}^{I_1\times I_2\times I_3}$ can be organized in three *unfolded matrices* $\mathbf{X}_1 \in \mathbb{C}^{I_3 I_1\times I_2}$, $\mathbf{X}_2 \in \mathbb{C}^{I_1 I_2\times I_3}$, and $\mathbf{X}_3 \in \mathbb{C}^{I_2 I_3\times I_1}$, constructed from the sets of matrix-slices, according to (1.15).

$\mathbf{X}_1$, $\mathbf{X}_2$, and $\mathbf{X}_3$ can be expressed by the following set of equations:

$$\begin{aligned}
\mathbf{X}_1 &= \big(\mathbf{C\Omega} \diamond \mathbf{A\Psi}\big)\big(\mathbf{B\Phi}\big)^T, \\
\mathbf{X}_2 &= \big(\mathbf{A\Psi} \diamond \mathbf{B\Phi}\big)\big(\mathbf{C\Omega}\big)^T, \\
\mathbf{X}_3 &= \big(\mathbf{B\Phi} \diamond \mathbf{C\Omega}\big)\big(\mathbf{A\Psi}\big)^T.
\end{aligned} \tag{1.87}$$

Demonstration: The demonstration of (1.86) and (1.87) is simple. It is similar to the one presented in [62] for the PARAFAC and Tucker decompositions. The CONFAC decomposition (1.77) can be rewritten as:

$$\begin{aligned}
x_{i_1,i_2,i_3} &= \sum_{f=1}^{F}\left(\sum_{r_2=1}^{R_2} b_{i_2,r_2}\phi_{r_2,f}\right)\left(\sum_{r_3=1}^{R_3} c_{i_3,r_3}\omega_{r_3,f}\right) \\
&\qquad \cdot\left(\sum_{r_1=1}^{R_1} a_{i_1,r_1}\psi_{r_1,f}\right) \\
&= \sum_{f=1}^{F}\big(\mathbf{B\Phi}\big)_{i_2,f}\big(\mathbf{C\Omega}\big)_{i_3,f}\big(\mathbf{A\Psi}\big)_{i_1,f},
\end{aligned} \tag{1.88}$$

which means that:

$$\begin{aligned}
\mathbf{X}_{\cdot\cdot i_3} &= \begin{bmatrix} x_{1,1,i_3} & \cdots & x_{1,I_2,i_3} \\ \vdots & & \vdots \\ x_{I_1,1,i_3} & \cdots & x_{I_1,I_2,i_3} \end{bmatrix} \\
&= \big(\mathbf{A\Psi}\big) D_{i_3}\big(\mathbf{C\Omega}\big)\big(\mathbf{B\Phi}\big)^T
\end{aligned}$$

and

$$\mathbf{X}_1 = \begin{bmatrix} \mathbf{X}_{..1} \\ \vdots \\ \mathbf{X}_{..I_3} \end{bmatrix} = \begin{bmatrix} \mathbf{A}\boldsymbol{\Psi} D_1\big(\mathbf{C}\boldsymbol{\Omega}\big) \\ \vdots \\ \mathbf{A}\boldsymbol{\Psi} D_{I_3}\big(\mathbf{C}\boldsymbol{\Omega}\big) \end{bmatrix} \big(\mathbf{B}\boldsymbol{\Phi}\big)^T, \\ = \big(\mathbf{C}\boldsymbol{\Omega} \diamond \mathbf{A}\boldsymbol{\Psi}\big)\big(\mathbf{B}\boldsymbol{\Phi}\big)^T. \quad (1.89)$$

The factorization of $\mathbf{X}_2$ and $\mathbf{X}_3$ can be demonstrated in a similar way.

Relation with the PARALIND model: By comparing (1.88) with the standard PARAFAC decomposition (1.85), we remark that the CONFAC decomposition can be viewed as an F-factor PARAFAC decomposition with equivalent (rank-deficient) matrices $\overline{\mathbf{A}} = \mathbf{A}\boldsymbol{\Psi} \in \mathbb{C}^{I_1 \times F}$, $\overline{\mathbf{B}} = \mathbf{B}\boldsymbol{\Phi} \in \mathbb{C}^{I_2 \times F}$, $\overline{\mathbf{C}} = \mathbf{C}\boldsymbol{\Omega} \in \mathbb{C}^{I_3 \times F}$. The rank-deficient structure due to the repetition of some columns of $\mathbf{A}$, $\mathbf{B}$ and $\mathbf{C}$, is controlled by the constraint matrices $\boldsymbol{\Psi}$, $\boldsymbol{\Phi}$ and $\boldsymbol{\Omega}$, respectively. A rank deficient tensor model using constraint matrices is proposed in [10]. This tensor model, which is called PARALIND, makes use of two constraint matrices to model interaction patterns between columns of different factor matrices. In the PARALIND model, the number of factor combinations/interactions is equal to the number of columns of the factor matrix that is not rank-deficient. The PARALIND model can be obtained from the CONFAC one by making $F = I_3$ and $\boldsymbol{\Omega} = \mathbf{I}_{I_3}$. Therefore, the CONFAC tensor model can be viewed as a generalization of the PARALIND one.

Interpretation as a constrained Tucker-3 decomposition: As previously mentioned, the CONFAC decomposition can be interpreted as a constrained Tucker-3 decomposition with PARAFAC-decomposed core tensor. We can also rewrite (1.87) as a function of the constrained core tensor $\mathcal{G}(\boldsymbol{\Psi}, \boldsymbol{\Phi}, \boldsymbol{\Omega})$. Let us define $\mathbf{G}_{r_1 \cdot \cdot} \in \mathbb{C}^{R_2 \times R_3}$, $\mathbf{G}_{\cdot r_2 \cdot} \in \mathbb{C}^{R_3 \times R_1}$ and $\mathbf{G}_{\cdot \cdot r_3} \in \mathbb{C}^{R_1 \times R_2}$ obtained by slicing the constrained core tensor along its first, second and third dimensions, respectively. In order to factorize the unfolded matrices $\mathbf{X}_{i=1,2,3}$ as a function of the constrained core tensor $\mathcal{G} \in \mathbb{C}^{R_1 \times R_2 \times R_3}$, we apply the property (1.57) to obtain the following

expressions:

$$\begin{aligned}
\mathbf{X}_1 &= \big(\mathbf{C} \otimes \mathbf{A}\big)\big(\mathbf{\Omega} \diamond \mathbf{\Psi}\big)\mathbf{\Phi}^T\mathbf{B}^T \\
&= \big(\mathbf{C} \otimes \mathbf{A}\big)\mathbf{G}_1\mathbf{B}^T, \\
\mathbf{X}_2 &= \big(\mathbf{A} \otimes \mathbf{B}\big)\big(\mathbf{\Psi} \diamond \mathbf{\Phi}\big)\mathbf{\Omega}^T\mathbf{C}^T \\
&= \big(\mathbf{A} \otimes \mathbf{B}\big)\mathbf{G}_2\mathbf{C}^T, \\
\mathbf{X}_3 &= \big(\mathbf{B} \otimes \mathbf{C}\big)\big(\mathbf{\Phi} \diamond \mathbf{\Omega}\big)\mathbf{\Psi}^T\mathbf{A}^T \\
&= \big(\mathbf{B} \otimes \mathbf{C}\big)\mathbf{G}_3\mathbf{A}^T,
\end{aligned} \tag{1.90}$$

where

$$\begin{aligned}
\mathbf{G}_1 &= \big(\mathbf{\Omega} \diamond \mathbf{\Psi}\big)\mathbf{\Phi}^T \ (R_3R_1 \times R_2), \\
\mathbf{G}_2 &= \big(\mathbf{\Psi} \diamond \mathbf{\Phi}\big)\mathbf{\Omega}^T \ (R_1R_2 \times R_3), \\
\mathbf{G}_3 &= \big(\mathbf{\Phi} \diamond \mathbf{\Omega}\big)\mathbf{\Psi}^T \ (R_2R_3 \times R_1),
\end{aligned} \tag{1.91}$$

are the three unfolded representations of the constrained core tensor $\mathcal{G}$, with

$$\begin{aligned}
[\mathbf{G}_1]_{(r_3-1)R_1+r_1,r_2} &= [\mathbf{G}_2]_{(r_1-1)R_2+r_2,r_3} \\
&= [\mathbf{G}_3]_{(r_2-1)R_3+r_3,r_1} = g_{r_1,r_2,r_3}.
\end{aligned}$$

Using the definition of the Khatri-Rao product, we have:

$$\mathbf{G}_1 = \begin{bmatrix} \mathbf{\Psi}D_1(\mathbf{\Omega}) \\ \vdots \\ \mathbf{\Psi}D_{R_3}(\mathbf{\Omega}) \end{bmatrix} \mathbf{\Phi}^T = \begin{bmatrix} \mathbf{G}_{\cdot\cdot 1} \\ \vdots \\ \mathbf{G}_{\cdot\cdot R_3} \end{bmatrix}, \tag{1.92}$$

where

$$\mathbf{G}_{\cdot\cdot r_3} = \mathbf{\Psi}D_{r_3}(\mathbf{\Omega})\mathbf{\Phi}^T \in \mathbb{C}^{R_1 \times R_2}. \tag{1.93}$$

In the same way, we get:

$$\begin{aligned}
\mathbf{G}_{r_1\cdot\cdot} &= \mathbf{\Phi}D_{r_1}(\mathbf{\Psi})\mathbf{\Omega}^T \in \mathbb{C}^{R_2 \times R_3}, \\
\mathbf{G}_{\cdot r_2\cdot} &= \mathbf{\Omega}D_{r_2}(\mathbf{\Phi})\mathbf{\Psi}^T \in \mathbb{C}^{R_3 \times R_1}.
\end{aligned} \tag{1.94}$$

Definition 1.11 (interaction matrices) *The* interaction matrices *of the CONFAC decomposition (1.77) characterize the interaction pattern involving the factors of*

different pairs of modes. They are defined by:

$$\begin{aligned}
\mathbf{G}^{(1,2)} &= \sum_{r_3=1}^{R_3} \mathbf{G}_{\cdot\cdot r_3} = \mathbf{\Psi}\mathbf{\Phi}^T\,(R_1 \times R_2), \\
\mathbf{G}^{(2,3)} &= \sum_{r_1=1}^{R_1} \mathbf{G}_{r_1\cdot\cdot} = \mathbf{\Phi}\mathbf{\Omega}^T\,(R_2 \times R_3), \\
\mathbf{G}^{(3,1)} &= \sum_{r_2=1}^{R_2} \mathbf{G}_{\cdot r_2 \cdot} = \mathbf{\Omega}\mathbf{\Psi}^T\,(R_3 \times R_1),
\end{aligned} \tag{1.95}$$

where we have used property (1.79).

Due to the canonical structure of the constraint matrices satisfying **A.1**-**A.2**, the three interaction matrices satisfy the following relation:

$$\sum_{r_1,r_2} g^{(1,2)}_{r_1,r_2} = \sum_{r_2,r_3} g^{(2,3)}_{r_2,r_3} = \sum_{r_3,r_1} g^{(3,1)}_{r_3,r_1} = F, \tag{1.96}$$

where $g^{(1,2)}_{r_1,r_2}$, $g^{(2,3)}_{r_2,r_3}$ and $g^{(3,1)}_{r_3,r_1}$ are the typical elements of $\mathbf{G}^{(1,2)}$, $\mathbf{G}^{(2,3)}$ and $\mathbf{G}^{(3,1)}$, respectively. We can distinguish the two following situations:

- $g^{(1,2)}_{r_1,r_2} = 0$ means that there is no interaction between the r_1-th column of $\mathbf{A}$ and the r_2-th column of $\mathbf{B}$;

- $g^{(1,2)}_{r_1,r_2} = \gamma_{1,2} > 0$ means that there are $\gamma_{1,2}$ interactions between the r_1-th column of $\mathbf{A}$ and the r_2-th column of $\mathbf{B}$.

The same is valid for $g^{(2,3)}_{r_2,r_3}$ (w.r.t $\mathbf{B}$ and $\mathbf{C}$) and $g^{(3,1)}_{r_3,r_1}$ (w.r.t $\mathbf{C}$ and $\mathbf{A}$).

Example 1.2: Let us consider the CONFAC decomposition of a third-order tensor with $F = 4$, $R_1 = R_2 = 2$, $R_3 = 3$ characterized by the following constraint matrices:

$$\mathbf{\Psi} = \mathbf{\Phi} = \begin{bmatrix} 1 & 1 & 0 & 0 \\ 0 & 0 & 1 & 1 \end{bmatrix}, \quad \mathbf{\Omega} = \begin{bmatrix} 1 & 0 & 1 & 0 \\ 0 & 1 & 0 & 0 \\ 0 & 0 & 0 & 1 \end{bmatrix}. \tag{1.97}$$

From (1.95) we have:

$$\mathbf{G}^{(1,2)} = \begin{bmatrix} 2 & 0 \\ 0 & 2 \end{bmatrix}, \quad \mathbf{G}^{(2,3)} = \begin{bmatrix} 1 & 1 & 0 \\ 1 & 0 & 1 \end{bmatrix},$$
$$\mathbf{G}^{(3,1)} = \begin{bmatrix} 1 & 1 \\ 1 & 0 \\ 0 & 1 \end{bmatrix}.$$

$\mathbf{G}^{(1,2)}$ indicates that $\mathbf{A}_{\cdot 1}$ and $\mathbf{B}_{\cdot 1}$ interact twice. The same is valid for $\mathbf{A}_{\cdot 2}$ and $\mathbf{B}_{\cdot 2}$. From $\mathbf{G}^{(2,3)}$, we can see that $\mathbf{B}_{\cdot 1}$ interacts with $\{\mathbf{C}_{\cdot 1}, \mathbf{C}_{\cdot 2}\}$ while $\mathbf{B}_{\cdot 2}$ interacts with $\{\mathbf{C}_{\cdot 1}, \mathbf{C}_{\cdot 3}\}$. According to $\mathbf{G}^{(3,1)}$, there is interaction between $\mathbf{C}_{\cdot 1}$ and $\{\mathbf{A}_{\cdot 1}, \mathbf{A}_{\cdot 2}\}$ while $\mathbf{C}_{\cdot 2}$ interacts with $\mathbf{A}_{\cdot 1}$, and $\mathbf{C}_{\cdot 3}$ interacts with $\mathbf{A}_{\cdot 2}$. Summing the nonzero elements of $\mathbf{G}^{(1,2)}$, $\mathbf{G}^{(2,3)}$ and $\mathbf{G}^{(3,1)}$ yields the number F of factor combinations.

Example 1.3: Now, consider $F = 4$, $R_1 = R_2 = 3$, $R_3 = 2$, with constraint matrices having the following structure:

$$\mathbf{\Psi} = \begin{bmatrix} 1 & 1 & 0 & 0 \\ 0 & 0 & 0 & 1 \\ 0 & 0 & 1 & 0 \end{bmatrix}, \quad \mathbf{\Phi} = \begin{bmatrix} 0 & 0 & 1 & 0 \\ 1 & 1 & 0 & 0 \\ 0 & 0 & 0 & 1 \end{bmatrix},$$
$$\mathbf{\Omega} = \begin{bmatrix} 1 & 1 & 1 & 0 \\ 0 & 0 & 0 & 1 \end{bmatrix}, \tag{1.98}$$

yielding the following interaction matrices:

$$\mathbf{G}^{(1,2)} = \begin{bmatrix} 0 & 2 & 0 \\ 0 & 0 & 1 \\ 1 & 0 & 0 \end{bmatrix}, \quad \mathbf{G}^{(2,3)} = \begin{bmatrix} 1 & 0 \\ 2 & 0 \\ 0 & 1 \end{bmatrix},$$
$$\mathbf{G}^{(3,1)} = \begin{bmatrix} 2 & 0 & 1 \\ 0 & 1 & 0 \end{bmatrix}.$$

According to $\mathbf{G}^{(1,2)}$, each column of $\mathbf{A}$ interacts with a different column of $\mathbf{B}$. In particular, $\mathbf{A}_{\cdot 1}$ interacts twice with $\mathbf{B}_{\cdot 2}$. We also have $\mathbf{C}_{\cdot 1}$ interacting once with $\mathbf{B}_{\cdot 1}$ and twice with $\mathbf{B}_{\cdot 2}$ as indicated by $\mathbf{G}^{(2,3)}$. On the other hand, $\mathbf{C}_{\cdot 1}$ interacts twice with $\mathbf{A}_{\cdot 1}$ and once with $\mathbf{A}_{\cdot 3}$.

1.4.1 Special CONFAC decompositions

Recall that the CONFAC decomposition allows arbitrary interaction patterns involving the factors of different modes. We have shown that the factors (i.e. the columns of the matrix) associated with a given mode can be recombined, or reused, more than once in the composition of the full tensor. However, when there is no recombination of factors along a given mode, simpler representations of the CONFAC decomposition are possible. Three special writings of this decomposition exist depending on which mode is free of interactions. When there is no interaction in the first mode, we have $\mathbf{\Psi} = \mathbf{I}_F$. Likewise, when no interaction takes place within the second and third modes, we have $\mathbf{\Phi} = \mathbf{I}_F$ and $\mathbf{\Omega} = \mathbf{I}_F$, respectively. In each case, we can simplify (1.77) as shown below:

1. *Type-1 CONFAC (no interactions in the first mode)*:

$$x_{i_1,i_2,i_3} = \sum_{f=1}^{F} \sum_{r_2=1}^{R_2} \sum_{r_3=1}^{R_3} a_{i_1,r_1} b_{i_2,r_2} c_{i_3,r_3} \phi_{r_2,f} \omega_{r_3,f}, \tag{1.99}$$

$$\text{with } F \geq \max(R_2, R_3).$$

2. *Type-2 CONFAC (no interactions in the second mode)*:

$$x_{i_1,i_2,i_3} = \sum_{f=1}^{F} \sum_{r_1=1}^{R_1} \sum_{r_3=1}^{R_3} a_{i_1,r_1} b_{i_2,r_2} c_{i_3,r_3} \psi_{r_1,f} \omega_{r_3,f}, \tag{1.100}$$

$$\text{with } F \geq \max(R_1, R_3).$$

3. *Type-3 CONFAC (no interactions in the third mode)*:

$$x_{i_1,i_2,i_3} = \sum_{f=1}^{F} \sum_{r_1=1}^{R_1} \sum_{r_2=1}^{R_2} a_{i_1,r_1} b_{i_2,r_2} c_{i_3,r_3} \psi_{r_1,f} \phi_{r_2,f}, \tag{1.101}$$

$$\text{with } F \geq \max(R_1, R_2).$$

In Chapter 4, the type-3 CONFAC decomposition will be exploited for designing blind multiple-antenna CDMA schemes. This application also appears in [37, 36]. The works [32, 33] can be viewed as a particular case of type-3 CONFAC, where the two corresponding constraint matrices have a fixed structure.

1.4.2 N-th order generalization

The CONFAC decomposition (1.77) can be straightforwardly generalized to tensors of any order higher than three. Let us consider an N-th order tensor $\mathcal{X} \in \mathbb{C}^{I_1 \times \cdots \times I_N}$, a set of N factor matrices $\{\mathbf{A}^{(n)}\} \in \mathbb{C}^{I_n \times R_n}$, and a set of N constraint matrices $\{\mathbf{\Psi}^{(n)}\} \in \mathbb{C}^{R_n \times F}$, $n = 1, \ldots, N$. The CONFAC decomposition of $\mathcal{X} \in \mathbb{C}^{I_1 \times \cdots \times I_N}$ with F factor combinations is given in scalar form by the following expression:

$$x_{i_1,\ldots,i_N} = \sum_{r_1=1}^{R_1} \cdots \sum_{r_N=1}^{R_N} \left(\prod_{n=1}^{N} a_{i_n,r_n}^{(n)} \right) g_{r_1,\ldots,r_N}(\mathbf{\Psi}^{(1)}, \ldots, \mathbf{\Psi}^{(N)}),$$

$$g_{r_1,\ldots,r_N}(\mathbf{\Psi}^{(1)}, \ldots, \mathbf{\Psi}^{(N)}) = \sum_{f=1}^{F} \prod_{n=1}^{N} \psi_{r_n,f}^{(n)},$$

where $g_{r_1,\ldots,r_N}(\mathbf{\Psi}^{(1)}, \ldots, \mathbf{\Psi}^{(N)})$ is the N-th order constrained core tensor.

1.4.3 Uniqueness results

The uniqueness of the factor matrices $\mathbf{A}$, $\mathbf{B}$, $\mathbf{C}$ of the CONFAC decomposition (up to permutation and scaling) depends on the particular structure of the constraint matrices $\mathbf{\Psi}$, $\mathbf{\Phi}$, $\mathbf{\Omega}$. Specifically, the degrees of freedom introduced in the decomposition by the three constraint matrices can induce a transformational ambiguity over (at least a subset of) the columns of the factor matrices.

Theorem 1.4 : *Let us consider the CONFAC decomposition (1.77) of a third-order tensor with F factor combinations. Suppose that $\mathbf{A}, \mathbf{B}$ and $\mathbf{C}$ are full column-rank, and that the joint structure of $\{\mathbf{\Psi}, \mathbf{\Phi}, \mathbf{\Omega}\}$ is such that $\mathbf{G}_1$ ($R_3R_1 \times R_2$), $\mathbf{G}_2$ ($R_1R_2 \times R_3$) and $\mathbf{G}_3$ ($R_2R_3 \times R_1$) are also full column-rank, then the decomposition is identifiable from equations (1.90).*

Identifiability of $\mathbf{A}, \mathbf{B}$ and $\mathbf{C}$ means that they are unique up to a multiplication by a nonsingular matrix, i.e. any alternative set $\{\tilde{\mathbf{A}}, \tilde{\mathbf{B}}, \tilde{\mathbf{C}}\}$ yielding the same tensor $\mathcal{X}$ is linked to the true set $\{\mathbf{A}, \mathbf{B}, \mathbf{C}\}$ by:

$$\tilde{\mathbf{A}} = \mathbf{A}\mathbf{T}^{(1)}, \quad \tilde{\mathbf{B}} = \mathbf{B}\mathbf{T}^{(2)}, \quad \tilde{\mathbf{C}} = \mathbf{C}\mathbf{T}^{(3)},$$

with $\mathbf{T}^{(1)} \in \mathbb{C}^{R_1 \times R_1}$, $\mathbf{T}^{(2)} \in \mathbb{C}^{R_2 \times R_2}$ and $\mathbf{T}^{(3)} \in \mathbb{C}^{R_3 \times R_3}$ satisfying the following equality:

$$\big((\mathbf{T}^{(1)})^{-1}\mathbf{\Psi} \diamond (\mathbf{T}^{(2)})^{-1}\mathbf{\Phi}\big)\big((\mathbf{T}^{(3)})^{-1}\mathbf{\Omega}\big)^T = \big(\mathbf{\Psi} \diamond \mathbf{\Phi}\big)\mathbf{\Omega}^T \tag{1.102}$$

Proof: Recall the following properties. For arbitrary matrices $\mathbf{A} \in \mathbb{C}^{I\times J}$, $\mathbf{B} \in \mathbb{C}^{K\times I}$ and $\mathbf{C} \in \mathbb{C}^{M\times J}$, with $\mathbf{B}$ full column-rank, we have:

$$\text{rank}(\mathbf{A} \otimes \mathbf{C}) = \text{rank}(\mathbf{A})\text{rank}(\mathbf{C}), \tag{1.103}$$
$$\text{rank}(\mathbf{BA}) = \text{rank}(\mathbf{A}). \tag{1.104}$$

Let us define the following quantities:

$$\begin{aligned}\mathbf{Z}_1 &= \big(\mathbf{C} \otimes \mathbf{A}\big)\mathbf{G}_1 \ \in \mathbb{C}^{I_3 I_1 \times R_2},\\ \mathbf{Z}_2 &= \big(\mathbf{A} \otimes \mathbf{B}\big)\mathbf{G}_2 \ \in \mathbb{C}^{I_1 I_2 \times R_3}\\ \mathbf{Z}_3 &= \big(\mathbf{B} \otimes \mathbf{C}\big)\mathbf{G}_3 \ \in \mathbb{C}^{I_2 I_3 \times R_1}.\end{aligned}$$

Identifiability of $\mathbf{A}$, $\mathbf{B}$ and $\mathbf{C}$ from (1.90) requires that $\mathbf{Z}_1$, $\mathbf{Z}_2$ and $\mathbf{Z}_3$ are full column-rank to be left-invertible. Since $\mathbf{A}$, $\mathbf{B}$ and $\mathbf{C}$ are full column-rank, using (1.103) implies that $\mathbf{C} \otimes \mathbf{A}$, $\mathbf{A} \otimes \mathbf{B}$, and $\mathbf{B} \otimes \mathbf{C}$ are also full column-rank. From (1.104), we can conclude that $\text{rank}(\mathbf{Z}_1) = \text{rank}(\mathbf{G}_1) = R_1$ since $\mathbf{G}_1$ is assumed to be full column-rank, and therefore $\mathbf{Z}_1$ is itself full column-rank. The reasoning is similar for $\mathbf{Z}_2$ and $\mathbf{Z}_3$. ■

Definition 1.12 (admissible transformation matrices): *The transformation matrices $\mathbf{T}^{(1)}$, $\mathbf{T}^{(2)}$ and $\mathbf{T}^{(3)}$ are called* admissible *i.i.f. they preserve the constrained structure of the decomposition satisfying (1.102).*

Definition 1.13 (essential uniqueness) [90]: *Essential uniqueness means that any alternative set $\{\tilde{\mathbf{A}}, \tilde{\mathbf{B}}, \tilde{\mathbf{C}}\}$ giving rise to the same tensor $\mathcal{X}$ is equal to the set $\{\mathbf{A}, \mathbf{B}, \mathbf{C}\}$ up to permutation and scaling of their columns, implying admissible transformation matrices of the form:*

$$\mathbf{T}^{(1)} = \mathbf{\Delta}_1\mathbf{\Pi}_1, \quad \mathbf{T}^{(2)} = \mathbf{\Delta}_2\mathbf{\Pi}_2, \quad \mathbf{T}^{(3)} = \mathbf{\Delta}_3\mathbf{\Pi}_3, \tag{1.105}$$

where $\mathbf{\Delta}_{i=1,2,3}$ are diagonal matrices satisfying the relation $\mathbf{\Delta}_1\mathbf{\Delta}_2\mathbf{\Delta}_3 = \mathbf{I}$, and $\mathbf{\Pi}_{i=1,2,3}$ are permutation matrices.

A proof of (1.105) is given in [136] for the standard PARAFAC decomposition, which also applies here.

Partial uniqueness

The CONFAC decomposition is said to be partially unique (or restrictively nonunique), when a subset of the columns belonging to the set $\{\mathbf{A}, \mathbf{B}, \mathbf{C}\}$ are essen-

tially unique while the remaining columns are affected by a linear transformation. Partial uniqueness was first observed in [74], and also investigated in [130] and [145] in the context of the standard PARAFAC decomposition. For the CONFAC decomposition, the partial uniqueness property is linked to the structure of the interaction matrices. It can also be studied from equivalence relations between pairs of constraint matrices. In this section, we present sufficient (but not necessary) conditions for the partial uniqueness of the CONFAC decomposition implying essential uniqueness in one or two modes.

We assume that $\mathbf{A}$, $\mathbf{B}$ and $\mathbf{C}$ do not contain a zero row. Introducing:

$$\tilde{\mathbf{A}} = \mathbf{A}\mathbf{T}^{(1)}, \quad \tilde{\mathbf{B}} = \mathbf{B}\mathbf{T}^{(2)}, \quad \tilde{\mathbf{C}} = \mathbf{C}\mathbf{T}^{(3)}$$

into the slice representations (1.86), we obtain:

$$\begin{aligned} \mathbf{X}_{i_1\cdot\cdot} &= \tilde{\mathbf{B}}\big[(\mathbf{T}^{(2)})^{-1}\overline{\mathbf{G}}_{i_1}^{(2,3)}(\mathbf{T}^{(3)})^{-T}\big]\tilde{\mathbf{C}}^T, \\ \mathbf{X}_{\cdot i_2\cdot} &= \tilde{\mathbf{C}}\big[(\mathbf{T}^{(3)})^{-1}\overline{\mathbf{G}}_{i_2}^{(3,1)}(\mathbf{T}^{(1)})^{-T}\big]\tilde{\mathbf{A}}^T, \\ \mathbf{X}_{\cdot\cdot i_3} &= \tilde{\mathbf{A}}\big[(\mathbf{T}^{(1)})^{-1}\overline{\mathbf{G}}_{i_3}^{(1,2)}(\mathbf{T}^{(2)})^{-T}\big]\tilde{\mathbf{B}}^T, \end{aligned} \tag{1.106}$$

where $\overline{\mathbf{G}}_{i_1}^{(2,3)} = \mathbf{\Phi} D_{i_1}\big(\tilde{\mathbf{A}}(\mathbf{T}^{(1)})^{-1}\mathbf{\Psi}\big)\mathbf{\Omega}^T$, $\overline{\mathbf{G}}_{i_2}^{(3,1)} = \mathbf{\Omega} D_{i_2}\big(\tilde{\mathbf{B}}(\mathbf{T}^{(2)})^{-1}\mathbf{\Phi}\big)\mathbf{\Psi}^T$, and $\overline{\mathbf{G}}_{i_3}^{(1,2)} = \mathbf{\Psi} D_{i_3}\big(\tilde{\mathbf{C}}(\mathbf{T}^{(3)})^{-1}\mathbf{\Omega}\big)\mathbf{\Phi}^T$. Note that $\overline{\mathbf{G}}_{i_1}^{(2,3)}$, $\overline{\mathbf{G}}_{i_2}^{(3,1)}$ and $\overline{\mathbf{G}}_{i_3}^{(1,2)}$ have the same pattern of zeros (up to permutation and scaling) as $\mathbf{G}^{(2,3)}$, $\mathbf{G}^{(3,1)}$ and $\mathbf{G}^{(1,2)}$, respectively. This comes from the assumption that $\mathbf{A}$, $\mathbf{B}$ and $\mathbf{C}$ do not contain a zero row. Therefore, the uniqueness property of $\mathbf{A}$, $\mathbf{B}$ and $\mathbf{C}$ is directly linked to the structure of the interaction matrices. For instance, uniqueness of $\mathbf{A}$ can be checked by searching the *admissible* structures of $\mathbf{T}^{(1)}$ preserving the pattern of zeros of $\mathbf{G}^{(1,2)}$ and $\mathbf{G}^{(3,1)}$. Similarly, uniqueness of $\mathbf{B}$ can be checked by searching the admissible structures of $\mathbf{T}^{(2)}$ preserving the pattern of zeros of $\mathbf{G}^{(2,3)}$ and $\mathbf{G}^{(1,2)}$. Finally, uniqueness of $\mathbf{C}$ can be checked by searching the admissible structures of $\mathbf{T}^{(3)}$ preserving the pattern of zeros of $\mathbf{G}^{(3,1)}$ and $\mathbf{G}^{(2,3)}$.

Theorem 1.5 (partial uniqueness): *Consider the CONFAC decomposition of $\mathcal{X} \in \mathbb{C}^{I_1\times I_2\times I_3}$ as a function of factor matrices $\mathbf{A}$, $\mathbf{B}$ and $\mathbf{C}$, and characterized by interaction matrices $\mathbf{G}^{(1,2)}$, $\mathbf{G}^{(2,3)}$ and $\mathbf{G}^{(3,1)}$. Suppose that the three factor matrices contain no zeros. We have:*

1. If $\text{rank}(\mathbf{G}^{(1,2)}) = \text{rank}(\mathbf{G}^{(3,1)}) = R_1$, then $\mathbf{A}$ is essentially unique;
2. If $\text{rank}(\mathbf{G}^{(2,3)}) = \text{rank}(\mathbf{G}^{(1,2)}) = R_2$, then $\mathbf{B}$ is essentially unique;
3. If $\text{rank}(\mathbf{G}^{(3,1)}) = \text{rank}(\mathbf{G}^{(2,3)}) = R_3$, then $\mathbf{C}$ is essentially unique.

Note that $\text{rank}(\mathbf{G}^{(1,2)}) = \text{rank}(\mathbf{G}^{(3,1)}) = R_1$ only happens when $R_1 \leq R_2$ and $R_1 \leq R_3$, i.e. when $R_1 \leq \min(R_2, R_3)$. Similarly, $\text{rank}(\mathbf{G}^{(2,3)}) = \text{rank}(\mathbf{G}^{(1,2)}) = R_2$ only happens when $R_2 \leq \min(R_1, R_3)$, and $\text{rank}(\mathbf{G}^{(3,1)}) = \text{rank}(\mathbf{G}^{(2,3)}) = R_3$ when $R_3 \leq \min(R_1, R_2)$. For instance, when $R_1 < R_2 < R_3$, only $\mathbf{A}$ is essentially unique, while $\mathbf{B}$ and $\mathbf{C}$ are not guaranteed to be unique since only condition 1 of Theorem 1.5 is satisfied. Nevertheless, partial uniqueness (i.e. essential uniqueness of a subset of columns) of $\mathbf{B}$ and $\mathbf{C}$ is possible.

The degree of partial uniqueness depends on the joint interaction structure of the decomposition. The only case where all the three above conditions are met is the one with $R_1 = R_2 = R_3$, in which the CONFAC decomposition is close to the PARAFAC one. If $\text{rank}(\mathbf{G}^{(1,2)}) < R_1$ and/or $\text{rank}(\mathbf{G}^{(3,1)}) < R_1$, the essential uniqueness of $\mathbf{A}$ is not guaranteed by Theorem 1.5. The same comments are valid for the essential uniqueness of $\mathbf{B}$ and $\mathbf{C}$. The three above conditions are sufficient but not necessary for the essential uniqueness of the factor matrices of the decomposition.

Definition 1.14 (equivalent constraint matrices): *When $R_1 = R_2$ (resp. $R_2 = R_3$ and $R_1 = R_3$), the matrix set $\{\boldsymbol{\Psi}, \boldsymbol{\Phi}\}$ (resp. $\{\boldsymbol{\Phi}, \boldsymbol{\Omega}\}$ and $\{\boldsymbol{\Omega}, \boldsymbol{\Psi}\}$) is said to be equivalent if*

$$\boldsymbol{\Psi} = \boldsymbol{\Pi}_1 \boldsymbol{\Phi}, \quad \Big(\textit{resp. } \boldsymbol{\Phi} = \boldsymbol{\Pi}_2 \boldsymbol{\Omega}, \quad \boldsymbol{\Omega} = \boldsymbol{\Pi}_3 \boldsymbol{\Psi}\Big), \tag{1.107}$$

where $\boldsymbol{\Pi}_{i=1,2,3}$ are arbitrary permutation matrices.

Note that the equivalence of two constraint matrices means that there is *no* interaction between the columns of the associated factor matrices. For instance, when $\boldsymbol{\Psi} = \boldsymbol{\Pi}_1 \boldsymbol{\Phi}$, we have:

$$\mathbf{G}^{(1,2)} = \boldsymbol{\Psi}\boldsymbol{\Phi}^T = \boldsymbol{\Pi}_1 \boldsymbol{\Phi}\boldsymbol{\Phi}^T = \boldsymbol{\Pi}_1 \mathbf{D}_1, \tag{1.108}$$

where $\mathbf{D}_1$ is defined in (1.81). Note that, in this case, $\mathbf{G}^{(1,2)}$ has only one nonzero element in each row and column, which means that there is a one-to-one correspondence between the columns of $\mathbf{A}$ and $\mathbf{B}$, i.e. there is no recombination of the columns of these matrices. In Example 1.2, where $\boldsymbol{\Psi} = \boldsymbol{\Phi}$ are given in (1.97) and $\mathbf{G}^{(1,2)}$ is given in (1.98), no interaction between columns of $\mathbf{A}$ and $\mathbf{B}$ exist. Similarly, when $\boldsymbol{\Phi} = \boldsymbol{\Pi}_2 \boldsymbol{\Omega}$ and $\boldsymbol{\Omega} = \boldsymbol{\Pi}_3 \boldsymbol{\Psi}$, we have:

$$\mathbf{G}^{(2,3)} = \boldsymbol{\Pi}_2 \mathbf{D}_3, \quad \mathbf{G}^{(3,1)} = \boldsymbol{\Pi}_3 \mathbf{D}_1. \tag{1.109}$$

Partial uniqueness corollaries: Based on such a concept of equivalence between constraint matrices, and from (1.107)-(1.109), we can deduce the following corollaries for partial uniqueness:

C.1 When $R_1 = R_2 = R < R_3$ and $\{\mathbf{\Psi}, \mathbf{\Phi}\}$ is an equivalent set, we have:

- $\{\mathbf{A}, \mathbf{B}\}$ essentially unique;

C.2 When $R_2 = R_3 = R < R_1$ and $\{\mathbf{\Phi}, \mathbf{\Omega}\}$ is an equivalent set, we have:

- $\{\mathbf{B}, \mathbf{C}\}$ essentially unique;

C.3 When $R_1 = R_3 = R < R_2$ and $\{\mathbf{\Psi}, \mathbf{\Omega}\}$ is an equivalent set, we have:

- $\{\mathbf{A}, \mathbf{C}\}$ essentially unique.

We can observe that the equivalence between $\mathbf{\Psi}$ and $\mathbf{\Phi}$ implies $\mathbf{G}^{(1,2)} = \mathbf{\Pi}_1\mathbf{D}_1$ (see (1.108)). In Corollary **C.1** the essential uniqueness of $\{\mathbf{A}, \mathbf{B}\}$ comes from the fact that the two first rank conditions of Theorem 1.5 are satisfied, i.e. $\text{rank}(\mathbf{G}^{(1,2)}) = \text{rank}(\mathbf{G}^{(2,3)}) = \text{rank}(\mathbf{G}^{(3,1)}) = R$. The same observation is valid for explaining the essential uniqueness of the matrix pair $\{\mathbf{B}, \mathbf{C}\}$ in **C.2** and $\{\mathbf{A}, \mathbf{C}\}$ in **C.3**.

These corollaries show that the essential uniqueness in one or two modes comes at the expense of a restrictive nonuniqueness in the remaining mode(s). Such a "uniqueness tradeoff" is inherent to the CONFAC decomposition. For an illustrative purpose, we can apply **C.1** to Examples 1.2 and 1.3, for evaluating the partial uniqueness property in each case. In Example 1.2, $\mathbf{A}$ and $\mathbf{B}$ are essentially unique while $\mathbf{C}$ is nonunique. In Example 1.3, $\mathbf{C}$ is essentially unique while $\mathbf{A}$ and $\mathbf{B}$ are partially unique.

1.5 Summary

This chapter has provided some fundamentals of multilinear algebra and tensor decompositions. In the first part of the chapter, we have provided some basic concepts related to the algebra of tensors. Some operations involving tensor objects have been defined. In the second part of this chapter, we have presented several tensor decompositions that are important to the context of this thesis. These decompositions have been formulated in both scalar (multi-indexed) and tensor (outer product or n-mode product) forms. In each case, the factorization of the tensor in slice and unfolded forms have been defined. The uniqueness property

of these decompositions has been discussed, and uniqueness conditions have been presented for these decompositions.

The chapter contains original contributions which are the development of two new tensor decompositions, namely, the block-constrained PARAFAC and the CONFAC decompositions. The block-constrained PARAFAC decomposition mixes some properties of the PARAFAC and Tucker-3 decompositions. At the same time, it falls within the framework of block term decompositions [50, 51]. We have shown that the CONFAC decomposition is more general than the block-constrained PARAFAC one, by allowing arbitrary interactions across all the modes of the decomposed tensor. The partial uniqueness of the CONFAC decomposition has been studied. A sufficient condition for the essential uniqueness in one or two modes has been derived.

The two proposed tensor decompositions will be exploited throughout the thesis in the context of the different applications we will address. For instance, a unified tensor modeling of the received signal in oversampled, DS-CDMA and OFDM systems along with blind multiuser detection/equalization will be presented based on the block-constrained PARAFAC decomposition. This decomposition will also be exploited for modeling multiple-antenna transmissions with block space-time spreading and blind detection. Concerning the CONFAC decomposition, we will show that it is useful for designing finite sets of multiple-antenna CDMA schemes with canonical precoding, where the allocation of multiple spreading codes and data streams to transmit antennas is modeled by means of the constraint matrices of this decomposition.

CHAPTER 2

Tensor Modeling for Wireless Communication Systems with Application to Blind Multiuser Equalization

This chapter presents a new tensor approach for modeling wireless communication systems with a receiver antenna array under the assumption of specular multipath propagation and frequency-selectivity. The proposed tensor model uses a third-order (3D) block-constrained PARAFAC decomposition with factor interactions. It aims at unifying the received signal modeling for (i) Temporally-Oversampled, (ii) Direct-Sequence Code Division Multiple Access (DS-CDMA) and (iii) Orthogonal Frequency Division Multiplexing (OFDM) systems. We show that the model for each particular system can be derived from the proposed model by making appropriate choices in its dimension and/or structure. As an application of the proposed tensor model to blind multiuser separation/equalization, a new receiver algorithm is derived, which combines tensor modeling (for multiuser signal separation) with a subspace method (for user-by-user equalization). Simulation results illustrate the Bit-Error-Rate (BER) performance of the proposed blind receiver.

2.1 Introduction and motivation

Most of existing array signal processing approaches rely on matrix (2D arrays) models for the received signal. In wireless communication systems, array signal processing is generally used at the receiver to mitigate multiuser (co-channel) interference, inter-symbol interference as well as to benefit from spatial diversity available in the wireless channel. Usually considered signal processing dimensions are *space* and *time* dimensions. In space-time matrix models, space dimension usually varies along the rows of the received signal matrix while time dimension varies along the columns. However, the main limitation of working with a matrix model for the received signal is its lack of inherent uniqueness. Regarding the blind recovery of information, blind algorithms generally take special (problem-specific) structural properties of the transmitted signals into account such as orthogonality, finite-alphabet, constant-modulus or cyclostationarity in order to overcome the non-uniqueness of matrix decompositions and successfully perform multiuser signal separation and equalization [114, 141, 150].

Unlike 2D (matrix) models, the use of 3D (tensor) received signal models in array signal processing problems result from the incorporation of a third "axis", also called dimension or mode, in addition to the usually considered *space* and *time* dimensions. For example, when temporal oversampling is used at the antenna array receiver, *oversampling* can be interpreted as the third dimension of the received signal. In a direct-sequence code division multiple access (DS-CDMA) system, *spreading* is the third dimension while in an orthogonal frequency division multiplexing (OFDM), *frequency* plays the role of this additional dimension. From a signal processing perspective, treating the received signal as a 3D tensor makes possible to simultaneously exploit the multiple forms of "diversity" inherent to it for a signal recovery purpose. In [128], the PARAFAC model has first appeared as a generalization of the ESPRIT method [120] for high-resolution direction finding. It has also been applied to the problem of multiuser detection for DS-CDMA systems in several works [131, 130, 47, 48]. In [81], a PARAFAC receiver was also proposed for blind channel estimation in OFDM systems.

In this chapter, we make use of the block-constrained PARAFAC decomposition for modeling the received signal in the uplink of some wireless communication systems subject to frequency-selective multipath fading. The proposed signal model unifies three systems: i)temporally-oversampled systems, ii) DS-CDMA systems [116], and iii) OFDM systems [152]. An antenna array is assumed at the base-station receiver. Each user contributes with a finite number of multipaths to the received signal. We show that the proposed model is subject to structural constraints in some of its component matrices, and that the same "general" tensor model is

shared by the three systems [28, 40]. For each particular system, the corresponding model can be obtained from the general one by making appropriate choices in the structure/dimension of its matrix components. For the DS-CDMA system, our tensor modeling approach generalizes those of [130] and [47], which are limited to special propagation models with a single path per user. Our modeling assumption are also more general than that of [133]. Therein, multiple paths per user were assumed but a frequency-selective channel model was not taken into account.

2.2 Channel and system models

Let us consider a uniform linear array of K half-wavelength spaced omnidirectional antennas receiving signals from Q co-channel users. The propagation channel is assumed to be time-dispersive and it is considered that multipath delay spread exceeds the inverse of the coherence bandwidth of the system, i.e. multipath fading is frequency-selective. The channel impulse response is assumed to span I symbols. Synchronization at the symbol level among the different user signals is assumed. The channel impulse response linking the q-th user to the k-th receive antenna has a finite duration and is assumed to be zero outside the interval $[0, (I-1)T)$, where T is the symbol period. The wireless channel is also assumed to be time-invariant over N symbols. In order to simplify the presentation of the signal model, we omit the additive white Gaussian noise term from the received signal throughout this section. The discrete-time baseband representation of the signal received at the n-th symbol period by the k-th antenna can be expressed as:

$$x_k(n) = \sum_{q=1}^{Q} x_k^{(q)}(n) = \sum_{q=1}^{Q} \sum_{i=1}^{I} h_k^{(q)}(i) s^{(q)}(n-i+1), \tag{2.1}$$

where $h_k^{(q)}(i)$ is the i-th component of the q-th user FIR channel, $s^{(q)}(n)$ is the n-th symbol transmitted by the q-th user.

Let us assume that the signal transmitted by each user is subject to multipath propagation and arrives at the receiver via L "effective" specular paths[1]. By "effective", we mean that each cluster of scatterers is associated with a dominant multipath (see Fig. 2.1). Each clustered multipath has a mean angle of arrival.

[1]In this model, we have assumed that all the users have the same number of multipaths in order to simplify the mathematical notation and the presentation of the model. In section 2.5,

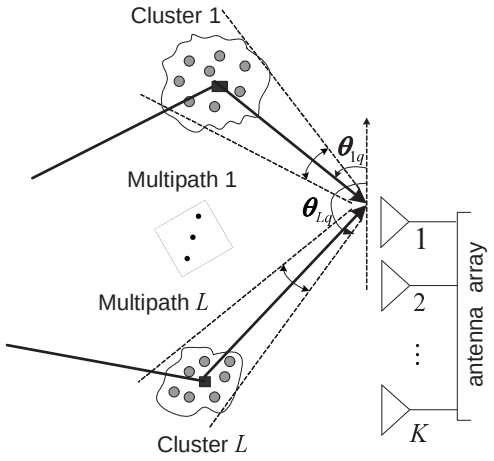

Figure 2.1: Schematic representation of the multipath propagation scenario.

We assume that the cluster angle spread around the mean angle of arrival is small compared to the spatial resolution of the antenna array and will not be considered in the received signal model. The adopted model is valid in practice, provided that the receive antenna array, generally located in a base transceiver station, is sufficiently high so that it is unobstructed and no local scattering occurs. These assumptions on the propagation scenario are typical for cellular suburban deployments [60], where the base transceiver station is on a tower or on the roof of a building. The multipath propagation channel is usually factored in the following manner [149]:

$$h_k^{(q)}(i) = \sum_{l=1}^{L} \beta_l^{(q)} a_k^{(q)}(\theta_l^{(q)}) g^{(q)}(i - 1 - \tau_l^{(q)}), \quad i = 1, \ldots, I, \tag{2.2}$$

where $\beta_l^{(q)}$ is the fading envelope of the l-th path of the q-th user. The term $a_k(\theta_l^{(q)})$ is the response of the k-th antenna to the l-th path of the q-th user, $\theta_l^{(q)}$ being the associated angle of arrival. Similarly, the term $\tau_l^{(q)}$ is the propagation delay (normalized by the symbol period T) and the term $g^{(q)}(i-1-\tau_l^{(q)})$ represents the i-th component of the pulse-shaping filter response. In matrix form, (2.2) can be written as:

$$\mathbf{H}^{(q)} = \sum_{l=1}^{L} \beta_l^{(q)} \mathbf{a}^{(q)}(\theta_l^{(q)}) \mathbf{g}^{(q)T}(\tau_l^{(q)}), \tag{2.3}$$

---

we will consider a more general model where users may have different number of multipaths.

where

$$\begin{aligned}\mathbf{a}^{(q)}(\theta_l^{(q)}) &= \left[a_1^{(q)}(\theta_l^{(q)}) \cdots a_K^{(q)}(\theta_l^{(q)})\right]^T \\ &= \left[1 \; e^{-j\pi \sin\theta_l^{(q)}} \cdots e^{-j\pi(K-1)\sin\theta_l^{(q)}}\right]^T \in \mathbb{C}^K, \end{aligned} \tag{2.4}$$

and

$$\mathbf{g}^{(q)}(\tau_l^{(q)}) = [g^{(q)}(-\tau_l^{(q)}) \cdots g^{(q)}(I-1-\tau_l^{(q)})]^T \in \mathbb{R}^I$$

as the vector antenna array responses and pulse-shape filter responses, respectively. Defining:

$$h_{k,i}^{(q)} \doteq \left[\mathbf{H}^{(q)}\right]_{k,i}, \quad \mathbf{a}_l^{(q)} \doteq \mathbf{a}^{(q)}(\theta_l^{(q)}) = \begin{bmatrix} a_{1,l}^{(q)} \\ \vdots \\ a_{k,l}^{(q)} \\ \vdots \\ a_{K,l}^{(q)} \end{bmatrix}, \quad \mathbf{g}_l^{(q)} \doteq \mathbf{g}^{(q)}(\tau_l^{(q)}) = \begin{bmatrix} g_{1,l}^{(q)} \\ \vdots \\ g_{i,l}^{(q)} \\ \vdots \\ g_{I,l}^{(q)} \end{bmatrix},$$

we can rewrite (2.2) in a simpler form as:

$$h_{k,i}^{(q)} = \sum_{l=1}^{L} \beta_l^{(q)} a_{k,l}^{(q)} g_{i,l}^{(q)}. \tag{2.5}$$

In order to write (2.3) in terms of matrix products, let us define:

$$\mathbf{A}^{(q)} = \left[\mathbf{a}_1^{(q)} \cdots \mathbf{a}_L^{(q)}\right] \in \mathbb{C}^{K\times L} \tag{2.6}$$

$$\mathbf{B}^{(q)} = \operatorname{diag}\left(\beta_1^{(q)} \cdots \beta_L^{(q)}\right) \in \mathbb{C}^{L\times L} \tag{2.7}$$

$$\mathbf{G}^{(q)} = \left[\mathbf{g}_1^{(q)} \cdots \mathbf{g}_L^{(q)}\right]^T \in \mathbb{R}^{L\times I} \tag{2.8}$$

as matrices concatenating L antenna array responses, multipath gains and pulse shape responses, respectively. Eliminating the summation in (2.3), we get:

$$\mathbf{H}^{(q)} = \begin{bmatrix} \mathbf{a}_1^{(q)} & \ldots & \mathbf{a}_L^{(q)} \end{bmatrix} \begin{bmatrix} \beta_1^{(q)} & & \\ & \ddots & \\ & & \beta_L^{(q)} \end{bmatrix} \begin{bmatrix} \mathbf{g}_1^{(q)T} \\ \vdots \\ \mathbf{g}_L^{(q)T} \end{bmatrix} = \mathbf{A}^{(q)}\mathbf{B}^{(q)}\mathbf{G}^{(q)}. \tag{2.9}$$

Using these definitions, the received signal vector $\mathbf{x}(n) = [x_1(n) \cdots x_K(n)]^T \in \mathbb{C}^K$

can be factored as:

$$\mathbf{x}(n) = \sum_{q=1}^{Q} \mathbf{H}^{(q)} \mathbf{s}^{(q)}(n), \tag{2.10}$$

where

$$\mathbf{s}^{(q)}(n) = \left[s^{(q)}(n) \cdots s^{(q)}(n-I+1) \right]^T \in \mathbb{C}^I, \tag{2.11}$$

is the q-th user symbol vector. Collecting the received signal samples during N symbol periods, yields [149]:

$$\mathbf{X} = [\mathbf{x}(1) \cdots \mathbf{x}(N)] = \sum_{q=1}^{Q} \mathbf{H}^{(q)} \mathbf{S}^{(q)T}, \tag{2.12}$$

where

$$\mathbf{S}^{(q)} = \begin{bmatrix} \mathbf{s}^{(q)T}(1) \\ \vdots \\ \mathbf{s}^{(q)T}(N) \end{bmatrix} \in \mathbb{C}^{N \times I}, \tag{2.13}$$

is a symbol matrix having a Toeplitz structure with (n,i)-th element defined as:

$$s_{n,i}^{(q)} = \left[\mathbf{S}^{(q)} \right]_{n,i} \doteq s^{(q)}(n-i+1).$$

Now, let us concatenate the Q user contributions in the following block-matrices:

$$\mathbf{A} = [\mathbf{A}^{(1)} \cdots \mathbf{A}^{(Q)}] \in \mathbb{C}^{K \times QL} \tag{2.14}$$

$$\mathbf{B} = \text{blockdiag}(\mathbf{B}^{(1)} \cdots \mathbf{B}^{(Q)}) \in \mathbb{C}^{QL \times QL} \tag{2.15}$$

$$\mathbf{G} = \text{blockdiag}(\mathbf{G}^{(1)} \cdots \mathbf{G}^{(Q)}) \in \mathbb{R}^{QL \times QI} \tag{2.16}$$

$$\mathbf{S} = [\mathbf{S}^{(1)} \cdots \mathbf{S}^{(Q)}] \in \mathbb{C}^{N \times QI}, \tag{2.17}$$

the received signal matrix (2.12) can be rewritten in a more compact form:

$$\mathbf{X} = \mathbf{A}\overline{\mathbf{H}}\mathbf{S}^T, \quad \text{where} \quad \overline{\mathbf{H}} = \mathbf{B}\mathbf{G}. \tag{2.18}$$

Model (2.18) is the reference model for the development of the block-constrained PARAFAC model for oversampled, DS-CDMA and OFDM systems.

2.3 Tensor signal models

In this section, we rewrite the received signal of each of the three considered communication systems using a tensor modeling approach [28, 46, 40]. The matrices $\mathbf{A}$ and $\mathbf{S}$ in (2.18) model the *space* and *time* dimensions of the 2D (matrix-based) received signal. As will be shown, when the tensor model is introduced, the matrix $\overline{\mathbf{H}}$ in (2.18) will depend on the third dimension of the 3D received signal tensor. The third dimension can be either an *oversampling*, a *spreading* or a *frequency* dimension. In the following, the tensor notation is introduced for modeling the received signal.

2.3.1 Model 1: Oversampled system

Typical wireless communication signals use some excess bandwidth, i.e., the Nyquist rate is larger but still close to the symbol rate. Some additional information can be extracted from the received signal by means of temporal oversampling. We assume an oversampling factor of P, which means that the signal at each receive antenna is sampled at T/P-spaced intervals. Consequently, each transmitted information symbol gives rise to P received over-samples. Temporal oversampling is applied at each receive antenna after the conversion of the received signal to the baseband format. The joint use of multiple receive antennas and oversampling has been studied in several works for blind channel identification/equalization, multiuser signal separation and multipath parameter estimation [101, 141, 150, 149, 151, 154].

Due to temporal oversampling at the receiver, the temporal resolution of the pulse-shaping filter response is increased by a factor P, which then increases the temporal resolution of the received signal by the same factor. We show that the use of oversampling can be interpreted as an incorporation of a third dimension to the received signal [29].

Defining the oversampled versions of the received signal and pulse shape response as:

$$x_{k,n,p} \doteq x_k(n + (p-1)/P), \quad g_{l,i,p} \doteq g\big(i - 1 + (p-1)/P - \tau_{lq}\big),$$

we can rewrite the received signal (2.1) and the multipath channel (2.5) as:

$$x_{k,n,p} = \sum_{q=1}^{Q} \sum_{i=1}^{I} h_{k,i,p}^{(q)} s_{n,i}^{(q)}. \tag{2.19}$$

and

$$h_{k,i,p}^{(q)} = \sum_{l=1}^{L} \beta_l^{(q)} a_{k,l}^{(q)} g_{l,i,p}^{(q)}, \tag{2.20}$$

Let us define the overall channel impulse response (or, simply, *channel response*) as:

$$\overline{h}_{l,i,p} \doteq \beta_l^{(q)}\, g_{l,i,p}^{(q)}.$$

Substituting (2.20) into (2.19), we obtain:

$$x_{k,n,p} = \sum_{q=1}^{Q} \sum_{l=1}^{L} \sum_{i=1}^{I} a_{k,l}^{(q)}\, \overline{h}_{l,i,p}^{(q)}\, s_{n,i}^{(q)}. \tag{2.21}$$

The received signal $x_{k,n,p}$ (k-th receive antena, n-th symbol, p-th oversample) can be interpreted as an element of a third-order tensor $\mathcal{X} \in \mathbb{C}^{K\times N\times P}$. The channel response $\overline{h}_{l,i,p}$ is also an element of a third-order tensor $\overline{\mathcal{H}} \in \mathbb{C}^{L\times I\times P}$. The received signal model (2.21) expresses the received signal tensor in the form of summations of products involving three factors $a_{k,l}^{(q)}$, $s_{n,i}^{(q)}$, and $\overline{h}_{l,i,p}^{(q)}$, associated with the space, time and oversampling dimensions of the received signal, respectively.

We define the l-th slice of the channel tensor as:

$$\overline{\mathbf{H}}_{l\cdot\cdot}^{(q)} = \begin{bmatrix} \overline{\mathbf{h}}_{l,1}^{(q)T} \\ \vdots \\ \overline{\mathbf{h}}_{l,I}^{(q)T} \end{bmatrix} \in \mathbb{C}^{I\times P}, \tag{2.22}$$

where $\overline{\mathbf{h}}_{l,i}^{(q)} = [\overline{h}_{l,i,1}^{(q)} \overline{h}_{l,i,2}^{(q)} \cdots \overline{h}_{l,i,P}^{(q)}]^T \in \mathbb{R}^P$ collects the P oversamples associated with the i-th component of the (l,q)-th channel response. A matrix concatenating the L channel response vectors is defined as:

$$\overline{\mathbf{H}}^{(q)} = [\overline{\mathbf{H}}_{1\cdot\cdot}^{(q)T} \cdots \overline{\mathbf{H}}_{L\cdot\cdot}^{(q)T}] \in \mathbb{C}^{P\times LI} \tag{2.23}$$

By comparing (2.21) with (1.48), we deduce the following correspondences:

$$(I_1, I_2, I_3, R_1^{(q)}, R_2^{(q)}, \mathbf{A}^{(q)}, \mathbf{B}^{(q)}, \mathbf{C}^{(q)}) \rightarrow (K, N, P, L, I, \mathbf{A}^{(q)}, \mathbf{S}^{(q)}, \overline{\mathbf{H}}^{(q)}), \tag{2.24}$$

By analogy with (1.51) and (1.54), and taking the above correspondences into

account, we can express the p-th slice $\mathbf{X}_{..p} \in \mathbb{C}^{K \times N}$ as:

$$\begin{aligned} \mathbf{X}_{..p} &= \sum_{q=1}^{Q} \mathbf{A}^{(q)} \mathbf{\Psi}^{(q)} D_p(\overline{\mathbf{H}}^{(q)}) (\mathbf{S}^{(q)} \mathbf{\Phi}^{(q)})^T \\ &= \mathbf{A} \mathbf{\Psi} D_p(\overline{\mathbf{H}}) (\mathbf{S} \mathbf{\Phi})^T \end{aligned} \tag{2.25}$$

where $\mathbf{\Psi}^{(q)} = \mathbf{I}_L \otimes \mathbf{1}_I^T$, $\mathbf{\Phi}^{(q)} = \mathbf{1}_L^T \otimes \mathbf{I}_I$, and

$$\begin{aligned} \mathbf{\Psi} &= \text{blockdiag}\big(\mathbf{\Psi}^{(1)} \cdots \mathbf{\Psi}^{(Q)}\big) = \mathbf{I}_Q \otimes (\mathbf{I}_L \otimes \mathbf{1}_I^T), \\ \mathbf{\Phi} &= \text{blockdiag}\big(\mathbf{\Phi}^{(1)} \cdots \mathbf{\Phi}^{(Q)}\big) = \mathbf{I}_Q \otimes (\mathbf{1}_L^T \otimes \mathbf{I}_I) \end{aligned}$$

are constraint matrices that depend on the number Q of users, on the number L of multipaths, and on the length I of the channel impulse response. The received signal follows a block-constrained PARAFAC model, the number of blocks corresponding to the number of users.

2.3.2 Model 2: DS-CDMA system

The DS-CDMA system enables multiple access by means of spread spectrum modulation [116]. In a classical DS-CDMA system, the transmitted symbol sequence is spread across the spectrum at a higher rate. The spreading operation consists in multiplying the narrowband signal to be transmitted by a spreading sequence, or *code* (see Fig. 2.2). In a DS-CDMA system, the users share the same frequency band and time slot to communicate, and each user is identified by a unique spreading code. At the receiver, the recovery of users' signals uses the same spreading code as the one used for spreading at the transmitter to perform correlation detection (also known as *despreading*) [116, 140]. Let us define $c^{(q)}(t)$ as the spreading sequence associated with the q-th user. The spreading sequences are symbol-periodic, i.e. their period is equal to the duration of one symbol, and are given by:

$$c^{(q)}(t) = \sum_{j=1}^{J} c_j^{(q)} g\big(t - (j-1)T_c\big), \tag{2.26}$$

where $c_j^{(q)} \in \{+1, -1\}$, $j = 1, \ldots, J$ is the spreading code, $g(t)$ is the pulse shaping filter, T_c is the chip period satisfying $T_c = T/J$, and J is the *spreading factor* (i.e. the ratio between chip- and symbol- rates).

Including the multipath propagation model of Section **??**, the spreading code is replaced by the *effective signature code*, given by the convolution of the spreading

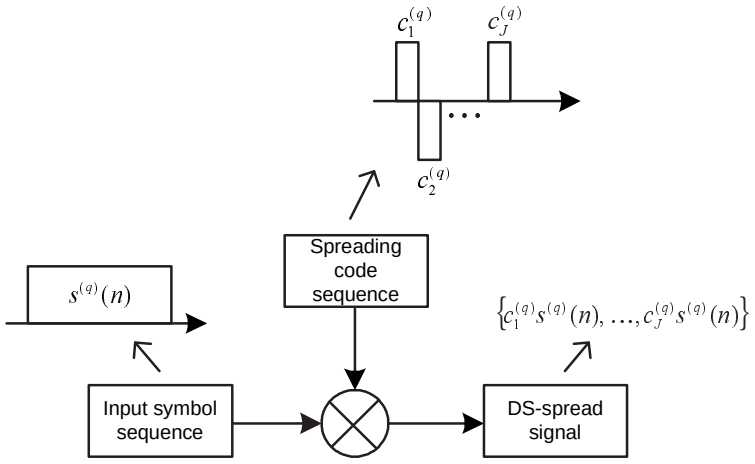

Figure 2.2: Simplified transmitter diagram of a DS-CDMA system.

code with the channel impulse response sampled at the chip-rate. Similarly to the oversampled system, we can define the chip-rate versions of the received signal and the channel impulse response as $x_{k,n,j} \doteq x_k(n + (j-1)/J)$ and $\overline{h}_{l,i,j} \doteq \beta_l^{(q)}\, g_{l,i,j}^{(q)}$. Define also:

$$u_{l,i,j}^{(q)} = \sum_{j'=1}^{J} \overline{h}_{l,i,j-j'}^{(q)}\, c_{j'}^{(q)}$$

as the convolution of the spreading codes with the channel response. With these definitions, the received signal model for oversampled and DS-CDMA systems are essentially the same, the only difference is that the spreading factor J plays the role of the oversampling factor P. Thus, the scalar component (k-th receive antenna, n-th symbol, j-th chip) of the distrete-time baseband received signal can be written in tensor notation as:

$$x_{k,n,j} = \sum_{q=1}^{Q} \sum_{l=1}^{L} \sum_{i=1}^{I} a_{k,l}^{(q)} u_{l,i,j}^{(q)}\, s_{n,i}^{(q)}. \tag{2.27}$$

Note that (2.27) is equivalent to (2.21), where $u_{l,i,j}^{(q)}$ plays the role of $h_{l,i,p}^{(q)}$ and $J \to P$. Therefore, the slice factorization of $\mathbf{X}_{\cdot\cdot j} \in \mathbb{C}^{K\times N}$ follows (2.25) and is given by:

$$\begin{aligned} \mathbf{X}_{\cdot\cdot j} &= \sum_{q=1}^{Q} \mathbf{A}^{(q)} \mathbf{\Psi}^{(q)} D_j(\mathbf{U}^{(q)}) (\mathbf{S}^{(q)} \mathbf{\Phi}^{(q)})^T \\ &= \mathbf{A}\mathbf{\Psi} D_j(\mathbf{U}) (\mathbf{S}\mathbf{\Phi})^T \end{aligned} \tag{2.28}$$

where $\mathbf{U}^{(q)}$ is defined as:

$$\mathbf{U}^{(q)} = \mathbf{C}^{(q)}\overline{\mathbf{H}}^{(q)} \in \mathbb{C}^{J\times IL}, \tag{2.29}$$

$\mathbf{C}^{(q)} \in \mathbb{C}^{J\times J}$ being a Toeplitz matrix with first row and column defined as $\mathbf{C}^{(q)}_{1\cdot} = [c_1^{(q)}\, 0\, \cdots\, 0]$ and $\mathbf{C}^{(q)}_{\cdot 1} = [c_1^{(q)}\, c_2^{(q)}\, \cdots\, c_J^{(q)}]^T$ respectively, and $\overline{\mathbf{H}}^{(q)}$ being analogous to that defined in (2.23), where J replaces P.

2.3.3 Model 3: OFDM system

OFDM is a special form of multicarrier modulation, where a single data stream is transmitted over a number of lower rate orthogonal subcarriers. One of the main reasons to use OFDM is to increase the robustness against frequency selective fading and narrowband interference. This characteristic is very attractive, especially for high-speed data transmission [152]. A simplified block-diagram of a multicarrier OFDM system is depicted in Fig. 2.3 focusing on the q-th user and considering a single-antenna system. In an OFDM system, the symbol sequence

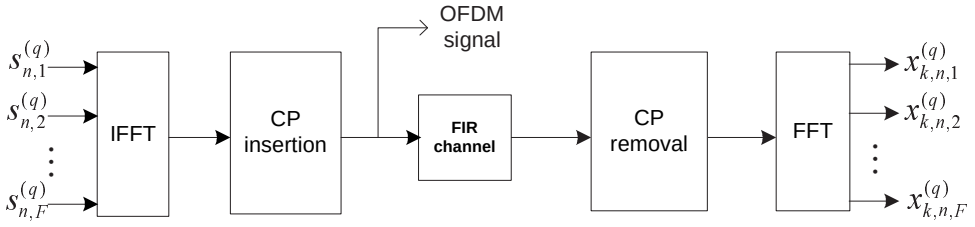

Figure 2.3: Simplified block-diagram of an OFDM system.

to be transmitted is organized into blocks of F symbols (serial-to-parallel conversion), where F is the number of subcarriers. Multicarrier modulation consists in linearly combining the F symbols using Inverse Fast Fourier Transform (IFFT).

Let us define $s^{(q)}_{n,f}$ as the f-th symbol of the n-th OFDM block associated with the q-th user. The signal at the output of the IFFT block is given by:

$$z^{(q)}_{n,f} = \frac{1}{\sqrt{F}} \sum_{i=1}^{F} s^{(q)}_{n,i} e^{j2\pi(i-1)(f-1)/F}, \quad n = 1, \ldots, N, \quad f = 1, \ldots, F, \tag{2.30}$$

where N denotes the number of transmitted OFDM blocks. After the IFFT, a guard period in the form of a cyclic prefix (CP) is inserted to each OFDM block.

The CP is used to avoid intercarrier interference, i.e. the interference between adjacent OFDM blocks [152]. We also assume that band-limited pulse shaping is employed at each frequency tone, and the spacing between the frequency-domain pulses is assumed to be sufficient so that they will not overlap each other. At the receiver, inverse processing is done, i.e. the CP is removed and the resulting OFDM block is linearly combined by means of Fast Fourier Transform (FFT). Defining:

$$\mathbf{\Gamma} = \frac{1}{\sqrt{F}} \begin{bmatrix} 1 & 1 & \cdots & 1 \\ 1 & \gamma^1 & \cdots & \gamma^{F-1} \\ \vdots & \vdots & \ddots & \vdots \\ 1 & \gamma^{F-1} & \cdots & \gamma^{(F-1)(F-1)} \end{bmatrix}, \tag{2.31}$$

as the FFT matrix, where $\gamma = e^{-j2\pi/F}$, the signal at the output of the IFFT block can be expressed by the following input-output relation:

$$\mathbf{z}_n^{(q)} = \mathbf{\Gamma}^H \mathbf{s}_n^{(q)} \in \mathbb{C}^F, \tag{2.32}$$

where

$$\mathbf{z}_n^{(q)} = \begin{bmatrix} z_{n,1}^{(q)} \\ \vdots \\ z_{n,F}^{(q)} \end{bmatrix}, \quad \mathbf{s}_n^{(q)} = \begin{bmatrix} s_{n,1}^{(q)} \\ \vdots \\ s_{n,F}^{(q)} \end{bmatrix}. \tag{2.33}$$

We assume that the length of the CP is equal to the memory $I-1$ of the channel impulse response. The CP insertion consists in copying the last $I-1$ samples of vector $\mathbf{z}_n^{(q)}$ to the beginning of it.Therefore, the augmented OFDM symbol block to be transmitted after the insertion of the CP is composed of $F+I$ samples. The transmitted signal of each user undergo frequency-selective propagation. Let $\{h_{k,1}^{(q)}, \ldots, h_{k,I}^{(q)}\}$ represent the length-I Finite Impulse Response (FIR) channel between the q-th user and the k-th receive antenna. At the receiver, the baseband signal at each receive antenna is then serial-to-parallel converted into blocks of $F+I$ samples. Then, the CP is removed from each block and the FFT is applied, yielding the following input-output relation [152]:

$$\mathbf{x}_{k,n} = \sum_{q=1}^{Q} \mathbf{D}_k^{(q)} \mathbf{s}_n^{(q)}. \tag{2.34}$$

where $\mathbf{D}_k^{(q)} = \operatorname{diag}\big(d_{k,1}^{(q)} \cdots d_{k,F}^{(q)}\big)$ and $d_{k,f}^{(q)}$ is the frequency-domain channel at the

f-th subcarrier, given by:

$$d_{k,f}^{(q)} = \sum_{i=1}^{I} h_{k,i}^{(q)} e^{j2\pi(f-1)(i-1)/F}. \tag{2.35}$$

In scalar form, (2.34) can be written as:

$$x_{k,n,f} = \sum_{q=1}^{Q} d_{k,f}^{(q)} s_{n,f}^{(q)}. \tag{2.36}$$

Using the multipath propagation model (2.5), the channel response (2.35) can be rewritten as:

$$\begin{aligned} d_{k,f}^{(q)} &= \sum_{l=1}^{L} \beta_l^{(q)} a_{k,l}^{(q)} \underbrace{\sum_{i=1}^{I} g_{i,l}^{(q)} e^{j2\pi(f-1)(i-1)/F}}_{\overline{g}_{f,l}^{(q)}} \\ &= \sum_{l=1}^{L} \beta_l^{(q)} a_{k,l}^{(q)} \overline{g}_{f,l}^{(q)}. \end{aligned} \tag{2.37}$$

Finally, substituting (2.37) into (2.36) and defining $\lambda_{f,l}^{(q)} = \beta_l^{(q)} \overline{g}_{f,l}^{(q)}$, yields:

$$x_{k,n,f} = \sum_{q=1}^{Q} \sum_{l=1}^{L} a_{k,l}^{(q)} \lambda_{f,l}^{(q)} s_{n,f}^{(q)}. \tag{2.38}$$

$x_{k,n,f}$ is a scalar component (k-th receive antenna, n-th symbol, f-th subcarrier) of the received signal tensor $\mathcal{X} \in \mathbb{C}^{K \times N \times F}$, the third-dimension of which corresponds to the number of subcarriers.

In order to allow for a direct comparison of (2.38) with (2.21) and (2.27), we rewrite (2.38) in the following equivalent manner:

$$x_{k,n,f} = \sum_{q=1}^{Q} \sum_{l=1}^{L} \sum_{i=1}^{F} a_{k,l}^{(q)} \lambda_{l,i,f}^{(q)} s_{n,i}^{(q)}, \quad \text{where} \quad \lambda_{l,i,f}^{(q)} = \lambda_{f,l}^{(q)} \delta_{if}. \tag{2.39}$$

As it has been done for the two previous communication systems, we are interested in representing the received signal tensor in slice notation. A matrix collecting the

F scalar channels associated with the l-th multipath is defined as:

$$\mathbf{\Lambda}_{..l}^{(q)} = \text{diag}\big(\lambda_{1,l}^{(q)} \cdots \lambda_{F,l}^{(q)}\big) \in \mathbb{C}^{F\times F}.$$

Now, let us concatenate the L multipath contributions into the following matrix:

$$\mathbf{\Lambda}^{(q)} = \big[\mathbf{\Lambda}_{..1}^{(q)} \cdots \mathbf{\Lambda}_{..L}^{(q)}\big] \in \mathbb{C}^{F\times LF}.$$

A symbol matrix collecting N OFDM symbols is defined as:

$$\mathbf{S}^{(q)} = \begin{bmatrix} \mathbf{s}_1^{(q)T} \\ \vdots \\ \mathbf{s}_N^{(q)T} \end{bmatrix} \in \mathbb{C}^{N\times F}$$

Taking these definitions into account, and comparing (2.39) with (1.48), we deduce the following correspondences:

$$(I_1, I_2, I_3, R_1^{(q)}, R_2^{(q)}, \mathbf{A}^{(q)}, \mathbf{B}^{(q)}, \mathbf{C}^{(q)}) \rightarrow (K, N, F, L, F, \mathbf{A}^{(q)}, \mathbf{S}^{(q)}, \mathbf{\Lambda}^{(q)}), \qquad (2.40)$$

By analogy with (1.51) and taking these correspondences into account, we obtain the following writing for the f-th slice $\mathbf{X}_{..f} \in \mathbb{C}^{K\times N}$ of $\mathcal{X} \in \mathbb{C}^{K\times N\times F}$:

$$\begin{aligned} \mathbf{X}_{..f} &= \sum_{q=1}^{Q} \mathbf{A}^{(q)}\mathbf{\Psi}^{(q)} D_f(\mathbf{\Lambda}^{(q)})(\mathbf{S}^{(q)}\mathbf{\Phi}^{(q)})^T \\ &= \mathbf{A}\mathbf{\Psi} D_f(\mathbf{\Lambda})(\mathbf{S}\mathbf{\Phi})^T. \end{aligned} \qquad (2.41)$$

Remark: The received signal models (2.25), (2.28) and (2.41) are similar, and all of them follow the block-constrained PARAFAC decomposition defined in (1.51). The main differences are in the structure and/or in dimension of certain component matrices. The general tensor formulation is identical. Such a similarity is our main motivation to formalize a unique tensor model that unifies the received signal model of the three systems. This is done in the following section.

2.4 Unified tensor model

In this section we formalize the unified tensor model for the oversampled, DS-CDMA and OFDM systems [40]. The proposed model brings together the received signal modeling for these systems in a single model using a unique mathematical

notation. The proposal of a unique model is based on the observation that the received signal in each system can be formulated as third-order tensors following fundamentally the same tensor model.

First note that the tensor models of the three systems are quite similar. The basic difference is in the definition of the term associated with the third-dimension of the received signal tensor, which is $\overline{h}_{l,i,p}^{(q)}$ for oversampled case, $u_{l,i,j}^{(q)}$ for the DS-CDMA case and $\lambda_{l,i,f}^{(q)}$ for the OFDM case (see (2.21), (2.27) and (2.39)). Another difference is in the structure of the component matrix $\mathbf{S}^{(q)}$, which is not Toeplitz in the OFDM model.

In order to link the unified tensor model to (1.48), let us define I_3 as the length of the third dimension of the received signal tensor. For the oversampled system $(I_3, R_2) = (P, I)$, for the DS-CDMA system $(I_3, R_2) = (J, I)$ and for the OFDM system $(I_3, R_2) = (F, F)$. The other parameters, which are common for all the systems are $I_1 = K$, $I_2 = N$, $R_1 = L$. In its general form, the tensor modeling of the three systems can be unified in the following expression:

$$\mathbf{X}_{..i_3} = \mathbf{A}\mathbf{\Psi} D_{i_3}(\mathbf{W})(\mathbf{S}\mathbf{\Phi})^T, \tag{2.42}$$

where

$$\mathbf{\Psi} = \mathbf{I}_Q \otimes (\mathbf{I}_L \otimes \mathbf{1}_{R_2}^T) \in \mathbb{C}^{QL \times LQR_2}, \quad \mathbf{\Phi} = \mathbf{I}_Q \otimes (\mathbf{1}_L^T \otimes \mathbf{I}_{R_2}) \in \mathbb{C}^{QLR_2 \times QR_2}, \tag{2.43}$$

and $\mathbf{W}$ is either $\overline{\mathbf{H}}$ (c.f. (2.25)), or $\mathbf{U}$ (c.f. ((2.28)) or $\mathbf{\Lambda}$ (c.f. (2.41)), depending on the considered system.

Concatenating I_3 slices $\mathbf{X}_{..i_3}$, $i_3 = 1, \ldots, I_3$, we get:

$$\mathbf{X}_1 = (\mathbf{W} \diamond \mathbf{A}\mathbf{\Psi})(\mathbf{S}\mathbf{\Phi})^T. \tag{2.44}$$

Comparing (2.44) with (1.55) we deduce the following correspondences:

$$\mathbf{A} \rightarrow \mathbf{A}, \quad \mathbf{B} \rightarrow \mathbf{S}, \quad \mathbf{C} \rightarrow \mathbf{W}.$$

The link of the block-constrained PARAFAC model to each considered system is provided in Table 2.1 for comparison.

In order to study the identifiability of the unified tensor model (2.44), we make use of the necessary uniqueness condition of the block-constrained PARAFAC model presented in (1.75).

Theorem 2.1 (identifiability condition) *For full-rank* $\mathbf{A}$, $\mathbf{S}$ *and* $\mathbf{W}$, *a necessary*

Table 2.1: Unified tensor model for the three wireless communication systems

	Oversampled	**DS-CDMA**	**OFDM**
(I_3)	oversampling(P)	spreading(J)	frequency(F)
(R_2)	delay(I)	delay(I)	frequency(F)
$\mathbf{W}$	$\overline{\mathbf{H}} = [\overline{\mathbf{H}}^{(1)}, \ldots, \overline{\mathbf{H}}^{(Q)}]$	$\mathbf{U} = [\mathbf{U}^{(1)}, \ldots, \mathbf{U}^{(Q)}]$	$\mathbf{\Lambda} = [\mathbf{\Lambda}^{(1)}, \ldots, \mathbf{\Lambda}^{(Q)}]$
dimensions	$P \times QLI$	$J \times QLI$	$F \times QLF$
structure	no structure	no structure	diagonal blocks
Matrix $\mathbf{S}$	$\mathbf{S} = [\mathbf{S}^{(1)}, \ldots, \mathbf{S}^{(Q)}]$	$\mathbf{S} = [\mathbf{S}^{(1)}, \ldots, \mathbf{S}^{(Q)}]$	$\mathbf{S} = [\mathbf{S}^{(1)}, \ldots, \mathbf{S}^{(Q)}]$
dimensions	$N \times QI$	$N \times QI$	$N \times QF$
structure	block-Toeplitz	block-Toeplitz	no structure

condition for the identifiability in the general case is given by the three following inequalities:

$$I_3 K \geq QR_2, \quad KN \geq QR_2 L, \quad NI_3 \geq QL. \tag{2.45}$$

From (2.45), the following corollaries can be obtained:

1. For $N \geq QL$ and $K \geq QR_2$, $I_3 \geq 1$ oversamples/chips per symbol/subcarriers are necessary for identifiability;
2. For $N \geq QL$ and $I_3 \geq QR_2$, $K = R_2$ receive antennas are necessary for identifiability;
3. For $I_3 \geq QL$ and $K \geq QR_2$, $N = L$ received samples are necessary for identifiability.

2.5 Generalization using Tucker-3 modeling

In the previous section, we have modeled the received signal of oversampled, DS-CDMA and OFDM systems using a block-constrained PARAFAC model, by considering that all the users have the same number of multipaths. We have also worked under the assumption of frequency-selective channel with specular multipath propagation. In this section, we provide a more general tensor formulation of the received signal, by assuming that the number of multipaths associated with each user can be different. Moreover, two practical multipath propagation scenarii are considered: i) far-field reflections without angular spread and ii) local scattering with small delay spread. For these scenarii, we present block-constrained Tucker-3 models, where the Tucker-3 core tensor is parameterized by the two constraint

matrices used in the block-PARAFAC model of the previous section [38]. The Tucker-3 core captures the spatial and temporal structure of the wireless channel.

Let us assume that the q-th user reaches the receiver via $L^{(q)}$ propagation paths. Recall the unified tensor model (2.44), which is rewritten here as a function of the q-th user contribution:

$$\mathbf{X}_2^{(q)} = \big(\mathbf{A}^{(q)}\mathbf{\Psi}^{(q)} \diamond \mathbf{S}^{(q)}\mathbf{\Phi}^{(q)}\big)\mathbf{W}^{(q)T}, \tag{2.46}$$

where

$$\mathbf{A}^{(q)} = [\underbrace{\mathbf{a}_1^{(q)} \cdots \mathbf{a}_{L^{(q)}}^{(q)}}_{L^{(q)}\text{paths}}] \in \mathbb{C}^{K \times L^{(q)}}, \tag{2.47}$$

concatenates the $L^{(q)}$ array responses for the q-th user,

$$\mathbf{\Psi}^{(q)} = \mathbf{I}_{L^{(q)}} \otimes \mathbf{1}_{R_2}^T, \quad \mathbf{\Phi}^{(q)} = \mathbf{1}_{L^{(q)}}^T \otimes \mathbf{I}_{R_2}, \tag{2.48}$$

and

$$\mathbf{W}^{(q)} = [\underbrace{\mathbf{W}_1^{(q)} \cdots \mathbf{W}_{L^{(q)}}^{(q)}}_{L^{(q)}\text{paths}}] \in \mathbb{C}^{I_3 \times R_2 L^{(q)}},$$

where $\mathbf{W}_{l^{(q)}}^{(q)}$ collects R_2 channel responses of the $l^{(q)}$-th multipath. Note also that $(R_2, I_3) = (I, P)$ or (I, J) or (F, F), where $\mathbf{W}^{(q)}$ is either $\mathbf{H}^{(q)}$ for the oversampled system, or $\mathbf{U}^{(q)}$ for the DS-CDMA system, or $\mathbf{\Lambda}^{(q)}$ for the OFDM system.

Using property (1.57), we can rewrite (2.46) as:

$$\mathbf{X}_2^{(q)} = \big(\mathbf{A}^{(q)} \otimes \mathbf{S}^{(q)}\big)\mathbf{G}_2^{(q)}\mathbf{W}^{(q)T},$$

where

$$\mathbf{G}_2^{(q)} = \mathbf{\Psi}^{(q)} \diamond \mathbf{\Phi}^{(q)}. \tag{2.49}$$

Substituting (2.48) into (2.49), we get:

$$\mathbf{G}_2^{(q)} \;=\; (\mathbf{I}_{L^{(q)}} \otimes \mathbf{1}_{R_2}^T) \diamond (\mathbf{1}_{L^{(q)}}^T \otimes \mathbf{I}_{R_2}) = (\mathbf{I}_{L^{(q)}} \otimes \mathbf{I}_{R_2}) = \mathbf{I}_{R_2 L^{(q)}}, \tag{2.50}$$

which allows us to rewrite the overall received signal (summed over all the users) in the following form:

$$\mathbf{X}_2 = \sum_{q=1}^{Q} \mathbf{X}_2^{(q)} = \sum_{q=1}^{Q} \big(\mathbf{A}^{(q)} \otimes \mathbf{S}^{(q)}\big)\mathbf{W}^{(q)T} \in \mathbb{C}^{KN \times I_3}, \tag{2.51}$$

or equivalently,

$$\mathbf{X}_2 \;=\; \Big[\mathbf{A}^{(1)} \otimes \mathbf{S}^{(1)} \cdots \mathbf{A}^{(Q)} \otimes \mathbf{S}^{(Q)}\Big] \begin{bmatrix} \mathbf{W}^{(1)T} \\ \vdots \\ \mathbf{W}^{(Q)T} \end{bmatrix} = \big(\mathbf{A} \,|\otimes|\, \mathbf{S}\big)\mathbf{W}^T \quad (2.52)$$

where $\mathbf{A} \in \mathbb{C}^{K \times \overline{L}}$, $\mathbf{S} \in \mathbb{C}^{N \times R_2 Q}$ and $\mathbf{W} \in \mathbb{C}^{I_3 \times R_2 \overline{L}}$ are block matrices (their matrix blocks can have different number of columns in this case), and

$$\overline{L} = \sum_{q=1}^{Q} L^{(q)}.$$

In a similar way, by taking property (1.57) into account, we can obtain two other equivalent Tucker-3 matrix representations $\mathbf{X}_3 \in \mathbb{C}^{I_3 N \times K}$ and $\mathbf{X}_1 \in \mathbb{C}^{K I_3 \times N}$:

$$\mathbf{X}_3 = \big(\mathbf{S} \,|\otimes|\, \mathbf{W}\big)\mathbf{G}_3\mathbf{A}^T, \quad \mathbf{X}_1 = \big(\mathbf{W} \,|\otimes|\, \mathbf{A}\big)\mathbf{G}_1\mathbf{S}^T.$$

Model (2.52) can be viewed as a constrained Tucker-3 decomposition [148, 144] with Tucker-3 core matrices given by:

$$\mathbf{G}_1 \;=\; \text{blockdiag}\big(\mathbf{G}_1^{(1)} \cdots \mathbf{G}_1^{(Q)}\big) = \mathbf{I}_{K\overline{L}}, \quad (2.53)$$

$$\mathbf{G}_2 \;=\; \text{blockdiag}\big(\mathbf{G}_2^{(1)} \cdots \mathbf{G}_2^{(Q)}\big) \;\in \mathbb{C}^{K^2\overline{L} \times \overline{L}} \quad (2.54)$$

$$\mathbf{G}_3 \;=\; \text{blockdiag}\big(\mathbf{G}_3^{(1)} \cdots \mathbf{G}_3^{(Q)}\big) \;\in \mathbb{C}^{K\overline{\overline{L}} \times KQ} \quad (2.55)$$

where

$$\overline{\overline{L}} = \sum_{q=1}^{Q} \big(L^{(q)}\big)^2,$$

$\mathbf{G}_1^{(q)} = \mathbf{I}_{KL^{(q)}}$, while $\mathbf{G}_2^{(q)}$ and $\mathbf{G}_3^{(q)}$ are factored in terms of $\mathbf{\Psi}^{(q)}$ and $\mathbf{\Phi}^{(q)}$ as follows:

$$\mathbf{G}_2^{(q)} \;=\; \big(\mathbf{\Phi}^{(q)} \diamond \mathbf{I}_{KL^{(q)}}\big)\mathbf{\Psi}^{(q)T} \;\in \mathbb{C}^{K^2 L^{(q)} \times L^{(q)}}, \quad (2.56)$$

$$\mathbf{G}_3^{(q)} \;=\; \big(\mathbf{I}_{KL^{(q)}} \diamond \mathbf{\Psi}^{(q)}\big)\mathbf{\Phi}^{(q)T} \;\in \mathbb{C}^{K(L^{(q)})^2 \times K}. \quad (2.57)$$

It is worth mentioning that the Tucker-3 model (2.52) can be viewed as a special case of the block-Tucker-3 model of [50, 109], where the Tucker-3 core has 1's and 0's elements.

2.5.1 Case 1: Far-field reflections without angular spread

In some practical propagation scenarii, multipath reflections occur in remote objects that are located in the far-field of the receive antenna array. We assume that most energy is concentrated in a single spatially resolvable path in the direction of the transmitter [149]. In [130] and [47], two different tensor modeling approaches for the received signal were proposed under the assumption of far-field reflection without angular spread. Here, we also work with this assumption and show that a constrained Tucker-3 formulation is also possible. Let us assume that the $L^{(q)}$ reflections relative to the q-th user are located in the far-field of the antenna array, so that the $L^{(q)}$ spatial signatures can be considered identical, i.e., $\mathbf{a}_1^{(q)} = \cdots = \mathbf{a}_{L^{(q)}}^{(q)} = \mathbf{a}^{(q)}, \quad q = 1, \ldots, Q$. Consequently, the array response matrix $\mathbf{A}$ defined in (2.14) is now constituted of Q blocks of $L^{(q)}$ identical columns each, and can be explicited as:

$$\mathbf{A} = \left[\mathbf{a}^{(1)} \otimes \mathbf{1}_{L^{(1)}}^T, \ldots, \mathbf{a}^{(Q)} \otimes \mathbf{1}_{L^{(Q)}}^T\right] = \overline{\mathbf{A}}\boldsymbol{\Upsilon}, \tag{2.58}$$

with $\overline{\mathbf{A}} = \left[\mathbf{a}^{(1)}, \ldots, \mathbf{a}^{(Q)}\right]$ and

$$\boldsymbol{\Upsilon} = \begin{bmatrix} \mathbf{1}_{L^{(1)}}^T & & \\ & \ddots & \\ & & \mathbf{1}_{L^{(Q)}}^T \end{bmatrix}. \tag{2.59}$$

Substituting (2.58) into (2.52) and (2.53) yields:

$$\begin{aligned} \mathbf{X}_2 &= \left(\overline{\mathbf{A}}\boldsymbol{\Upsilon} \,|\otimes|\, \mathbf{S}\right) \mathbf{W}^T, \\ \mathbf{X}_3 &= \left(\mathbf{S} \,|\otimes|\, \mathbf{W}\right) \mathbf{G}_2 \left(\overline{\mathbf{A}}\boldsymbol{\Upsilon}\right)^T, \\ \mathbf{X}_1 &= \left(\mathbf{W} \,|\otimes|\, \overline{\mathbf{A}}\boldsymbol{\Upsilon}\right) \mathbf{G}_3 \mathbf{S}^T. \end{aligned} \tag{2.60}$$

Let us consider the following property of the block-wise Kronecker product:

Property 2.1 : For arbitrary block-matrices $\mathbf{A}$, $\mathbf{B}$, $\mathbf{C}$ and $\mathbf{D}$ composed of Q blocks, with $\mathbf{C}$ and $\mathbf{D}$ block-diagonal matrices with compatible dimensions, we have:

$$\mathbf{AC} \,|\otimes|\, \mathbf{BD} = (\mathbf{A} \,|\otimes|\, \mathbf{B}) diag\left(\mathbf{C}^{(1)} \otimes \mathbf{D}^{(1)}, \ldots, \mathbf{C}^{(Q)} \otimes \mathbf{D}^{(Q)}\right), \tag{2.61}$$

Using this property in each of the three unfolded representations (2.60), we get the following equivalent constrained Tucker-3 representations:

$$\mathbf{X}_2 = \big(\overline{\mathbf{A}} \,|\otimes|\, \mathbf{S}\big)\, \overline{\mathbf{G}}_1 \mathbf{W}^T, \quad \mathbf{X}_3 = (\mathbf{S} \,|\otimes|\, \mathbf{W})\, \overline{\mathbf{G}}_2 \overline{\mathbf{A}}^T, \quad \mathbf{X}_1 = \big(\mathbf{W} \,|\otimes|\, \overline{\mathbf{A}}\big)\, \overline{\mathbf{G}}_3 \mathbf{S}^T, \tag{2.62}$$

where $\overline{\mathbf{G}}_1 = diag\big(\overline{\mathbf{G}}_1^{(1)}, \ldots, \overline{\mathbf{G}}_1^{(Q)}\big)$, $\overline{\mathbf{G}}_2 = \mathbf{G}_2 \boldsymbol{\Upsilon}^T$ and $\overline{\mathbf{G}}_3 = diag\big(\overline{\mathbf{G}}_3^{(1)}, \ldots, \overline{\mathbf{G}}_3^{(Q)}\big)$ are the associated constrained core matrices, with $\overline{\mathbf{G}}_1^{(q)} = \mathbf{1}_{L^{(q)}}^T \otimes \mathbf{I}_K$ and $\overline{\mathbf{G}}_3^{(q)} = \big(\mathbf{I}_{KL^{(q)}} \otimes \mathbf{1}_{L^{(q)}}^T\big)\mathbf{G}_3^{(q)}$.

2.5.2 Case 2: Local scattering with small delay spread

Now, consider that all scattering objects are local to the receive antenna array so that the relative propagation delays are much smaller than the symbol period, i.e. $max(\tau_{lq}) << T$, $q = 1, \ldots, Q$. It is assumed that multipath delays are different. This is also known as the incoherent multipath assumption with small delay spread, which was addressed in [133] using tensor modeling. Since temporal dispersion at the symbol-level is no longer present ($R_2 = 1$), we can drop the dependence of both the pulse-shape matrix and symbol matrix on the index r_2. These matrices can be rewritten as:

$$\overline{\mathbf{W}} = \Big[\underbrace{\mathbf{w}_1^{(1)} \cdots \mathbf{w}_{L^{(1)}}^{(1)}}_{L^{(1)} \text{ paths}} \cdots \underbrace{\mathbf{w}_1^{(Q)} \cdots \mathbf{w}_{L^{(Q)}}^{(Q)}}_{L^{(Q)} \text{ paths}} \Big] \in \mathbb{C}^{I_3 \times \overline{L}} \tag{2.63}$$

and $\overline{\mathbf{S}} = [\mathbf{s}^{(1)} \cdots \mathbf{s}^{(Q)}] \in \mathbb{C}^{N \times Q}$, where $\mathbf{s}^{(q)} = [s_1^{(q)} s_2^{(q)} \cdots s_N^{(q)}]^T \in \mathbb{C}^N$. Substituting $\overline{\mathbf{W}}$ and $\overline{\mathbf{S}}$ into (2.52) we can rewrite the resulting model as:

$$\mathbf{X}_2 = \Big[\mathbf{A}^{(1)} \otimes \mathbf{s}^{(1)} \cdots \mathbf{A}^{(Q)} \otimes \mathbf{s}^{(Q)}\Big] \overline{\mathbf{W}}^T = \big(\mathbf{A} \,|\otimes|\, \overline{\mathbf{S}}\big)\, \mathbf{G}_2 \overline{\mathbf{W}}^T,$$

$$\mathbf{X}_3 = \big(\overline{\mathbf{S}} \,|\otimes|\, \overline{\mathbf{W}}\big)\mathbf{G}_3 \mathbf{A}^T, \quad \mathbf{X}_1 = \big(\overline{\mathbf{W}} \,|\otimes|\, \mathbf{A}\big)\mathbf{G}_1 \overline{\mathbf{S}}^T. \tag{2.64}$$

Using (2.48), we have:

$$\boldsymbol{\Psi}^{(q)} = \mathbf{I}_{L^{(q)}}, \quad \boldsymbol{\Phi}^{(q)} = \mathbf{1}_{L^{(q)}}^T,$$

and (2.49), (2.56) and (2.57) are reduced to:

$$\mathbf{G}_2^{(q)} = \mathbf{I}_{L^{(q)}} \diamond \mathbf{1}_{L^{(q)}}^T = \mathbf{I}_{L^{(q)}},$$

$$\mathbf{G}_3^{(q)} = \mathbf{1}_{L^{(q)}}^T \diamond \mathbf{I}_{L^{(q)}} = \mathbf{I}_{L^{(q)}}, \quad \mathbf{G}_1^{(q)} = \big(\mathbf{I}_{L^{(q)}} \diamond \mathbf{I}_{L^{(q)}}\big)\mathbf{1}_{L^{(q)}}.$$

Using (2.43), (2.49), (2.56)-(2.57) with $R_2 = 1$, we get the following constraint matrices: $\mathbf{\Psi}^{(q)} = \mathbf{I}_{L^{(q)}}$ and $\mathbf{\Phi}^{(q)} = \mathbf{1}_{L^{(q)}}^T$, which gives $\mathbf{G}_1 = \mathbf{G}_2 = \mathbf{I}_{\overline{L}}$ and $\mathbf{G}_3 = diag(\mathbf{G}_3^{(1)} \cdots \mathbf{G}_3^{(Q)})$ with $\mathbf{G}_3^{(q)} = (\mathbf{I}_{L^{(q)}} \diamond \mathbf{I}_{L^{(q)}})\mathbf{1}_{L^{(q)}}$. Table 2.2 summarizes the constrained Tucker-3 models presented in this paper for each scenario.

Table 2.2: Unification of constrained Tucker-3 models for blind beamforming

Factor matrices : $\{\overline{\mathbf{A}}, \mathbf{S}, \mathbf{W}\}$, Core matrices : $\{\overline{\mathbf{G}}_1, \overline{\mathbf{G}}_2, \overline{\mathbf{G}}_3\}$

Unfolded matrices of the received signal:

$\mathbf{X}_1 = \big(\overline{\mathbf{A}} \,|\otimes|\, \mathbf{S}\big)\,\overline{\mathbf{G}}_1\mathbf{W}^T, \qquad \mathbf{X}_2 = (\mathbf{S} \,|\otimes|\, \mathbf{W})\,\overline{\mathbf{G}}_2\overline{\mathbf{A}}^T, \qquad \mathbf{X}_3 = \big(\mathbf{W} \,|\otimes|\, \overline{\mathbf{A}}\big)\,\overline{\mathbf{G}}_3\mathbf{S}^T$

General case	**Case 1: no angular spread**	**Case 2: small delay spread**
$\overline{\mathbf{A}} = \mathbf{A} = [\mathbf{A}^{(1)}, \ldots, \mathbf{A}^{(Q)}]$ $\mathbf{A}^{(q)} \in \mathbb{C}^{M \times L^{(q)}}$	$\overline{\mathbf{A}} = [\mathbf{a}^{(1)}, \ldots, \mathbf{a}^{(Q)}]$ $\mathbf{a}^{(q)} \in \mathbb{C}^{M}$	$\overline{\mathbf{A}} = \mathbf{A} = [\mathbf{A}^{(1)}, \ldots, \mathbf{A}^{(Q)}]$ $\mathbf{A}^{(q)} \in \mathbb{C}^{M \times L^{(q)}}$
$\mathbf{S} = [\mathbf{S}^{(1)}, \ldots, \mathbf{S}^{(Q)}]$ $\mathbf{S}^{(q)} \in \mathbb{C}^{N \times R_2}$	$\mathbf{S} = [\mathbf{S}^{(1)}, \ldots, \mathbf{S}^{(Q)}]$ $\mathbf{S}^{(q)} \in \mathbb{C}^{N \times R_2}$	$\mathbf{S} = [\mathbf{s}^{(1)}, \ldots, \mathbf{s}^{(Q)}]$ $\mathbf{s}^{(q)} \in \mathbb{C}^{N}$
$\mathbf{W} = [\mathbf{W}^{(1)}, \ldots, \mathbf{W}^{(Q)}]$ $\mathbf{W}^{(q)} \in \mathbb{C}^{P \times R_2 L^{(q)}}$	$\mathbf{W} = [\mathbf{W}^{(1)}, \ldots, \mathbf{W}^{(Q)}]$ $\mathbf{W}^{(q)} \in \mathbb{C}^{P \times R_2 L^{(q)}}$	$\mathbf{W} = [\mathbf{W}^{(1)}, \ldots, \mathbf{W}^{(Q)}]$ $\mathbf{W}^{(q)} \in \mathbb{C}^{P \times L^{(q)}}$
$\overline{\mathbf{G}}_i = diag\big(\mathbf{G}_i^{(1)}, \ldots \mathbf{G}_i^{(Q)}\big), \quad i = 1, 2, 3$		
$\overline{\mathbf{G}}_1^{(q)} = \mathbf{G}_1^{(q)}$	$\overline{\mathbf{G}}_1^{(q)} = \mathbf{1}_{L^{(q)}}^T \otimes \mathbf{I}_{R_2}$	$\overline{\mathbf{G}}_1^{(q)} = \mathbf{I}_{L^{(q)}}$
$\overline{\mathbf{G}}_2^{(q)} = \mathbf{G}_2^{(q)}$	$\overline{\mathbf{G}}_2^{(q)} = \mathbf{G}_2^{(q)}\mathbf{1}_{L^{(q)}}$	$\overline{\mathbf{G}}_2^{(q)} = \mathbf{I}_{L^{(q)}}$
$\overline{\mathbf{G}}_3^{(q)} = \mathbf{G}_3^{(q)}$	$\overline{\mathbf{G}}_3^{(q)} = (\mathbf{I}_{R_2 L^{(q)}} \otimes \mathbf{1}_{L^{(q)}}^T)\mathbf{G}_3^{(q)}$	$\overline{\mathbf{G}}_3^{(q)} = (\mathbf{I}_{L^{(q)}} \diamond \mathbf{I}_{L^{(q)}})\mathbf{1}_{L^{(q)}}$
with $\mathbf{G}_1^{(q)}$, $\mathbf{G}_2^{(q)}$ and $\mathbf{G}_3^{(q)}$ given in (2.50), (2.56) and (2.57).		

2.6 Application to blind multiuser equalization

The blind multiuser equalization problem consists in recovering the information sequence from several users under the assumption of frequency-selective fading. We propose a deterministic tensor-based blind multiuser receiver performing user separation and equalization iteratively [26, 40]. We consider the oversampled system. The receiver makes use of the block-constrained PARAFAC model. Multiuser signal separation is carried out in the 3D tensor space, exploiting *space*, *time* and *oversampling* dimensions of the received signal. Our tensor-based receiver does not require the use of training sequences, nor the knowledge of the channel impulse responses and antenna array responses. Moreover, it does not rely on statistical

independence between the transmitted signals. The number Q of users is, however, assumed to be known at the receiver.

The Alternating Least Squares (ALS) algorithm [73] is used for this purpose. Equalization is done in the 2D matrix space, where the Toeplitz structure of the symbol matrix as well as the Finite-Alphabet (FA) property of the transmitted symbols are exploited to estimate the transmitted symbols via a subspace method. The key aspect of the proposed algorithm is that multiuser signal separation (PARAFAC stage) and equalization (Subspace+FA stage) is done in an iterative way. The goal of the PARAFAC stage is to estimate three component matrices from which the PARAFAC model parameters can be determined. In turn, the goal of the subspace+FA stage is to solve the transformation ambiguity problem that is inherent to the proposed model as well as to estimate the transmitted symbols in the 2D space, exploiting the FA property. The FA-projected symbols are in turn used as an input to the PARAFAC stage to refine the multiuser signal separation in the 3D space. In the following, we describe the proposed algorithm.

2.6.1 Iterative PARAFAC-Subspace receiver

For the received signal tensor $\mathcal{X}$ $(K \times N \times P)$, multiuser signal separation is carried out in the 3D tensor space using the ALS algorithm, which consists in estimating in an alternating way three matrices $\mathbf{Z}_1 \in \mathbb{C}^{N \times IQ}$, $\mathbf{Z}_2 \in \mathbb{C}^{K \times LQ}$ and $\mathbf{Z}_3 \in \mathbb{C}^{P \times ILQ}$ from the matrix representations $\mathbf{X}_{i=1,2,3}$ of the received signal tensor (see Sec. 1.2.3). The multiuser signal separation problem is formulated as a set of three independent nonlinear least squares problems:

$$\begin{aligned} \widehat{\mathbf{Z}}_2 &= \underset{\mathbf{Z}_2}{\operatorname{argmin}} \|\mathbf{X}_1 - (\mathbf{Z}_3 \diamond \mathbf{Z}_1\mathbf{\Psi})(\mathbf{Z}_2\mathbf{\Phi})^T\|_F^2, \\ \widehat{\mathbf{Z}}_3 &= \underset{\mathbf{Z}_3}{\operatorname{argmin}} \|\mathbf{X}_2 - (\mathbf{Z}_1\mathbf{\Psi} \diamond \mathbf{Z}_2\mathbf{\Phi})(\mathbf{Z}_3)^T\|_F^2, \\ \widehat{\mathbf{Z}}_1 &= \underset{\mathbf{Z}_1}{\operatorname{argmin}} \|\mathbf{X}_3 - (\mathbf{Z}_2\mathbf{\Phi} \diamond \mathbf{Z}_3)(\mathbf{Z}_1\mathbf{\Psi})^T\|_F^2. \end{aligned} \tag{2.65}$$

Thus, one iteration of the multiuser signal separation stage has three steps. At each step one component matrix is updated while the others are fixed to the values obtained at the previous steps. By analogy with (2.44), we have $\mathbf{Z}_1 \to \mathbf{A}$, $\mathbf{Z}_2 \to \mathbf{S}$ and $\mathbf{Z}_3 \to \mathbf{W}$. Uniqueness of $\mathbf{A}$ and $\mathbf{W}$ is not important in the present context since we are interested in recovering the user symbol sequences (which is the final goal in the blind multiuser equalization problem) that should be extracted from $\mathbf{S}$. We have:

$$\widehat{\mathbf{S}}^{(1)} = \mathbf{S}^{(1)}\mathbf{T}^{(1)} \quad , \ldots , \quad \widehat{\mathbf{S}}^{(Q)} = \mathbf{S}^{(Q)}\mathbf{T}^{(Q)},$$

Table 2.3: Pseudo-code for the iterative PARAFAC-Subspace algorithm

$i = 0$; Initialize $\widehat{\mathbf{Z}}_2(0)$ and $\widehat{\mathbf{Z}}_3(0)$

1. $i = i + 1$;
2. Update $\widehat{\mathbf{Z}}_2^T(i) = \left[\left(\widehat{\mathbf{Z}}_3(i-1) \diamond \widehat{\mathbf{Z}}_1(i-1)\mathbf{\Psi}\right)\mathbf{\Phi}^T\right]^\dagger \mathbf{X}_1$;
3. Subspace+FA stage (go to table 2.4);
4. Form $\widehat{\mathbf{Z}}_2(i) = \left[\widehat{\mathbf{Z}}_2^{(1)}(i), \ldots, \widehat{\mathbf{Z}}_2^{(Q)}(i)\right]$;
5. Update $\widehat{\mathbf{Z}}_3^T(i) = \left[\widehat{\mathbf{Z}}_1(i-1)\mathbf{\Psi} \diamond \widehat{\mathbf{Z}}_2(i)\mathbf{\Phi}\right]^\dagger \mathbf{X}_2$;
6. Update $\widehat{\mathbf{Z}}_1^T(i) = \left[\left(\widehat{\mathbf{Z}}_2(i)\mathbf{\Phi} \diamond \widehat{\mathbf{Z}}_3(i)\right)\mathbf{\Psi}^T\right]^\dagger \mathbf{X}_3$;
7. Go to step 1 until convergence.

where $\mathbf{T}^{(q)} \in \mathbb{C}^{I\times I}$, $q = 1, \ldots, Q$ are non-singular (ambiguity) matrices to be determined. The determination of $\mathbf{T}^{(q)}$ and $\widehat{\mathbf{S}}^{(q)}$ can be viewed as an equivalent single-input multiple-output (SIMO) blind channel identification problem, where $\mathbf{T}^{(q)}$, $q = 1, \ldots, Q$ play the role of virtual length-I SIMO channels with I outputs.

The subspace+FA stage of the proposed receiver aims at determining $\mathbf{T}^{(q)}$, $q = 1, \ldots, Q$, by the following steps. Matrices $\widehat{\mathbf{T}}^{(1)}, \cdots, \widehat{\mathbf{T}}^{(Q)}$ are determined at each ALS iteration, via a subspace method. We use the subspace method originally proposed by Moulines et al. in [101]. For reasons of space, we report the interested reader to the original work for further details. After determining $\widehat{\mathbf{T}}^{(q)}$, the associated symbol matrix $\widehat{\mathbf{S}}^{(q)}$ can be estimated (up to permutation) by pseudo-inversion. An estimation of user symbol sequences $\widehat{\mathbf{s}}^{(q)} \in \mathbb{C}^N$ is obtained by properly averaging over the columns of $\widehat{\mathbf{S}}^{(q)}$ followed by a FA-projection. We assume that the first symbol of each user sequence is known and equal to 1. This allows us to eliminate scaling ambiguity by normalizing each estimated symbol sequence $\widetilde{\mathbf{s}}^{(q)}(i)$ by its first element. An updated (post-equalized) version of $\widehat{\mathbf{Z}}_1$ is then formed and used as an input to the PARAFAC stage to refine user signal separation in the 3D space. At the end of the algorithm, the permutation ambiguity is resolved using a greedy least squares $(\mathbf{S}^{(q)}, \widehat{\mathbf{S}}^{(q)})$-column matching algorithm [131].

Tables 2.3 and 2.4 summarize the proposed iterative PARAFAC-Subspace algorithm. Table 2.3 describes the steps of the proposed algorithm, with emphasis on the ALS algorithm, while in Table 2.4 the steps associated with the subspace+FA stage are detailed. The operator $\mathrm{proj}(\cdot)$ projects each entry of its vector argument to the closest point of the finite symbol-alphabet. At the end of the i-th iteration, an overall error measurement between the estimated model and the received signal

Table 2.4: Pseudo-code for the subspace + FA projection stage

for $q = 1$ to Q,
- Partition $\widehat{\mathbf{Z}}_2(i) = \left[\widehat{\mathbf{Z}}_2^{(1)}(i), \ldots, \widehat{\mathbf{Z}}_2^{(Q)}(i)\right]$;
- Determine $\mathbf{T}^{(q)}(i)$ from $\widehat{\mathbf{Z}}_2^{(q)}(i)$ (subspace method);
- $\widehat{\mathbf{S}}^{(q)}(i) = \widehat{\mathbf{Z}}_2^{(q)}(i)[\widehat{\mathbf{T}}^{(q)}(i)]^{-1}$;
- $\widehat{\mathbf{s}}^{(q)}(i) =$*Average over the columns of* $\widehat{\mathbf{S}}^{(q)}(i)$;
- $\widetilde{\mathbf{s}}^{(q)}(i) = \text{proj}\left(\widehat{\mathbf{s}}^{(q)}(i)\right)$;
- $\widehat{\mathbf{Z}}_2^{(q)}(i) = \text{Toeplitz}\ \left(\widetilde{\mathbf{s}}^{(q)}(i)\right)$;

end q

tensor can be obtained from the following equation:

$$e_i = \left\| \mathbf{X}_1 - \left(\widehat{\mathbf{Z}}_3(i) \diamond \widehat{\mathbf{Z}}_1(i)\mathbf{\Psi}\right)\left(\widehat{\mathbf{Z}}_2(i)\mathbf{\Phi}\right)^T \right\|_F . \tag{2.66}$$

We declare convergence at the i-th iteration when $|e_i - e_{i-1}| \leq 10^{-5}$.

2.6.2 Simulation results

In this section, the performance of the proposed tensor-based blind multiuser receiver is evaluated through computer simulations. Each obtained result is an average over $R = 1000$ independent Monte Carlo runs. For each run, multipath fading gains are generated from an i.i.d. Rayleigh generator while the user symbols are generated from an i.i.d. distribution and are modulated using binary-phase shift keying (BPSK). Perfect synchronization is assumed at the receiver. In all cases, a block of $N = 100$ received samples is used in the blind estimation process. The channel impulse response follows a raised cosine pulse shape with roll-off factor 0.35. We consider $I = 2$ channel taps, $Q = 2$ users and a fixed oversampling factor $P = 8$. At the beginning of the algorithm $\widehat{\mathbf{Z}}_1^{(0)}$ and $\widehat{\mathbf{Z}}_3^{(0)}$ are randomly initialized. More sophisticated initialization strategies exist, which are based on Tucker-3 compression [131] or on eigenanalysis [130], but they are beyond the scope of this thesis. We have observed however that convergence of the estimates is rapidly achieved (within 10 ALS iterations in most of cases), and this is attributed to the use of the FA property within the ALS loops.

BER calculation

We adopt the following criterion for the Bit-Error-Rate (BER) calculation. 1% of the total number of runs are discarded, corresponding to inevitable bad runs that reach a local minimum. The criterion for selecting the bad runs is based on the observation of the steady state estimation error, i.e., the error between the received tensor and the tensor reconstructed from estimated components matrices after convergence. The runs with the highest error values are discarded from the BER averaging process. For the bit-error-rate (BER) *versus* signal-to-noise ratio (SNR) results, the BER shown is the BER averaged over both users and R independent runs, i.e.:

$$\mathrm{BER} = \frac{1}{R}\sum_{r=1}^{R}\frac{\mathrm{BER}_1(r)+\mathrm{BER}_2(r)}{2},$$

where $\mathrm{BER}_1(r)$ and $\mathrm{BER}_2(r)$ are the BER of the first and second users at the r-th run, respectively.

Propagation scenarii

We adopt the multipath propagation model described in Section 2.2 and consider $L = 2$ effective multipaths per user, each path being associated with a different cluster of scatterers. Cluster angle spreads are the same for both users and are given by $(\Delta\theta_{1q}, \Delta\theta_{2q}) = (0^\circ, 5^\circ)$, $q = 1, 2$. Concerning the mean angle of arrival, we consider two propagation scenarii. In the first one, we have $(\theta_{11}, \theta_{21}) = (0^\circ, 20^\circ)$ for the first user and $(\theta_{12}, \theta_{22}) = (-10^\circ, 10^\circ)$ for the second one. The second propagation scenario is more challenging. The mean angle of arrival of the first (zero-delayed) path of both users is identical, and we have $\theta_{11} = \theta_{12} = 0^\circ$, while the other multipaths have the same angles as those of the first scenario. All multipaths have the same average power $E[\beta_{lq}\beta_{lq}^*] = 1$, $l = 1, \ldots, L$, $q = 1, \ldots, Q$.

Performance results

We begin by evaluating the convergence of the proposed PARAFAC-Subspace algorithm. Figure 2.4 shows typical convergence curves, considering the first propagation scenario. The median values of the normalized error $e_i^2/(MPN)$, where e_i is given in (2.66), are plotted as a function of the iterations for various SNR values. It can be seen from Fig. 2.4 that the algorithm rapidly converges, usually

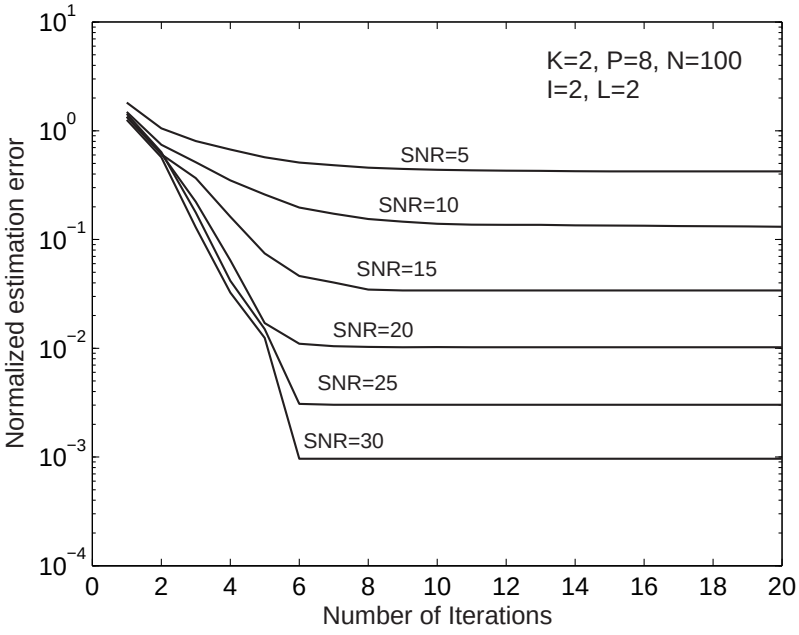

Figure 2.4: Convergence of the PARAFAC-Subspace receiver.

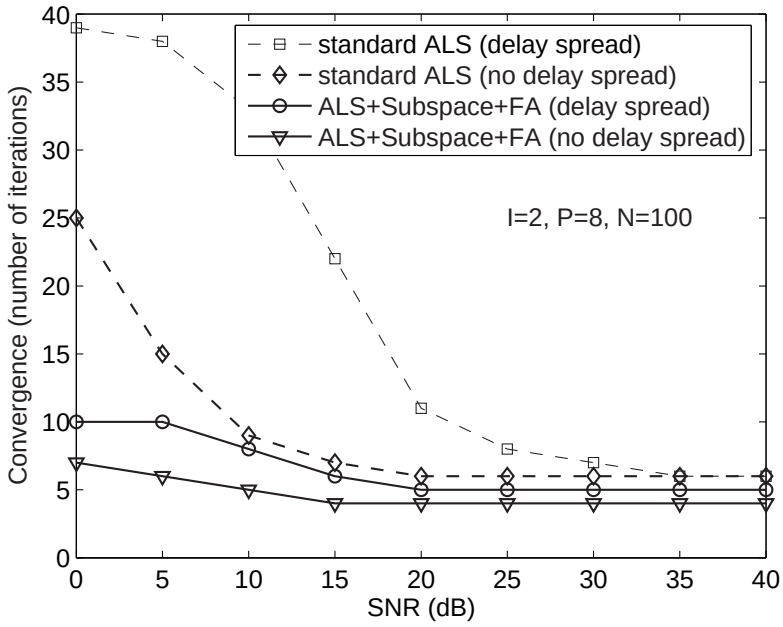

Figure 2.5: Convergence of ALS+Subspace+FA and standard ALS as a function of the SNR.

within 10 iterations. We have observed that convergence is actually accelerated due to the use of FA property within the ALS loops.

In Fig. 2.5, we compare the proposed algorithm with the standard ALS algorithm in terms of convergence speed. We plot the number of iterations for convergence as a function of the SNR. We consider two propagation scenarii, the first one with delay spread ($I = 2$) and the second one without delay spread ($I = 1$). We can observe that the proposed algorithm converges with fewer iterations than the standard ALS algorithm. In particular, note that the convergence of the standard ALS algorithm is more sensitive to the delay spread, in contrast to the proposed algorithm. The difference on the required number of iterations between both algorithms is more pronounced for low to medium SNR values.

The BER versus SNR results are evaluated considering the first scenario, where the users have distinct spatial signatures. In order to verify the influence of the multipath delay spread, we consider two cases. In the first one $(\tau_{1q}, \tau_{2q}) = (0, \tau) = (0, T)$, while in the second one $(\tau_{1q}, \tau_{2q}) = (0, \tau) = (0, 0.25T)$, $q = 1, 2$. The results are shown in Figure 2.6, for $K = 2$ and 4 receive antennas. It can be seen that the BER performance of the proposed receiver is remarkable, even with $K = 2$ receive antennas only. A significant performance gain is observed when the number of receive antennas is increased from 2 to 4, since more degrees of freedom are available in the space domain to separate the two user signals. Improved performance is obtained when $\tau = T$, i.e., when the delay of the second multipath (for both users) coincides with one symbol period. Multipath combination is more effective when $\tau = T$, since the multipaths are better distinguished in the time domain. Moreover, when $\tau = 0.25T$, some multipath energy is spread beyond $I = 2$ symbol periods and this is ignored in our tensor model.

We now consider the second propagation scenario, where the first path of both users have identical directions of arrival. We want to illustrate that in this type of scenario, path diversity becomes important and frequency-selectivity indeed helps the separability of the user signals in the time domain. In order to evaluate this, the average power of the second (one-symbol delayed) path of each user is varied. We define δ as the average ratio between the gain of the second and first multipaths, which are assumed equal for both users. We consider $\delta = 0.1, 0.25, 0.5$ and 1. According to Figure 2.7, improved performance is obtained when the first and second paths have the same average power, i.e., $\delta = 1$. In this case, the path diversity gain is maximum. The worst result is obtained with $\delta = 0.1$ (nearly flat-fading channel). These results indicate that the proposed PARAFAC-Subspace receiver effectively combines the multipaths of each user to provide a path diversity gain, being able to blindly separate the two user signals.

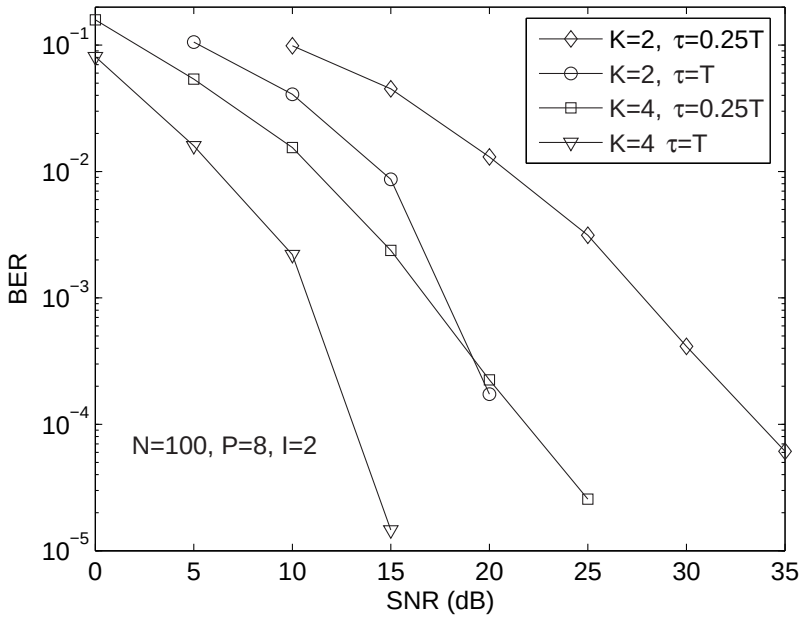

Figure 2.6: BER versus SNR results. First propagation scenario.

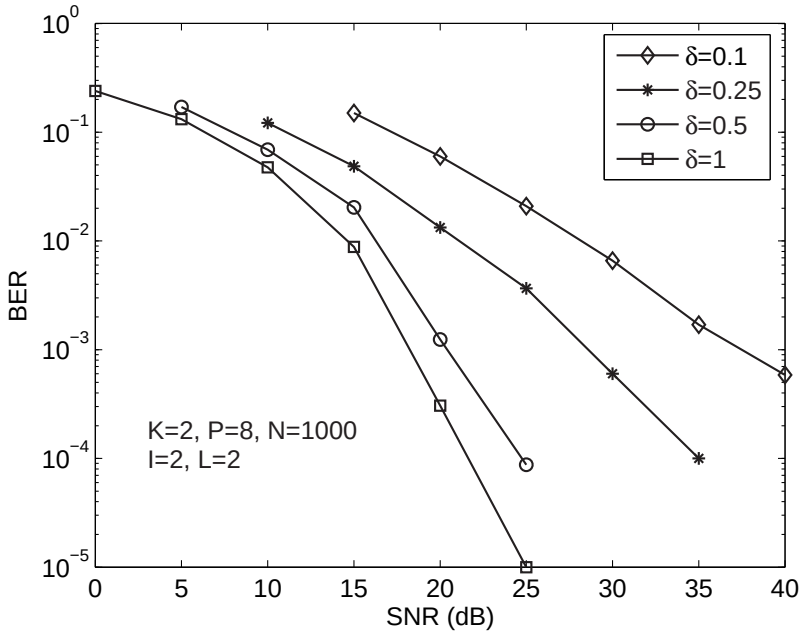

Figure 2.7: BER versus SNR results. Second propagation scenario.

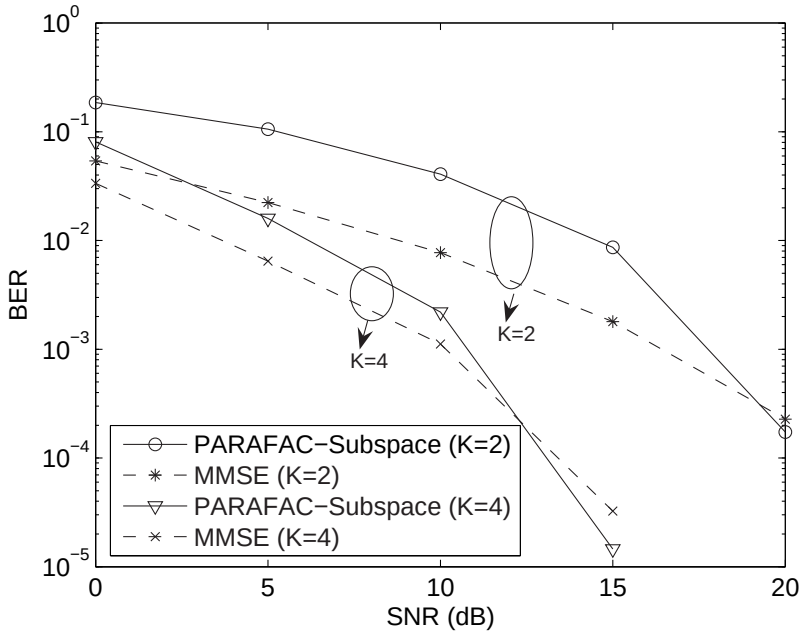

Figure 2.8: Blind PARAFAC-Subspace receiver versus MMSE receiver with perfect channel knowledge.

In order to provide a performance reference for the proposed PARAFAC-Subspace receiver, we also evaluate the performance of the Minimum Mean Square Error (MMSE) receiver. In contrast to our blind iterative PARAFAC-Subspace receiver, the MMSE one assumes perfect knowledge of all channel parameters as well as the knowledge of the SNR. We consider $K = 2$ and 4 receive antennas. Figure 2.8 shows that the PARAFAC-Subspace receiver has nearly the same BER vs. SNR improvement than that of MMSE with perfect channel knowledge. The gap between both receivers is smaller for $K = 4$. For example, considering a target BER of 10^{-2}, the proposed receiver provides a loss in performance of 5dB for $K = 2$ and 3dB for $K = 4$, with respect to the MMSE receiver.

In the next experiment, we consider $Q = 2$ users, $I = 3$, $L^{(1)} = 2$, $L^{(2)} = 3$, $N = 50$, $P = 12$ and $K = \{2, 3\}$. The angles-of-arrival and the time-delays are described in Table 2.5. Figure 2.9 shows that the performance of source 2 is better than that of source 1. Indeed, the signal from source 2 is received via $L^{(2)} = 3$ paths (against $L^{(2)} = 2$ paths for source 1), thus achieving a higher path diversity gain. Performance is also improved for both users, when the number of receive antennas is increased. The figure also shows the performance of the non-blind MMSE receiver which assumes perfect knowledge of $\mathbf{A}$ and $\mathbf{H}$ for source 2 with $K = 3$. The performance loss of the proposed receiver with respect to the MMSE

one is 3dB for a BER of 10^{-2}.

Table 2.5: Multipath parameters for the simulated scenario.

	angles-of-arrival	time-delays
Source 1	$(-50°, -20°)$	$(0, T)$
Source 2	$(0°, 30°, 50°)$	$(0, 0.2T, T)$

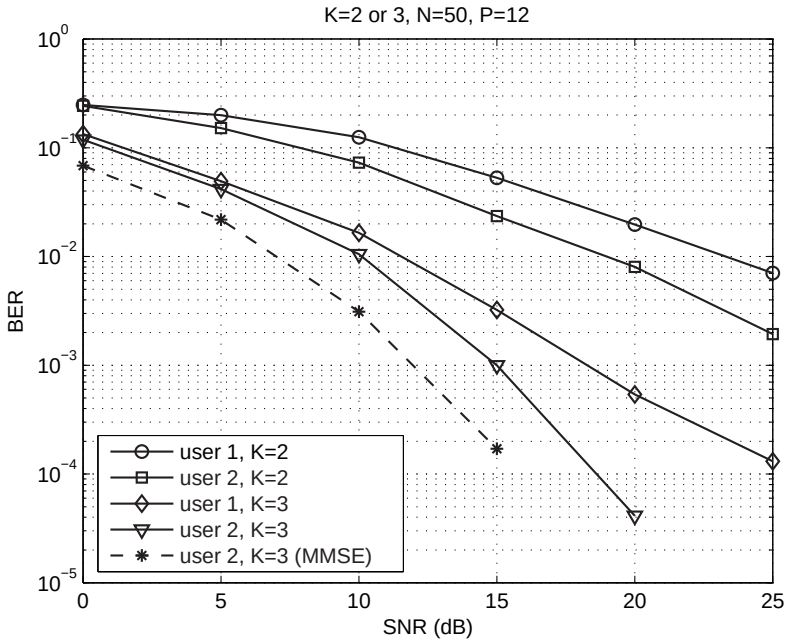

Figure 2.9: Receiver performance for two users with different number of multipaths.

2.7 Summary

This chapter has proposed a new tensor modeling approach for the received signal in three wireless communication systems, namely, the oversampled, DS-CDMA and OFDM systems. The tensor models assume frequency-selective channel with multipath propagation characterized by a few dominant paths. The first and second dimensions of the received signal is common for the three systems, while the third-dimension is associated with *oversampling*, *spreading* or *frequency*. We have seen that the received signal tensor in each of these systems can be unified by means of the block-constrained PARAFAC decomposition.

A generalization of this unified model has been presented by considering that the number of paths of each user can be different. The formulation of this generalized model is based on a constrained Tucker-3 model. Based on the generalized model, two practical multipath propagation scenarii have been considered, namely, far-field reflections without angular spread and local scattering with small delay spread.

A blind receiver based on the proposed tensor model has been presented for multiuser separation/equalization under the assumption of frequency-selective fading and in the oversampled case. The proposed receiver is deterministic, and does not require the use of training sequences, nor the knowledge of the channel impulse responses and antenna array responses. The IPSP receiver iteratively combines the ALS algorithm (for multiuser separation in the tensor space) with a subspace method (for single-user equalization in the matrix space). The FA property of the transmitted symbols is also used. The BER performance of this receiver has been evaluated for some propagation scenarii.

In the next two chapters, we will show that the block-constrained PARAFAC decomposition is also useful for modeling multiple-antenna systems with space-time spreading and multiplexing in the context of MIMO systems.

CHAPTER 3

Multiuser MIMO Systems Using Block Space-Time Spreading

In this chapter, we consider a point-to-multipoint downlink multiuser wireless communication system, where a multiple-antenna base station simultaneously transmits data to several users equipped with multiple receive antennas. The transmit antenna array is partitioned into transmission blocks, each one being associated with a given user. Space-time spreading is performed within each block using a transmit antenna subset. We formulate block space-time spreading using a tensor modeling. The space-time spreading structure is chosen to allow a deterministic MUltiuser Interference (MUI) elimination by each user. A block-constrained PARAFAC model is then presented for the received signal, where the fixed constraint matrices reveal the overall space-time spreading pattern used at the transmitter. The distinguishing feature of the space-time spreading model of this chapter, is the possibility of modeling a multiuser space-time transmission with different spatial spreading factors (diversity gains) as well as different multiplexing factors (code rates) for the users. Simulation results illustrate the performance of the proposed transceiver model in terms of bit-error-rate and link-level throughput.

3.1 Motivation and previous work

Several works have addressed the design of MIMO signaling techniques for multiuser multiple-access systems, especially in the downlink, by using space-time spreading in conjunction with DS/CDMA techniques (see e.g. [103, 56, 22, 57] and the references therein). By exploiting excess bandwidth, these approaches are generally based on the combination of linear space-time spreading codes and multiuser spatial multiplexing, and rely on linear multiuser detection at the receiver side to handle Multiuser Interference (MUI). [103] proposes a space-time multiplexing model that allows several users to simultaneously access all the spatial channels, by using mutually-orthogonal spreading codes for the transmit antennas. This idea is pursued in [56], by using different space-time multiplexing matrices (i.e. different 2-D spreading codes) for each user. In [22], space-time multiplexing and algebraic rotation are combined to yield full transmit diversity to each user. The receiver is based on linear multiuser detection followed by single-user sphere decoding. [57] proposes a space-time multiplexing model for the downlink of a Multiuser (MU) Space-Time (ST) MIMO system and a new spreading matrix structure. All these approaches assume that the channel is perfectly known at the transmitter (or it has been estimated using training sequences), and rely on the orthogonality properties of the spreading codes to handle MUI at the receiver. They also focus on suboptimal receiver structures as an alternative to Maximum Likelihood (ML) detection.

The use of tensor decompositions in MIMO antenna systems has been addressed in [129, 48, 32, 33] by focusing on single-user transmissions. In [48], a generalized tensor model for MIMO systems was proposed. However, this modeling approach only considers spatial multiplexing. The MIMO system model of [129] considers spreading of each data stream in the temporal dimension only, i.e., across consecutive chips. There is no spreading across the transmit antennas. In [32], we proposed a constrained tensor model for MIMO systems which allows spreading of each data stream across both space and time dimensions.

The proposed block-constrained tensor based MU-MIMO system can be viewed as a generalization of [129] and [24, 32] due to the fact that i) it is designed to cope with multiuser MIMO transmission and ii) it jointly performs space-time spreading and multiuser spatial multiplexing. The MU-MIMO framework proposed here is close to those of [103, 56, 57], which use space-time multiplexing codes for downlink MU-MIMO systems. Our block space-time spreading structure acts as a tridimensional (3-D) spreading sequence [39].

The tensor model presented in this chapter is more general than that of the pre-

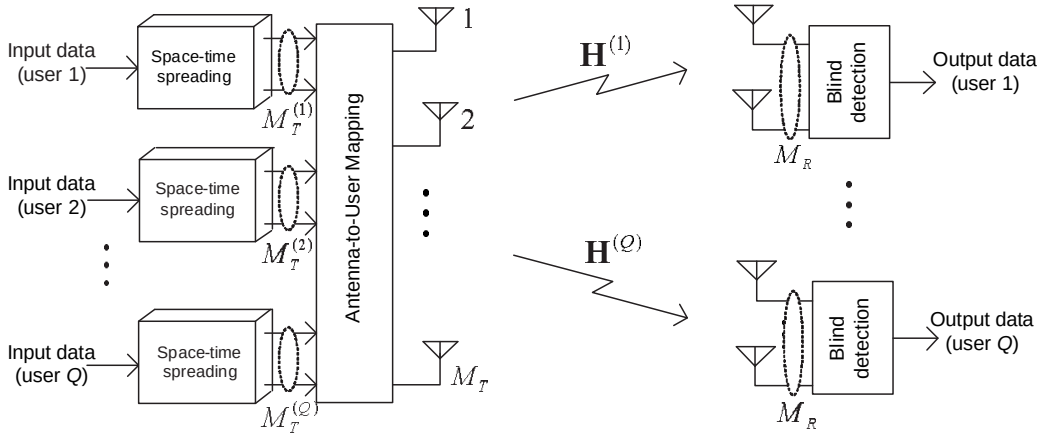

Figure 3.1: Block-diagram of the considered MU-MIMO system.

vious chapter in the sense that it allows constrained PARAFAC blocks with different interaction structure per block. We limit ourselves to a flat-fading channel model.

3.2 System model and assumptions

Let us consider the downlink of a multiuser MIMO wireless communication system where a multiple-antenna base station simultaneously transmits data to Q users equipped with multiple receive antennas. Let P denote the temporal spreading factor of the system. The base station is equipped with M transmit antennas, and the q-th user is equipped with K receive antennas, $q = 1, \ldots, Q$ (see Fig. 3.1). It is assumed that the base station has no knowledge of the downlink channels[1].

The transmission is organized into time-slots of N symbols, each one being composed of P chips. We assume that the wireless channel is characterized by scattering-rich propagation and is frequency-flat. The channel is also assumed to be constant during the time necessary to transmit a time-slot, but varies between two consecutive time-slots. For the q-th user, the discrete-time baseband version of the signal

[1]When *a priori* information of the users' channels is available at the transmitter, multiuser scheduling policies can be used to allocate the transmit antennas to the users. This is the role of the antenna-to-user mapping block shown in Fig. 3.1. Although interesting, we do not pursue the antenna allocation issue here by simply bypassing this stage.

received at the k-th receive antenna, associated with the p-th chip of the n-th transmitted symbol, can be written as:

$$x_k^{(q)}\big((n-1)P+p\big) = \sum_{m=1}^{M} h_{k,m}^{(q)}\, c_m\big((n-1)P+p\big),$$

$$n = 1, \ldots, N,\ p = 1, \ldots, P,$$

where $h_{k,m}^{(q)}$ is the complex channel gain between the m-th transmit and the k-th receive antenna and $c_m\big((n-1)P+p\big)$ is the $\big((n-1)P+p\big)$-th sample of the signal transmitted by the m-th transmit antenna. Let $\mathbf{H}^{(q)} \in \mathbb{C}^{K\times M}$ and $\mathbf{C}_n \in \mathbb{C}^{P\times M}$ denote the MIMO channel matrix and the transmitted signal matrix at the n-th symbol period. Let $h_{k,m}^{(q)} \doteq [\mathbf{H}^{(q)}]_{k,m}$ and $c_m\big((n-1)P+p\big) \doteq [\mathbf{C}_n]_{p,m}$ be the entries of these matrices. Taking these definitions into account, we can represent the noiseless received signal at the n-th symbol period by a $P \times K$ matrix $\mathbf{X}_n^{(q)}$, with $x_k^{(q)}\big((n-1)P+p\big) = [\mathbf{X}_n^{(q)}]_{p,k}$. This matrix can be expressed as:

$$\mathbf{X}_n^{(q)} = \mathbf{C}_n \mathbf{H}^{(q)T}, \quad n = 1, \ldots, N. \tag{3.1}$$

We assume that the channel matrix has i.i.d. entries following a zero-mean unit-variance complex-Gaussian distribution with $E[\mathrm{trace}(\mathbf{H}^{(q)}\mathbf{H}^{(q)H})] = MK$, where $\mathrm{trace}(\cdot)$ is the *trace* operator. We also have $E[\mathrm{trace}(\mathbf{C}_n\mathbf{C}_n^H)] = P_T$, ensuring that the total transmitted power P_T is maintained irrespective of M and P.

3.3 Block space-time spreading model

In this section, we describe the proposed transmitter/receiver model by using the tensor formalism [39]. We assume that the M transmit antennas are associated with Q transmission blocks of $M^{(i)}$ antennas each, $i = 1, \ldots, Q$. These Q transmission blocks are disjoint in the sense that they do not share a common transmit antenna. The total number of transmit antennas is then given by $M = M^{(1)} + \cdots + M^{(Q)}$. Each transmission block is associated with a different user to be served. At the i-th block, a serial input data stream is parsed into $R^{(i)}$ parallel streams, which are individually spread in the *space* and *time* domains over $M^{(i)}$ transmit antennas and P chips, respectively. After space-time spreading, these $R^{(i)}$ data streams are summed up at each transmit antenna to yield the coded signal tensor that is effectively transmitted. Let us denote the total number of multiplexed data streams by $R = R^{(1)} + \cdots + R^{(Q)}$. After serial-to-parallel conversion, the n-th symbol of the $r^{(i)}$-th data stream of the i-th transmission block is

given by:

$$s^{(i)}_{n,r^{(i)}} = s\big((r^{(i)}-1)N+n\big), \tag{3.2}$$

where $n = 1,\ldots,N$, $r^{(i)} = 1,\ldots,R^{(i)}$, $i = 1,\ldots,Q$. Let us define a symbol matrix concatenating these $R^{(i)}$ data streams as:

$$\mathbf{S}^{(i)} = [\mathbf{S}^{(i)}_{\cdot 1} \cdots \mathbf{S}^{(i)}_{\cdot R^{(i)}}] \in \mathbb{C}^{N\times R^{(i)}}, \tag{3.3}$$

where $\mathbf{S}^{(i)}_{\cdot r^{(i)}} = [s^{(i)}_{1,r^{(i)}} \cdots s^{(i)}_{N,r^{(i)}}]^T \in \mathbb{C}^{N\times 1}$, $i = 1,\ldots,Q$. The aggregate symbol matrix is defined as the concatenation of the Q symbol matrices:

$$\mathbf{S} = [\mathbf{S}^{(1)} \cdots \mathbf{S}^{(Q)}] \in \mathbb{C}^{N\times R}.$$

Due to the partitioning of the M transmit antennas into Q disjoint blocks, we can view the MIMO channel matrix $\mathbf{H}^{(q)}$ defined in Section 3.2 as a block-partitioned matrix:

$$\mathbf{H}^{(q)} = \Big[\mathbf{H}^{(q,\,1)} \cdots \mathbf{H}^{(q,\,Q)}\Big] \in \mathbb{C}^{K\times M}, \tag{3.4}$$

with $\mathbf{H}^{(q,\,i)} \in \mathbb{C}^{K\times M^{(i)}}$. Taking the above definitions into account, we can visualize the block space-time spreading process as a tensor transformation. Define $\mathcal{W}^{(i)} \in \mathbb{C}^{M^{(i)}\times P\times R^{(i)}}$ as the 3-D *spreading code tensor* having three dimensions: the first one is equal to the number of transmit antennas $M^{(i)}$, the second one defines the temporal spreading factor P, while the third one is equal to the number of multiplexed data sub-streams $R^{(i)}$. Space-time spreading is formulated as:

$$\mathcal{W}^{(i)} : \mathbf{S}^{(i)} \to \mathcal{C}^{(i)}, \quad i = 1,\ldots,Q, \tag{3.5}$$

where $\mathcal{C}^{(i)} \in \mathbb{C}^{M^{(i)}\times N\times P}$ is a tensor collecting the coded signals over $M^{(i)}$ transmit antennas, N symbols and P chips/symbol, associated with the i-th space-time spreading block.

3.3.1 Scalar writing

The block space-time spreading model can be written in scalar form. Defining $w^{(i)}_{m^{(i)},r^{(i)},p}$ and $c^{(i)}_{m^{(i)},n,p}$ as the entries of $\mathcal{W}^{(i)}$ and $\mathcal{C}^{(i)}$, respectively, we have:

$$c^{(i)}_{m^{(i)},n,p} = \sum_{r^{(i)}=1}^{R^{(i)}} s^{(i)}_{n,r^{(i)}} w^{(i)}_{m^{(i)},r^{(i)},p}, \quad i = 1,\ldots,Q. \tag{3.6}$$

Note that the transmitted signal tensor is given by a linear combination of $R^{(i)}$ signal contributions. Let $h^{(q,i)}_{k,m^{(i)}}$ be the channel gain between the $m^{(i)}$-th transmit antenna and the k-th receive antenna of the q-th user. The discrete-time baseband signal received by the q-th user is a third-order tensor $\mathcal{X}^{(q)} \in \mathbb{C}^{K \times N \times P}$ with typical element $x^{(q)}_{k,n,p}$ representing the signal received by the k-th receive antenna of the q-th user, associated with the n-th symbol and p-th chip. In absence of noise, $x^{(q)}_{k,n,p}$ can be written as:

$$\begin{aligned} x^{(q)}_{k,n,p} &= \sum_{i=1}^{Q} x^{(q,\,i)}_{k,n,p} = \sum_{i=1}^{Q} \sum_{m^{(i)}=1}^{M^{(i)}} h^{(q,i)}_{k,m^{(i)}} c^{(i)}_{m^{(i)},n,p} \\ &= \sum_{i=1}^{Q} \sum_{m^{(i)}=1}^{M^{(i)}} \sum_{r^{(i)}=1}^{R^{(i)}} h^{(q,i)}_{k,m^{(i)}} s^{(i)}_{n,r^{(i)}} w^{(i)}_{m^{(i)},r^{(i)},p} \end{aligned} \tag{3.7}$$

Figure 3.2 illustrates the proposed block space-time spreading MU-MIMO system, where $\mathcal{W}^{(i)}$ is interpreted as a 3-D spreading code for multiple data streams and multiple transmit channels.

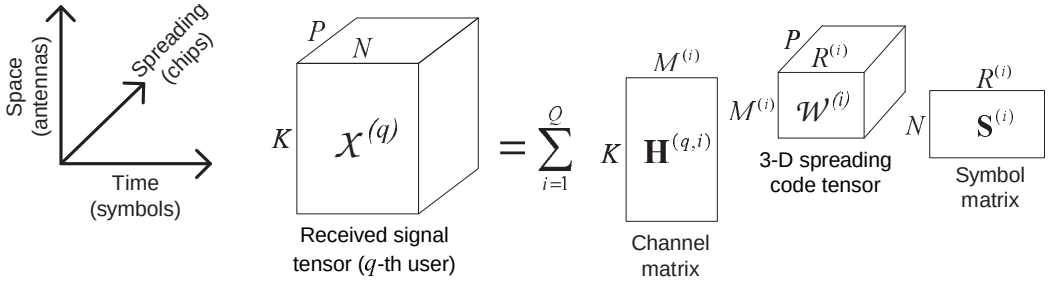

Figure 3.2: Decomposition of the received signal tensor (q-th user) in absence of noise.

Generalization to frequency-selective channels using MIMO-OFDM

The generalization of the proposed model to frequency-selective channel is straightforward under certain assumptions by considering OFDM [33]. In a MIMO-OFDM system, the R data streams are spread over an $M^{(i)} \times P \times F$ space-time-frequency grid associated with $M^{(i)}$ transmit antennas, P OFDM symbols and F subcarriers, and then linearly combined. The resulting signal at each transmit antenna is parsed into blocks of N_c symbols, and an Inverse Fast Fourier Transform (IFFT) is applied to each block followed by the insertion of a Cyclic Prefix (CP) before

transmission. It is assumed that the Q transmission blocks use the same set of subcarriers at the same time. After baseband conversion, the CP is removed and Fast Fourier Transform (FFT) is applied at each receive antenna. Perfect timing and synchronization are assumed at the receiver. We suppose that the frequency selective fading channels between each pair of transmit and receive antennas have L independent delay paths and the same power-delay profile. It is also assumed that all path gains are constant over the N time-slots.

From the assumption of subcarrier orthogonality, the overall system is modeled as N_c/F parallel sub-systems of F subcarriers each. In order to benefit from the frequency diversity, the F frequencies can be taken N_c/L apart or more.

The received signal model is similar to (3.7), and the main difference is the presence of the frequency-dependent index f, which adds a fourth dimension to the received signal tensor. In absence of noise, the received signal is given by:

$$x^{(q)}_{f,k,n,p} = \sum_{i=1}^{Q} \sum_{m^{(i)}=1}^{M^{(i)}} \sum_{r^{(i)}=1}^{R^{(i)}} h^{(q,i)}_{f,k,m^{(i)}} s^{(i)}_{n,r^{(i)}} w^{(i)}_{m^{(i)},r^{(i)},p},$$

where $x^{(q)}_{f,k,n,p}$ is the q-th user received signal at the k-th receive antenna, f-th subcarrier, p-th OFDM symbol and n-th time-slot. $x_{f,k,n,p}$ is a $F \times K \times N \times P$ fourth-order tensor. We are interested in working with an equivalent third-order tensor of dimensions $FK \times N \times P$ obtained by concatenating the space and frequency dimensions into one dimension. The unfolded representations of the received signal also follow a block-constrained PARAFAC model, and are similar to those of the flat-fading case. For further details, we refer to [33].

3.3.2 Matrix writing

Model (3.6)-(3.7) admits an equivalent matrix writing. Let us define $\mathbf{W}^{(i)}_{m^{(i)}..} \in \mathbb{C}^{R^{(i)} \times P}$ as the $m^{(i)}$-th slice of the spreading code tensor $\mathcal{W}^{(i)}$. This matrix models the joint temporal spreading and spatial multiplexing of $R^{(i)}$ data streams at the $m^{(i)}$-th transmit antenna. Let us define:

$$\mathbf{C}^{(i)}_{.n.} = \begin{bmatrix} c^{(i)}_{1,n,1} & \cdots & c^{(i)}_{M^{(i)},n,1} \\ \vdots & & \vdots \\ c^{(i)}_{1,n,P} & \cdots & c^{(i)}_{M^{(i)},n,P} \end{bmatrix} \in \mathbb{C}^{P \times M^{(i)}}, \tag{3.8}$$

as a n-th second-mode matrix slice of the transmitted signal tensor $\mathcal{C}^{(i)} \in \mathbb{C}^{M^{(i)} \times N \times P}$, containing the received signal samples associated with the n-th symbol. We can rewrite (3.6) as:

$$\begin{aligned} \mathbf{C}^{(i)}_{\cdot n \cdot} &= \left[\left(\mathbf{S}^{(i)}_{n \cdot} \mathbf{W}^{(i)}_{1 \cdot \cdot} \right)^T, \ldots, \left(\mathbf{S}^{(i)}_{n \cdot} \mathbf{W}^{(i)}_{M^{(i)} \cdot \cdot} \right)^T \right] \\ &= \left[\mathbf{W}^{(i)T}_{1 \cdot \cdot}, \ldots, \mathbf{W}^{(i)T}_{M^{(i)} \cdot \cdot} \right] \begin{bmatrix} \mathbf{S}^{(i)T}_{n \cdot} & & \\ & \ddots & \\ & & \mathbf{S}^{(i)T}_{n \cdot} \end{bmatrix}, \end{aligned} \tag{3.9}$$

i.e.

$$\mathbf{C}^{(i)}_{\cdot n \cdot} = \mathbf{W}^{(i)} \big(\mathbf{I}_{M^{(i)}} \otimes \mathbf{S}^{(i)T}_{n \cdot} \big), \tag{3.10}$$

where

$$\mathbf{S}^{(i)}_{n \cdot} = \left[s^{(i)}_{n,1} \cdots s^{(i)}_{n,R^{(i)}} \right] \in \mathbb{C}^{1 \times R^{(i)}},$$

and

$$\mathbf{W}^{(i)} = \left[\mathbf{W}^{(i)T}_{1 \cdot \cdot}, \ldots, \mathbf{W}^{(i)T}_{M^{(i)} \cdot \cdot} \right] \in \mathbb{C}^{P \times M^{(i)} R^{(i)}}$$

is a *space-time spreading matrix*. This matrix is linked to the spreading tensor $\mathcal{W}^{(i)} \in \mathbb{C}^{M^{(i)} \times R^{(i)} \times P}$ by:

$$[\mathbf{W}^{(i)}]_{p,(m^{(i)}-1)R^{(i)}+r^{(i)}} = w^{(i)}_{m^{(i)},r^{(i)},p}. \tag{3.11}$$

Substituting (3.10) into (3.1) and using (3.4), the signal received by the q-th user from the $M^{(i)}$ transmit antennas corresponding to the i-th space-time spreading block, is given by:

$$\mathbf{X}^{(q,i)}_{\cdot n \cdot} = \mathbf{C}^{(i)}_{\cdot n \cdot} \mathbf{H}^{(q,i)T} = \mathbf{W}^{(i)} \big(\mathbf{I}_{M^{(i)}} \otimes \mathbf{S}^{(i)T}_{n \cdot} \big) \mathbf{H}^{(q,\,i)T}. \tag{3.12}$$

The overall signal received by the q-th user is then written as:

$$\begin{aligned} \mathbf{X}^{(q)}_{\cdot n \cdot} &= \sum_{i=1}^{Q} \mathbf{X}^{(q,i)}_{\cdot n \cdot} \\ &= \sum_{i=1}^{Q} \mathbf{W}^{(i)} \big(\mathbf{I}_{M^{(i)}} \otimes \mathbf{S}^{(i)T}_{n \cdot} \big) \mathbf{H}^{(q,\,i)T}. \end{aligned} \tag{3.13}$$

Figure 3.3 illustrates the overall signal transmission/reception scheme in absence of noise, by focusing on the link between the i-th space-time spreading block and the q-th user.

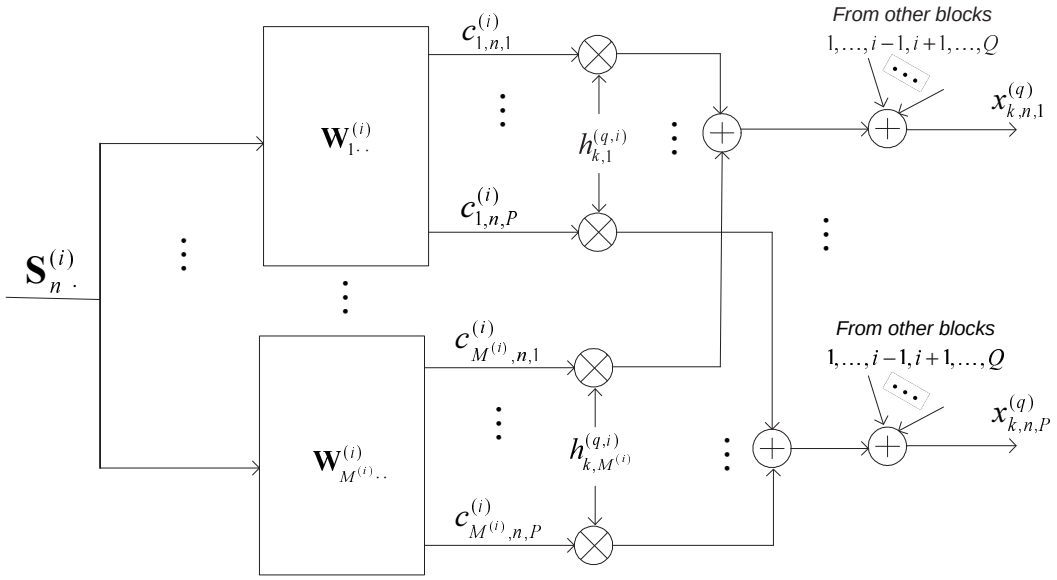

Figure 3.3: Signal transmission/reception model linking the i-th transmission block to the k-th receive antenna of the q-th user.

Let us define an aggregate transmitted signal matrix $\mathbf{C}_{\cdot n \cdot} \in \mathbb{C}^{P \times M}$ and an aggregate spreading matrix $\mathbf{W} \in \mathbb{C}^{P \times R_M}$ concatenating the Q users contributions as:

$$\mathbf{C}_{\cdot n \cdot} = \left[\mathbf{C}^{(1)}_{\cdot n \cdot}, \ldots, \mathbf{C}^{(Q)}_{\cdot n \cdot} \right], \quad \mathbf{W} = \begin{bmatrix} \mathbf{W}^{(1)} \\ \vdots \\ \mathbf{W}^{(Q)} \end{bmatrix}, \tag{3.14}$$

where

$$R_M = \sum_{i=1}^{Q} R^{(i)} M^{(i)} = \sum_{i=1}^{Q} R^{(i)}_M.$$

Note that $\mathbf{C}_{\cdot n \cdot}$ corresponds to the $\mathbf{C}_n$ matrix defined in Section 3.2, now interpreted as a concatenation of Q blocks. Using the partitioned forms (3.4) and (3.14) of $\mathbf{H}^{(q)}$ and $\mathbf{C}_{\cdot n \cdot}$, the received signal matrix $\mathbf{X}^{(q)}_{\cdot n \cdot}$ given in (3.13) can be written as:

$$\mathbf{X}^{(q)}_{\cdot n \cdot} = \mathbf{C}_{\cdot n \cdot} \mathbf{H}^{(q)T} = \mathbf{W} \overline{\mathbf{S}}_n \mathbf{H}^{(q)T}, \tag{3.15}$$

where

$$\mathbf{C}_{\cdot n\cdot} = \mathbf{W}\begin{bmatrix} \left(\mathbf{I}_{M^{(1)}} \otimes \mathbf{S}_{n\cdot}^{(1)T}\right) & & \\ & \ddots & \\ & & \left(\mathbf{I}_{M^{(Q)}} \otimes \mathbf{S}_{n\cdot}^{(Q)T}\right) \end{bmatrix}, \tag{3.16}$$

$\overline{\mathbf{S}}_n \in \mathbb{C}^{R_M \times M}$ being an aggregate block-diagonal symbol matrix.

3.3.3 Relation with the Khatri-Rao coding model [129]

In [129] a space-time encoding technique based on the properties of the Khatri-Rao product was proposed for single-user MIMO antenna systems. In the Khatri-Rao Space-Time (KRST) coding model, each transmit antenna transmits a single data stream which is spread in the temporal domain (i.e. across P chips). Let us see that model (3.15) includes the KRST coding model [129] as a special case. By setting $M^{(i)} = R^{(i)} = 1$, $i = 1, \ldots, Q$, we have $M = R = Q$. In this particular case, model (3.15) can be viewed as a single-user MIMO system transmitting Q data streams using Q transmit antennas. Then, (3.10) is reduced to the following form:

$$\mathbf{C}_{\cdot n}^{(i)} = \begin{bmatrix} w_1^{(i)} \\ \vdots \\ w_P^{(i)} \end{bmatrix} s_n^{(i)},$$

so that (3.13) simplifies to:

$$\mathbf{X}_{\cdot n\cdot}^{(q)} = \sum_{i=1}^{Q} \mathbf{w}^{(i)} s_n^{(i)} \mathbf{h}^{(q,\,i)T} = \mathbf{W}\mathrm{diag}(\mathbf{S}_{n\cdot})\mathbf{H}^{(q)T} = \mathbf{W} D_n(\mathbf{S})\mathbf{H}^{(q)T}, \tag{3.17}$$

where

$$\begin{aligned} \mathbf{H}^{(q)} &= \left[\mathbf{h}^{(q,\,1)} \cdots \mathbf{h}^{(q,\,Q)}\right] \in \mathbb{C}^{K \times Q}, \\ \mathbf{S}_{n\cdot} &= \left[s_n^{(1)} \cdots s_n^{(Q)}\right] \in \mathbb{C}^{1 \times Q}, \\ \mathbf{W} &= \left[\mathbf{w}^{(1)} \cdots \mathbf{w}^{(Q)}\right] \in \mathbb{C}^{P \times Q}, \end{aligned}$$

are the channel, symbol and code matrices. Comparing (3.13) with (3.17), we can see that the proposed space-time spreading model can be viewed as a generalized KRST coding model where the data streams are also spread in the spatial domain, i.e. across the transmit antennas.

3.3.4 Relation with the ST spreading model [32]

In [32], a space-time spreading model was proposed using tensor modeling. This model is similar to the present one in the sense that each data stream is spread across several antennas and chips. It can be obtained from (3.15) by setting $Q = 1$ (single-user/single-block system) with $M^{(1)} = M$. The proposed block space-time spreading model generalizes [32] by considering multiuser block transmission with different space-time spreading patterns for the users/blocks. As will be detailed in Section 3.4, a distinguishing feature of the block space-time spreading model is its flexibility to share multiplexing (data-rate) and spatial spreading (transmit diversity) among the different blocks (when $Q \geq 2$).

3.3.5 Relation with LD coding [76]

The principle of block space-time spreading is similar to that of Linear Dispersion (LD) coding. Both approaches propose to transmit multiple data streams in linear combinations over space and time. In principle, the proposed approach can be viewed as a sort of LD coding formulated using tensor notation. However, both approaches differ in some aspects. In LD coding, space-time signal design is based on numerical optimization with mutual information as the objective function. LD coding does not necessarily provide full diversity and assumes accurate channel estimation using training sequences. The proposed block space-time spreading also provides different data rates and diversity gains, and has the distinguishing feature of allowing a blind joint channel and symbol recovery.

3.4 Performance analysis

We apply the rank criterion for space-time code design [142] to the equivalent matrix model (3.16) for performance analysis in terms of diversity gain. Suppose that the joint Maximum Likelihood (ML) decoding is performed at the receiver to recover $\mathbf{C}_{\cdot n \cdot}$ using perfect channel knowledge. Consider an erroneous decoding leading to an estimation of the transmitted signal matrix $\mathbf{C}'_{\cdot n \cdot}$, with $\mathbf{C}_{\cdot n \cdot} \neq \mathbf{C}'_{\cdot n \cdot}$. The pairwise error probability can be upper bounded by [142]:

$$P(\mathbf{C}_{\cdot n \cdot} \rightarrow \mathbf{C}'_{\cdot n \cdot}) \leq \left(\frac{2\nu - 1}{\nu}\right) \left(\prod_{i=1}^{\nu} \lambda_i\right)^{-1} \left(\frac{\mathrm{SNR}}{M}\right)^{-\nu},$$

where ν is given by:

$$\nu = r_{\mathbf{E}_n} = r_{(\mathbf{C}_{\cdot n \cdot} - \mathbf{C}'_{\cdot n \cdot})},$$

$\lambda_1, \ldots, \lambda_\nu$ are the nonzero eigenvalues of $\mathbf{E}_n$. Full transmit diversity gain is obtained when $\mathbf{E}_n$ is full-rank, i.e. $\nu = r_{\mathbf{E}_n} = \min(P, M)$, for all $\mathbf{C}_{\cdot n \cdot} \neq \mathbf{C}'_{\cdot n \cdot}$. Using (3.15), we have:

$$\mathbf{E}_n \;=\; \mathbf{C}_{\cdot n \cdot} - \mathbf{C}'_{\cdot n \cdot} = \mathbf{W}\big(\overline{\mathbf{S}}_n - \overline{\mathbf{S}}'_n\big). \tag{3.18}$$

In our analysis, we must ensure that $\overline{\mathbf{S}}_n - \overline{\mathbf{S}}'_n$ is full rank. From (3.16)), this requires that $\mathbf{S}_{n\cdot}^{(i)} - \mathbf{S}_{n\cdot}^{(i)'}$ contains no zeros, for all $\mathbf{S}_{n\cdot}^{(i)} \neq \mathbf{S}_{n\cdot}^{(i)'}$. This holds if appropriate linear precoding over the symbol vectors $\mathbf{S}_{n\cdot}^{(1)}, \ldots, \mathbf{S}_{n\cdot}^{(Q)}$ is used [21, 155, 59, 94]. The use of linear precoding by means of constellation rotation is important to ensure maximum diversity gain in MIMO systems with space-time coding. These constructions are generally based either on algebraic number-theoretic constructions or on exhaustive computer search. This issue is beyond the scope of this work and is not addressed here.

Under the assumption that $\overline{\mathbf{S}}_n - \overline{\mathbf{S}}'_n$ is full rank, the diversity gain, denoted by ν, is upper-bounded by:

$$K \min(P, M).$$

In frequency-selective channels and assuming $F > L$, the diversity gain is given by:

$$\nu \leq KL \min(P, M). \tag{3.19}$$

In the MIMO-OFDM case, the overall rate is given by:

$$\text{Rate} = \left(\frac{QR}{PF}\right) \cdot \log_2(\mu) \text{ bits/channel use.} \tag{3.20}$$

3.4.1 Design requirement and spreading structure

In order to achieve an aggregate transmit diversity gain of order M, we must have $\text{rank}(\mathbf{E}_n) = \text{rank}(\overline{\mathbf{S}}_n - \overline{\mathbf{S}}'_n) = M$, which implies that the spreading matrix $\mathbf{W}$ must be *full column rank*, i.e.:

$$P \geq \sum_{i=1}^{Q} R^{(i)} M^{(i)} = \sum_{i=1}^{Q} R_M^{(i)} = R_M. \tag{3.21}$$

Note that this design requirement relates the temporal spreading factor P to both the spatial spreading and multiplexing factors $\{M^{(i)}, R^{(i)}\}$, $i = 1, \ldots, Q$. We choose the spreading matrix $\mathbf{W}$ as the following Vandermonde matrix [129]:

$$[\mathbf{W}]_{p,r'} = \frac{1}{\sqrt{P}} \cdot e^{j\frac{2\pi(p-1)}{P}(r'-1)}, \quad p = 1, \ldots, P, \quad r' = 1, \ldots, R_M.$$

Note that $\mathbf{W}$ is a full rank semi-unitary matrix which satisfies the following conditions:

$$\mathbf{W}^H\mathbf{W} = \mathbf{I}_{R_M}.$$

This structure of $\mathbf{W}$ has the attractive feature of allowing MUI elimination deterministically at the receiver, provided that all the receivers have knowledge of their corresponding spreading matrix [94]. Moreover, the chosen structure allows to control the number of transmit antennas $M^{(i)}$ as well as the number of multiplexed data-streams $R^{(i)}$ by simple truncation of $\mathbf{W}$. Using this Vandermonde structure can be beneficial when the channel matrix is rank-deficient (e.g. due to strong correlation of the spatial channels). In such a situation, an equivalent full rank channel matrix is created from the combination of the original (rank-deficient) channel matrix with the space-time spreading matrix. A similar structure is also considered for constructing the KRST coding model [129].

Remark: The spreading matrix $\mathbf{W}$ can, in principle, be any matrix satisfying the condition for full diversity and deterministic MUI elimination. For instance, $\mathbf{W}$ can be chosen as a Hadamard matrix associated with an orthogonal transformation existing for dimensions two and all dimensions multiple of 4, which satisfies $\mathbf{W}^T\mathbf{W} = \mathbf{I}_{R_M}$ up to a scalar factor [22]. In this case, our transmission model can be interpreted as a sort of space-time spreading DS/CDMA model, and is close in structure to those proposed in [103, 56, 57] with $\mathbf{W}$ being a matrix of spreading sequences of length $P = R_M$. It is to be noticed that the Hadamard transform is also used to design quasi-optimal constellation rotations in space-time coding [21], and has the property of reducing the peak to mean envelope power ratio [23].

3.4.2 Rate issues

Taking the above design requirement and spreading matrix structure into account, the rate of the proposed space-time spreading model can be calculated by using

the simple formula:

$$\rho^{(q)} = \left(\frac{R^{(q)}}{P}\right) \log_2(\mu) \ \text{(bits per channel use)}, \tag{3.22}$$

where μ is the modulation cardinality. Note that the Q data streams can share different rates, depending on their spatial spreading factors $\{M^{(q)}\}$ and multiplexing factors $\{R^{(q)}\}$, $q = 1, \ldots, Q$. Such a rate sharing characteristic comes from the design requirement (3.21) which establishes a lower bound for the spreading factor (which is common for all the users) function of the multiplexing factors (which can vary across users). Table 3.1 shows different rates (in bits per channel use) for $Q = 2$ and different values of $\{M^{(1)}, R^{(1)}\}$ and $\{M^{(2)}, R^{(2)}\}$. The users' rates are calculated using (3.22) considering 64-QAM modulation ($\mu = 64$) with $P = R_M$.

Table 3.1: User rates for different spatial spreading and multiplexing factors.

$\{M^{(1)}, R^{(1)}\}$; $\{M^{(2)}, R^{(2)}\}$	$\{\rho^{(1)}, \rho^{(2)}\}$	$\rho^{(1)}/\rho^{(2)}$
$\{2,1\}$; $\{1,1\}$	$\{2,2\}$	1
$\{2,2\}$; $\{1,1\}$	$\{2.4,1.2\}$	2
$\{2,1\}$; $\{1,2\}$	$\{1.5,3\}$	1/2
$\{2,1\}$; $\{2,1\}$	$\{1.5,1.5\}$	1
$\{2,2\}$; $\{2,1\}$	$\{2,1\}$	2
$\{2,3\}$; $\{2,1\}$	$\{2.25,0.75\}$	3
$\{3,1\}$; $\{1,1\}$	$\{1.5,1.5\}$	1
$\{3,3\}$; $\{1,1\}$	$\{1.8,0.6\}$	3
$\{3,1\}$; $\{1,2\}$	$\{1.2,2.4\}$	1/2

In order to illustrate the rate sharing characteristic of the proposed block space-time spreading model, let us consider a system with $Q = 2$ and $M = 2$. The modulation has cardinality $\mu = 16$. Assume that the space-time spreading blocks of both users have the same number of transmit antennas, i.e. $M^{(1)} = M^{(2)} = 1$. Figure 3.4 illustrates the theoretical (maximum) rate sharing between two users as the multiplexing factor $R^{(1)}$ of the first user is increased while that of the second one is fixed at $R^{(2)} = 1$ or 2. The rates are calculated using (3.22) with P satisfying the design requirement (3.21) in each case. First of all, note that the total rate $\rho^{(1)} + \rho^{(2)}$ is constant. The increase of $\rho^{(1)}$ comes at the expense of a decrease of $\rho^{(2)}$. The crossing of both rate curves occurs when $R^{(1)} = R^{(2)} = 1$ and 2. This figure suggests that the rate of the different space-time spreading blocks can be controlled by varying their multiplexing factors.

In Fig. 3.5, we show the influence of the number of transmit antennas on the achievable rate for fixed multiplexing factors $\{R^{(1)}, R^{(2)}\} = \{2,1\}$ and $\mu = 64$.

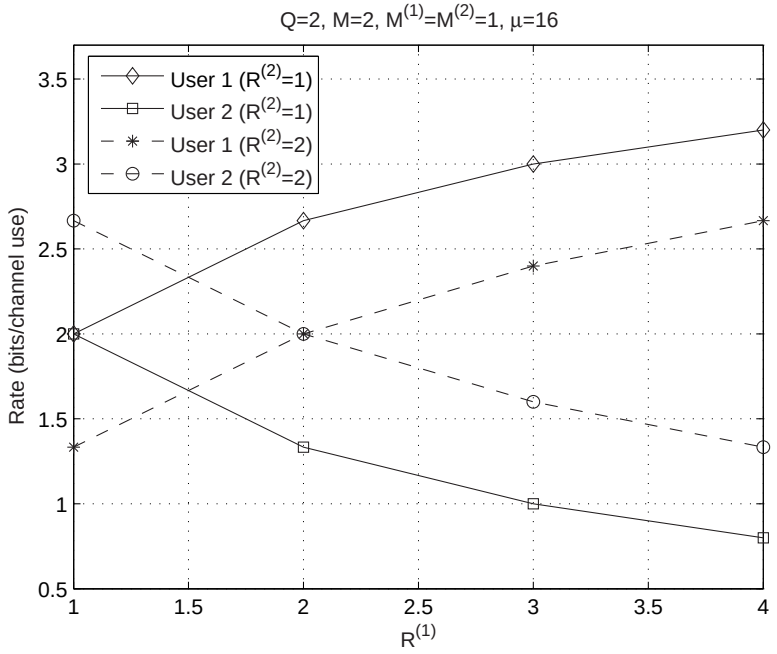

Figure 3.4: Rate sharing between two users.

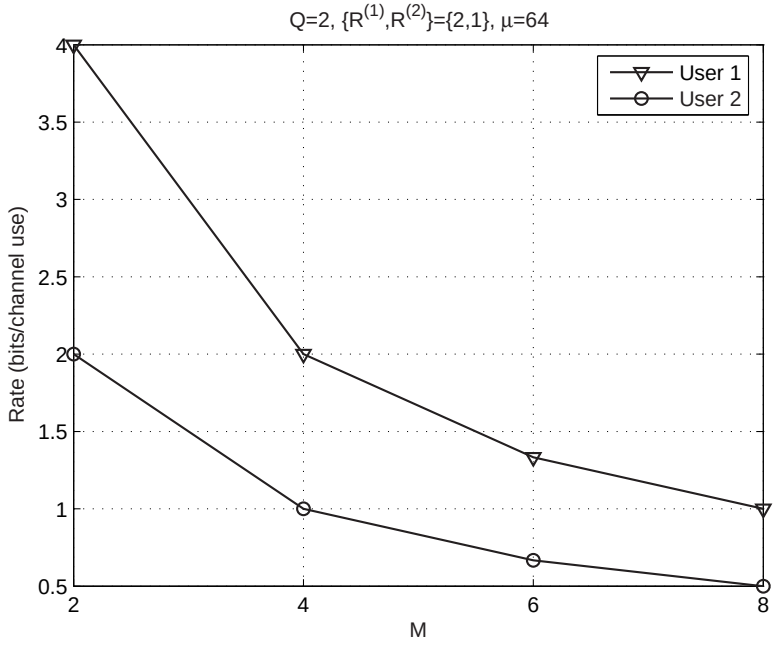

Figure 3.5: Rate *versus* number of antennas, for fixed multiplexing factors.

Users' space-time spreading blocks have the same number of transmit antennas. As the number of transmit antennas used for spatial spreading is increased (so is the transmit diversity gain), the achievable rate of both users is decreased. Such a rate decrease comes from the fact that P must be increased according to the number of transmit antennas in order to satisfy (3.21).

3.5 Block-constrained received signal model

We formulate the received signal tensor (3.7) in equivalent matrix forms associated with a block-constrained PARAFAC model. Moreover, we show how the constrained structure of this model is linked to the block space-time spreading pattern used at the transmitter.

Recall the scalar writing of the received signal model (3.7). By analogy with (1.48), and using (1.55), we can deduce the following correspondences:

$$(I_1, I_2, I_3, R_1^{(q)}, R_2^{(q)}, \mathbf{A}, \mathbf{B}, \mathbf{C}) \rightarrow (K, N, P, M^{(q)}, R^{(q)}, \mathbf{H}^{(q)}, \mathbf{S}, \mathbf{W}),$$

so that the unfolded matrices of the received signal $\mathbf{X}_1^{(q)} \in \mathbb{C}^{PK \times N}$, $\mathbf{X}_2^{(q)} \in \mathbb{C}^{KN \times P}$ and $\mathbf{X}_3^{(q)} \in \mathbb{C}^{NP \times K}$ are factored as:

$$\mathbf{X}_1^{(q)} = \big(\mathbf{W} \diamond (\mathbf{H}^{(q)}\mathbf{\Psi})\big)(\mathbf{S}\mathbf{\Phi})^T, \tag{3.23}$$

$$\mathbf{X}_2^{(q)} = \big((\mathbf{H}^{(q)}\mathbf{\Psi}) \diamond (\mathbf{S}\mathbf{\Phi})\big)\mathbf{W}^T, \tag{3.24}$$

$$\mathbf{X}_3^{(q)} = \big((\mathbf{S}\mathbf{\Phi}) \diamond \mathbf{W}\big)\big(\mathbf{H}^{(q)}\mathbf{\Psi}\big)^T, \tag{3.25}$$

where $\mathbf{H}^{(q)}$ is defined in (3.4), $\mathbf{S} = [\mathbf{S}^{(1)} \cdots \mathbf{S}^{(Q)}]$, while $\mathbf{\Psi}$ and $\mathbf{\Phi}$ are block-diagonal *constraint matrices*:

$$\mathbf{\Psi} = \begin{bmatrix} \mathbf{\Psi}^{(1)} & & \\ & \ddots & \\ & & \mathbf{\Psi}^{(Q)} \end{bmatrix} \in \mathbb{R}^{M \times R_M}, \tag{3.26}$$

$$\mathbf{\Phi} = \begin{bmatrix} \mathbf{\Phi}^{(1)} & & \\ & \ddots & \\ & & \mathbf{\Phi}^{(Q)} \end{bmatrix} \in \mathbb{R}^{R \times R_M}, \tag{3.27}$$

where their i-th blocks have, respectively, the following Kronecker structures:

$$\begin{aligned} \boldsymbol{\Psi}^{(i)} &= \mathbf{I}_{M^{(i)}} \otimes \mathbf{1}_{R^{(i)}}^T \in \mathbb{C}^{M^{(i)} \times R_M^{(i)}}, \\ \boldsymbol{\Phi}^{(i)} &= \mathbf{1}_{M^{(i)}}^T \otimes \mathbf{I}_{R^{(i)}} \in \mathbb{C}^{R^{(i)} \times R_M^{(i)}}. \end{aligned} \tag{3.28}$$

with $R_M^{(i)}$ defined in (3.21).

3.6 Physical meaning of the constraint matrices

In the present context, the constraint matrices $\boldsymbol{\Psi}$ and $\boldsymbol{\Phi}$ admit an interesting physical interpretation. They can be viewed as *symbol-to-antenna allocation matrices* and their structure reveals the overall block space-time spreading pattern considered at the transmitter. This interpretation sheds light on the different space-time spreading designs that can be achieved by properly configuring these matrices with 1's and 0's. For example, let us consider $M = 3$ transmit antennas and a transmission for $Q = 2$ users, which implies $Q = 2$ transmission blocks. Assume $\{M^{(1)}, R^{(1)}\} = \{2, 1\}$, $\{M^{(2)}, R^{(2)}\} = \{1, 3\}$. From (3.26)-(3.28), $\boldsymbol{\Psi}$ and $\boldsymbol{\Phi}$ have the following structures:

$$\boldsymbol{\Psi} = \begin{bmatrix} 1 & 0 & 0 & 0 & 0 \\ 0 & 1 & 0 & 0 & 0 \\ 0 & 0 & 1 & 1 & 1 \end{bmatrix}, \quad \boldsymbol{\Phi} = \begin{bmatrix} 1 & 1 & 0 & 0 & 0 \\ 0 & 0 & 1 & 0 & 0 \\ 0 & 0 & 0 & 1 & 0 \\ 0 & 0 & 0 & 0 & 1 \end{bmatrix}.$$

First, note that both $\boldsymbol{\Psi}$ and $\boldsymbol{\Phi}$ are block-diagonal matrices with two diagonal blocks, i.e.:

$$\{\boldsymbol{\Psi}^{(1)}, \boldsymbol{\Psi}^{(2)}\} = \{\mathbf{I}_2, \mathbf{1}_3^T\}, \quad \{\boldsymbol{\Phi}^{(1)}, \boldsymbol{\Phi}^{(2)}\} = \{\mathbf{1}_2^T, \mathbf{I}_3\}.$$

Each row of $\boldsymbol{\Psi}$ defines the *multiplexing factor* at each transmit antenna. The number of 1's entries in each row of $\boldsymbol{\Psi}$ defines the number of symbols combined into each transmit antenna. Observe that the first and second rows of $\boldsymbol{\Psi}$ (both associated with the first transmission block) have only one non-zero entry, which indicates that both transmit antennas of this block transmit only one symbol at a time. The third row contains three non-zero entries, meaning that three symbols are simultaneously transmitted by the antenna of the second block.

Now, let us look at the structure of $\boldsymbol{\Phi}$. Its number of rows corresponds to the total number of multiplexed data streams. Each row of $\boldsymbol{\Phi}$ defines the *spatial spreading factor* associated with each data-stream: The number of 1's entries in each row of $\boldsymbol{\Phi}$ defines the number of antennas used to transmit each data-stream. Note that its

first row has two non-zero entries, which means that the first data-stream is spread over the two first transmit antennas. The three other rows have only one non-zero entry, which indicates that the three other data-streams are transmitted using only one transmit antenna, i.e., they are not spatially spread at the transmitter. The chosen spreading-multiplexing configuration can be checked by means of the following matrix:

$$\mathbf{\Psi}\mathbf{\Phi}^T = \begin{bmatrix} 1 & 0 & 0 & 0 \\ 1 & 0 & 0 & 0 \\ 0 & 1 & 1 & 1 \end{bmatrix} \in \mathbb{C}^{M \times R}.$$

This matrix product reveals the *joint* spreading-multiplexing pattern. For a fixed row, one can check for the number of data-streams multiplexed at a given antenna by counting the number of 1's entries in that row. On the other hand, for a fixed column, one can check for the number of antennas over which a given data-stream is spread.

3.7 Receiver algorithm

As mentioned in the last section, the choice of a semi-unitary (Vandermonde) matrix $\mathbf{W}$ allows the separation of users' transmissions deterministically, so that the detection of each user transmitted data can be carried out independently. In the following, we exploit the knowledge and structure of $\mathbf{W}$ for MUI elimination and then the tensor structure of the received signal for a blind joint channel estimation and symbol recovery.

3.7.1 MUI elimination

The first processing step at each receiver performs a deterministic MUI elimination, by relying on the structure of the unfolded spreading matrix $\mathbf{W} \in \mathbb{C}^{P \times R_M}$ and assuming $P \geq R_M$. Let us define $\mathbf{F}^{(q)} = \mathbf{W}^{(q)*} \in \mathbb{C}^{P \times R_M^{(q)}}$ as the q-th user receive filter. For the q-th user, the elimination of the MUI coming from the transmission blocks $\{1, \ldots, q-1, q+1, \ldots, Q\}$, consists in post-multiplying the received signal matrix $\mathbf{X}_2^{(q)}$ given in (3.24) by $\mathbf{F}^{(q)}$, which gives:

$$\mathbf{Y}_2^{(q)} \;=\; \mathbf{X}_2^{(q)}\mathbf{F}^{(q)} = \left((\mathbf{H}^{(q)}\mathbf{\Psi}) \diamond (\mathbf{S}\mathbf{\Phi})\right)\mathbf{D}^{(q)}, \tag{3.29}$$

where

$$\mathbf{D}^{(q)} = \mathbf{W}^T\mathbf{F}^{(q)} = \begin{bmatrix} \mathbf{0}_{\overline{R}_M^{(q-1)} \times R_M^{(q)}} \\ \mathbf{I}_{R_M^{(q)}} \\ \mathbf{0}_{(R_M - \overline{R}_M^{(q)}) \times R_M^{(q)}} \end{bmatrix} \in \mathbb{C}^{R_M \times R^{(q)}},$$

$$\text{with } \overline{R}_M^{(q)} = \sum_{i=1}^{q} R_M^{(i)}.$$

Note that all the blocks in $\mathbf{D}^{(q)}$ except the one corresponding to the q-th user are zero. This allows us to rewrite (3.29) as a MUI-free model:

$$\mathbf{Y}_2^{(q)} = \left((\mathbf{H}^{(q,q)}\mathbf{\Psi}^{(q)}) \diamond (\mathbf{S}^{(q)}\mathbf{\Phi}^{(q)})\right)\mathbf{I}_{R_M^{(q)}}, \tag{3.30}$$

which can be viewed as a single-user tensor model with constrained structure. Therefore, $\mathbf{Y}_1^{(q)}$ is an unfolded matrix of a tensor $\mathcal{Y}^{(q)} \in \mathbb{C}^{R_M \times R_M^{(q)} \times N}$ resulting from a linear transformation of the received signal tensor $\mathcal{X}^{(q)} \in \mathbb{C}^{R_M \times P \times N}$ by the associated receive filter $\mathbf{F}^{(q)} \in \mathbb{C}^{P \times R_M^{(q)}}$ as shown in (3.29). A one-to-one correspondence between the multiuser and single-user tensor models can be obtained by comparing $\mathbf{X}_2^{(q)}$ in (3.23) with $\mathbf{Y}_2^{(q)}$ in (3.30). This correspondence is:

$$\left(\mathbf{H}^{(q)}, \mathbf{S}, \mathbf{W}, \mathbf{\Psi}, \mathbf{\Phi}\right) \rightarrow \left(\mathbf{H}^{(q,q)}, \mathbf{S}^{(q)}, \mathbf{I}_{R_M^{(q)}}, \mathbf{\Psi}^{(q)}, \mathbf{\Phi}^{(q)}\right).$$

By analogy with (3.23) and (3.25), we can also represent the information contained in $\mathbf{Y}_1^{(q)}$ by means of two other unfolded matrices:

$$\mathbf{Y}_3^{(q)} = \left((\mathbf{S}^{(q)}\mathbf{\Phi}^{(q)}) \diamond \mathbf{I}_{R_M^{(q)}}\right)\left(\mathbf{H}^{(q,q)}\mathbf{\Psi}^{(q)}\right)^T, \tag{3.31}$$

$$\mathbf{Y}_1^{(q)} = \left(\mathbf{I}_{R_M^{(q)}} \diamond (\mathbf{H}^{(q,q)}\mathbf{\Psi}^{(q)})\right)\left(\mathbf{S}^{(q)}\mathbf{\Phi}^{(q)}\right)^T. \tag{3.32}$$

Note that $\mathbf{Y}_3^{(q)} \in \mathbb{C}^{R_M^{(q)}N \times K}$ and $\mathbf{Y}_1^{(q)} \in \mathbb{C}^{KR_M^{(q)} \times N}$ are "reshaped" versions of $\mathbf{Y}_2^{(q)} \in \mathbb{C}^{NK \times R_M^{(q)}}$. Defining:

$$\mathbf{Z}_3\left(\mathbf{S}^{(q)}\right) = \left((\mathbf{S}^{(q)}\mathbf{\Phi}^{(q)}) \diamond \mathbf{I}_{R_M^{(q)}}\right)\mathbf{\Psi}^{(q)T}, \in \mathbb{C}^{R_M^{(q)}N \times M^{(q)}} \tag{3.33}$$

$$\mathbf{Z}_1\left(\mathbf{H}^{(q,q)}\right) = \left(\mathbf{I}_{R_M^{(q)}} \diamond (\mathbf{H}^{(q,q)}\mathbf{\Psi}^{(q)})\right)\mathbf{\Phi}^{(q)T} \in \mathbb{C}^{KR_M^{(q)} \times R^{(q)}}, \tag{3.34}$$

we can rewrite $\mathbf{Y}_3^{(q)}$ and $\mathbf{Y}_1^{(q)}$ as:

$$\mathbf{Y}_3^{(q)} = \mathbf{Z}_3\left(\mathbf{S}^{(q)}\right)\mathbf{H}^{(q,q)T}, \quad \mathbf{Y}_1^{(q)} = \mathbf{Z}_1\left(\mathbf{H}^{(q,q)}\right)\mathbf{S}^{(q)T}. \tag{3.35}$$

3.7.2 Identifiability

For studying the identifiability of model (3.35), let us make the following assumptions concerning the structure of $\mathbf{S}^{(q)}$ and $\mathbf{H}^{(q,q)}$:

A1: "Persistence of excitation" of the transmitted symbols which implies, in our context, that $\mathbf{S}^{(q)}$ can be considered as a full rank matrix with probability one if N is large enough.

A2: An "ideal" MIMO channel so that the entries of the channel matrix are assumed to be independent and randomly drawn from an absolutely continuous distribution, which implies that $\mathbf{H}^{(q,q)}$ is full rank with probability one.

Under assumptions $\mathbf{A1}-\mathbf{A2}$, joint channel-symbol identifiability from the MUI-free model defined in (3.35) requires that $\mathbf{Z}_3\big(\mathbf{S}^{(q)}\big)$ and $\mathbf{Z}_1\big(\mathbf{H}^{(q,q)}\big)$ in (3.33) and (3.34) be full column-rank, since these matrices must have a left-inverse. Let us study the rank properties of $\mathbf{Z}_3\big(\mathbf{S}^{(q)}\big)$ and $\mathbf{Z}_1\big(\mathbf{H}^{(q,q)}\big)$. We make use of the concept of k-rank [131], which is recalled here for convenience:

Definition 1: The k-rank of $\mathbf{A} \in \mathbb{C}^{I\times F}$, denoted by $k_{\mathbf{A}}$, is equal to r if *any* set of r columns of $\mathbf{A}$ is independent, but there exists a set of $r+1$ linearly dependent columns in $\mathbf{A}$. We have $k_{\mathbf{A}} \leq \text{rank}(\mathbf{A}) \leq \min(I,F)$.

We have to note that if two columns in $\mathbf{A}$ are repeated, and if $\mathbf{A}$ does not contain a zero column, then we have $k_{\mathbf{A}} = 1$. Let us also recall the two following lemmae:

Lemma 1 (k-rank of the Khari-Rao product)[133]: Suppose that $\mathbf{A} \in \mathbb{C}^{I\times F}$ and $\mathbf{B} \in \mathbb{C}^{J\times F}$ are such that $k_{\mathbf{A}} \geq 1$ and $k_{\mathbf{B}} \geq 1$ (i.e. neither $\mathbf{A}$ nor $\mathbf{B}$ has a zero column). If $k_{\mathbf{A}} + k_{\mathbf{B}} = F+1$, then $\mathbf{A} \diamond \mathbf{B}$ is full column-rank.

Lemma 2: If $\mathbf{A}$ is full column-rank, then we have $\text{rank}(\mathbf{AB}) = \text{rank}(\mathbf{B})$.

Taking the definitions (3.28) of $\mathbf{\Psi}^{(q)}$ and $\mathbf{\Phi}^{(q)}$ into account, we have:

$$\mathbf{\Psi}^{(q)} = \underbrace{\begin{bmatrix} \mathbf{1}_{R^{(q)}}^T & & \\ & \ddots & \\ & & \mathbf{1}_{R^{(q)}}^T \end{bmatrix}}_{M^{(q)} \text{ times}} \Rightarrow \text{rank}(\mathbf{\Psi}^{(q)}) = M^{(q)}.$$

$$\mathbf{\Phi}^{(q)} = \underbrace{\begin{bmatrix}\mathbf{I}_{R^{(q)}} \cdots \mathbf{I}_{R^{(q)}}\end{bmatrix}}_{M^{(q)} \text{ times}} \Rightarrow \text{rank}(\mathbf{\Phi}^{(q)}) = R^{(q)},$$

which implies that $\mathbf{\Psi}^{(q)}$ and $\mathbf{\Phi}^{(q)}$ be full row-rank. From these expressions of $\mathbf{\Psi}^{(q)}$ and $\mathbf{\Phi}^{(q)}$, we get:

$$\mathbf{S}^{(q)}\mathbf{\Phi}^{(q)} = \underbrace{\left[\mathbf{S}^{(q)} \cdots \mathbf{S}^{(q)}\right]}_{M^{(q)} \text{ times}},$$

and

$$\mathbf{H}^{(q,q)}\mathbf{\Psi}^{(q)} = [\underbrace{\mathbf{H}_{\cdot 1}^{(q,q)} \cdots \mathbf{H}_{\cdot 1}^{(q,q)}}_{R^{(q)} \text{ times}} \cdots \underbrace{\mathbf{H}_{\cdot M^{(q)}}^{(q,q)} \cdots \mathbf{H}_{\cdot M^{(q)}}^{(q,q)}}_{R^{(q)} \text{ times}}],$$

which implies that:

$$k_{\mathbf{S}^{(q)}\mathbf{\Phi}^{(q)}} = k_{\mathbf{H}^{(q,q)}\mathbf{\Psi}^{(q)}} = 1.$$

As we have $k_{\mathbf{I}_{K^{(q)}}} + k_{\mathbf{S}^{(q)}\mathbf{\Phi}^{(q)}} = K^{(q)} + 1$, application of Lemma 1 to the Khatri-Rao product in (3.33) implies that $\mathbf{I}_{K^{(q)}} \diamond (\mathbf{S}^{(q)}\mathbf{\Phi}^{(q)})$ be full column-rank, i.e. $\text{rank}(\mathbf{I}_{K^{(q)}} \diamond (\mathbf{S}^{(q)}\mathbf{\Phi}^{(q)})) = R^{(q)}$. Application of Lemma 2 leads to $\text{rank}\big(\mathbf{Z}_3\big(\mathbf{S}^{(q)}\big)\big) = \text{rank}\big(\mathbf{\Psi}^{(q)T}\big) = \text{rank}\big(\mathbf{\Psi}^{(q)}\big) = M^{(q)}$, i.e. $\mathbf{Z}_3\big(\mathbf{S}^{(q)}\big)$ is full column-rank. The same reasoning applies for showing that $\mathbf{Z}_1\big(\mathbf{H}^{(q,q)}\big)$ is also full column-rank.

3.7.3 Blind joint channel and symbol recovery

After MUI elimination at each receiver, we propose to apply the ALS algorithm on the resulting interference-free tensor model (3.35) in order to blindly recover the transmitted symbols jointly with channel estimation. As in the previous chapters,the algorithm is initialized using a random value $\widehat{\mathbf{S}}_{t=0}^{(q)}$. At the t-th iteration, the two least-squares update equations are:

$$\widehat{\mathbf{H}}_t^{(q,q)T} = \left[\mathbf{Z}_3\big(\widehat{\mathbf{S}}_{t-1}^{(q)}\big)\right]^{\dagger} \mathbf{Y}_3^{(q)}, \tag{3.36}$$

$$\widehat{\mathbf{S}}_t^{(q)T} = \left[\mathbf{Z}_1\big(\widehat{\mathbf{H}}_t^{(q,q)}\big)\right]^{\dagger} \mathbf{Y}_1^{(q)}. \tag{3.37}$$

For the q-th receiver, the following error measure is computed at the t-th iteration:

$$e_t^{(q)} = \left\| \mathbf{Y}_1^{(q)} - \mathbf{Z}_1\big(\widehat{\mathbf{H}}_t^{(q,q)}\big)\widehat{\mathbf{S}}_t^{(q)} \right\|_F, \tag{3.38}$$

We choose $|e_t^{(q)} - e_{t-1}^{(q)}| \leq 10^{-6}$ as the convergence threshold, $q = 1, \ldots, Q$. The estimation of both $\mathbf{H}^{(q,q)}$ and $\mathbf{S}^{(q)}$ is affected by a scaling ambiguity. In other words, the columns of the estimated channel and symbol matrices are affected by unknown scaling factors that compensate each other. Following [129], we eliminate this scaling ambiguity by assuming that the first transmitted symbol of each data stream is equal to one, which corresponds to have all the elements in the first row

of $\mathbf{S}$ equal to one. Thus, we eliminate the scaling ambiguity by normalizing each column of $\widehat{\mathbf{S}}$ by its first element yielding:

$$\widetilde{\mathbf{S}}_{\infty}^{(q)} = \widehat{\mathbf{S}}_{\infty}^{(q)} D_1^{-1}\big(\widehat{\mathbf{S}}_{\infty}^{(q)}\big),$$

where $\widehat{\mathbf{S}}_{\infty}^{(q)}$ corresponds to the estimated value obtained after convergence and $D_1(\cdot)$ denotes the diagonal matrix formed from the first row of its matrix argument. After such a normalization, we obtain a final estimate of the channel matrix without scaling ambiguity using (3.36):

$$\widetilde{\mathbf{H}}_{\infty}^{(q,q)T} = \Big[\mathbf{Z}_3\big(\widetilde{\mathbf{S}}_{\infty}^{(q)}\big)\Big]^{\dagger} \mathbf{Y}_3^{(q)}.$$

Discussion: Recall that we have modeled the channel between each transmit and receive antenna by a flat-fading coefficient. In a more practical scenario with time-dispersive multipath propagation, the channel between each pair of transmit and receive antennas is usually characterized by a number of resolvable multipaths with different relative propagation delays. In this scenario, we can still work with the proposed block space-time spreading model by assuming that the spreading codes are augmented by a number of trailing zeros, or "guard chips" in order to avoid inter-symbol interference. The main impact is that, in this case, the spreading matrix $\mathbf{W}$ is *unknown* at the receiver due to the convolution of the transmitted spreading codes with the impulse response of the multipath channel. Since the orthogonality between the transmitted data streams is destroyed by multipath propagation, the two-steps receiver algorithm (MUI elimination + ALS) should be replaced by a multiuser detection receiver based on the classical three-steps ALS algorithm where the *channel*, *symbol* and *spreading* matrices are iteratively estimated [131]. The price to pay is, of course, the increased complexity of the receiver algorithm.

3.8 Simulation Results

In this section, the performance of the proposed block space-time spreading based MU-MIMO system using the ALS algorithm is illustrated by means of computer simulations. The number of Monte Carlo runs vary from 1000 to 5000 depending on the simulated Signal-to-Noise Ratio (SNR) value. At each run, the noise power is generated according to the sample SNR value given by $\text{SNR}=10\log_{10}\big(\|\mathbf{X}_1^{(q)}\|_F^2/\|\mathbf{V}_1^{(q)}\|_F^2\big)$, where $\mathbf{V}_1^{(q)}$ represents the additive noise matrix. A Rayleigh fading MIMO channel is assumed. The elements of the channel ma-

trix $\mathbf{H}^{(q)}$ are independent and identically distributed (i.i.d) samples of a complex Gaussian process with zero mean and unit variance.

Each run represents a different realization of the MIMO channel and the transmitted symbols are drawn from a pseudo-random QPSK or QAM sequence. The BER curves represent the performance averaged on the transmitted data streams. In all the results, we focus on system configurations with a small number K of receive antennas ($K \leq M$ is generally assumed). For clarity of presentation, we consider $Q = 1$, 2 or 3 users. In some simulations, we focus on the individual performance of each user by averaging the performance over the data streams of each user. In some others, the performance is averaged over all the transmitted data streams o all the users.

3.8.1 BER performance

We begin by evaluating the BER performance of the block space-time spreading based MU-MIMO system using the ALS algorithm. We consider a two-users system ($Q = 2$) with corresponding transmission blocks parameterized by $\{M^{(1)}, R^{(1)}\} = \{1, 2\}$ and $\{M^{(2)}, R^{(2)}\} = \{2, 2\}$. A time-slot containing $N = 10$ symbols is processed at the receiver. QPSK modulation is used ($\mu = 4$). Unless otherwise stated, we assume $P = M^{(1)}R^{(1)} + M^{(2)}R^{(2)}$ in order to satisfy the requirement (3.21) for maximum transmit diversity. In this case we have $P = 6$ and both users have the same rate $\rho^{(1)} = \rho^{(2)} = 2/3$ bits per channel use. A single transmit antenna is used to transmit the two data streams of the first user, while two transmit antennas are dedicated to the second user. Figure 3.6 shows the individual performance of each user assuming $K = 1$ and 2 receive antennas. We can clearly see that the second user has an improved performance over the first one, due to a higher transmit diversity gain obtained by spreading the data streams across two transmit antennas.

Now, we investigate the influence of the spreading factor P on the receiver performance. We assume $Q = 1$ (single-user/single-block case) and consider two space-time spreading configurations $\{M, R\} = \{2, 2\}$ and $\{M, R\} = \{4, 2\}$. As shown in Fig. 3.7, for $\{M, R\} = \{2, 2\}$, the transmit diversity gain is degraded with $P = 3$ (note that $P = 3$ does not satisfy (3.21)) in comparison with $P = 4$ (satisfying (3.21)). The same comment is valid for $P = 6$ with respect to $P = 8$. Such a lack of diversity, explaining the BER floors in the figure, comes with a marginal increase in rate. Indeed, the rate is $\rho = 4/3$ for $P = 3$ and $\rho = 1$ for $P = 4$. These comments are also valid for $\{M, R\} = \{4, 2\}$. These results confirm that the receiver performance is sensitive to the spreading factor.

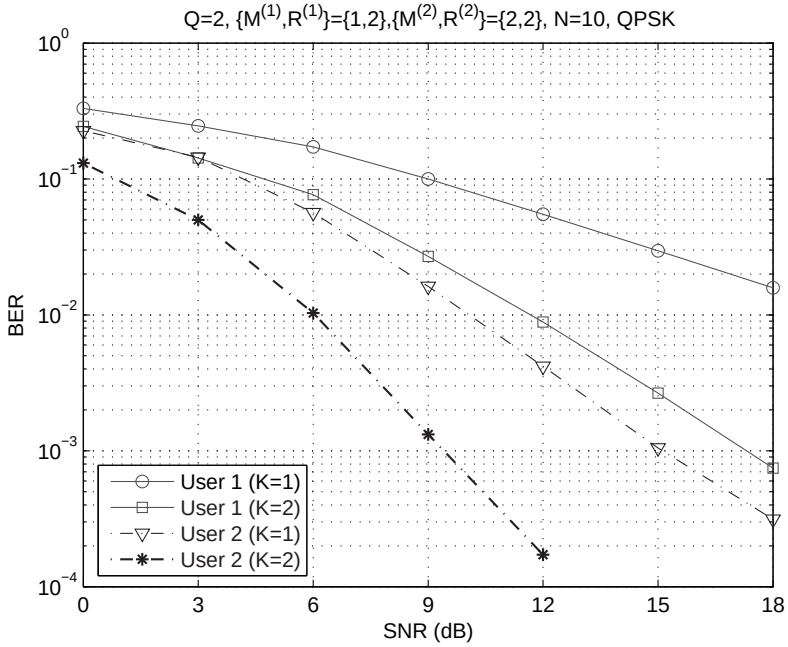

Figure 3.6: BER *versus* SNR for $K = 1$ and 2.

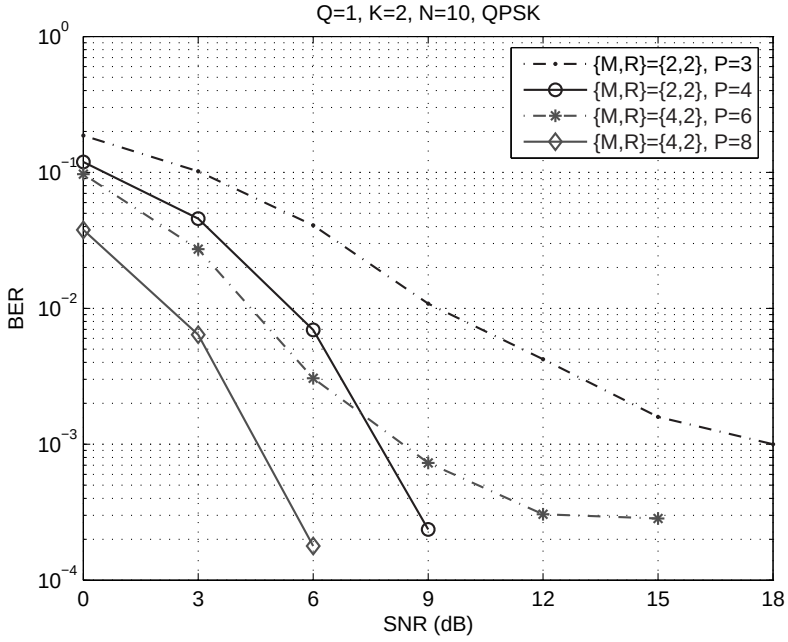

Figure 3.7: BER *versus* SNR for different values of P.

In Fig. 3.8, we compare block space-time spreading with KRST coding [129]. We consider $M = 4$, $K = 2$ and 16-QAM. Different space-time spreading configurations are simulated by varying the number of space-time spreading blocks/users. We consider the following cases: i) $Q = 3$ with $\{M^{(1)}, M^{(2)}, M^{(3)}\} = \{2, 1, 1\}$, ii) $Q = 2$ with $\{M^{(1)}, M^{(2)}\} = \{2, 2\}$, iii) $Q = 1$ with $\{M\} = 4$. Note that KRST coding is a special case of the proposed approach for $Q = M = 4$ (constellation rotation is not considered here for simulating KRST coding). KRST coding provides the best performance in terms of rate, but the worst performance in terms of BER. In the proposed approach, by decreasing the number of space-time spreading blocks, the BER performance is improved since more transmit antennas are used to achieve higher transmit diversity gains. However, this comes at the expense of a decrease in rate.

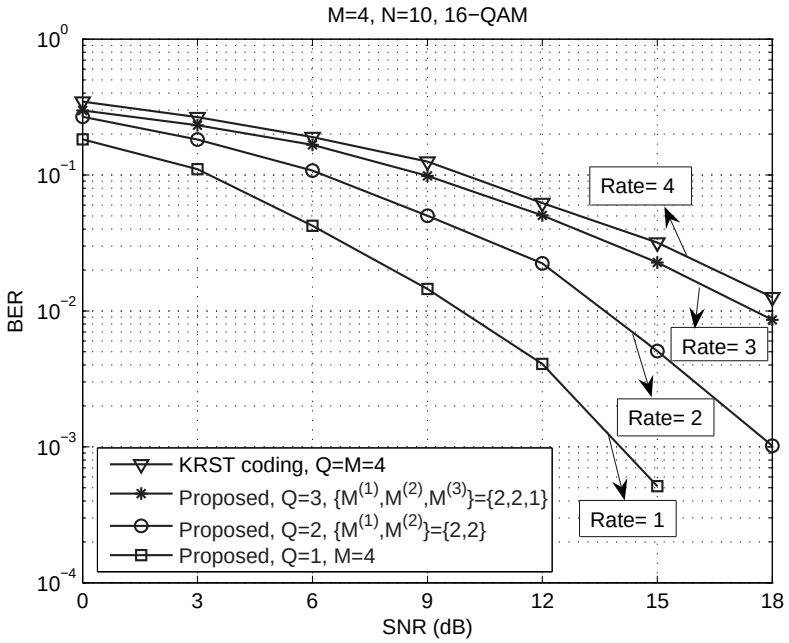

Figure 3.8: Block space-time spreading *versus* KRST coding.

Figure 3.9 compares the proposed MIMO system with the Alamouti code [2] in the particular single-user case with $Q = 1$, $M = K = 2$ and $R = 2$. For the Alamouti code, perfect channel knowledge is assumed at the receiver, contrarily to our system which uses blind detection. In order to keep the same rate (1 bit/channel use) for a fair comparison, the Alamouti code uses BPSK while the proposed MIMO system uses QPSK. The performance gap between the proposed approach and the Alamouti code is 3dB for a BER of $2 \cdot 10^{-3}$. The slope of the BER curves indicate that both approaches have the same diversity gain.

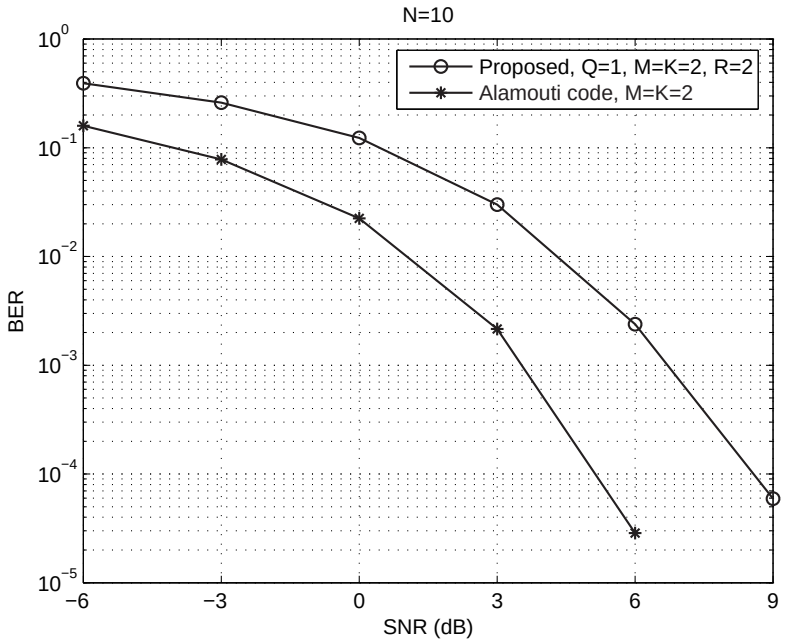

Figure 3.9: Block space-time spreading *versus* Alamouti code.

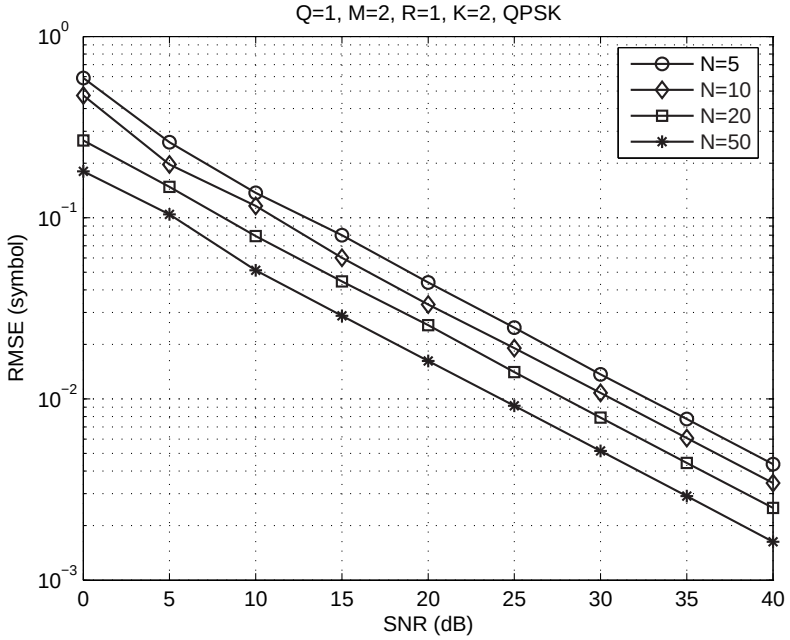

Figure 3.10: Symbol RMSE for different values of N.

3.8.2 RMSE performance

In the next experiment, we investigate the accuracy of the ALS algorithm in recovering the channel and symbol matrices. The fixed simulation parameters are $Q = 1$, $M = 2$, $R = 1$, $K = 2$. The evaluation is based on the Root-Mean-Square Error (RMSE) between the estimated and true matrices calculated according to the following formulae:

$$\begin{aligned} \text{RMSE}(\mathbf{S}) &= \sqrt{\frac{1}{LNR}\sum_{l=1}^{L}\left\|\widehat{\mathbf{S}}_{\infty}(l)-\mathbf{S}\right\|_F^2}, \\ \text{RMSE}(\mathbf{H}) &= \sqrt{\frac{1}{LMK}\sum_{l=1}^{L}\left\|\widehat{\mathbf{H}}_{\infty}(l)-\mathbf{H}\right\|_F^2}, \end{aligned}$$

where L is the number of Monte Carlo runs, while $\widehat{\mathbf{S}}_{\infty}(l)$ and $\widehat{\mathbf{H}}_{\infty}(l)$ are the estimated matrices after convergence at the l-th run. In this experiment, we assume $L = 1000$. Figure 3.10 shows that the RMSE associated with the estimation of the transmitted symbols exhibits a linear decrease as a function of the SNR. Estimation accuracy also improves as N increases.

In Fig. 3.11, the RMSE associated with the channel estimation is depicted for different numbers M of transmit antennas with $Q = 1$, $R = 2$, $K = 2$ and $N = 10$. Improved estimation of the channel matrix is obtained as M is increased. Note that, despite the increase of the number of channel parameters to be estimated when M is increased, this performance improvement is attributed to the higher transmit diversity gain.

3.8.3 Comparison with classical MIMO schemes

In this section, we are interested in comparing the proposed MIMO system with classical schemes such as Spatial Multiplexing (SM) [69] and Orthogonal Transmit Diversity (OTD) [142], also known as V-BLAST and "Alamouti" schemes, respectively. These schemes provide a performance reference for the proposed MIMO system. The simulation of both SM and OTD consider a single-user system (no multiuser interference) with perfect channel knowledge, which leads to the best performance they can achieve. Contrarily to SM and OTD, the proposed space-time spreading system is simulated in a blind setting using the ALS algorithm.

Figure 3.12 shows the BER performance of the proposed system with $P = 2$,

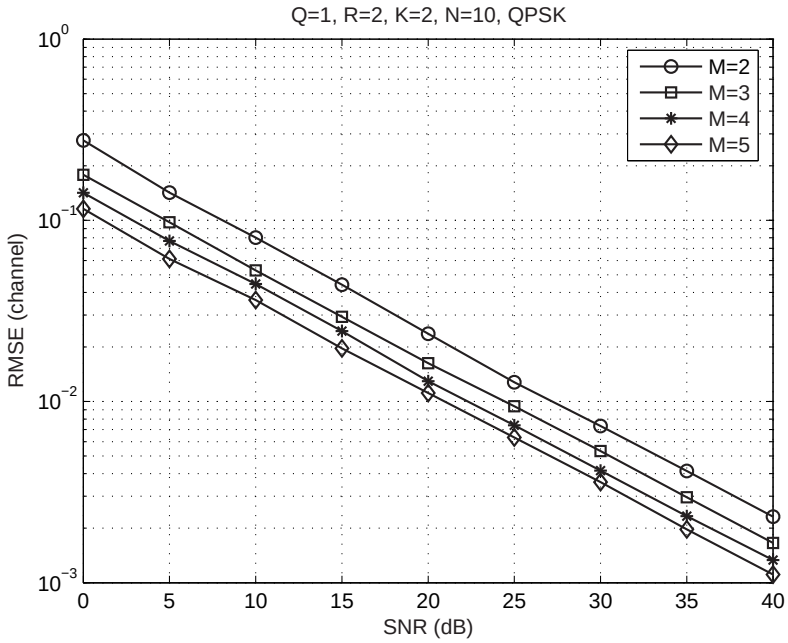

Figure 3.11: Channel RMSE for different values of M.

compared with that of SM, for two different spectral efficiencies (2 and 4 bps/Hz), and for $M = 2$ and $K = 2$ or 3. For achieving 2 and 4 bps/Hz, the proposed system uses 4-PSK and 16-QAM, respectively while SM uses 2-PSK and 4-PSK, respectively. In can be seen that, at 4bps/Hz, the proposed system is worse at low-to-medium SNR and tends to be better at high SNR. From the slope of the two BER curves, it can be noted that the block space-time spreading MIMO system has a higher diversity gain than the classical SM scheme. We attribute such a gain to the use of the spreading structure, which enforces orthogonality between the transmit spatial channels. At 2 bps/Hz, the proposed MIMO system outperforms SM. Note that the proposed system $K = 2$ has the same diversity gain as SM with $K = 3$ (see the slope of the curves).

Figure 3.13 compares the proposed MIMO system with the OTD scheme. Differently from the previous results, we now include channel frequency-selectivity and OFDM. We consider a two-path channel ($L = 2$) with independent (zero and one symbol-delayed) equal power taps and $N_c = 64$ subcarriers. The other transmit parameters are $Q = 1$, $M = K = 2$, $R = 2$, $P = 2$ and $F = 1$. The OTD scheme codes the input symbols in the time-domain (i.e. across $P = 2$ consecutive OFDM symbols) and *not* in the frequency-domain. It can be seen that both systems achieve the same diversity gain and the gap between the proposed MIMO system and OTD is approximately 6 dB for BER=10^{-3}.

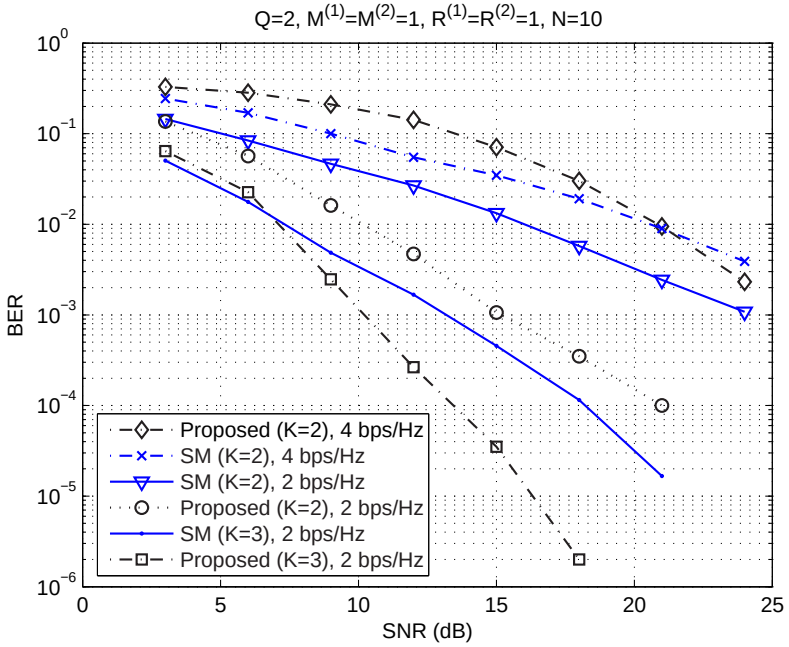

Figure 3.12: Proposed MIMO system *versus* SM (V-BLAST scheme)

3.8.4 Performance with pilot symbols

In a practical system, a training sequence in the form of pilot symbols is used for channel estimation. Here, we aim at evaluating possible performance gains obtained when pilot symbols are used in conjunction with the ALS algorithm. We make use of the Pilot-Assisted Channel Estimation (PACE) method for obtaining an initial (more accurate) initialization of the channel matrix for the ALS algorithm. The PACE method consists in estimating the frequency-selective MIMO channel by using an orthogonal training sequence structure (see [93, 5] for details).

We evaluate the BER performance of the block space-time spreading MIMO system for $Q = 2$, using i) standard PACE followed by LS symbol detection and ii) ALS-based detection with joint channel-symbol estimation. It is worth mentioning that the PACE method is sensitive to the number of pilot subcarriers, and its performance considerably degrades when a small number of pilot subcarriers is used. The proposed system uses $Q = 2$ with $\{M^{(1)}, M^{(2)}\} = \{2, 2\}$, $\{R^{(1)}, R^{(2)}\} = \{1, 1\}$, $N_c = 64$ and $F = L = 2$. Figure 3.14 shows the performance of the proposed system with PACE and ALS based detection for $N_c = 16$. We can observe that the ALS based receiver outperforms the conventional PACE receiver. The gain is more pronounced when the number of receive antennas is increased.

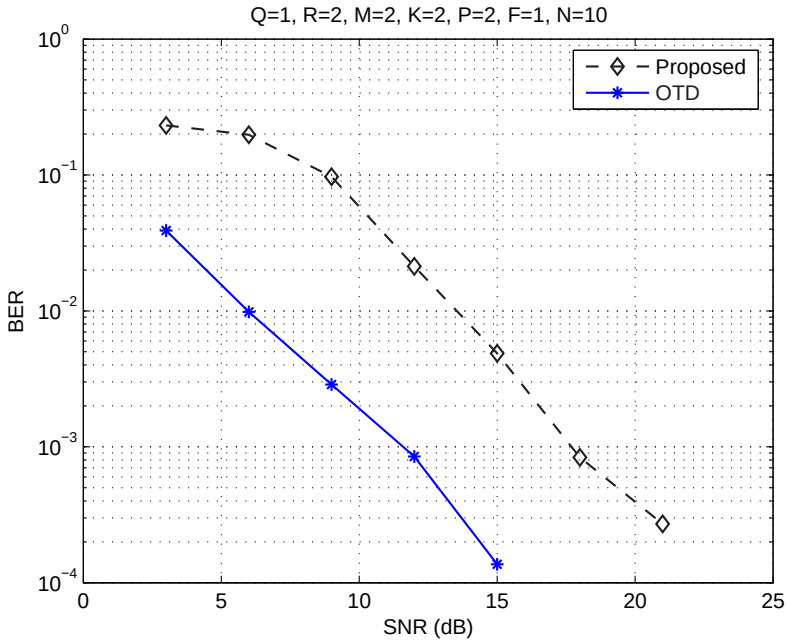

Figure 3.13: Proposed MIMO system *versus* OTD (Alamouti scheme)

3.8.5 Throughput performance

In this section, the average throughput of the proposed MIMO system is studied for some system configurations. Our aim is to show that the block space-time spreading model covers different "transmission modes" that could be adapted according to the SNR in a practical transmission setting. Throughput results are interesting from a practical point of view, since they provide a more realistic insight on the physical-layer performance of the proposed receiver strategy.

In order to obtain Block Error Rate (BLER) measures for throughput calculation, we introduce an 8-bit Cyclic Redundancy Check (CRC) scheme at each data block, which is defined as a collection of NR symbols (N symbols per data stream $\times$ R data streams). We only vary the temporal spreading factor P which can be viewed as a parameter controlling the redundancy of the transmitted symbols in the time domain. The average values for the BLER are calculated over 1000 independent runs for each SNR value. No channel coding is used. The calculation of the total

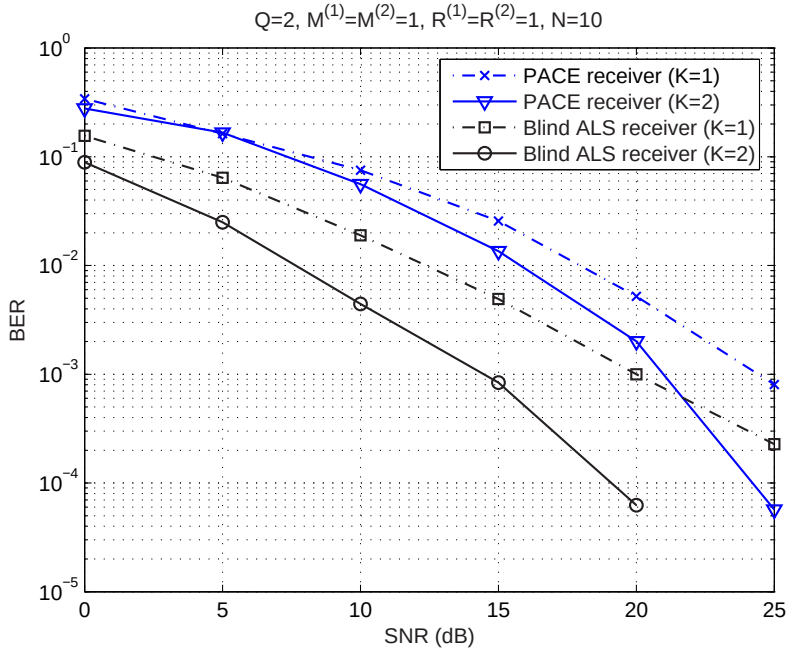

Figure 3.14: Comparison between PACE and ALS based receivers.

throughput Γ (summed over the Q users) is made using the following formula:

$$\Gamma = \sum_{q=1}^{Q} \Gamma^{(q)} = \sum_{q=1}^{Q} (1 - \mathrm{BLER}^{(q)}) \cdot \rho^{(q)} \quad (\mathrm{bits}/T_{\mathrm{block}}),$$

where $\mathrm{BLER}^{(q)}$ is the block-error-rate of the q-th user, $\rho^{(q)}$ is the nominal rate of the q-th transmission block defined in (3.22), and $T_{\mathrm{block}} = NRT_s$ denotes the duration of one transmission block of NR symbols, T_s being the symbol period. The number of symbols per data stream is fixed at $N = 10$. In Fig. 3.15, we consider $Q = 2$ users with $\{M^{(1)}, R^{(1)}\} = \{2, 1\}$ and $\{M^{(2)}, R^{(2)}\} = \{1, 1\}$. Note that both users have the same multiplexing factor (thus the same nominal rate) but different spatial spreading factors. In this figure, we evaluate the individual throughput performance of each user. Each user throughput curve is reproduced for two values of P. In the first case, we have $P = M^{(1)}R^{(1)} + M^{(2)}R^{(2)} = 3$. In the second case, $P = 2$ is assumed, which is below the required value for achieving the maximum transmit diversity gain. Considering first $P = 3$, we verify from Fig. 3.15 that the expected transmit diversity gain of the first user is effectively translated into a higher throughput gain with respect to the second user. When P is decreased, we observe an increase in the first user's throughput for medium-to-high SNR

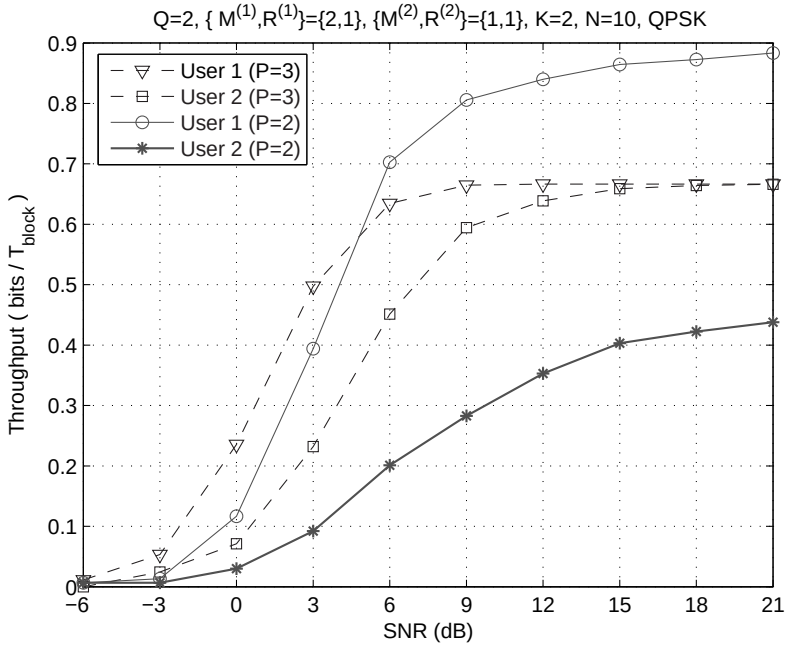

Figure 3.15: Per-user throughput performance for $P = 2$ and $P = 3$

levels, while, for low SNR levels, a throughput loss is observed. Therefore, the diversity loss that occurs when P is decreased is compensated by a throughput gain, especially for high SNR levels. For the second user, where no transmit diversity is available, a significant degradation in the throughput performance is observed.

Figure 3.16 shows a set of throughput curves for different values of P considering $Q = 1$, $M = 4$, $R = 4$, $K = 2$, and using 16-QAM. This figure indicates that it is possible to obtain a variable throughput performance by adjusting P according to the SNR. Otherwise stated, this experiment suggests that a sort of *link adaptation* could be implemented by varying the temporal spreading factor P in order to keep the best throughput within each SNR region. In this case, the switching points between different values of P occur at a SNR of 15, 21 and 28 dB.

3.9 Summary

This chapter has presented a new block space-time spreading model for the downlink of MU-MIMO system based on tensor modeling. The core of the transmitter is a 3-D *spreading code tensor* that jointly spreads and combines independent data

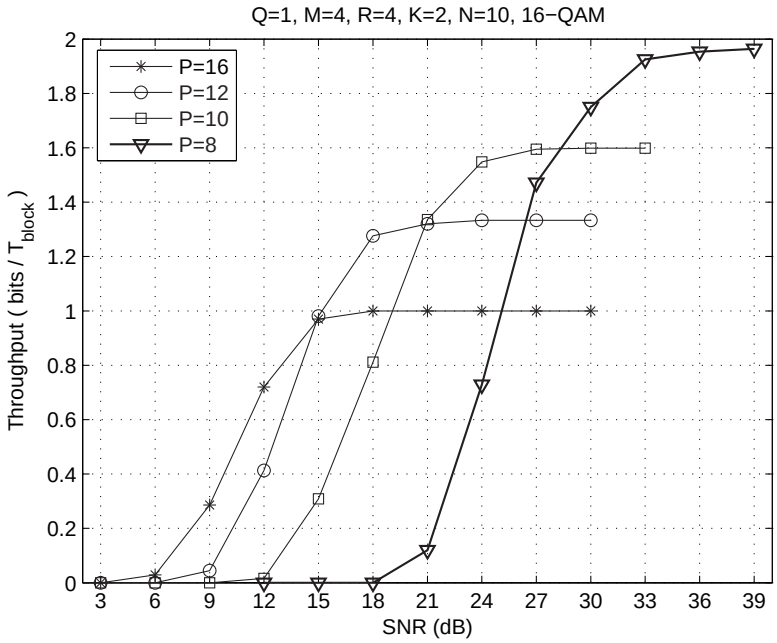

Figure 3.16: Throughput performance for different values of P.

streams across multiple transmit antennas. We have formulated the received signal as a block-constrained PARAFAC model, where the two fixed constraint matrices reveal the overall space-time spreading pattern at the transmitter. The proposed approach is flexible in the sense that it allows different spatial spreading factors (diversity gains) as well as different multiplexing factors (code rates) for the users. At the receiver, deterministic MUI elimination is performed by each user, followed by a blind joint channel and symbol recovery stage using the ALS algorithm.

Simulation results have shown that the proposed MU-MIMO system is not far from the classical SM receiver with perfect channel knowledge. We have considered the use of pilot-assisted channel estimation in conjunction with the ALS algorithm. According to the obtained results, significant performance gains can be obtained when pilot symbols are used for initializing the ALS receiver. Our simulation results have also shown that the block space-time spreading based MU-MIMO system can achieve variable BER and throughput performances by adjusting the three transmit parameters which are the *spatial spreading*, *multiplexing* and *temporal spreading* factors.

In the next chapter, we show that the constraint matrices $\mathbf{\Psi}$ and $\mathbf{\Phi}$ can be exploited for designing more general MIMO transmit schemes. This is done by relying on a CONFAC decomposition of the transmitted and received signals.

CHAPTER 4

Constrained Tensor Modeling Approaches to MIMO-CDMA Systems

This chapter presents new modeling approaches to MIMO-CDMA transmit schemes based on the CONstrained FACtor (CONFAC) decomposition. The constraint matrices of the CONFAC decomposition are the core of the proposed transmission model. They are exploited as allocation matrices that define the allocation of users' data streams and spreading codes to the transmit antennas. We begin by considering a MIMO-CDMA transmission model based on the type-3 CONFAC decomposition with two constraint matrices only. A systematic design procedure for the allocation matrices leading to unique blind symbol recovery is proposed. We show that a finite-set of spatial spreading schemes using multiple spreading codes can be derived by controlling the canonical structure of the CONFAC constraint matrices. In the second part of this chapter, a generalized transmission model is proposed which fully exploits all the three constraint matrices of the CONFAC decomposition. The core of the generalized model consists of a precoder tensor decomposed as a function of three constraint matrices. Identifiability issues for blind symbol/code/channel recovery are discussed. The bit-error-rate performance of several MIMO-CDMA schemes are evaluated for different structures of the constraint matrices.

4.1 Introduction

Several transmission models for MIMO systems using CDMA codes have been the subject of recent research [79]. Spatial multiplexing strategies in conjunction with CDMA is addressed in a few recent works [123, 97, 55] with focus on layered space-time processing. In [123], the multiple transmit antennas are organized in groups and a unique spreading code is allocated within the same group. The separation of the different groups at the receiver is done by using a layered spacetime algorithm [69]. Focusing on the downlink reception, [97] also considers the spatial reuse of the spreading codes and proposes a chip-level equalizer at the receiver to handle the loss of code orthogonality. A space-time receiver for block-spread MIMO-CDMA is proposed in [55]. In this case, block-despreading is used prior to space-time filtering in order to eliminate multi-user interference and reduce receiver complexity.

On the other hand, CDMA-based transmit diversity schemes have been proposed earlier in [78, 56] and recently in [57]. These methods, commonly called *space-time spreading*, are capable of providing maximum transmit diversity gain without using extra spreading codes and without an increased transmit power. However, space-time spreading methods put more emphasis on diversity than on multiple-access interference. [158] investigates the performance of a range of linear single-user and multiuser detectors for MIMO-CDMA schemes with space-time spreading. In practice, due to the joint presence of multiple-access interference and time-dispersive multipath propagation, the large number of parameters to be estimated at the receiver (e.g. users' multipath channels, received powers, spreading codes) may require too much processing/training overhead and degrade receiver performance.

In this chapter, we show that several MIMO-CDMA schemes ranging from full transmit diversity to full spatial multiplexing and using different patterns of spatial reuse of the spreading codes can be modeled with the aid of the constraint matrices of the CONFAC decomposition introduced in Chapter 1. The distinguishing features of the proposed approaches w.r.t existing tensor-based CDMA models can be briefly summarized as follows:

- The constraints in the tensor model allow to cope with multiple transmit antennas and spreading codes per user or per data-stream, which provides an extension of [129, 48, 32] where each data stream is associated with only one spreading code;
- Several transmit schemes with varying degree of spatial spreading, spatial multiplexing and spreading code reuse can be obtained by adjusting the constraint matrices of the tensor signal model accordingly.

4.2 System model and assumptions

We consider the uplink of a single cell synchronous MIMO-CDMA system with Q active users and spreading factor P. The base-station receiver is equipped with K antennas and the q-th user transmits R_q independent data streams using M_q antennas. Multiple spreading codes per user are allowed, and J_q denotes the number of spreading codes associated with the q-th user. Each transmitted data stream contains N symbols. The wireless channel is assumed to be constant during N symbol periods. Flat-fading and user-wise independent multipath propagation are assumed. The transmit parameter set $\{R_q, M_q, J_q\}$, $q = 1, \ldots, Q$, utilized by the q-th user, as well as the number Q of active users are considered to be known at the base-station receiver. Users' spreading codes are assumed to be symbol-periodic spreading codes.

We assume that the propagation channel between each pair of transmit and receive antennas is characterized by L resolvable multipaths, where the l-th path delay is $(l-1)T_c$, T_c being the chip duration in seconds, i.e., the maximum path delay is equal to $\tau_{max} = (L-1)T_c$. The multipath channel is assumed to be constant during N symbols. We assume small angle-spread around the receiver, which arises when the multipath reflectors are in the far field of the receive antenna array [149]. Inter-Symbol Interference (ISI) is handled by assuming that the codes include L trailing zeros (or "guard chips") [131]. In this case, only Inter-Chip Interference (ICI) exists, and the *known* codes are interpreted as *unknown* "effective signature codes", and are given by the convolution of the transmitted spreading codes with the impulse response of the multipath channel [156], with P denoting the number of ISI-free chips per symbol. Under the assumption of independent multipath propagation, the effective signature codes (henceforth referred to as "spreading codes") are pseudo-random and mutually independent codes. We simply adopt the term "spreading code" for simplicity reasons.

4.3 Type-3 CONFAC-based MIMO-CDMA

For the considered multiuser MIMO-CDMA system, we formulate a new tensor model for the received signal [37, 36]. This model is based on the type-3 CONFAC decomposition introduced in Chapter 1 (c.f. Section 1.4). We start with a single-user model for simplicity reasons. Let $h_{k,m}$ be the spatial fading channel gain between the m-th transmit antenna and the k-th receive antenna, $s_{n,r} \doteq s((r-1)N+n)$ be the n-th symbol of the r-th data stream, and $c_{p,j}$ be the p-th element

of the j-th spreading code. Let us define $\mathbf{H} \in \mathbb{C}^{K\times M}$, $\mathbf{S} \in \mathbb{C}^{N\times R}$ and $\mathbf{C} \in \mathbb{C}^{P\times J}$ as the channel, symbol and code matrices, where $h_{k,m} \doteq [\mathbf{H}]_{k,m}$, $s_{n,r} \doteq [\mathbf{S}]_{n,r}$, and $c_{p,j} \doteq [\mathbf{C}]_{p,j}$ are, respectively, the entries of these matrices. We can view the discrete-time baseband version of the noise-free received signal at the n-th symbol period, p-th chip, and k-th receive antenna as a third-order tensor $\mathcal{X} \in \mathbb{C}^{N\times P\times K}$ with the (n,p,k)-th element defined as $x_{n,p,k} \doteq x_k((n-1)P+p)$. We propose the following input-output model for the considered MIMO- CDMA system:

$$x_{n,p,k} = \sum_{m=1}^{M} u_{n,p,m} h_{k,m}, \tag{4.1}$$

where $u_{n,p,m} \doteq u_m((n-1)P+p)$ is the (n,p,m)-th element of the third-order tensor $\mathcal{U} \in \mathbb{C}^{N\times P\times M}$ representing the effective transmitted signal. We treat $\mathcal{U}$ as the output of a *constrained space-time spreading* operation, which is modeled by the following constrained tensorial transformation:

$$u_{n,p,m} = \sum_{r=1}^{R}\sum_{j=1}^{J} g_m(r,j) s_{n,r} c_{p,j}, \quad g_m(r,j) \doteq \psi_{r,m}\phi_{j,m}, \tag{4.2}$$

where $g_m(r,j)$ is the (r,j)-th element of $\mathbf{G}_m \in \mathbb{C}^{R\times J}$. This matrix defines the allocation of R data streams and J spreading codes to the m-th transmit antenna. Let us define:

$$\mathbf{G} = \mathbf{\Psi}\mathbf{\Phi}^T \in \mathbb{C}^{R\times J}$$

as the *stream-to-code allocation matrix*. This matrix synthesizes the constrained structure of the model. It is given by the inner product of two *allocation matrices* $\mathbf{\Psi} \in \mathbb{C}^{R\times M}$ and $\mathbf{\Phi} \in \mathbb{C}^{J\times M}$, respectively. Note that $\mathbf{\Psi}$ and $\mathbf{\Phi}$ controls, respectively, the allocation of R data streams and J spreading codes to M transmit antennas. $\mathbf{\Psi}$ can be viewed as a *stream-to-antenna allocation matrix* and $\mathbf{\Phi}$ as a *code-to-antenna allocation matrix*.

The physical interpretation of (4.2) is that each data symbol $s_{n,r}$ is spread up to J times using the spreading codes $c_{p,1},\ldots,c_{p,J}$. Each spread symbol $s_{n,r}c_{p,j}$ is then loaded at the m-th transmit antenna. Depending on the structure of the $g_m(r,j)$'s, the same spread symbol $s_{n,r}c_{p,j}$ may simultaneously be loaded at several transmit antennas in order to benefit from transmit spatial diversity. From (4.1) and (4.2), we can express the received signal as

$$x_{n,p,k} = \sum_{m=1}^{M}\sum_{r=1}^{R}\sum_{j=1}^{J} g_m(r,j) s_{n,r} c_{p,j} h_{k,m} \tag{4.3}$$

By comparing (4.3) with (1.101), we can deduce the following correspondences:

$$\begin{aligned}(I_1, I_2, I_3, R_1, R_2, F) &\rightarrow (N, P, K, R, J, M),\\ (\mathbf{A}, \mathbf{B}, \mathbf{C}) &\rightarrow (\mathbf{S}, \mathbf{C}, \mathbf{H}),\end{aligned} \tag{4.4}$$

which means that the received signal model follows a type-3 CONFAC decomposition.

4.3.1 Multiuser signal model

Some definitions are now introduced, which allow us to view (4.3) also as a multiuser signal model. In the multiuser case, $R = R_1 + \cdots + R_Q$, $J = J_1 + \cdots + J_Q$, and $M = M_1 + \cdots + M_Q$ denote, respectively, the total number of data streams, spreading codes and transmit antennas considered, i.e., summed over all the Q users. In this case, $\mathbf{H}$, $\mathbf{S}$ and $\mathbf{C}$ are interpreted as *aggregate* channel, symbol and code matrices concatenating Q matrix-blocks, i.e.:

$$\begin{aligned}\mathbf{H} &= [\mathbf{H}^{(1)}, \ldots, \mathbf{H}^{(Q)}] \in \mathbb{C}^{K \times M},\\ \mathbf{S} &= [\mathbf{S}^{(1)}, \ldots, \mathbf{S}^{(Q)}] \in \mathbb{C}^{N \times R},\\ \mathbf{C} &= [\mathbf{C}^{(1)}, \ldots, \mathbf{C}^{(Q)}] \in \mathbb{C}^{P \times J},\end{aligned} \tag{4.5}$$

where $h^{(q)}_{k,m_q} \doteq [\mathbf{H}^{(q)}]_{k,m_q} \doteq [\mathbf{H}]_{k,\sum_{i=1}^{q-1} M_i + m_q}$, $s^{(q)}_{n,r_q} \doteq [\mathbf{S}^{(q)}]_{n,r_q} \doteq [\mathbf{S}]_{n,\sum_{i=1}^{q-1} R_i + r_q}$, and $c^{(q)}_{p,j_q} \doteq [\mathbf{C}^{(q)}]_{p,j_q} \doteq [\mathbf{C}]_{p,\sum_{i=1}^{q-1} J_i + j_q}$ define the entries of the q-th user channel, symbol and code matrices, respectively. We can also view the aggregate allocation matrices as a block-diagonal concatenation of Q matrix-blocks:

$$\begin{aligned}\mathbf{\Psi} &= \text{blockdiag}(\mathbf{\Psi}^{(1)} \cdots \mathbf{\Psi}^{(Q)}) \in \mathbb{C}^{R \times M}\\ \mathbf{\Phi} &= \text{blockdiag}(\mathbf{\Phi}^{(1)} \cdots \mathbf{\Phi}^{(Q)}) \in \mathbb{C}^{J \times M}\end{aligned} \tag{4.6}$$

where $\psi^{(q)}_{r_q,m_q} \doteq [\mathbf{\Psi}^{(q)}]_{r_q,m_q} \doteq [\mathbf{\Psi}]_{\sum_{i=1}^{q-1} R_i + r_q, \sum_{i=1}^{q-1} M_i + m_q}$ and $\phi^{(q)}_{j_q,m_q} \doteq [\mathbf{\Phi}^{(q)}]_{j_q,m_q} = [\mathbf{\Phi}]_{\sum_{i=1}^{q-1} J_i + j_q, \sum_{i=1}^{q-1} M_i + m_q}$ define the entries of the q-th user allocation matrices. Similarly, the aggregate stream-to-code allocation matrix is defined as:

$$\begin{aligned}\mathbf{G} &= \text{blockdiag}(\mathbf{G}^{(1)}, \cdots, \mathbf{G}^{(Q)}) = \mathbf{\Psi}\mathbf{\Phi}^T \in \mathbb{C}^{R \times J},\\ &\quad \text{with } \mathbf{G}^{(q)} = \mathbf{\Psi}^{(q)}\mathbf{\Phi}^{(q)T},\ q = 1, \ldots, Q.\end{aligned} \tag{4.7}$$

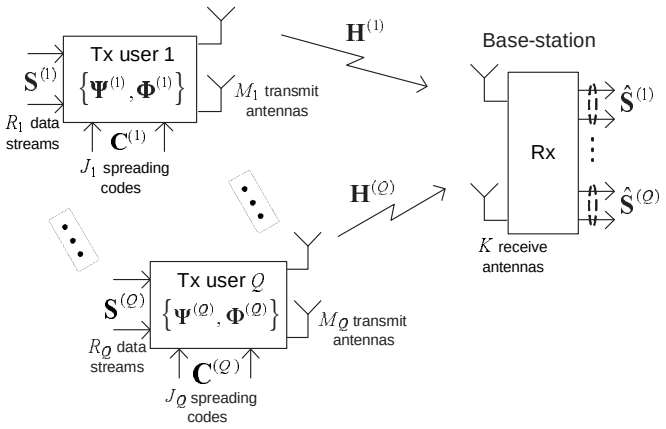

Figure 4.1: Uplink model of the proposed multiuser MIMO-CDMA system.

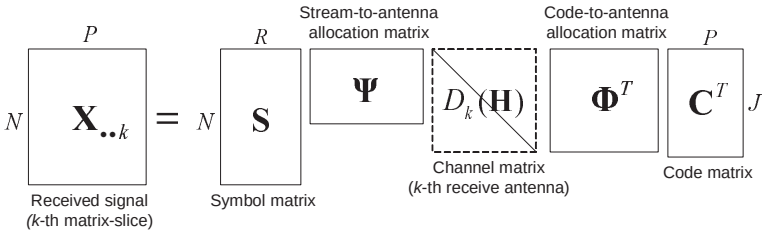

Figure 4.2: Constrained decomposition of the received signal tensor (k-th third-mode matrix slice).

Figure 4.1 depicts the proposed multiuser MIMO-CDMA model. Figure 4.2 illustrates the constrained factorization of the k-th third-mode slice of the received signal tensor.

Note that the received signal model (4.3) can be expressed in equivalent matrix forms. Let us define the three unfolded matrices of the received signal tensor as:

$$[\mathbf{X}_1]_{(k-1)N+n,p} = [\mathbf{X}_2]_{(n-1)P+p,k} = [\mathbf{X}_3]_{(p-1)K+k,n} = x_{n,p,k}$$

Comparing (4.3) with (1.83) and using (1.87), we have:

$$\mathbf{X}_1 = \big(\mathbf{H} \diamond (\mathbf{S\Psi})\big)(\mathbf{C\Phi})^T, \quad \mathbf{X}_2 = \big((\mathbf{S\Psi}) \diamond (\mathbf{C\Phi})\big)\mathbf{H}^T$$

$$\mathbf{X}_3 = \big((\mathbf{C\Phi}) \diamond \mathbf{H}\big)(\mathbf{S\Psi})^T. \tag{4.8}$$

Relation to the PARAFAC model of [131]

The parallel can be made by assuming $\{R_q\} = \{J_q\} = \{M_q\} = 1$. In this case, the correspondences between both tensor signal models are $(M, R, J) \rightarrow (Q, Q, Q)$, and we have $\mathbf{\Psi} = \mathbf{\Phi} = \mathbf{I}_Q$, meaning that the noiseless received signal model reduces to a single-antenna CDMA tensor model [131]:

$$x_{n,p,k} = \sum_{q=1}^{Q} s_{n,q} c_{p,q} h_{k,q}. \tag{4.9}$$

Therefore, the proposed model can be viewed as a generalization of the one in [131], which is restricted to the single-antenna CDMA case. The introduction of $\mathbf{\Psi}$ and $\mathbf{\Phi}$ gives flexibility (and more degrees of freedom) to our tensor signal modeling, in the sense that it models CDMA systems with multiple transmit antennas, multiple data streams and multiple spreading codes per user.

Remark 4.1: This constrained tensor model has properties similar to those of the tensor model proposed in [130] for blind single-antenna CDMA systems with large delay spread. This model can be also viewed as a constrained tensor model where the constrained structure is fixed and intrinsic to the propagation channel (and not to the multiple-antenna transmitter design as in our context).

Example 4.1: In order to illustrate the physical meaning of the allocation matrices, let us consider the simple example of a single-user multiple-antenna system ($Q = 1$). Assume that the serial input stream is divided into $R = 2$ parallel data streams transmitted by $M = 4$ transmit antennas using $J = 3$ orthogonal spreading codes. Suppose that the allocation scheme is defined by the following constraint matrices:

$$\mathbf{\Psi} = \begin{bmatrix} 1 & 1 & 0 & 0 \\ 0 & 0 & 1 & 1 \end{bmatrix}, \quad \mathbf{\Phi} = \begin{bmatrix} 1 & 1 & 0 & 0 \\ 0 & 0 & 1 & 0 \\ 0 & 0 & 0 & 1 \end{bmatrix} \tag{4.10}$$

The unitary entries in the first row of the stream-to-antenna matrix $\mathbf{\Psi}$ means that the first data stream is spread across the first and second transmit antennas. Likewise, the second row of $\mathbf{\Psi}$ shows that the second data stream is spread across the third and fourth transmit antennas. Now, looking at the code-to-antenna matrix $\mathbf{\Phi}$, we can see that the first two antennas share the same spreading code for transmission while the third and fourth transmit antennas are associated with different spreading codes. Several allocation structures with different allocation patterns

involving data streams and spreading codes for an arbitrary number of transmit antennas can be accommodated in our tensor model. However, the question is whether or not the chosen structure guarantees the uniqueness of the parameters of interest which is the symbol matrix and, possibly, the code matrix. In the next section, the design of the allocation matrices is studied.

4.4 Design of the allocation matrices

In this section, we study the design of the allocation matrices for ensuring blind symbol recovery (i.e. uniqueness of $\mathbf{S}$). Then, we describe a procedure for designing $\mathbf{\Psi}$ and $\mathbf{\Phi}$ which allows us to derive a set of multiple-antenna schemes for a fixed number of transmit antennas.

4.4.1 Generating vectors

For simplicity reasons, we omit the user-dependent index q in the design of the allocation matrices by considering a single-user system. Since the design criterion for these matrices is exactly the same for all the users, we can bypass the user-dependent notation without loss of generality while simplifying the notation.

We propose to parameterize the two allocation matrices $\mathbf{\Psi}$ and $\mathbf{\Phi}$ by their *generating vectors*. Let us define $\boldsymbol{\alpha} = [\alpha_1 \cdots \alpha_R]$ and $\boldsymbol{\beta} = [\boldsymbol{\beta}_1 \cdots \boldsymbol{\beta}_R]$, where $\boldsymbol{\beta}_r = [\beta_{r,1} \cdots \beta_{r,J_r}]$ as the generating vectors of $\mathbf{\Psi}$ and $\mathbf{\Phi}$, respectively. These vectors completely characterize the allocation structure in the considered MIMO system. Note that:

- α_r is the r-th *spatial spreading factor*, and denotes the number of transmit antennas associated with the r-th data stream;
- β_{r,j_r} is the j_r-th *code reuse factor*, and denotes the number of transmit antennas reusing the j_r-th spreading code of the r-th data stream, $j_r = 1, \ldots, J_r$.

The generating vectors are linked to the allocation matrices by the following relations:

$$\begin{aligned} \mathbf{\Psi}\mathbf{\Psi}^T &= \operatorname{diag}(\alpha_1, \ldots, \alpha_R) = \operatorname{diag}(\boldsymbol{\alpha}), \\ \mathbf{\Phi}\mathbf{\Phi}^T &= \operatorname{diag}(\boldsymbol{\beta}_1, \ldots, \boldsymbol{\beta}_R) = \operatorname{diag}(\boldsymbol{\beta}), \end{aligned}$$

For instance, in Example 4.1 the generating vectors of $\mathbf{\Psi}$ and $\mathbf{\Phi}$ are respectively:

$$\boldsymbol{\alpha} = [2\ 2], \quad \boldsymbol{\beta} = [2\ 1\ 1],$$

where $\alpha_1 = 2$, $\alpha_2 = 2$, $\beta_{1,1} = 2$, $\beta_{2,1} = 1$ and $\beta_{2,2} = 1$. Note that $\boldsymbol{\alpha}$ and $\boldsymbol{\beta}$ satisfy the following constraint:

$$\sum_{r=1}^{R} \alpha_r = \sum_{r=1}^{R} \sum_{j_r=1}^{J_r} \beta_{r,j_r} = M. \tag{4.11}$$

4.4.2 Design criterion

We borrow some basic concepts from partition theory [4] in order to design the allocation matrices. Specifically, the generating vectors $\boldsymbol{\alpha} = [\alpha_1 \cdots \alpha_R]$ and $\boldsymbol{\beta} = [\boldsymbol{\beta}_1 \cdots \boldsymbol{\beta}_R]$ are interpreted here as *partitions* of size M and dimensions R and J, respectively. The fact that $\boldsymbol{\alpha}$ and $\boldsymbol{\beta}$ are partitions of the same size is due to (4.11). Physically, $\boldsymbol{\alpha}$ is a partition of M transmit antennas into R subsets transmitting *different* data streams (i.e.,the r-th data stream is spread across α_r antennas). Likewise, $\boldsymbol{\beta}$ is a partition of M transmit antennas into J subsets, each one of which is associated with a *different* code (i.e., the j_r-th code is reused by β_{r,j_r} antennas). We suppose that $\boldsymbol{\alpha}$ and $\boldsymbol{\beta}$ satisfy the following design criterion:

$$\sum_{j_r=1}^{J_r} \beta_{r,j_r} = \|\boldsymbol{\beta}_r\|_1 = \alpha_r, \quad 1 \leq r \leq R, \tag{4.12}$$

where J_r is the dimension of the r-th subpartition $\boldsymbol{\beta}_r = [\beta_{r,1} \cdots \beta_{r,J_r}]$ of $\boldsymbol{\beta}$, with $J_1 + \cdots + J_R = J$. β_{r,j_r} corresponds to the number of times the j_r-th spreading code is reused by the r-th data stream, while J_r corresponds to the number of different spreading codes within the r-th antenna set.

Based on (4.12), we propose the following partitioned construction for $\mathbf{\Psi}$ and $\mathbf{\Phi}$:

$$\begin{aligned} \mathbf{\Psi} \quad &= \quad [\mathbf{\Psi}_1, \ldots, \mathbf{\Psi}_r, \ldots, \mathbf{\Psi}_R], \\ &\text{with} \quad \mathbf{\Psi}_r = \mathbf{1}_{\alpha_r}^T \otimes \mathbf{e}_r^{(R)}\ (R \times \alpha_r),\ r = 1, \ldots, R, \end{aligned} \tag{4.13}$$

and

$$\begin{aligned} \boldsymbol{\Phi} &= [\boldsymbol{\Phi}_1, \ldots, \boldsymbol{\Phi}_r, \ldots, \boldsymbol{\Phi}_R], \\ \text{with} \quad & \boldsymbol{\Phi}_r = [\boldsymbol{\Phi}_{r,1}, \ldots, \boldsymbol{\Phi}_{r,j_r}, \ldots, \boldsymbol{\Phi}_{r,J_r}] \ (J \times \alpha_r), \\ \text{and} \quad & \boldsymbol{\Phi}_{r,j_r} = \begin{bmatrix} \mathbf{0}_{\overline{J}_{r-1} \times \beta_{r,j_r}} \\ \mathbf{1}_{\beta_{r,j_r}}^T \otimes \mathbf{e}_{j_r}^{(J_r)} \\ \mathbf{0}_{(J-\overline{J}_r) \times \beta_{r,j_r}} \end{bmatrix} \ (J \times \beta_{r,j_r}), \end{aligned} \tag{4.14}$$

where $\mathbf{1}_n = [1\,1\,\cdots\,1]^T$ is an n-dimensional vector of ones, and $\overline{J}_r = \sum_{i=1}^{r} J_i$. Note that $\boldsymbol{\Psi}_r$ is the allocation matrix associated with the r-th transmitted data stream, and $\boldsymbol{\Phi}_{r,j_r}$ is the allocation matrix associated with the j_r-th spreading code used by the r-th data stream.

Constructing $\boldsymbol{\Psi}(\boldsymbol{\alpha})$ and $\boldsymbol{\Phi}(\boldsymbol{\beta})$ according to the design criterion (4.12), we can verify (see Appendix B) that any $\tilde{\mathbf{S}}$ and $\tilde{\mathbf{C}}$ satisfying the model are related to $\mathbf{S}$ and $\mathbf{C}$, respectively, by:

$$\begin{aligned} \tilde{\mathbf{S}} &= \mathbf{S}\mathbf{T}, \quad \mathbf{T} = \text{diag}(t_1, \ldots, t_R)\boldsymbol{\Pi}_R, \\ \tilde{\mathbf{C}} &= \mathbf{C}\mathbf{U}, \quad \mathbf{U} = \text{blockdiag}(\mathbf{U}_1, \ldots, \mathbf{U}_R)\overline{\boldsymbol{\Pi}}_J, \end{aligned} \tag{4.15}$$

where $\mathbf{U}_r \in \mathbb{C}^{J_r \times J_r}$ is a non-singular transformation ambiguity matrix, $\boldsymbol{\Pi}_R \in \mathbb{C}^{R \times R}$ is a permutation matrix and $\overline{\boldsymbol{\Pi}}_J \in \mathbb{C}^{J \times J}$ is a block-diagonal permutation matrix. In other words, the symbol matrix $\mathbf{S}$ is unique up to column permutation and scaling while the code matrix $\mathbf{C}$ is unique up to a multiplication by a non-singular block-diagonal matrix and column permutation. It is worth noting that the simultaneous uniqueness of $\mathbf{S}$ and $\mathbf{C}$ up to permutation and scaling arises in a particular case of (4.12) where $R = J$ and $\alpha_r = \beta_r$, $r = 1, \ldots, R$.

Remark 4.2: The uniqueness of $\mathbf{S}$ is the major concern here, since our final goal is the blind recovery of the transmitted data streams. On the other hand, the uniqueness of $\mathbf{H}$ is not required in our context, since we are mostly interested in a "direct" detection without using any knowledge about the channel.

Practical implications of the proposed design criterion: The proposed design criterion based on $\boldsymbol{\alpha}$ and $\boldsymbol{\beta}$ has some practical implications. First, we can observe that the spatial spreading of the data streams and the reuse of the spreading codes are restricted to adjacent transmit antennas only. This restriction can easily be deduced from the repetition pattern of identical canonical vectors in these matrices. Another implication of this construction is that different data

streams cannot be associated with the same spreading code for transmission. In other words, spreading code reuse only takes place across the transmit antennas transmitting the same data stream.

4.4.3 Design procedure

We propose a systematic procedure for building the allocation matrices $\mathbf{\Psi}$ and $\mathbf{\Phi}$ in (4.13)-(4.14) based only on the generating vectors $\boldsymbol{\alpha}$ and $\boldsymbol{\beta}$, according to the following steps:

(i) *A choice of $\boldsymbol{\alpha}$ is made for a fixed number M of transmit antennas (partition size) and a fixed number R of input data streams (partition dimension)*;

(ii) *For every α_r, a sub-partition $\boldsymbol{\beta}_r = [\beta_{r,1} \cdots \beta_{r,J_r}]$ of size α_r and dimension J_r is formed so that (4.12) is satisfied, and $\boldsymbol{\beta} = [\boldsymbol{\beta}_1 \cdots \boldsymbol{\beta}_R]$. The value of J_r, i.e. the number of spreading codes for the r-th data stream, is a design parameter.*

(iii) *$\mathbf{\Psi}$ and $\mathbf{\Phi}$ are built according to (4.13)-(4.14).*

4.4.4 Set of allocation schemes

More than one choice for $\boldsymbol{\beta}$ may be possible for a fixed $\boldsymbol{\alpha}$. This is due to the fact that more than one way of choosing a sub-partition $\boldsymbol{\beta}_r$ from α_r, $r = 1 \ldots, R$ may be possible without affecting the uniqueness property of the model. Each choice will lead to a different allocation structure $\mathbf{G} = \mathbf{\Psi}(\boldsymbol{\alpha})\mathbf{\Phi}(\boldsymbol{\beta})^T$. Following the proposed design procedure, a set of MIMO-CDMA schemes can be derived from the different possible choices of $\boldsymbol{\alpha}$ and $\boldsymbol{\beta}$. Table 4.1 shows the set of schemes for $M = 4$ transmit antennas. We assume that $\alpha_1 \geq \cdots \geq \alpha_R$, and $\beta_{1,1} \geq \cdots \geq \beta_{1,J_1} \geq \cdots \geq \beta_{R,1} \geq \cdots \geq \beta_{R,J_R}$. This assumption eliminates equivalent (redundant) schemes. For example, an allocation scheme with $\boldsymbol{\alpha} = [1\ 3]$ and $\boldsymbol{\beta} = [1\ 2\ 1]$ is considered equivalent to the one with $\boldsymbol{\alpha} = [3\ 1]$ and $\boldsymbol{\beta} = [2\ 1\ 1]$. Both schemes have the same spreading and multiplexing pattern (the order of association of data streams and spreading codes with the transmit antennas is irrelevant), and have the same uniqueness property (both schemes satisfy condition (4.12)). In this table, the different schemes are listed according to increasing values of R and J.

It can be seen from this table that 14 allocation schemes are possible. Note that for some values of R and J, 2 schemes exist. Let us consider the case $(R, J) = (1, 2)$,

Table 4.1: Set of schemes for $M = 4$.

(R, J)	$\boldsymbol{\alpha}$'s	$\boldsymbol{\beta}$'s	nb. of schemes
(1, 1)	4	4	1
(1, 2)	4	{[3 1]; [2 2]}	2
(1, 3)	4	[2 1 1]	1
(1, 4)	4	[1 1 1 1]	1
(2, 2)	{[3 1]; [2 2]}	{[3 1]; [2 2]}	2
(2, 3)	{[3 1]; [2 2]}	[2 1 1]	2
(2, 4)	{[3 1]; [2 2]}	[1 1 1 1]	2
(3, 3)	[2 1 1]	[2 1 1]	1
(3, 4)	[2 1 1]	[1 1 1 1]	1
(4, 4)	[1 1 1 1]	[1 1 1 1]	1

where we have 2 possible choices. For $\boldsymbol{\beta} = [3\ 1]$, antennas 1, 2 and 3 use the same spreading code, which is different from the one used by antenna 4. On the other hand, for $\boldsymbol{\beta} = [2\ 2]$ each spreading code is used twice by two different antenna sets. Both are full spatial spreading schemes, but having different code reuse patterns. For $(R, J) = (2, 2)$, we have 2 feasible schemes, and they correspond to those satisfying $\boldsymbol{\alpha} = \boldsymbol{\beta}$. For $(R, J) = (2, 3)$ and $(2, 4)$ we also have 2 schemes. Note that the basic difference between the schemes $(R, J) = (2, 2)$, $(2, 3)$ and $(2, 4)$ is on the code reuse/multiplexing pattern, the spatial spreading pattern being the same.

Remark 4.3: In this chapter, we have considered an uplink MIMO-CDMA system model, with multiple transmitters/users and a single (base-station) receiver. In [41], we address the downlink case with multiuser/multicode transmission. From the viewpoint of tensor modeling, this model is a generalization of the uplink model of this chapter to the case of multiuser spatial multiplexing, since several user transmissions are multiplexed across the same set of transmit antennas. Another distinguishing feature of [41] is the design of the allocation matrices. This work proposes a complete parametrization of the two allocation matrices along with new design constraints that allow to easily derive sets of downlink allocation schemes for a fixed number of transmit antennas.

4.4.5 Discussion

In practice, $\boldsymbol{\Psi}$ and $\boldsymbol{\Phi}$ can be designed based on practical restrictions such as the number of available spreading codes and transmit antennas, data-rate and diversity requirements. One way of optimizing the allocation matrices is to take advantage

of *a priori* channel state information at the transmitter. Since our design procedure allows the determination of a finite-set, or codebook, of feasible allocation schemes, limited feedback precoding methods [77, 95] can be used to select the best pair of constraint matrices at the transmitter. Although interesting, performance-oriented optimization of $\mathbf{\Psi}$ and $\mathbf{\Phi}$ is a topic beyond the scope of the thesis and will be elaborated in the future. Here, we only focus on uniqueness aspects for designing the transmit schemes. However, we conjecture that the optimization of the allocation structure can allow substantial performance gains compared to the non-optimized case. This issue is under investigation.

4.4.6 Identifiability

Let us rewrite the three unfolded matrices of the received signal (4.8) in the following equivalent manner:

$$\mathbf{X}_1 = \mathbf{Z}_1\big(\mathbf{H},\mathbf{S}\big)\mathbf{C}^T, \quad \mathbf{X}_2 = \mathbf{Z}_2\big(\mathbf{S},\mathbf{C}\big)\mathbf{H}^T, \quad \mathbf{X}_3 = \mathbf{Z}_3\big(\mathbf{C},\mathbf{H}\big)\mathbf{S}^T. \tag{4.16}$$

where

$$\mathbf{Z}_1\big(\mathbf{H},\mathbf{S}\big) = \big(\mathbf{H}\diamond(\mathbf{S}\mathbf{\Psi})\big)\mathbf{\Phi}^T \in \mathbb{C}^{KN\times J}, \quad \mathbf{Z}_2\big(\mathbf{S},\mathbf{C}\big) = (\mathbf{S}\mathbf{\Psi})\diamond(\mathbf{C}\mathbf{\Phi}) \in \mathbb{C}^{NP\times M},$$
$$\mathbf{Z}_3\big(\mathbf{C},\mathbf{H}\big) = \big((\mathbf{C}\mathbf{\Phi})\diamond\mathbf{H}\big)\mathbf{\Psi}^T \in \mathbb{C}^{PK\times R},$$

are the three constrained Khatri-Rao factorizations of the received signal model.

Theorem 5.1 (identifiability): *The identifiability of the constrained tensor model (4.3) in the Least Square (LS) sense requires that* $\mathbf{Z}_1\big(\mathbf{H},\mathbf{S}\big)$, $\mathbf{Z}_2\big(\mathbf{S},\mathbf{C}\big)$, *and* $\mathbf{Z}_3\big(\mathbf{C},\mathbf{H}\big)$ *are full column-rank, i.e.:*

$$KN \geq J, \quad NP \geq M, \quad \textit{and} \quad PK \geq R. \tag{4.17}$$

Proof: The proof is equal to that of Theorem 1.3 by using the following correspondences: $(I_1, I_2, I_3, R_1, R_2, R_3) \rightarrow (N, P, K, R, J, M)$. ■

From (4.17), the following corollaries can be obtained:

1. For $R = J = M$ (equal number of data streams, spreading codes and transmit antennas), the type-3 CONFAC decomposition of the received signal reduces to the PARAFAC decomposition of M factors, and (4.17) is equivalent to condition [132]:

$$\min(KN, NP, PK) \geq M$$

2. For $1 < R = J < M$ (equal number of data streams and spreading codes) we can decouple (4.17) into the two following conditions:

$$K \cdot \min(N, P) \geq R, \quad \text{and} \quad NP \geq M.$$

3. For $1 < R < J = M$ (equal number of spreading codes and transmit antennas), we obtain the two following conditions:

$$N \cdot \min(K, P) \geq M, \quad \text{and} \quad KP \geq R.$$

4.4.7 Discussion on the identifiability conditions:

Interpretation of (4.17)

These conditions relate all the system parameters of interest, which belong either to the transmitted or to the received signal dimensions. The transmitted signal dimensions are (R, J, M) while the receiver dimensions are (N, P, K). These identifiability conditions can be interpreted in the following manner. An increase in a transmitted signal dimension (e.g. *data stream*, *spreading code*, or *transmit antenna* dimension), representing an increase in the number of system parameters to be identified at the receiver, must be compensated by an increase in the corresponding received signal dimension(s). As a consequence of tensor modeling, an identifiability tradeoff arises in (4.17). For instance, an increase in the number R of data streams can be compensated by increasing the number K of receive antennas or by increasing the spreading factor P, or both, accordingly. A similar reasoning applies when the number of spreading codes or transmit antennas is increased.

On k-rank based conditions

Model (4.8) can be viewed as a third-order PARAFAC model with three equivalent factor matrices $\overline{\mathbf{S}} = \mathbf{S}\boldsymbol{\Psi}$, $\overline{\mathbf{C}} = \mathbf{C}\boldsymbol{\Phi}$ and $\mathbf{H}$. Due to the presence of sets of identical columns in $\boldsymbol{\Psi}$ and $\boldsymbol{\Phi}$, and consequently in $\overline{\mathbf{S}}$ and $\overline{\mathbf{C}}$, the identifiability result of [131], which is based on the concept of k-rank, does not apply to this constrained tensor model. This is due to the fact that $\overline{\mathbf{S}}$ and $\overline{\mathbf{C}}$ have k-rank equal to one, and the sufficient condition of [131] fails (see [131] for further details). The same comment is valid for the PARALIND model of [130] and [10], which exhibits similar constrained structure.

4.5 CONFAC-based MIMO-CDMA

Now, we present a CONFAC-based MIMO-CDMA model which generalizes the one proposed in the previous section [44, 35, 42]. At the transmitter, R input data streams are transmitted using J spreading codes and M transmit antennas. The proposed transmission model consists in: i) generating F precoded signals to be transmitted by spreading R input data streams[1] with the aid of J spreading codes and then ii) associating these F precoded signals with the M transmit antennas. The simultaneous transmission of the data streams across multiple transmit antennas may use different codes, or fully reuse the same code, or partially reuse one, or a set of, spreading code(s). Such a code reuse pattern will be explicitly modeled by fully exploiting the CONFAC decomposition structure.

4.5.1 Precoder decomposition

The signal to be transmitted is modeled by the sum of F *precoded* signal components. Let $g_{r,j,m}$ be the (r,j,m)-th element of the *precoder tensor* $\mathcal{G} \in \mathbb{C}^{R\times J\times M}$. This tensor determines the allocation of the r-th data stream and the j-th spreading code to the m-th transmit antenna. The F-factor decomposition of the precoder tensor is given, in scalar form, by the following "constrained" PARAFAC decomposition:

$$g_{r,j,m}(\mathbf{\Psi},\mathbf{\Phi},\mathbf{\Omega}) = \sum_{f=1}^{F} \psi_{r,f}\phi_{j,f}\omega_{m,f}. \tag{4.18}$$

$\mathbf{\Psi} \in \mathbb{C}^{R\times F}$, $\mathbf{\Phi} \in \mathbb{C}^{J\times F}$, $\mathbf{\Omega} \in \mathbb{C}^{M\times F}$ are *stream reuse*, *code reuse* and *antenna reuse* matrices, respectively. Therefore, the precoder tensor $\mathcal{G} \in \mathbb{C}^{R\times J\times M}$ can be viewed as a *joint stream-code-antenna multiplexer* which is decomposed in terms of elementary stream, code and antenna reuse matrices. For instance, $\psi_{r,f}\phi_{j,f}\omega_{m,f} = 1$ means that the r-th data stream is spread by the j-th spreading code and then transmitted by the m-th transmit antenna.

[1] Although not mentioned, the R input data streams can be associated with R users in a multiuser model.

4.5.2 Transmitted signal model

The transmitted signal is represented by the third-order tensor $\mathcal{U} \in \mathbb{C}^{N\times P\times M}$ with entry $u_{n,p,m}$. The discrete-time baseband version of the transmitted signal associated with the m-th transmit antenna, n-th symbol and p-th chip, is defined as $u_{n,p,m} \doteq u_m\big((n-1)P+p\big)$. We propose the following constrained factorization for modeling the effective transmitted signal:

$$\begin{aligned} u_{n,p,m} &= \sum_{r=1}^{R}\sum_{j=1}^{J} s_{n,r}c_{p,j}\, g_{r,j,m}(\boldsymbol{\Psi},\boldsymbol{\Phi},\boldsymbol{\Omega}), \\ &= \sum_{f=1}^{F}\sum_{r=1}^{R}\sum_{j=1}^{J} s_{n,r}c_{p,j}\, \psi_{r,f}\phi_{j,f}\omega_{m,f}, \end{aligned} \tag{4.19}$$

By comparing (4.19) with (1.83), we have the following correspondences:

$$\begin{gathered} (I_1, I_2, I_3, R_1, R_2, R_3, F) \leftrightarrow (N, P, M, R, J, M, F), \\ (\mathbf{A}, \mathbf{B}, \mathbf{C}) \leftrightarrow (\mathbf{S}, \mathbf{C}, \mathbf{I}_M). \end{gathered}$$

Hence, the transmitted signal model is a special case of the CONFAC decomposition, where the third-mode matrix is equal to the identity matrix.

We can rewrite (4.19) in the following form:

$$\begin{aligned} u_{n,p,m} &= \sum_{r=1}^{R}\sum_{j=1}^{J}\left(\sum_{f=1}^{F}\psi_{r,f}\phi_{j,f},\omega_{m,f}\right) s_{n,r}c_{p,j} \\ &= \sum_{r=1}^{R}\sum_{j=1}^{J}\Big[\boldsymbol{\Psi}D_m(\boldsymbol{\Omega})\boldsymbol{\Phi}^T\Big]_{r,j} s_{n,r}c_{p,j}. \end{aligned} \tag{4.20}$$

$\kappa_{r,j} = \Big[\boldsymbol{\Psi}D_m(\boldsymbol{\Omega})\boldsymbol{\Phi}^T\Big]_{r,j} = 1$ means that the m-th transmit antenna transmits the r-th data stream using the j-th spreading code. The transmitted signal slice $\mathbf{U}_{\cdot\cdot m} \in \mathbb{C}^{N\times P}$ associated with the m-th transmit antenna can be expressed as:

$$\mathbf{U}_{\cdot\cdot m} = \sum_{r,j/\kappa_{r,j}=1} \mathbf{S}_{\cdot r}\mathbf{C}_{\cdot j}^T, \tag{4.21}$$

or, equivalently, in terms of the constraint matrices:

$$\mathbf{U}_{\cdot\cdot m} = \mathbf{S}\big(\boldsymbol{\Psi}D_m(\boldsymbol{\Omega})\boldsymbol{\Phi}^T\big)\mathbf{C}^T. \tag{4.22}$$

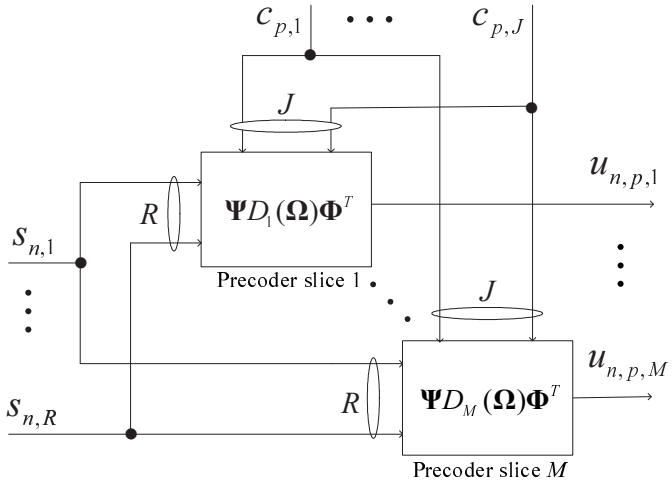

Figure 4.3: Block-diagram of the CONFAC-based MIMO transmission system.

The block diagram of the proposed MIMO transmission system is shown in Fig. 4.3. In this figure, the precoder tensor is shown in terms of its M matrix-slices. The m-th precoder slice generates a tensor signal component $u_{n,p,m}$ at the m-th transmit antenna by combining transmitted symbols and spreading codes, the combination pattern being determined by $\mathbf{\Psi}$, $\mathbf{\Phi}$ and $D_m(\mathbf{\Omega})$.

Example 4.2: In order to illustrate the physical meaning of the precoder decomposition, let us consider a MIMO-CDMA system transmitting $R = 2$ data streams with $J = 3$ spreading codes across $M = 3$ transmit antennas. Assume that $F = 3$ precoded signals are generated using the following constraint matrices:

$$\mathbf{\Psi} = \begin{bmatrix} 1 & 0 & 1 \\ 0 & 1 & 0 \end{bmatrix}, \quad \mathbf{\Phi} = \mathbf{\Omega} = \begin{bmatrix} 1 & 0 & 0 \\ 0 & 1 & 0 \\ 0 & 0 & 1 \end{bmatrix} = \mathbf{I}_3.$$

We have:

$$\mathbf{\Psi} D_1(\mathbf{\Omega})\mathbf{\Phi}^T = \begin{bmatrix} 1 & 0 & 0 \\ 0 & 0 & 0 \end{bmatrix}, \quad \mathbf{\Psi} D_2(\mathbf{\Omega})\mathbf{\Phi}^T = \begin{bmatrix} 0 & 0 & 0 \\ 0 & 1 & 0 \end{bmatrix},$$

$$\mathbf{\Psi} D_3(\mathbf{\Omega})\mathbf{\Phi}^T = \begin{bmatrix} 0 & 0 & 1 \\ 0 & 0 & 0 \end{bmatrix},$$

resulting in the following decomposition of $\mathbf{U}_{..1}$, $\mathbf{U}_{..2}$ and $\mathbf{U}_{..3}$:

$$\underbrace{\mathbf{U}_{..1} = \mathbf{S}_{.1}\mathbf{C}_{.1}^T}_{\text{signal at tx antenna 1}} \ , \quad \underbrace{\mathbf{U}_{..2} = \mathbf{S}_{.2}\mathbf{C}_{.2}^T}_{\text{signal at tx antenna 2}} \ , \quad \underbrace{\mathbf{U}_{..3} = \mathbf{S}_{.1}\mathbf{C}_{.3}^T}_{\text{signal at tx antenna 3}}$$

The first data stream is reused at the first and third transmit antennas with two different spreading codes, while the second data stream is transmitted by a single antenna using a single spreading code.

Example 4.3: Now, consider that we have $R = J = 2$, $M = 3$ and $F = 4$, with the following precoder constraint matrices:

$$\mathbf{\Psi} = \mathbf{\Phi} = \begin{bmatrix} 1 & 1 & 0 & 0 \\ 0 & 0 & 1 & 1 \end{bmatrix}, \quad \mathbf{\Omega} = \begin{bmatrix} 1 & 0 & 1 & 0 \\ 0 & 1 & 0 & 0 \\ 0 & 0 & 0 & 1 \end{bmatrix}.$$

We have:

$$\mathbf{\Psi} D_1(\mathbf{\Omega})\mathbf{\Phi}^T = \begin{bmatrix} 1 & 0 \\ 0 & 1 \end{bmatrix}, \quad \mathbf{\Psi} D_2(\mathbf{\Omega})\mathbf{\Phi}^T = \begin{bmatrix} 1 & 0 \\ 0 & 0 \end{bmatrix}, \quad \mathbf{\Psi} D_3(\mathbf{\Omega})\mathbf{\Phi}^T = \begin{bmatrix} 0 & 0 \\ 0 & 1 \end{bmatrix},$$

From (4.21), we deduce that:

$$\underbrace{\mathbf{U}_{..1} = \mathbf{S}_{.1}\mathbf{C}_{.1}^T + \mathbf{S}_{.2}\mathbf{C}_{.2}^T}_{\text{signal at tx antenna 1}}, \quad \underbrace{\mathbf{U}_{..2} = \mathbf{S}_{.1}\mathbf{C}_{.1}^T}_{\text{signal at tx antenna 2}} \ , \quad \underbrace{\mathbf{U}_{..3} = \mathbf{S}_{.2}\mathbf{C}_{.2}^T}_{\text{signal at tx antenna 3}}$$

In this case, the first and second data streams are code-multiplexed at the first transmit antenna. The first and second data streams are reused respectively by the second and third transmit antennas in order to achieve transmit spatial diversity.

Several transmit schemes can be designed for a fixed parameter set (R, J, M, F), by varying the pattern of 1's and 0's of the precoder constraint matrices.

4.5.3 Received signal model

The scalar component $x_{n,p,k}$ of the *received signal tensor* $\mathcal{X} \in \mathbb{C}^{N\times P\times K}$ is factored, in absence of noise, as:

$$\begin{aligned} x_{n,p,k} &= \sum_{m=1}^{M} h_{k,m} u_{n,p,m} \\ &= \sum_{r=1}^{R}\sum_{j=1}^{J}\sum_{m=1}^{M} s_{n,r} c_{p,j} h_{k,m}\, g_{r,j,m}(\mathbf{\Psi},\mathbf{\Phi},\mathbf{\Omega}) \end{aligned} \tag{4.23}$$

which is a CONFAC decomposition of the received signal as a function of symbol, code and channel matrices, the constrained structure being determined by the precoder tensor $g_{r,j,m}(\mathbf{\Psi},\mathbf{\Phi},\mathbf{\Omega})$. The following correspondences can be deduced by comparing (4.23) with (1.83):

$$\begin{aligned} (I_1, I_2, I_3, R_1, R_2, R_3, F) &\leftrightarrow (N, P, K, R, J, M, F), \\ (\mathbf{A}, \mathbf{B}, \mathbf{C}) &\leftrightarrow (\mathbf{S}, \mathbf{C}, \mathbf{H}). \end{aligned} \tag{4.24}$$

The unfolded matrices $\mathbf{X}_1 \in \mathbb{C}^{PK\times N}$, $\mathbf{X}_2 \in \mathbb{C}^{KN\times P}$ and $\mathbf{X}_3 \in \mathbb{C}^{NP\times K}$ can be factored as in (1.87) by taking the correspondences (4.24) into account.

4.6 Blind detection: uniqueness tradeoffs

As discussed in Chapter 1 (c.f. Section 1.4.3), the partial uniqueness property of the CONFAC decomposition leads to a "uniqueness tradeoff", where the essential uniqueness in one or two modes comes at the expense of a restrictive nonuniqueness in the other mode(s). The implications of this uniqueness tradeoff in terms of blind symbol/code/channel recovery are now studied.

Recall that the uniqueness conditions of Section 1.4.3 establish equivalences between pairs of constraint matrices ensuring essential uniqueness in two factor matrices of the CONFAC decomposition. Having in mind the correspondences (4.24), these equivalences admit a physical interpretation in terms of allocation of data streams and spreading codes to transmit antennas, leading to different blind symbol/code/channel recovery properties. We shall distinguish the precoder strategies in two groups: i) those with reuse across two dimensions only and; ii) those allowing reuse across all the dimensions. These two cases are now detailed:

4.6.1 Reuse across two dimensions only

We assume that either i) data streams and spreading codes (but not the transmit antennas) are reused more than once in the composition of the F precoded signals, or ii) transmit antennas and data streams (but not the spreading codes) are reused more than once. These two configurations are detailed below:

(1.a) $\underline{R = J < M = F}$ (no transmit antenna reuse): Each data stream is associated with a different spreading code. Each data stream/spreading code can be reused more than once by different transmit antennas (spatial diversity).

(2.a) $\underline{M = R < J = F}$ (no spreading code reuse): Each transmit antenna is associated with a different data stream. Each data stream/transmit antenna can be reused more than once by different spreading codes (code diversity);

4.6.2 Reuse across all the dimensions

We assume that data streams, spreading codes and transmit antennas are reused more than once in the composition of the F precoded signals. We consider two different situations:

(1.b) $\underline{R = J \leq M < F}$: Equal number of data streams and codes.

(2.b) $\underline{M = R \leq J < F}$: Equal number of data streams and antennas.

Resorting to the partial uniqueness corollaries **C.1** (for (1.a) and (1.b)) and **C.3** (for (2.a) and (2.b)) given in Section 1.4.3, we have the following results:

- For configurations (1.a) and (1.b), if $\mathbf{\Psi}$ and $\mathbf{\Phi}$ are equivalent, then both $\mathbf{S}$ and $\mathbf{C}$ are essentially unique, i.e. *joint symbol-code* recovery is achieved.
- For configurations (2.a) and (2.b), if $\mathbf{\Psi}$ and $\mathbf{\Omega}$ are equivalent, then both $\mathbf{S}$ and $\mathbf{H}$ are essentially unique, i.e. *joint symbol-channel* recovery is achieved.

These results illustrate the existing link between the space-time precoder structure with constraints used at the transmitter and the resulting blind symbol/code/channel recovery property at the receiver using the proposed CONFAC model. Several degrees of freedom for space-time precoder design are available for ensuring the blind symbol recovery.

It is worth noting that for configurations with more transmit antennas than data streams (meaning that there is one or more data streams spatially spread using multiple transmit antennas), the proposed transmission model is similar to space-time spreading [103, 78, 56]. On the other hand, if we have more data streams than transmit antennas (meaning that two or more data streams are code-multiplexed at the same transmit antenna), the proposed transmission model is close to space-time multiplexing [102, 57].

4.6.3 Receiver algorithm

As in the previous chapters, we make use of the ALS algorithm. In the present context, this algorithm consists in fitting a CONFAC model to the received signal tensor in order to estimate the symbol, code and channel matrices in presence of an additive white Gaussian noise. Since the precoder constraint matrices $\mathbf{\Psi}$, $\mathbf{\Phi}$ and $\mathbf{\Omega}$ are known at the receiver, they are fixed during the whole iterative estimation process.

Define $\tilde{\mathbf{X}}_i = \mathbf{X}_i + \mathbf{V}_i$, $i = 1, 2, 3$, as the noisy versions of $\mathbf{X}_i$, where $\mathbf{V}_i$ is an additive complex-valued white gaussian noise matrix. The algorithm consists of the following steps:

1. Set $i = 0$;
   Randomly initialize $\widehat{\mathbf{S}}_{(i=0)}$ and $\widehat{\mathbf{H}}_{(i=0)}$;

2. $i = i + 1$;

3. Using $\tilde{\mathbf{X}}_1$, find an LS estimate of $\mathbf{C}_{(i)}$:
   $\widehat{\mathbf{C}}_{(i)}^T = \left[(\widehat{\mathbf{H}}_{(i-1)}\mathbf{\Omega} \diamond \widehat{\mathbf{S}}_{(i-1)}\mathbf{\Psi})\mathbf{\Phi}^T\right]^\dagger \tilde{\mathbf{X}}_1$;

4. Using $\tilde{\mathbf{X}}_2$, find an LS estimate of $\mathbf{H}_{(i)}$:
   $\widehat{\mathbf{H}}_{(i)}^T = \left[(\widehat{\mathbf{S}}_{(i-1)}\mathbf{\Psi} \diamond \widehat{\mathbf{C}}_{(i)}\mathbf{\Phi})\mathbf{\Omega}^T\right]^\dagger \tilde{\mathbf{X}}_2$;

5. Using $\tilde{\mathbf{X}}_3$, find an LS estimate of $\mathbf{S}_{(i)}$:
   $\widehat{\mathbf{S}}_{(i)}^T = \left[(\widehat{\mathbf{C}}_{(i)}\mathbf{\Phi} \diamond \widehat{\mathbf{H}}_{(i)}\mathbf{\Omega})\mathbf{\Psi}^T\right]^\dagger \tilde{\mathbf{X}}_3$;

6. Repeat steps 2-5 until convergence.

In practice, it is reasonable to assume known spreading codes at the receiver. In this case, the matrix $\mathbf{C}$ is fixed during the ALS algorithm and Step 3 is skipped. The knowledge of one factor matrix generally accelerates the convergence of the ALS algorithm, even with small blocks of received samples [129]. Therefore, exploiting the knowledge of the spreading code matrix (whenever it is available) is beneficial from this viewpoint.

4.7 Performance evaluation

We present some simulation results for illustrating the performance of the proposed MIMO-CDMA transmission models. We are interested in the symbol and channel recovery with the knowledge or not of the spreading codes at the receiver. Therefore, two different detection assumptions are considered:

- *Code-assisted detection*: The spreading code matrix $\mathbf{C}$ is assumed to be *known* at the receiver so that Step 3 of the ALS algorithm is skipped. Hadamard(P) spreading codes are used in this case.
- *Code-blind detection*: The spreading code matrix $\mathbf{C}$ is assumed to be *unknown* at the receiver as a consequence of multipath delay propagation. In this case, the ALS receiver fully iterates for estimating the code matrix $\mathbf{C}$. The spreading code matrix is generated by convolving the Hadamard(P) code with the considered multipath delay channel [156].

Performance evaluation is based on average Bit-Error-Rate (BER) *versus* Signal-to-Noise Ratio (SNR) plots, obtained by means of Monte Carlo runs. The number of runs vary from 1000 to 5000 depending on the simulated SNR value. At each run, the additive noise power is generated according to the SNR value given by:

$$\text{SNR} = 10\log_{10}\frac{\|\mathbf{X}_1\|_F^2}{\|\mathbf{V}_1\|_F^2}\,\text{dB}.$$

This SNR measure takes into account the effects of multiple transmit/receive antennas, fading and multipath. The spatial channel gains and multipath fading are drawn from an i.i.d. complex-valued Gaussian generator while the transmitted symbols are drawn from a pseudo-random Quaternary Phase Shift Keying (QPSK) sequence. Our simulations focus on challenging system configurations with a small number of receive antennas and short received data blocks, which is more attractive in practice.

It is known that the ALS algorithm is strongly dependent on the initialization in the completely blind case (where $\mathbf{S}$, $\mathbf{C}$ and $\mathbf{H}$ are unknown). Indeed, ill-convergence to local minima generally occurs for bad initializations. At each run, we consider 10 different random initializations and the best one is chosen for performance evaluation. The best initialization corresponds to the one with the smallest error. The scaling ambiguity affecting the estimates of the symbol matrix is resolved by assuming that the first symbol of each data stream is equal to 1. We recall that the unknown scaling factor that is inherent to the blind estimation process is eliminated by normalizing each column of the estimated symbol matrix by its first element. Differential modulation/encoding can optionally be used to eliminate this ambiguity [131]. In the unknown spreading code case, the inherent column permutation ambiguity in $\mathbf{S}$ is resolved using a greedy least squares $(\mathbf{S}, \hat{\mathbf{S}})$-column matching algorithm [131].

4.8 Simulation results–Part 1

This section contains the first part of our computer simulation results. We evaluate the BER performance of the type-3 CONFAC-based MIMO-CDMA model of Section 4.3. The second part will be dedicated to the CONFAC-based model of Section 4.5. Different allocation structures for $M = 2, 3$ and 4 are considered. The ALS algorithm is used as the multiuser detection receiver. Note that for the type-3 CONFAC MIMO-CDMA model, the ALS algorithm coincides with the one described in (4.6.3) with $\mathbf{\Omega} = \mathbf{I}_R$.

The BER curves represent the performance averaged on the R transmitted data streams, except in some figures, where we plot the individual performance of each data stream for a more detailed analysis. We assume $K = 2$ and $N = 10$ throughout the simulations, unless otherwise stated. The most relevant parameters to be considered here are the generating vectors $\boldsymbol{\alpha}$ and $\boldsymbol{\beta}$ of the allocation structure, defining the spatial spreading and code reuse factors, respectively. In all the simulations, the transmit parameters are shown at the top of each figure. We recall that for given $\boldsymbol{\alpha}$ and $\boldsymbol{\beta}$, the corresponding values of R and J can be deduced, as shown in Table 4.1 for $M = 4$.

It is worth mentioning that our simulation results do not distinguish between the detection of Q user signals with M_q transmit antennas, R_q data streams and J_q spreading codes each, or the detection of a single-user signal with $M = M_1 + \cdots + M_Q$ antennas, $R = R_1 + \cdots + R_Q$ data streams and $J = J_1 + \cdots + J_Q$ spreading codes. Since the ALS receiver is based on a joint multiuser detection, distinguishing between both cases is not relevant for purposes of performance evaluation.

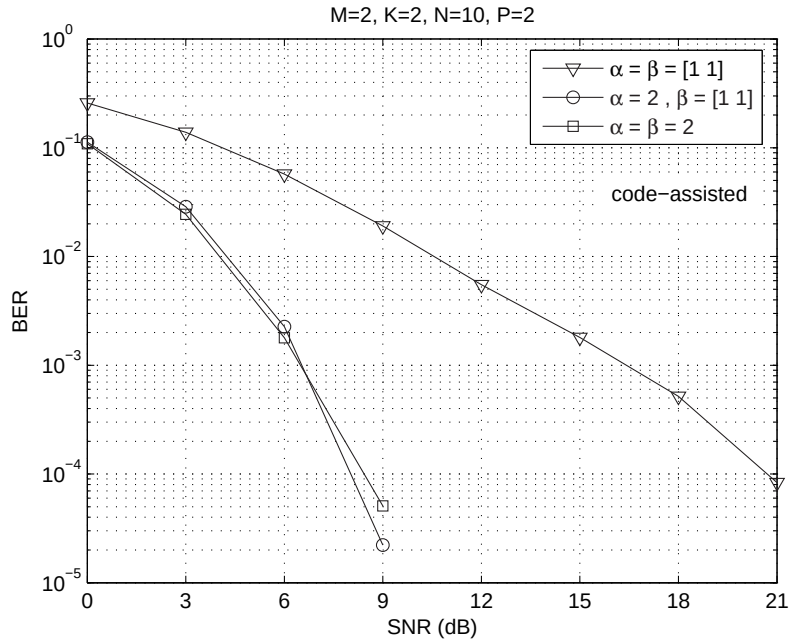

Figure 4.4: Average performance of 3 different transmit schemes with $M = 2$.

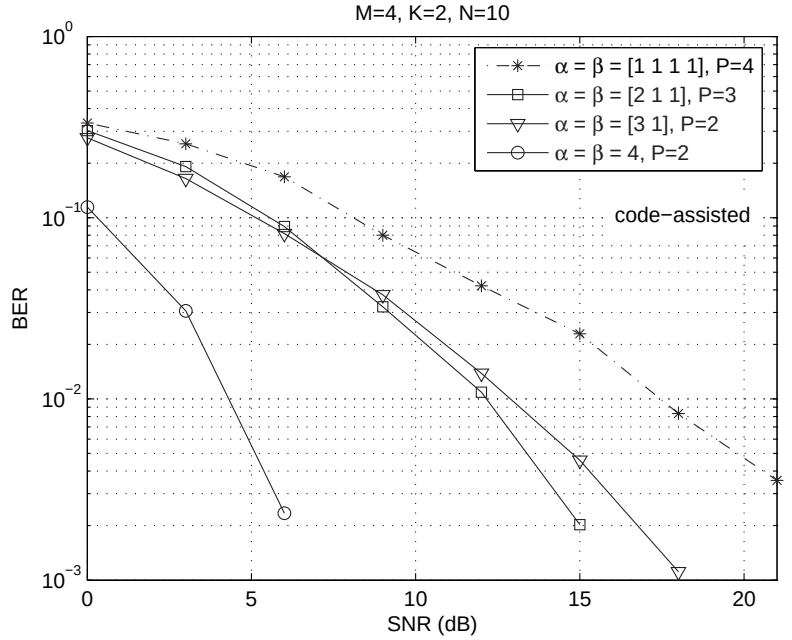

Figure 4.5: Average performance of 4 different transmit schemes with $M = 4$.

4.8.1 Performance of different schemes ($M = 2$ and $M = 4$)

First, we consider the code-assisted detection and investigate the performance of some MIMO-CDMA schemes for $M = 2$ and $M = 4$ transmit antennas. Figure 4.4 depicts the performance of 3 different schemes for $M = 2$. The allocation matrices for these schemes are given by:

generating vectors	allocation matrices
$\boldsymbol{\alpha} = \boldsymbol{\beta} = [1\ 1]$	$\boldsymbol{\Psi} = \boldsymbol{\Phi} = \mathbf{I}_2$
$\boldsymbol{\alpha} = 2, \quad \boldsymbol{\beta} = [1\ 1]$	$\boldsymbol{\Psi} = [1\,1], \quad \boldsymbol{\Phi} = \mathbf{I}_2$
$\boldsymbol{\alpha} = \boldsymbol{\beta} = 2$	$\boldsymbol{\Psi} = \boldsymbol{\Phi} = [1\ 1]$

We can observe that performance improves when going from full spatial multiplexing ($\boldsymbol{\alpha} = \boldsymbol{\beta} = [1\ 1]$) to full spatial spreading with code reuse ($\boldsymbol{\alpha} = \boldsymbol{\beta} = 2$). Such a performance gain comes at the expense of a reduction of the spectral efficiency P/R by a factor of two. Spatial spreading with code multiplexing ($\boldsymbol{\alpha} = [2], \boldsymbol{\beta} = [1\ 1]$) offers nearly the same average performance as spatial spreading with code reuse. The use of code multiplexing in place of code reuse can be more attractive in scenarii where the spatial channels from the different transmit antennas are correlated and transmit spatial signatures are poor [102]. We shall come back to this issue latter in our simulation results. Figure 4.5 shows the performance of 4 different schemes for $M = 4$, considering $R = J$ and $\boldsymbol{\alpha} = \boldsymbol{\beta}$. The spreading factor P is adjusted for keeping the spectral efficiency P/R constant (except for $\boldsymbol{\alpha} = \boldsymbol{\beta} = 4$ where spectral efficiency is reduced twice). A variable degree of spatial diversity is afforded by the different choices of $\boldsymbol{\alpha}$ and $\boldsymbol{\beta}$.

4.8.2 Influence of the code reuse pattern (choice of $\boldsymbol{\beta}$)

Figure 4.6 compares the performance of two different schemes combining spatial spreading and spatial multiplexing for $M = 3$. Both schemes have the same spatial spreading pattern, the difference being on the code reuse/multiplexing pattern. In contrast to previous figures, we plot the individual performance for each data stream in order to verify the influence of code reuse/multiplexing. It can be concluded that the difference between these transmit schemes is basically on the performance of the second data stream, which is significantly better as code multiplexing is used. This result confirms that using different codes for transmitting the same data stream across different antennas allows the receiver to use both spatial and code information to distinguish the transmitted substreams, corroborating with [79] and [102].

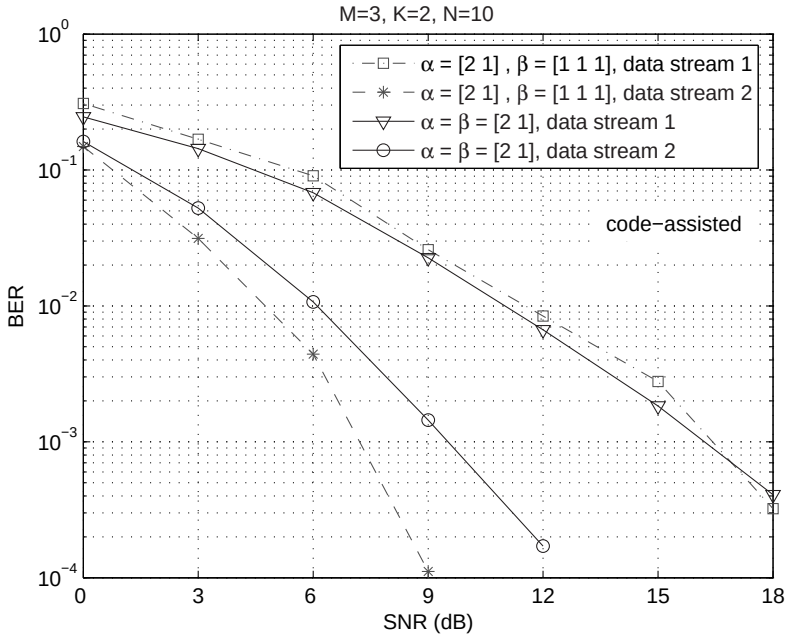

Figure 4.6: Individual data stream performance for 2 different transmit schemes with $M = 3$ and different choices of $\boldsymbol{\beta}$

4.8.3 Performance over spatially-correlated channel

Now, we are interested in investigating the impact of using different codes for transmitting the same data stream over a practical (non-ideal) channel with transmit correlation. We assume that only the transmit antennas are correlated, which can be a reasonable assumption in uplink transmission with poor scattering around the transmitter. At the base-station receiver, we assume sufficient scattering so that the receive antennas are uncorrelated. We adopt the following channel model with transmit correlation [125]:

$$\mathbf{H} = \mathbf{H}_o \mathbf{R}_t^{1/2},$$

where $\mathbf{H}_o$ is a matrix of complex i.i.d. Gaussian variables of unity variance and $\mathbf{R}_t$ the transmit covariance matrix. In this experiment, we assume $M = 4$ and $\mathbf{R}_t$ is given by [71]:

$$\mathbf{R}_t = \begin{bmatrix} 1 & 0.57e^{-2.25j} & 0.17e^{0.02j} & 0.29e^{-2.94j} \\ 0.57e^{2.25j} & 1 & 0.57e^{-2.25j} & 0.17e^{0.02j} \\ 0.17e^{-0.02j} & 0.57e^{2.25j} & 1 & 0.57e^{-2.25j} \\ 0.29e^{2.94j} & 0.17e^{-0.02j} & 0.57e^{2.25j} & 1 \end{bmatrix}$$

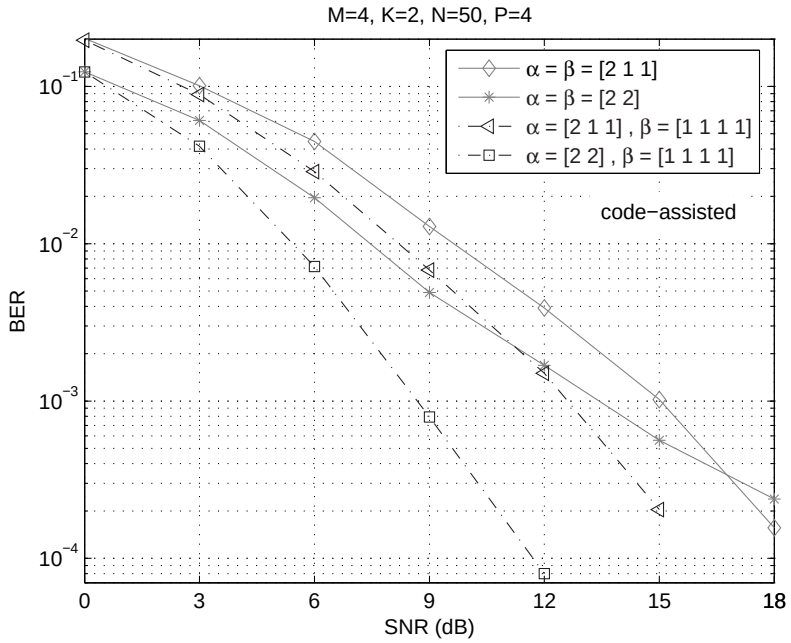

Figure 4.7: Average performance of 4 different transmit schemes with $M = 4$ over a channel with transmit spatial correlation.

We consider four allocation schemes having different spatial spreading/multiplexing and code reuse/multiplexing patterns. We focus on the isolated performance for each data stream. According to Figure 4.7, for a fixed choice of $\boldsymbol{\alpha}$ and $\boldsymbol{\beta}$, better results are obtained when full code multiplexing is used ($\boldsymbol{\beta} = [1\ 1\ 1\ 1]$). Note that, when $\boldsymbol{\alpha} = \boldsymbol{\beta} = [2\ 2]$, the performance tends to saturate at high SNR as a consequence of transmit spatial correlation. Keeping $\boldsymbol{\alpha} = [2\ 2]$ and using $\boldsymbol{\beta} = [1\ 1\ 1\ 1]$ in place of $\boldsymbol{\beta} = [2\ 2]$, a significant performance improvement is obtained at the expense of using twice the number of spreading codes. The same comment is valid for $\boldsymbol{\alpha} = [2\ 1\ 1]$. These results show that the choice of the generating vectors is important in practical scenarii.

4.8.4 Code-blind versus code-assisted detection

In all the previously obtained results, we have considered code-assisted detection by assuming perfectly orthogonal spreading codes (no inter-chip interference). The next results consider the more challenging code-blind detection, where the (effective) spreading codes are unknown to the receiver due to multipath propagation. The effective spreading codes are generated by convolving a Hadamard code with

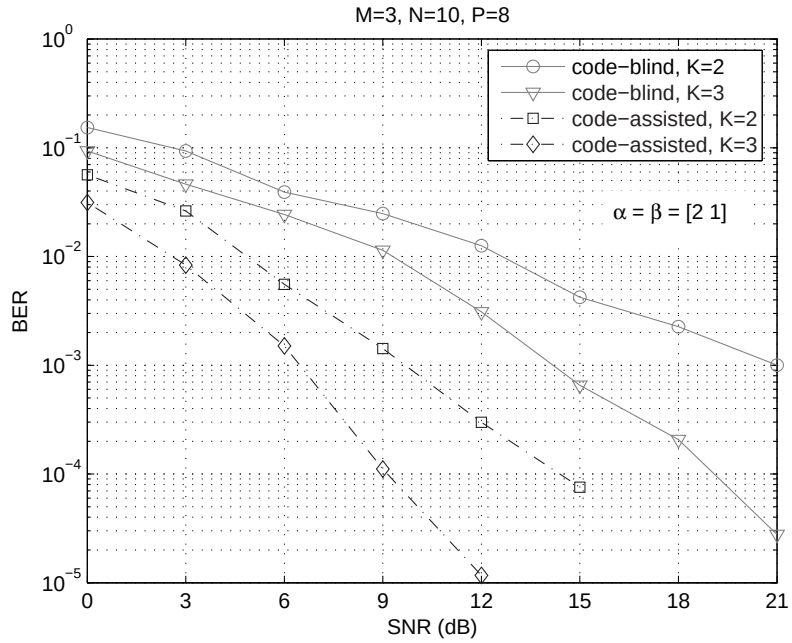

Figure 4.8: Comparison between code-assisted and code-blind detection with $M = 3$.

a two-tap multipath delay channel, the delay between the two taps being equal to two chip periods. At each run, these multipath components are drawn from an i.i.d. complex-valued Gaussian generator. Figure 4.8 compares the performance of code-blind and code-assisted detection. In this case we fix $N = 10$, $P = 8$, $\boldsymbol{\alpha} = \boldsymbol{\beta} = [2\ 1]$ while K is varied. We can observe a performance loss of the code-blind receiver with respect to the code-assisted one. The performance gap is attributed, in part, to the presence of inter-chip interference and the lack of knowledge of the code matrix which induces more parameters to be estimated by means of the ALS algorithm.

4.8.5 Comparison with the optimum ZF receiver

As a reference for comparison, we now consider the performance of the Zero Forcing (ZF) receiver with perfect knowledge of the channel and code matrices. The ZF receiver is compared with the channel- and code-blind ALS receiver. The ZF receiver consists in a single-step estimation of the symbol matrix given by

$$\widehat{\mathbf{S}}_{\mathrm{ZF}}^{T} = \left[\left((\mathbf{C}\boldsymbol{\Phi}) \diamond \mathbf{H}\right)\boldsymbol{\Psi}^{T}\right]^{\dagger} \tilde{\mathbf{X}}_{3},$$

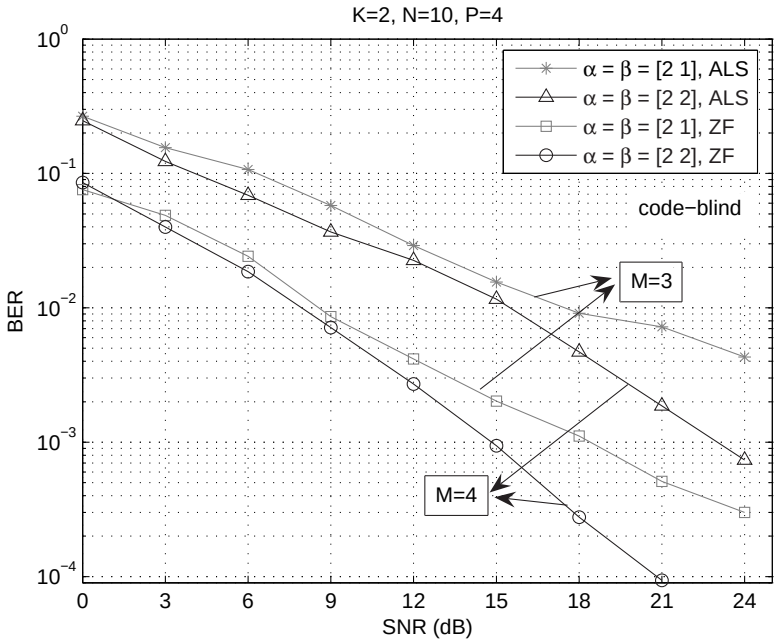

Figure 4.9: Comparison between code-blind ALS and ZF receivers (Perfect channel/code knowledge is assumed for the ZF receiver).

$\mathbf{H}$ and $\mathbf{C}$ being perfectly known. We consider two allocation schemes with $\boldsymbol{\alpha} = \boldsymbol{\beta} = [2\ 1]$ ($M = 3$) and $[2\ 2]$ ($M = 4$). It can be seen from Figure 4.9 that the gap between ALS and ZF is around 6dB in terms of SNR for BER=$2 \cdot 10^{-2}$. We can observe that the same performance improvement is obtained for both ZF and ALS when M is increased.

4.9 Simulation results–Part 2

In this section, simulation results are provided for performance assessment of the CONFAC-based MIMO-CDMA model (4.23). Unless otherwise stated, $K = 2$ receive antennas and $N = 50$ signal samples are assumed throughout the simulations.

4.9.1 Performance of different allocation schemes

We evaluate the receiver BER performance for some choices of the precoder constraint matrices. We begin by considering a flat-fading channel with the knowledge of the spreading codes at the receiver. We assume $F = 3$ precoded signals, $J = 2$ or 3 spreading codes, and $M = 2$ or 3 transmit antennas. The spreading factor is set to $P = 4$. The orthogonal spreading codes are columns of a Hadamard(4) matrix. The data stream allocation matrix $\mathbf{\Psi}$ is the one of Example 3 of Section 4.5.2, which is recalled here for convenience:

$$\mathbf{\Psi} = \begin{bmatrix} 1 & 0 & 1 \\ 0 & 1 & 0 \end{bmatrix}.$$

Three different precoding schemes for 2 or 3 spreading codes/transmit antennas are tested by varying the structure of the code and antenna allocation matrices $\mathbf{\Phi}$ and $\mathbf{\Omega}$:

$$\mathbf{\Phi} = \mathbf{\Psi}, \quad \mathbf{\Omega} = \mathbf{I}_3 \ (J = 2, M = 3),$$

$$\mathbf{\Phi} = \mathbf{\Psi}, \quad \mathbf{\Omega} = \begin{bmatrix} 1 & 0 & 0 \\ 0 & 1 & 1 \end{bmatrix} \ (J = 2, M = 2),$$

$$\mathbf{\Phi} = \mathbf{I}_3, \quad \mathbf{\Omega} = \begin{bmatrix} 1 & 0 & 0 \\ 0 & 1 & 1 \end{bmatrix} \ (J = 3, M = 2).$$

The BER performance of the three schemes are depicted in Figure 4.10. It can be seen that the first and second schemes have similar performance. The third scheme provides the best performance due to the fact that the two first schemes reuse one spreading code which is not the case for the third scheme.

In a second experiment, we assume $F = 4$ precoded signals, and $J = 2$, 3 or 4 orthogonal spreading codes. The number of transmit antennas is fixed at $M = 4$, and the spreading factor at $P = 4$. The fixed structure of $\mathbf{\Psi}$ and $\mathbf{\Omega}$ is as follows (the same used in Example 4 of Section 4.5.2):

$$\mathbf{\Psi} = \begin{bmatrix} 1 & 1 & 0 & 0 \\ 0 & 0 & 1 & 1 \end{bmatrix}, \quad \mathbf{\Omega} = \begin{bmatrix} 1 & 0 & 1 & 0 \\ 0 & 1 & 0 & 0 \\ 0 & 0 & 0 & 1 \end{bmatrix} \tag{4.25}$$

According to the structure of $\mathbf{\Psi}$ and $\mathbf{\Omega}$, we can see that each data stream is simultaneously transmitted by two transmit antennas. We consider three code

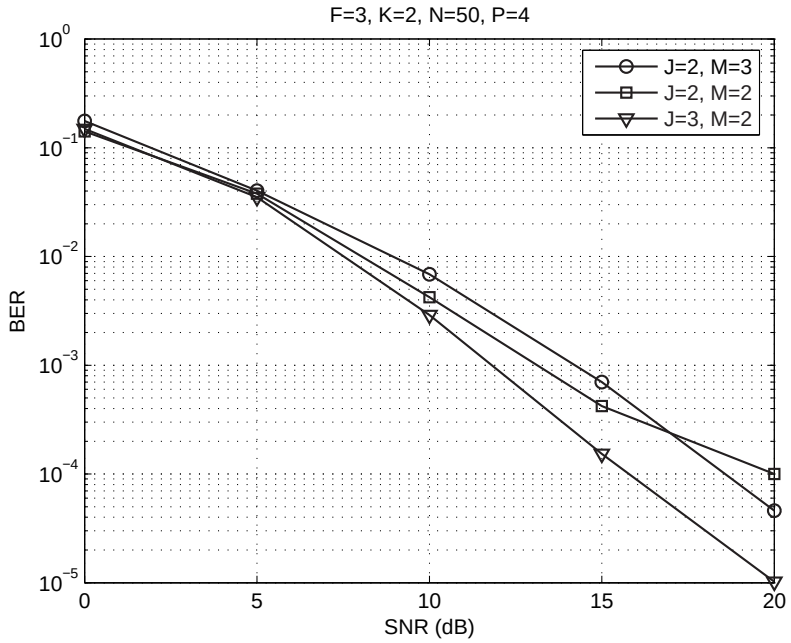

Figure 4.10: Performance of different allocation schemes with $F = 3$.

reuse patterns. The three choices for the code allocation matrix $\mathbf{\Phi}$ are:

$$\mathbf{\Phi} = \mathbf{\Psi} \ (J = 2), \quad \mathbf{\Phi} = \begin{bmatrix} 1 & 1 & 0 & 0 \\ 0 & 0 & 1 & 0 \\ 0 & 0 & 0 & 1 \end{bmatrix} \ (J = 3),$$

$$\mathbf{\Phi} = \mathbf{I}_4 \ (J = 4). \tag{4.26}$$

The first scheme reuses twice both spreading codes. The second one reuses only the first spreading code while the third one uses different spreading codes. The results are shown in Figure 4.11. As expected, the performance improves at the expense of using more orthogonal codes. From the slope of the BER curves, we remark that an increased spatial diversity gain is obtained with the third precoding scheme.

4.9.2 Performance with unknown spreading codes

We now consider the case where the spreading codes are unknown at the receiver resulting from the presence of ICI due to multipath/delay propagation. We assume that the channel has $L = 3$ chip-spaced multipath components. The multipaths

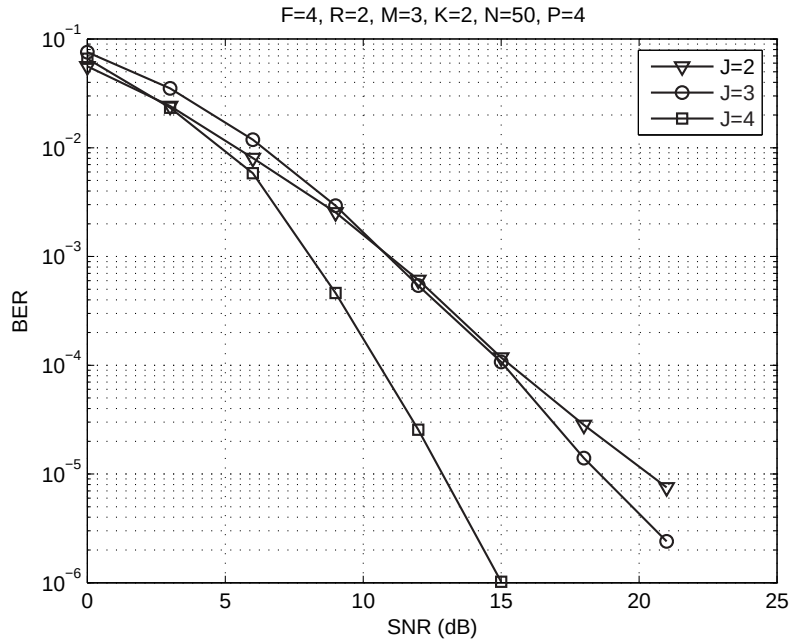

Figure 4.11: Performance of different allocation schemes with $F = 4$.

undergo independent Rayleigh fading. In order to avoid ISI, $L = 2$ trailing zeros (guard chips) are included in each spreading code, as discussed in Section 4.5. We consider two transmit schemes with $F = 4$. The first one with $R = J = 2$ and $P = 4$ ISI-free chips (Hadamard(2) codes increased by $L = 2$ trailing zeros) and the second one with $R = J = 3$ and $P = 6$ ISI-free chips. Both schemes have the same antenna reuse pattern and the chosen $\mathbf{\Omega}$ is the one given in (4.25). The two other precoding constraint matrices are given below for the first and second schemes, respectively:

$$\mathbf{\Psi} = \mathbf{\Phi} = \begin{bmatrix} 1 & 1 & 0 & 0 \\ 0 & 0 & 1 & 1 \end{bmatrix} \quad (R = J = 2) \tag{4.27}$$

$$\mathbf{\Psi} = \mathbf{\Phi} = \begin{bmatrix} 1 & 0 & 0 & 0 \\ 0 & 1 & 0 & 0 \\ 0 & 0 & 1 & 1 \end{bmatrix} \quad (R = J = 3).$$

Note that both schemes trade off spatial multiplexing and transmit diversity. In the first one, each data stream is transmitted by two transmit antennas. In the second one, spatial multiplexing takes place within the first and second antennas. Both schemes have the same spectral efficiency (the ratio R/P is constant). According to Figure 4.12, the first scheme outperforms the second one. This is due to the

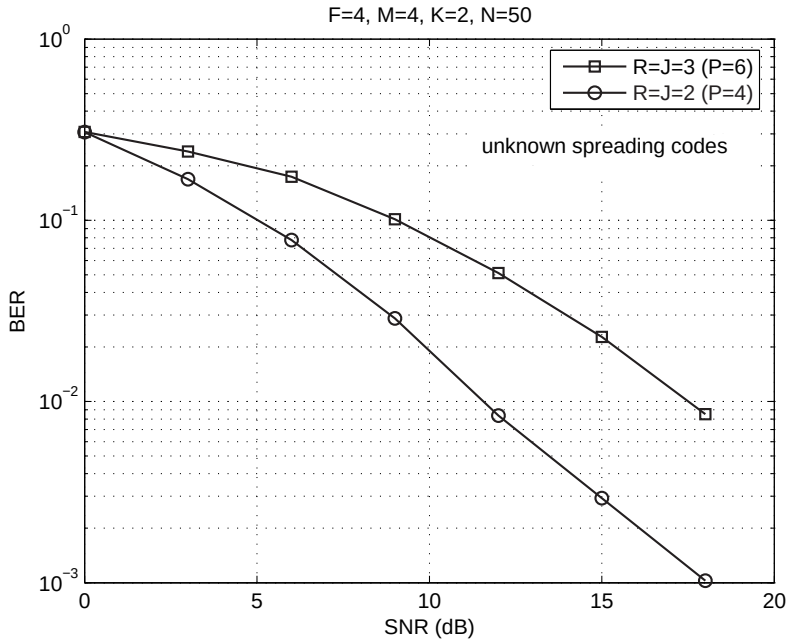

Figure 4.12: Performance of two transmit schemes with multipath/delay propagation and unknown spreading codes, for $R = 2$ and 3 data streams.

improved signal separation/resolution that is obtained at the receiver when fewer data streams are transmitted.

4.9.3 Comparison with a PARAFAC scheme

Now, we consider three transmit schemes with $F = M = 4$ (i.e. $\mathbf{\Omega} = I_4$) and $R = J = 2$. In the first scheme, $\mathbf{\Psi}$ and $\mathbf{\Phi}$ are given by (4.27). In the second one, we have:

$$\mathbf{\Phi} = \mathbf{\Psi} = \begin{bmatrix} 1 & 1 & 1 & 0 \\ 0 & 0 & 0 & 1 \end{bmatrix}.$$

The third scheme coincides with the PARAFAC scheme of [131], where $R = J = M$ and $\mathbf{\Psi} = \mathbf{\Phi} = \mathbf{\Omega} = \mathbf{I}_4$ (no stream/code/antenna reuse takes place). The results are shown in Figure 4.13. The first and second schemes offer improved performance over the third (PARAFAC) one. Note that the CONFAC schemes transmit fewer data streams than transmit antennas, in order to achieve spatial spreading. Consequently, more degrees of freedom are available at the receiver for separating the data streams as compared to the PARAFAC scheme, which is a full spatial multiplexing scheme. It is worth noting, however, that the PARAFAC

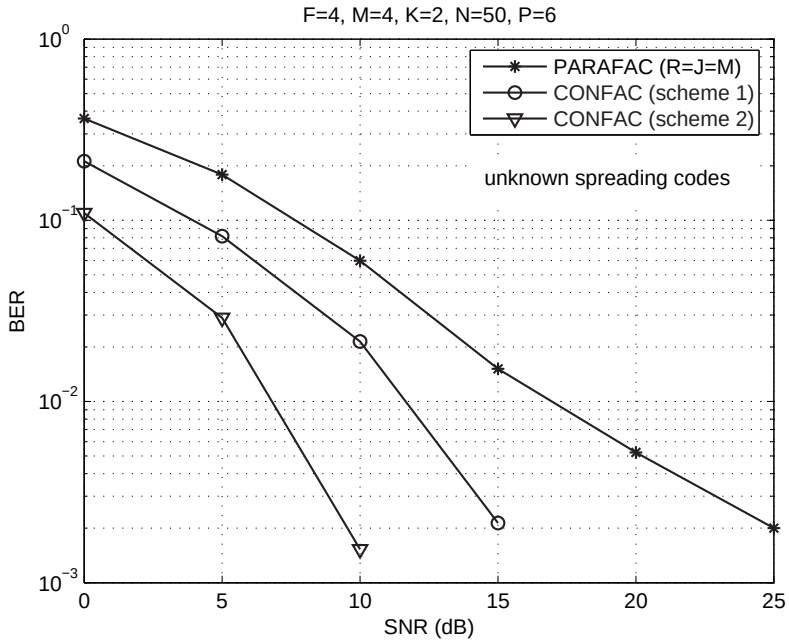

Figure 4.13: Comparison of two CONFAC schemes with a PARAFAC scheme for $M = 4$.

scheme has twice the spectral efficiency as the CONFAC schemes by simultaneously transmitting four data streams instead of two.

4.9.4 Comparison with the nonblind ZF receiver

In order to provide a performance reference of the proposed blind receiver (CONFAC-ALS), we have plotted the performance of the nonblind Zero Forcing (ZF) receiver. Contrarily to the proposed receiver, the nonblind ZF one assumes perfect knowledge of the channel parameters (fading gains and multipath/delay response) as well as the knowledge of the spreading codes. We consider a frequency-selective channel with $L = 2$ multipaths. The spreading codes are unknown at the receiver and $P = 6$. The results are depicted in Figure 4.14. The chosen $\mathbf{\Psi}$ and $\mathbf{\Phi}$ are given by (4.27) and $\mathbf{\Omega} = \mathbf{I}_4$. We can observe a gap of, approximately, 7dB in terms of SNR between blind ALS and nonblind ZF receivers for BER$= 2 \cdot 10^{-3}$.

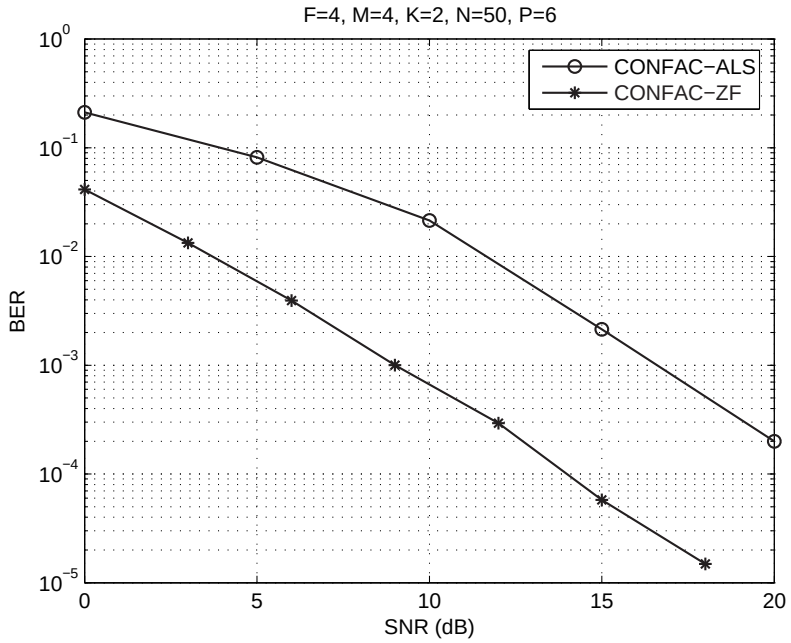

Figure 4.14: Comparison between blind CONFAC-ALS with nonblind CONFAC-ZF receivers.

4.9.5 Blind channel recovery

As discussed in the previous section, joint blind symbol and channel recovery is possible for some precoder structures with antenna reuse. We evaluate the accuracy of the blind channel estimation from the Root Mean Square Error (RMSE) measure averaged over 100 Monte Carlo runs and defined as follows:

$$\mathrm{RMSE}(\mathbf{H}) = \sqrt{\frac{1}{100MK}\sum_{t=1}^{100}\left\|\widehat{\mathbf{H}}(t) - \mathbf{H}\right\|_F^2},$$

where $\widehat{\mathbf{H}}(t)$ is the channel matrix estimated at the t-th run. We consider two schemes with $R = M$ and $\mathbf{\Psi} = \mathbf{\Omega}$. Orthogonal and known spreading codes are assumed with $P = 4$. The structure of these matrices for the first and second schemes are as follows:

$$\mathbf{\Psi} = \mathbf{\Omega} = \begin{bmatrix} 1 & 1 & 0 & 0 \\ 0 & 0 & 1 & 1 \end{bmatrix} \ (R = M = 2).$$

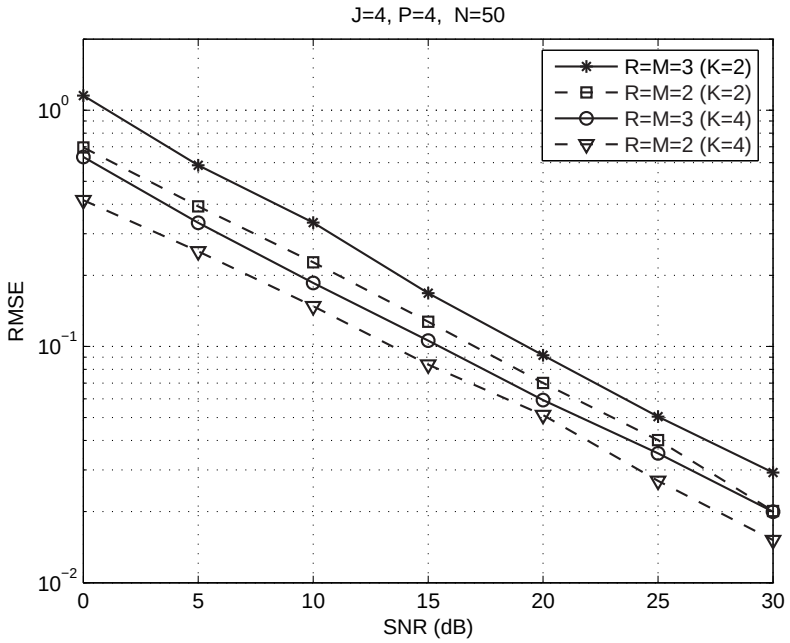

Figure 4.15: RMSE performance for the blind channel estimation.

$$\mathbf{\Psi} = \mathbf{\Omega} = \begin{bmatrix} 1 & 0 & 0 & 0 \\ 0 & 1 & 0 & 0 \\ 0 & 0 & 1 & 1 \end{bmatrix} \quad (R = M = 3).$$

Figure 4.15 displays the results. The dashed lines are for $R = M = 2$ and the solid lines for $R = M = 3$. The results are shown for $K = 2$ and 4 receive antennas. In all the simulated configurations, a linear decrease in the channel estimation error as a function of the SNR is observed. The RMSE increases as the number of data streams/transmit antennas is increased. On the other hand, the estimation accuracy is improved as the number of receive antennas is increased.

4.9.6 Evaluation of the convergence

Figure 4.16 depicts an ALS convergence histogram (for 100 Monte Carlo runs) for two transmit schemes: i) CONFAC scheme with $(F, R, J, M) = (4, 2, 2, 3)$; ii) PARAFAC scheme with $(F = R = J = M = 4)$. For the CONFAC scheme, $\mathbf{\Psi} = \mathbf{\Phi}$ and $\mathbf{\Omega}$ are given by (4.25). We remark that the convergence of the CONFAC scheme is achieved within 500 iterations for approximatively 90 % of runs. In average, the PARAFAC scheme has a slower convergence, with less than 40 % of runs converging within 500 iterations. Such a difference certainly comes

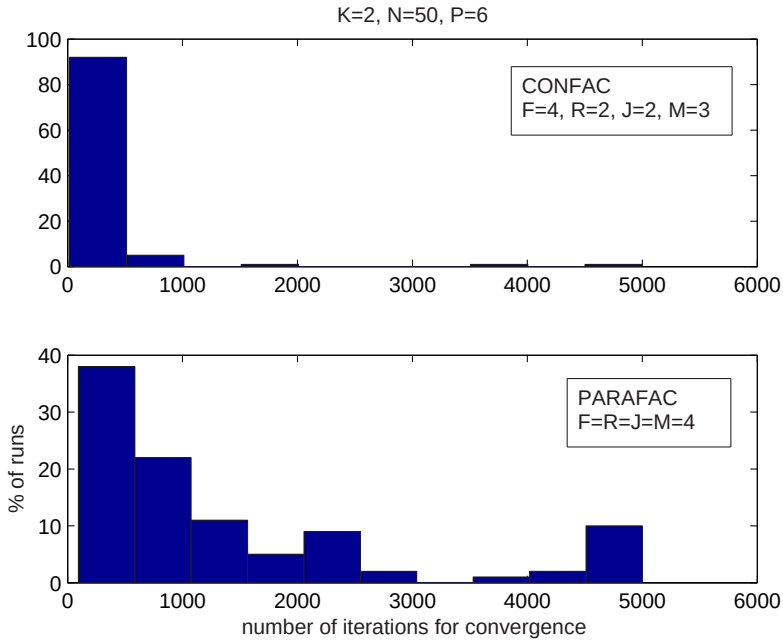

Figure 4.16: Convergence histogram for CONFAC and PARAFAC for 100 runs.

from the exploitation of the known interaction structure incorporated into the received signal model by means of the constraint matrices. Consequently, the number of parameters to be estimated is smaller with the CONFAC scheme as compared to the PARAFAC one.

4.10 Summary

This chapter has presented new tensor modeling approaches for multiuser MIMO-CDMA systems with blind detection based on the CONFAC decomposition. We have shown that this decomposition can be exploited to design space-time spreading/allocation schemes for MIMO-CDMA systems with a meaningful physical interpretation for the constraint matrices of the decomposition. First, we have presented a transmission model based on the type-3 CONFAC decomposition with two constraint matrices only. The two constraint matrices of the tensor model act as *allocation matrices* and control the spatial spreading of the data streams and the spatial reuse of the spreading codes. We have parameterized the two allocation matrices by their corresponding generating vectors, and have presented a design procedure for systematically deriving a set of transmit schemes with guaranteed

blind symbol recovery.

In the second part of the chapter, we have presented a CONFAC-based transmission model, where a precoder tensor fully exploiting the CONFAC decomposition structure defines the allocation of the data streams and spreading codes to transmit antennas. Based on the CONFAC modeling of the received signal, we have discussed blind symbol/code/channel recovery from the partial uniqueness properties of this decomposition. The BER performance of several transmit schemes has been evaluated. Simulation results have shown that remarkable performance is obtained with only two receive antennas and short data blocks.

The key difference between the type-3 CONFAC- and the CONFAC-based modeling approaches is on the transmission flexibility that the second approach offers as compared to the first one. As opposed to the type-3 CONFAC MIMO-CDMA model, the CONFAC-based model allows the reuse of the same transmit antenna by different data streams/speading codes. This comes from the introduction of a third constraint matrix. Thanks to the transmit antenna reuse, the CONFAC-based model covers a wider class of MIMO-CDMA transmit schemes.

We emphasize that the introduction of the two allocation matrices into the MIMO-CDMA model can be further exploited. For a fixed number M of transmit antennas, we could resort to limited feedback precoding [77, 95] to properly select the allocation matrices from the finite-set of feasible choices (c.f. Table 4.1 for $M = 4$) by taking practical requirements into account such as diversity and data-rate. We conjecture that antenna subset selection can be implemented by introducing more degrees of freedom in the structure of the constraint matrices of the tensor signal model. Generalization of the CONFAC tensor modeling approach to multi-carrier CDMA systems with space-time and frequency-domain spreading is an interesting topic for future work.

CHAPTER 5

Trilinear Space-Time-Frequency Spreading for MIMO Wireless Systems

We consider a point-to-point Multiple Input Multiple Output (MIMO) multicarrier multiple-access wireless communication system. For this system, a new Space-Time-Frequency (STF) spreading model is proposed. A tridimensional (3-D) spreading code with trilinear decomposition structure is used for modeling the core of an STF transmitter that jointly multiplexes and spreads multiple data streams across space (transmit antennas), time (chips) and frequency (subcarriers). The proposed model, called Trilinear Space-Time-Frequency Spreading (T-STFS), covers different orthogonal signaling techniques using multiple antennas, while allowing a variable degree of multiplexing and spreading over each one of the three signal dimensions. The diversity performance of the proposed T-STFS model is analyzed and a necessary condition for maximum diversity gain is derived. A trilinear (PARAFAC) model of the received signal is developed. Thanks to the identifiability property of this model, blind joint detection and channel estimation is possible using the alternating least squares algorithm. The bit-error-rate of T-STFS with blind detection is evaluated from computer simulations in a variety of system configurations. The simulations also compare T-STFS with some existing Space-Time (ST)/STF spreading models.

5.1 Introduction

Recently, Space-Time-Frequency Spreading (STFS) transceivers were proposed relying on a combination of direct-sequence spread spectrum and multicarrier modulations, to enable orthogonal multiple-access in multiuser multi-antenna systems. [58] proposed space-frequency spreading codes for the downlink of a multiuser MIMO-OFDM system. The transmission is designed to support more multiplexed signals than transmit antennas and to provide full-diversity for each multiplexed signal. Another STF transmission framework based on spread spectrum modulation is proposed in [104] for Multicarrier Spread Space Spectrum Multiple Access (MC-SSSMA), with the idea of fully spreading each user symbol over space, time and frequency. MC-SSSMA is a generalization of the single-carrier SSSMA model proposed in [105, 106]. Despite the spectral efficiency gains achieved, the design of [104] was restricted to the case where the number of transmit and receive antennas is equal to the spreading gain. In [157], a STF transmit diversity strategy was proposed for multicarrier DS-CDMA, which is based on the concatenation of a space-time spreading code with a frequency-domain spreading code. A common characteristic of these works is the assumption of perfect channel knowledge at the receiver, which is an optimistic assumption in practice. The decoding complexity of these codes is considerably high and prohibitive in some cases.

The distinguishing feature of the proposed T-STFS model when compared to the existing models is the flexibility for controlling both the spreading and the multiplexing pattern over space, time and frequency dimensions by adjusting the corresponding spreading matrices. In our context, the trilinear decomposition acts as a *triple product code* that allows several data streams to simultaneously access all the three signal diversity dimensions [34, 43, 45]. The blind joint detection/channel estimation that is possible thanks to the identifiability property of the PARAFAC model is a distinguishing feature of the proposed approach.

5.2 System model

Consider a MIMO multicarrier system with M transmit antennas, K receive antennas and N_c subcarriers. The transmission of information is organized in a time-frequency grid of $N_t \times N_f$ symbols, where N_t denotes the number of *time-slots* and $N_f = N_c/F$ denotes the number of *frequency-slots*. Each time-slot is composed of P chips, and each frequency-slot is composed of F subcarriers. This means that

the N_c subcarriers are partitioned into N_f frequency-slots of F subcarriers[1].

The proposed system uses jointly space-, time- and frequency-domain spreading. At the transmitter, each one of the R input data streams is spread across M transmit antennas, P chips and F subcarriers. After such a spreading operation, the R spread data streams are summed up to generate the transmitted signal. In order to allow a full spreading of the R data streams over space, time and frequency dimensions, three spreading code sequences are employed for transmitting each data stream, namely, the Space(S)-, Time(T)- Frequency(F)-domain spreading codes.

The transmitted signal is interpreted as a concatenation of *signal tensor blocks* over a tridimensional (3-D) space-time-frequency grid, as shown in Fig. 5.1. Each STF symbol is interpreted as an $M \times P \times F$ tensor spanning M transmit antennas, P chips and F subcarriers. Note that each point $x_{m,p,f}^{(n_t,n_f)}$ in the n_f versus n_t coordinate system on the left, is an element of a transmitted signal tensor of third-order $\mathcal{X}^{(n_t,n_f)} \in \mathbb{C}^{M\times P\times F}$ on the right.

The construction of the transmitted signal is now formalized. Let us define the r-th symbol to be spread within the (n_t, n_f)-th *time-frequency slot* as:

$$\begin{aligned} s_r^{(n_t,n_f)} \quad &\doteq s_r\big((n_t-1)N_f + n_f\big), \\ &n_t = 1,\ldots,N_t, \quad n_f = 1,\ldots,N_f. \end{aligned} \tag{5.1}$$

A 1-D vector representation of the 3-D STF spreading sequence associated with the r-th data stream is given by:

$$\begin{aligned} \mathbf{c}_r &= \Big[\mathbf{c}_r^T(1)\cdots\mathbf{c}_r^T(F)\Big]^T \in \mathbb{C}^{MPF}, \\ \text{with} \quad \mathbf{c}_r(f) &= \big[c_{1,1,f}^{(r)}\cdots c_{M,1,f}^{(r)}\cdots c_{M,P,f}^{(r)}\big]^T, \ \in \mathbb{C}^{MP}, \end{aligned} \tag{5.2}$$

where $c_{m,p,f}^{(r)}$ is the p-th chip through the m-th antenna and the f-th frequency subcarrier from the r-th data stream. Each STF-spread symbol is then generated by:

$$\mathbf{x}^{(n_t,n_f)} = \sum_{r=1}^{R} \mathbf{c}_r s_r^{(n_t,n_f)},$$

[1]Interleaving in the frequency-domain can be used after the STF spreading process for achieving frequency diversity. In this case, the F subcarriers are not necessarily adjacent. We bypass the frequency interleaving stage here for ease of explanation.

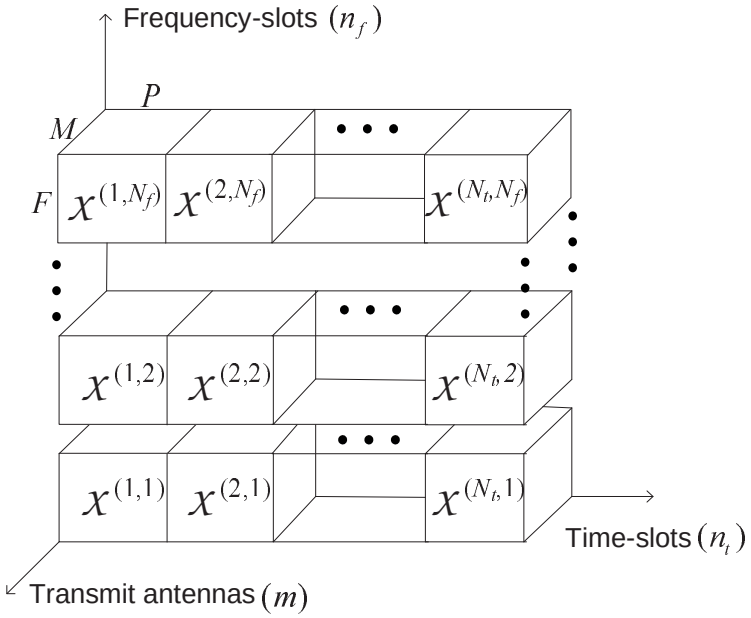

Figure 5.1: Illustration of the STF-spread sample $x_{m,p,f}^{(n_t,n_f)}$ as an element of the (n_t, n_f)-th signal tensor block.

or, equivalently,

$$x_{(f-1)MP+(p-1)M+m}^{(n_t,n_f)} = \sum_{r=1}^{R} c_{m,p,f}^{(r)} s_r^{(n_t,n_f)},$$

where $\mathbf{x}^{(n_t,n_f)} = \left[\mathbf{x}_{(1)}^{(n_t,n_f)T} \cdots \mathbf{x}_{(F)}^{(n_t,n_f)T}\right]^T \in \mathbb{C}^{MPF}$ concatenates F space-time-spread symbols, $\mathbf{x}_{(f)}^{(n_t,n_f)} \in \mathbb{C}^{MP}$.

Figure 5.2 depicts the baseband representation of the STF spreading transmitter focusing on the r-th data stream. At the output of the STF transmission block , the structure of which will be detailed in Section 5.3, the resulting signal vector $\mathbf{x}^{(n_t,n_f)}$ is serial-to-parallel converted, and then organized as a concatenation of N_c space-time signal vectors of MP components each: An N_c-point Inverse Fast Fourier Transform (IFFT) is applied. Then, a Cyclic Prefix (CP) of appropriate length is inserted. We assume that the length of the CP is at least equal to the multipath delay spread. Band-limited pulse shaping is employed at each frequency subcarrier. The spacing between the frequency-domain pulses is assumed to be sufficient so that they will not overlap one another, avoiding intercarrier interference. Under these assumptions, the time-dispersive channel between each transmit and receive antenna can be modeled as a set of N_c scalar (flat-fading) components. The channel is assumed to be constant across the N_t time-slots. At the receiver, and after

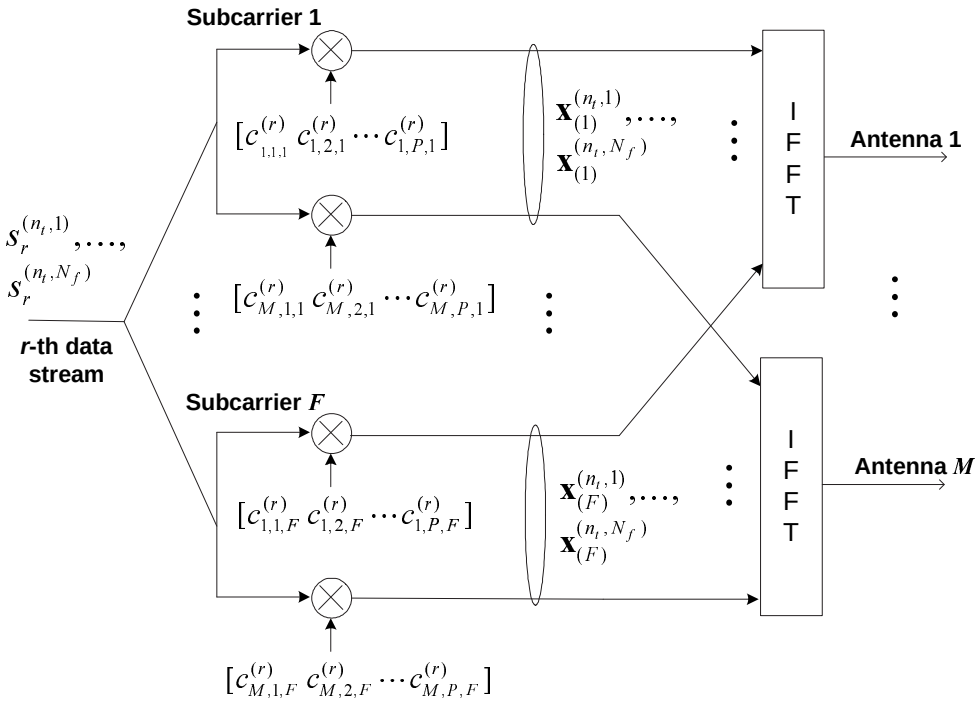

Figure 5.2: Baseband representation of the STF spreading transmitter.

baseband conversion, matched filtering and sampling, the CP is properly removed and an N_c-point Fast Fourier Transform (FFT) is applied to the resulting signal. The modeling of the received signal will be discussed in the next section.

5.3 Trilinear STF spreading (T-STFS) model

The basic idea of the proposed STF spreading model is to treat the 3-D spreading code vector defined in (5.2) as the Kronecker product of three spreading code vectors:

$$\mathbf{c}_r = \mathbf{u}_r \otimes \mathbf{v}_r \otimes \mathbf{w}_r, \tag{5.3}$$

where $\mathbf{u}_r \doteq [u_{r,1} \cdots u_{r,M}]^T \in \mathbb{C}^M$, $\mathbf{v}_r \doteq [v_{r,1} \cdots v_{r,P}]^T \in \mathbb{C}^P$ and $\mathbf{w}_r \doteq [w_{r,1} \cdots w_{r,F}]^T \in \mathbb{C}^F$ are the Space(S)-, Time(T) and Frequency(F)-domain spreading code vectors associated with the spreading of the r-th data stream over the transmit antennas, chips and subcarriers, respectively. Let us define three *spreading matrices* $\mathbf{U} \doteq [\mathbf{u}_1 \mathbf{u}_2 \cdots \mathbf{u}_R] \in \mathbb{C}^{M \times R}$, $\mathbf{V} \doteq [\mathbf{v}_1 \mathbf{v}_2 \cdots \mathbf{v}_R] \in \mathbb{C}^{P \times R}$ and $\mathbf{W} \doteq [\mathbf{w}_1 \mathbf{w}_2 \cdots \mathbf{w}_R] \in \mathbb{C}^{F \times R}$ with entries $[\mathbf{U}]_{m,r} \doteq u_{m,r}$, $[\mathbf{V}]_{p,r} \doteq v_{p,r}$ and $[\mathbf{W}]_{f,r} \doteq w_{f,r}$.

Due to the Kronecker (trilinear) product structure of the 3-D spreading code in (5.3), we can naturally formulate the 3-D spreading model as a tensor model. Let $\mathcal{X}^{(n_t,n_f)} \in \mathbb{C}^{M\times P\times F}$ be the (n_t, n_f)-th transmitted signal tensor with entry $x_{m,p,f}^{(n_t,n_f)}$. Similarly, we can define $\mathcal{C}_r \in \mathbb{C}^{M\times P\times F}$ as the r-th *spreading code tensor* with typical element $c_{m,p,f}^{(r)}$. Using the outer product notation, $\mathcal{C}_r$ is given by:

$$\mathcal{C}_r = \mathbf{u}_r \circ \mathbf{v}_r \circ \mathbf{w}_r. \tag{5.4}$$

Note that (5.3) and (5.4) are two different (resp. vector and tensor) writings of the 3-D spreading code.

Let us define a vector containing the R data symbols transmitted within the n_t-th time-slot and n_f-th frequency-slot as:

$$\mathbf{s}^{(n_t,n_f)} \doteq [s_1^{(n_t,n_f)} s_2^{(n_t,n_f)} \cdots s_R^{(n_t,n_f)}]^T \in \mathbb{C}^R. \tag{5.5}$$

In order to satisfy the transmit power constraint, the input symbols are normalized so that $E[\|\mathbf{s}^{(n_t,n_f)}\|^2] = 1$.

Definition 5.1 (Trilinear STF spreading): *Given the input symbol vector* $\mathbf{s}^{(n_t,n_f)}$ *and the three spreading matrices* $\mathbf{U}, \mathbf{V}$ *and* $\mathbf{W}$*, we define the following trilinear mapping:*

$$f(\mathbf{U}, \mathbf{V}, \mathbf{W}) : \mathbf{s}^{(n_t,n_f)} \rightarrow \mathcal{X}^{(n_t,n_f)}.$$

The STF signal tensor transmitted at the n_t-th time-slot and n_f-th frequency-slot is a trilinear combination of R rank-1 outer product terms:

$$\begin{aligned} \mathcal{X}^{(n_t,n_f)} &= \sum_{r=1}^{R} s_r^{(n_t,n_f)} \mathcal{C}_r \\ &= \sum_{r=1}^{R} s_r^{(n_t,n_f)} (\mathbf{u}_r \circ \mathbf{v}_r \circ \mathbf{w}_r). \end{aligned} \tag{5.6}$$

Figure 5.3 depicts the transmission block-diagram of the T-STFS model using tensor notation.

We can express (5.6) in scalar form:

$$x_{m,p,f}^{(n_t,n_f)} = \sum_{r=1}^{R} s_r^{(n_t,n_f)} u_{m,r} v_{p,r} w_{f,r}. \tag{5.7}$$

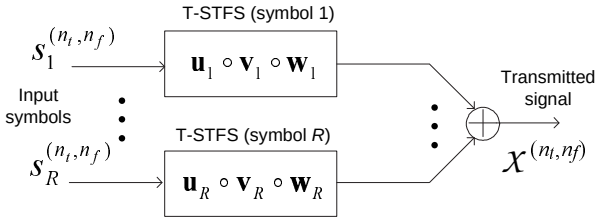

Figure 5.3: Transmission block-diagram of the T-STFS model.

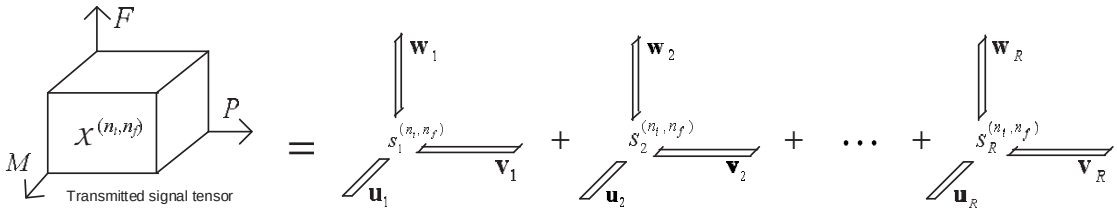

Figure 5.4: PARAFAC decomposition of the STF signal tensor at the (n_t, n_f)-th time-frequency slot.

We clearly recognize (5.7) as a PARAFAC decomposition. It expresses the third-order STF tensor $\mathcal{X}^{(n_t,n_f)}$ as a sum of R trilinear terms (rank-1 tensors), each one being the outer product of three spreading code vectors scaled by the corresponding information symbol to be transmitted. Figure 5.4 illustrates the PARAFAC decomposition of the (n_t, n_f)-th transmitted signal tensor.

Definition 5.2 (Multiplexing and spreading factors): *The multiplexing factor of the T-STFS model is defined as the rank of the PARAFAC decomposition (5.7). It corresponds to the number of data streams that simultaneously access the same STF resource. The spreading factors are defined as the dimensions of $\mathcal{X}^{(n_t,n_f)}$, corresponding to the lengths of the code vectors $\mathbf{u}_r$, $\mathbf{v}_r$, $\mathbf{w}_r$, $r = 1, \ldots, R$.*

Note that in (5.6), the r-th term contributing to the generation of the resulting signal tensor can be interpreted as a *modulated* version of the STF spreading code vectors, the modulating factor being the r-th information symbol $s_r^{(n_t,n_f)}$. Therefore, the proposed T-STFS model can be viewed as a STF modulation scheme written with the tensor formalism. It is worth noting that, in a multiuser transmission, the R data streams can be associated with R different users sharing the same STF resource.

Let us define $\mathbf{X}_{..f}^{(n_t,n_f)}$ as the f-th slice of $\mathcal{X}^{(n_t,n_f)}$ with $\left[\mathbf{X}_{..f}^{(n_t,n_f)}\right]_{m,p} = x_{m,p,f}^{(n_t,n_f)}$. This

slice admits the following factorization:

$$\mathbf{X}_{\cdot\cdot f}^{(n_t,n_f)} = \mathbf{U} D_f(\mathbf{W}) \mathrm{diag}\big(\mathbf{s}^{(n_t,n_f)}\big) \mathbf{V}^T, \tag{5.8}$$

with $\mathbf{s}^{(n_t,n_f)}$ defined in (5.5). By stacking column-wise these F slices in a matrix $\mathbf{X}^{(n_t,n_f)} \in \mathbb{C}^{FM \times P}$, we get:

$$\mathbf{X}^{(n_t,n_f)} = \begin{bmatrix} \mathbf{X}_{\cdot\cdot 1}^{(n_t,n_f)} \\ \vdots \\ \mathbf{X}_{\cdot\cdot F}^{(n_t,n_f)} \end{bmatrix} = (\mathbf{W} \diamond \mathbf{U}) \mathrm{diag}\big(\mathbf{s}^{(n_t,n_f)}\big) \mathbf{V}^T. \tag{5.9}$$

Special cases:

The T-STFS model (5.9) subsumes some existing space-time signaling schemes depending on the structure assumed for the spreading matrices $\mathbf{U}, \mathbf{V}, \mathbf{W}$:

- *Space-time spreading*: For $N_c = 1$ (single-carrier transmission, flat-fading channel), we can abandon the frequency-dependent index in (5.8) and our model reduces to space-time spreading using multiple spreading codes, which is close to several existing approaches [102, 78, 104, 56, 57, 22]. From (5.8), we get the following factorization of the space-time spread signal:

$$\mathbf{X}^{(n_t)} = \mathbf{U} \mathrm{diag}\big(\mathbf{s}^{(n_t)}\big) \mathbf{V}^T \in \mathbb{C}^{M \times P}.$$

- *Spatial multiplexing*: For $N_c = 1$, $R = M$ and $\mathbf{U} = \mathbf{I}_M$, model (5.8) coincides with a spatial multiplexing multiple-antenna CDMA system using a different spreading code per transmit antenna [79]. This is the case of the Khatri-Rao Space-Time (KRST) coding model [129]. The n_t-th transmitted signal in (5.8) is then factored as:

$$\mathbf{X}^{(n_t)} = \mathrm{diag}\big(\mathbf{s}^{(n_t)}\big) \mathbf{V}^T \in \mathbb{C}^{M \times P}.$$

- *Spatial spreading*: For $N_c = 1$, $R = M$ and $\mathbf{V} = \mathbf{I}_M$, model (5.8) reduces to full spatial spreading transmission:

$$\mathbf{X}^{(n_t)} = \mathbf{U} \mathrm{diag}\big(\mathbf{s}^{(n_t)}\big) \in \mathbb{C}^{M \times M}.$$

- *Time-frequency spreading*: For $N_c > 1$, $R = M$ and $\mathbf{U} = \mathbf{I}_M$, only time- and frequency-domain spreading takes place and T-STFS reduces to the multicarrier CDMA model of [158].

5.3.1 Channel modeling

The frequency-selective MIMO channel between each transmit-receive antenna pair is assumed to have L independent multipaths and the same power-delay profile. Let $a_{k,m,l}$ denote the complex amplitude of the l-th path between the m-th transmit antenna and the k-th receive antenna, modeled as a zero-mean complex Gaussian random variable, for any (k,m,l), $k=1,\ldots,K$, $m=1,\ldots,M$, $l=1,\ldots,L$. The $a_{k,m,l}$'s are assumed to be mutually independent. The average power of each path, assumed to be the same for every transmit-receive antenna pair, is denoted by $\gamma_l^2 = E[|a_{k,m,l}|^2], \forall(k,m,l)$, where $E[\cdot]$ stands for the mathematical expectation. They are normalized such that $\gamma_1^2 + \ldots + \gamma_L^2 = 1$. Due to the partitioning of subcarriers in $N_f = N_c/F$ frequency-slots, the frequency response of the n_f-th STF "subchannel" can be expressed as:

$$h_{k,m,f}^{(n_f)} = \sum_{l=1}^{L} a_{k,m,l}\omega_{f,l}^{(n_f)}, \quad n_f = 1,\ldots,N_f, \tag{5.10}$$

where $\omega_{f,l}^{(n_f)} = e^{-j2\pi\left(\frac{(n_f-1)F+f-1}{N_c}\right)\tau_l}$ and τ_l is the delay of the l-th path.

The n_f-th MIMO channel matrix at the f-th subcarrier is defined as:

$$\mathbf{H}_{\cdot\cdot f}^{(n_f)} = \begin{bmatrix} h_{1,1,f}^{(n_f)} & h_{1,2,f}^{(n_f)} & \cdots & h_{1,M,f}^{(n_f)} \\ h_{2,1,f}^{(n_f)} & h_{2,2,f}^{(n_f)} & \cdots & h_{2,M,f}^{(n_f)} \\ \vdots & \vdots & & \vdots \\ h_{K,1,f}^{(n_f)} & h_{K,2,f}^{(n_f)} & \cdots & h_{K,M,f}^{(n_f)} \end{bmatrix} \in \mathbb{C}^{K\times M}. \tag{5.11}$$

5.3.2 Received signal modeling

By exploiting the T-STFS structure of the transmitted signal, we now formulate the received signal as a trilinear (PARAFAC) model. This model is considered in Section 5.5 for blind detection. At the receiver, perfect synchronization is assumed. The received signal is down-converted, and matched-filtering at each receive antenna and subcarrier is applied. The CP is removed and then an FFT transform is applied. After the FFT block, we can write the (n_t,n_f)-th scalar component of the discrete-time baseband received signal as:

$$y_{k,p,f}^{(n_t,n_f)} = \sum_{m=1}^{M} h_{k,m,f}^{(n_f)} x_{m,p,f}^{(n_t,n_f)} \tag{5.12}$$

Using (5.8), we can write (5.12) in slice form in the following manner:

$$\begin{aligned}\mathbf{Y}_{\cdot\cdot f}^{(n_t,n_f)} &= \mathbf{H}_{\cdot\cdot f}^{(n_f)}\mathbf{X}_{\cdot\cdot f}^{(n_t,n_f)} \\ &= \underbrace{\mathbf{H}_{\cdot\cdot f}^{(n_f)}\mathbf{U}D_f(\mathbf{W})}_{\mathbf{G}_{\cdot\cdot f}^{(n_f)}}\mathrm{diag}\big(\mathbf{s}^{(n_t,n_f)}\big)\mathbf{V}^T, \end{aligned} \tag{5.13}$$

i.e.,

$$\mathbf{Y}_{\cdot\cdot f}^{(n_t,n_f)} = \mathbf{G}_{\cdot\cdot f}^{(n_f)}\mathrm{diag}\big(\mathbf{s}^{(n_t,n_f)}\big)\mathbf{V}^T,$$

where

$$\mathbf{G}_{\cdot\cdot f}^{(n_f)} = \mathbf{H}_{\cdot\cdot f}^{(n_f)}\mathbf{U}D_f(\mathbf{W}). \tag{5.14}$$

Note that $\mathbf{G}_{\cdot\cdot f}^{(n_f)}$ is the *effective* space-frequency channel, i.e. the original channel combined with the space- and frequency-domain spreading codes.

By stacking column-wise the slices $\mathbf{Y}_{\cdot\cdot 1}^{(n_t,n_f)},\ldots,\mathbf{Y}_{\cdot\cdot F}^{(n_t,n_f)}$ and the slices $\mathbf{G}_{\cdot\cdot 1}^{(n_f)},\ldots,\mathbf{G}_{\cdot\cdot F}^{(n_f)}$, we obtain:

$$\underbrace{\begin{bmatrix}\mathbf{Y}_{\cdot\cdot 1}^{(n_t,n_f)}\\ \vdots \\ \mathbf{Y}_{\cdot\cdot F}^{(n_t,n_f)}\end{bmatrix}}_{\mathbf{Y}^{(n_t,n_f)}\in\mathbb{C}^{FK\times P}} = \underbrace{\begin{bmatrix}\mathbf{G}_{\cdot\cdot 1}^{(n_f)}\\ \vdots \\ \mathbf{G}_{\cdot\cdot F}^{(n_f)}\end{bmatrix}}_{\mathbf{G}^{(n_f)}\in\mathbb{C}^{FK\times R}}\mathrm{diag}\big(\mathbf{s}^{(n_t,n_f)}\big)\mathbf{V}^T,$$

i.e.

$$\mathbf{Y}^{(n_t,n_f)} = \mathbf{G}^{(n_f)}\mathrm{diag}\big(\mathbf{s}^{(n_t,n_f)}\big)\mathbf{V}^T. \tag{5.15}$$

Collecting the received signal over N_t time-slots, we obtain:

$$\begin{aligned}\mathbf{Y}_1^{(n_f)} &= \begin{bmatrix}\mathbf{Y}^{(1,n_f)T}\\ \vdots \\ \mathbf{Y}^{(N_t,n_f)T}\end{bmatrix} \\ &= \begin{bmatrix}\mathbf{V}\mathrm{diag}\big(\mathbf{s}^{(1,n_f)}\big)\\ \vdots \\ \mathbf{V}\mathrm{diag}\big(\mathbf{s}^{(N_t,n_f)}\big)\end{bmatrix}\mathbf{G}^{(n_f)T}.\end{aligned}$$

Using the definition of the Khatri-Rao product, we get:

$$\mathbf{Y}_1^{(n_f)} = \big(\mathbf{S}^{(n_f)}\diamond\mathbf{V}\big)\mathbf{G}^{(n_f)T}. \tag{5.16}$$

where

$$\mathbf{S}^{(n_f)} \doteq \left[\mathbf{s}^{(1,n_f)}\mathbf{s}^{(2,n_f)}\cdots\mathbf{s}^{(N_t,n_f)}\right]^T \in \mathbb{C}^{N_t\times R}.$$

Consider the following property:

Property 5.1 : For $\mathbf{A}\in\mathbb{C}^{I\times R}$, $\mathbf{B}\in\mathbb{C}^{J\times K}$, and $\mathbf{c}\in\mathbb{C}^{R}$, we have:

$$\text{vec}(\mathbf{A}\text{diag}(\mathbf{c})\mathbf{B}^T) = (\mathbf{B}\diamond\mathbf{A})\mathbf{c}. \tag{5.17}$$

From (5.15) and property (5.17), we get:

$$\text{vec}\big(\mathbf{Y}^{(n_t,n_f)}\big) = \big(\mathbf{V}\diamond\mathbf{G}^{(n_f)}\big)\mathbf{s}^{(n_t,n_f)} \in \mathbb{C}^{FKP},$$

and then, collecting the received signal over N_t time-slots, we obtain:

$$\begin{aligned}\mathbf{Y}_2^{(n_f)} &= \left[\text{vec}\big(\mathbf{Y}^{(1,n_f)}\big)\cdots\text{vec}\big(\mathbf{Y}^{(N_t,n_f)}\big)\right] \in \mathbb{C}^{FKP\times N_t}\\ &= \big(\mathbf{V}\diamond\mathbf{G}^{(n_f)}\big)\left[\mathbf{s}^{(1,n_f)}\ \cdots\mathbf{s}^{(N_t,n_f)}\right],\end{aligned} \tag{5.18}$$

i.e.

$$\mathbf{Y}_2^{(n_f)} = \big(\mathbf{V}\diamond\mathbf{G}^{(n_f)}\big)\mathbf{S}^{(n_f)T}. \tag{5.19}$$

Note that (5.16) and (5.19) are two different matrix writings of the received data, which follow a PARAFAC model. Both $\mathbf{Y}_1^{(n_f)}$ and $\mathbf{Y}_2^{(n_f)}$ concatenate the information contained in the received signal tensors $\mathcal{Y}^{(1,n_f)},\ldots,\mathcal{Y}^{(N_t,n_f)}\in\mathbb{C}^{K\times P\times F}$ across the N_t time-slots.

5.4 Performance analysis/spreading structure

In this section, we study the diversity gain of the T-STFS model (5.9) from a code design viewpoint. Then, a necessary condition for maximum diversity gain is derived. The structure chosen for the three spreading matrices $\mathbf{U}$, $\mathbf{V}$ and $\mathbf{W}$ is also presented.

Recall the input-output model (5.15) with an Additive White Gaussian (AWG) noise:

$$\mathbf{Y}^{(n_t,n_f)} = \mathbf{G}^{(n_f)}\text{diag}\big(\mathbf{s}^{(n_t,n_f)}\big)\mathbf{V}^T + \mathbf{N}^{(n_t,n_f)},$$

where $\mathbf{N}^{(n_t,n_f)}\in\mathbb{C}^{FK\times P}$ is the AWG noise matrix. Our analysis supposes that joint

Maximum Likelihood (ML) decoding is performed at the receiver to recover $\mathbf{s}^{(n_t,n_f)}$. We assume a perfect channel knowledge at the receiver. Uncorrelated multipath propagation with equal multipath profile for each transmit-receive antenna pair is assumed. Let us consider an erroneous decoding in favor of the "codeword" $\tilde{\mathbf{X}}^{(n_t,n_f)}$, where $\mathbf{X}^{(n_t,n_f)} \neq \tilde{\mathbf{X}}^{(n_t,n_f)}$. Under the above assumptions, the pairwise error probability can be upper bounded by [142]:

$$P\Big(\mathbf{X}^{(n_t,n_f)} \to \tilde{\mathbf{X}}^{(n_t,n_f)}\Big) \leq \left(\frac{2\nu-1}{\nu}\right)\left(\prod_{i=1}^{\nu}\lambda_i\right)^{-1}\left(\frac{\mathrm{SNR}}{M}\right)^{-\nu},$$

where ν is the rank of $\mathbf{E}^{(n_t,n_f)} = \mathbf{X}^{(n_t,n_f)} - \tilde{\mathbf{X}}^{(n_t,n_f)} \in \mathbb{C}^{FM\times P}$, and $\lambda_1,\ldots,\lambda_\nu$ are its nonzero eigenvalues. Provided that $\mathbf{E}^{(n_t,n_f)}$ is full rank, the diversity gain is given by:

$$K\cdot\nu = K\cdot\min(FM,P). \tag{5.20}$$

Theorem 5.1: *Suppose that* $\mathbf{E}^{(n_t,n_f)}$ *is full rank, for all* $\mathbf{X}^{(n_t,n_f)} \neq \tilde{\mathbf{X}}^{(n_t,n_f)}$. *For* $F = L$, *a diversity gain* MKL *requires:*

$$P \geq FM. \tag{5.21}$$

From condition (5.21), we have:

- For the single-carrier flat-fading case ($F = L = 1$), T-STFS reduces to space-time spreading, and a diversity gain KM requires $P \geq M$;
- For the single transmit antenna case ($M = 1$), with $F = L$, T-STFS reduces to time-frequency spreading, and a diversity gain of KL requires $P \geq F$.

This illustrates the existing tradeoff between space- and frequency-domain spreading which is inherent to the T-STFS model.

The rate of the T-STFS code is given by:

$$\mathrm{Rate} = \left(\frac{R}{FP}\right)\log_2(\mu)\ \text{bits/channel use}, \tag{5.22}$$

where μ is the cardinality of a μ-Quadrature Amplitude Modulation (QAM). We call attention that it is possible to choose $P \leq MF$ to tradeoff diversity and rate.

From (5.9), let us define:

$$\mathbf{E}^{(n_t,n_f)} = (\mathbf{W} \diamond \mathbf{U})\text{diag}\big(\mathbf{e}^{(n_t,n_f)}\big)\mathbf{V}^T, \quad \text{where } \mathbf{e}^{(n_t,n_f)} = \mathbf{s}^{(n_t,n_f)} - \tilde{\mathbf{s}}^{(n_t,n_f)}.$$

We remark that linear precoding in the form of constellation rotation can be used [155] to ensure $\mathbf{e}^{(n_t,n_f)} \neq \mathbf{0}_R$. We assume that the elements of $\mathbf{s}^{(n_t,n_f)}$ are coordinates of a rotated constellation of dimension R with full modulation diversity [68]. The rank of $\mathbf{E}^{(n_t,n_f)}$ is still dependent on the structure of $\mathbf{U}$, $\mathbf{V}$ and $\mathbf{W}$. We consider the two following criteria for choosing these matrices:

1. $\mathbf{U} \in \mathbb{C}^{M\times R}$, $\mathbf{V} \in \mathbb{C}^{P\times R}$ and $\mathbf{W} \in \mathbb{C}^{F\times R}$ are full rank;
2. $[\mathbf{U}]_{m,r}$, $[\mathbf{V}]_{p,r}$ and $[\mathbf{W}]_{f,r}$ have unit magnitudes;

Both criteria are satisfied if $\mathbf{U}$, $\mathbf{V}$ and $\mathbf{W}$ are Vandermonde matrices defined as:

$$\begin{aligned}
[\mathbf{U}]_{m,r} &\doteq e^{j2\pi\left(\frac{r-1}{R}\right)(m-1)},\\
[\mathbf{V}]_{p,r} &\doteq e^{j2\pi\left(\frac{r-1}{R}\right)(p-1)},\\
[\mathbf{W}]_{f,r} &\doteq e^{j2\pi\left(\frac{r-1}{R}\right)(f-1)}.
\end{aligned} \tag{5.23}$$

With this choice, $\mathbf{U}$, $\mathbf{V}$ and $\mathbf{W}$ are full-rank semi-unitary matrices, as required for maximum diversity gain. It is to be noted that this spreading structure is not necessarily optimal for a code design viewpoint. However, using the Vandermonde structure we can independently control both the spreading degree in each one of the three signal dimensions as well as the number of multiplexed data streams by truncating the spreading matrices. To be specific, a subset of columns and/or rows of a Vandermonde matrix forms another semi-unitary Vandermode matrix satisfying the maximum diversity criterion [100]. Therefore, the Vandermonde design gives some spreading flexibility.

Remarks:

1. The generators of the spreading matrices can alternatively be chosen using an algebraic number-theoretic criterium. As an example, in the case $M = R$ we can choose $\theta_m = e^{j\frac{\pi}{M}(2m+1)}$, $m = 1, \ldots, M$, as the generators of $\mathbf{U}$. This structure can provide full diversity in space-time transmission with M transmit antennas for finite QAM symbol constellations [68],[99]. A satisfactory choice is to use $M = 2^i$, $i \in \mathbb{N}$. A jointly optimized design of the trilinear spreading set $\{\mathbf{U}, \mathbf{V}, \mathbf{W}\}$ using information-theoretic tools is under investigation.

2. An alternative design approach for the three spreading matrices is based on the Walsh-Hadamard codes. This code structure was considered in the design of DAST codes [22] and is also applicable to the proposed STF spreading model. In this case, the proposed T-STFS transmission model is close to a multicarrier CDMA transmission using space-, time-, and frequency-domain spreading codes [157],[104] (the columns of $\mathbf{U}$, $\mathbf{V}$, $\mathbf{W}$ are orthogonal spreading codes). In contrast to the Vandermonde structure, the Walsh-Hadamard design can be useful for reducing the peak-to-mean power ratio which results from the multiplexing of the R symbols.

5.5 Blind receiver

A distinguishing feature of the T-STFS approach is the possibility of blind detection without a priori channel estimation or training sequences. The PARAFAC model of the received signal derived in Section 5.3.2 is exploited here for blind joint detection/channel estimation. We present an identifiability condition, and the blind receiver algorithm is detailed.

Recall the two matrix writings of the received signal $\mathbf{Y}_1^{(n_f)}$ and $\mathbf{Y}_2^{(n_f)}$ in (5.16) and (5.19), in presence of an AWG noise:

$$\begin{aligned} \tilde{\mathbf{Y}}_1^{(n_f)} &= \big(\mathbf{S}^{(n_f)} \diamond \mathbf{V}\big)\mathbf{G}^{(n_f)T} + \mathbf{N}_1^{(n_f)}, \\ \tilde{\mathbf{Y}}_2^{(n_f)} &= \big(\mathbf{V} \diamond \mathbf{G}^{(n_f)}\big)\mathbf{S}^{(n_f)T} + \mathbf{N}_2^{(n_f)}. \end{aligned} \tag{5.24}$$

The two matrix writings (5.24) reveal the trilinear structure of the received signal, which can be viewed as a third-order tensor $\mathcal{Y} \in \mathbb{C}^{FK \times N_t \times P}$ following a rank-R PARAFAC decomposition with factor matrices $\mathbf{G}^{(n_f)} \in \mathbb{C}^{FK \times R}$, $\mathbf{S}^{(n_f)} \in \mathbb{C}^{N_t \times R}$ and $\mathbf{V} \in \mathbb{C}^{P \times R}$.

5.5.1 Identifiability

Applying the identifiability result of PARAFAC [136], we present the following theorem:

Theorem 5.2: *Suppose that* $\mathbf{G}^{(n_f)}, \mathbf{S}^{(n_f)}$ *and* $\mathbf{V}$ *are full rank matrices,* $\mathbf{V}$ *is known,*

and $R > 1$. *If*

$$min(FK, R) + min(P, R) + min(N_t, R) \geq 2R + 2, \tag{5.25}$$

then $\mathbf{G}^{(n_f)}$ *and* $\mathbf{S}^{(n_f)}$ *are unique up to scaling of their columns, i.e.:*

$$\tilde{\mathbf{G}}^{(n_f)} = \mathbf{G}^{(n_f)}\mathbf{\Delta}_g, \quad \tilde{\mathbf{S}}^{(n_f)} = \mathbf{S}^{(n_f)}\mathbf{\Delta}_s, \tag{5.26}$$

where $\tilde{\mathbf{G}}^{(n_f)}$ *and* $\tilde{\mathbf{S}}^{(n_f)}$ *are any alternative matrices satisfying the model, while* $\mathbf{\Delta}_g$ *and* $\mathbf{\Delta}_s$ *are diagonal (scaling) matrices satisfying* $\mathbf{\Delta}_g\mathbf{\Delta}_s = \mathbf{I}_R$.

We assume that $N_t > R$, which is generally the case in practice. In this case, (5.25) reduces to the following identifiability condition:

$$\min(FK, R) + \min(P, R) \geq R + 2. \tag{5.27}$$

Proof: The complete uniqueness proof is given in [136]. The proof relies on the fundamental concept of "Kruskal rank" [90]. In the general proof, the uniqueness of the three factor matrices of the PARAFAC model are also affected by a column-permutation ambiguity. In our case, this ambiguity does not exist since $\mathbf{V}$ is known.

Note that this condition links the received signal diversity dimensions (F, K, P) to the number R of multiplexed data streams. From (5.21) and (5.27), we can obtain the following corollaries:

Corollary 5.1: For $M = K = 1$ (single transmit/receive antenna case) and $P \geq R$, spreading across $F = 2$ subcarriers is enough for blind symbol recovery. On the other hand, condition (5.27) is equivalent to $P \geq 2$. Therefore, for satisfying both diversity and identifiability conditions we must have:

$$P \geq \max(R, 2).$$

In this case, the (frequency) diversity gain is equal to F.

Corollary 5.2: For $F = L = 1$ (single-carrier flat-fading case), with $P \geq R > 1$ and $K = 2$, the identifiability condition is always satisfied, which means that two receive antennas are enough for blind symbol recovery (regardless of the number M of used transmit antennas). In this case, for achieving a diversity gain MK,

we must have:

$$P \geq M,$$

which means that it is enough to temporally spread across $P = M$ chips.

Example: Consider a system with $M = 4$ transmit antennas and $K = 3$ receive antennas. Suppose that $R = 8$ data streams should be spread across space- and time- dimensions using $P = 4$ chips. The identifiability condition (5.27) yields:

$$\min(3F, 8) \geq 6,$$

i.e. $F \geq 2$ subcarriers are enough to guarantee blind detection. In a single-carrier system, where frequency-domain spreading is not available ($F = 1$), we should have $K \geq 6$ receive antennas for satisfying this identifiability condition. On the other hand, if a single receive antenna is used ($K = 1$), spreading across $F = 6$ subcarriers is sufficient. Therefore, space- and frequency- spreading diversities can be exchanged for allowing blind detection.

The use of frequency-domain spreading is beneficial in situations where the number of receive antennas is small (e.g. $K = 1$ or 2). Although condition (5.21) for maximum diversity is not satisfied in the considered configuration (since $P < MF$), blind detection is still possible.

5.5.2 Receiver algorithm

In this context, the ALS receiver alternates between LS estimations of $\mathbf{S}^{(n_f)}$ and $\mathbf{G}^{(n_f)}$ based on the two matrix writings of the received data $\mathbf{Y}_1^{(n_f)}$ and $\mathbf{Y}_2^{(n_f)}$. This is the first stage of the blind receiver. After obtaining the final estimate of the symbol matrix, the second stage of this receiver consists in recovering the MIMO channel response. The proposed blind receiver benefits from the knowledge of the trilinear spreading set $\{\mathbf{U}, \mathbf{V}, \mathbf{W}\}$ in the following manner:

1. The knowledge of $\mathbf{V}$ allows some complexity reduction (otherwise a third LS estimation step for updating $\mathbf{V}$ would be necessary).

2. The knowledge of $\mathbf{U}$ and $\mathbf{W}$ is exploited in the second stage of the receiver for estimating the MIMO channel.

The overall receiver algorithm is summarized as follows:

1st Stage (blind symbol recovery):

for $n_f = 1, 2, \cdots N_f$:

1. Set $i = 0$; Randomly initialize $\mathbf{S}_{(0)}^{(n_f)}$;
2. $i = i + 1$;
3. From $\mathbf{Y}_1^{(n_f)}$, find an LS estimate of $\widehat{\mathbf{G}}_{(i)}^{(n_f)}$:
   $\widehat{\mathbf{G}}_{(i)}^{(n_f)T} = \left[\mathbf{S}_{(i-1)}^{(n_f)} \diamond \mathbf{V}\right]^{\dagger} \tilde{\mathbf{Y}}_1^{(n_f)}$;
4. From $\mathbf{Y}_2^{(n_f)}$, find an LS estimate of $\mathbf{S}_{(i)}^{(n_f)}$:
   $\mathbf{S}_{(i)}^{(n_f)T} = \left[\mathbf{V} \diamond \mathbf{G}_{(i)}^{(n_f)}\right]^{\dagger} \tilde{\mathbf{Y}}_2^{(n_f)}$;
5. Repeat steps 2-4 until convergence;

   $\widehat{\mathbf{S}}_{(\text{conv})}^{(n_f)} \leftarrow \widehat{\mathbf{S}}_{(i)}^{(n_f)}$; $\widehat{\mathbf{G}}_{\text{conv}}^{(n_f)} \leftarrow \mathbf{G}_{(i)}^{(n_f)}$;

end n_f;

2nd Stage (channel estimation):

for $n_f = 1, 2, \cdots N_f$:

1. From $\widehat{\mathbf{G}}_{\text{conv}}^{(n_f)} = \begin{bmatrix} \mathbf{G}_{\cdot\cdot 1}^{(n_f)} \\ \vdots \\ \mathbf{G}_{\cdot\cdot F}^{(n_f)} \end{bmatrix} = \begin{bmatrix} \mathbf{H}_{\cdot\cdot 1}^{(n_f)} \mathbf{U} D_1(\mathbf{W}) \\ \vdots \\ \mathbf{H}_{\cdot\cdot F}^{(n_f)} \mathbf{U} D_F(\mathbf{W}) \end{bmatrix}$, find LS estimates of $\mathbf{H}_{\cdot\cdot f}^{(n_f)}$, $f = 1, \ldots, F$, by solving the following LS problem:

   $$\widehat{\mathbf{H}}_{\cdot\cdot f}^{(n_f)} = \underset{\mathbf{H}_{\cdot\cdot f}^{(n_f)}}{\text{argmin}} \left\| \mathbf{G}_{\cdot\cdot f}^{(n_f)} - \mathbf{H}_{\cdot\cdot f}^{(n_f)} \mathbf{U} D_f(\mathbf{W}) \right\|_F^2,$$

   the analytic solution of which is given by:

   $$\widehat{\mathbf{H}}_{\cdot\cdot f}^{(n_f)} = \mathbf{G}_{\cdot\cdot f}^{(n_f)} \left[\mathbf{U} D_f(\mathbf{W})\right]^{\dagger}, \quad f = 1, \ldots, F;$$

end n_f;

Remarks:

- Convergence of the estimates at the first stage is declared at the i-th iteration when the error between the received signal tensor and its reconstructed version from the estimated matrices does not significantly change between iterations i and $i+1$.
- In order to eliminate the column scaling ambiguity affecting $\widehat{\mathbf{G}}^{(n_f)}$ and $\widehat{\mathbf{S}}^{(n_f)}$, we assume that an "all ones" data stream is transmitted at the first time-slot $n_t = 1$, i.e:
$$\mathbf{S}_{1\cdot}^{(n_f)} = [1\ 1\ \cdots\ 1], \quad n_f = 1, \ldots, N_f.$$
In this case, the arbitrary scaling matrices $\mathbf{\Delta}_s$ and $\mathbf{\Delta}_g$ in (5.26) can be estimated and then eliminated.

5.6 Performance evaluation

The performance of the T-STFS model using the proposed blind receiver is evaluated. In all the results, the BER is shown as a function of the SNR. Each plotted BER curve is an average over 1000 independent Monte Carlo runs. At each run, the additive noise power is generated according to the sample SNR value given by:

$$\text{SNR} = 10\log_{10}\left(\frac{\|\mathbf{Y}_1^{(n_f)}\|_F^2}{\|\mathbf{N}_1^{(n_f)}\|_F^2}\right),$$

$n_f = 1, \ldots, N_f$. The MIMO channel coefficients are drawn from an i.i.d. complex-valued Gaussian generator while the transmitted symbols are drawn from a pseudo-random μ-QAM sequence. The BER curves represent the performance averaged on the R transmitted data streams. Unless otherwise stated, we assume $N_t = 10$ time-slots. Multicarrier transmission is simulated with $N_c = 64$ orthogonal subcarriers over a total bandwidth of 1MHz, which means that the chip duration (corresponding to one multicarrier symbol) is $T = 64\mu s$ without the cyclic prefix. We assume that multipath delays are equal to $\tau_l = (l-1)T/N_c$, $l = 1, \ldots L$. When considering frequency-domain spreading, $F = L$ spreading subcarriers is always assumed. We recall that a CP of appropriate length is used along with band-limited frequency-domain pulses with sufficient spacing in order to avoid intercarrier interference. Perfect synchronization is assumed.

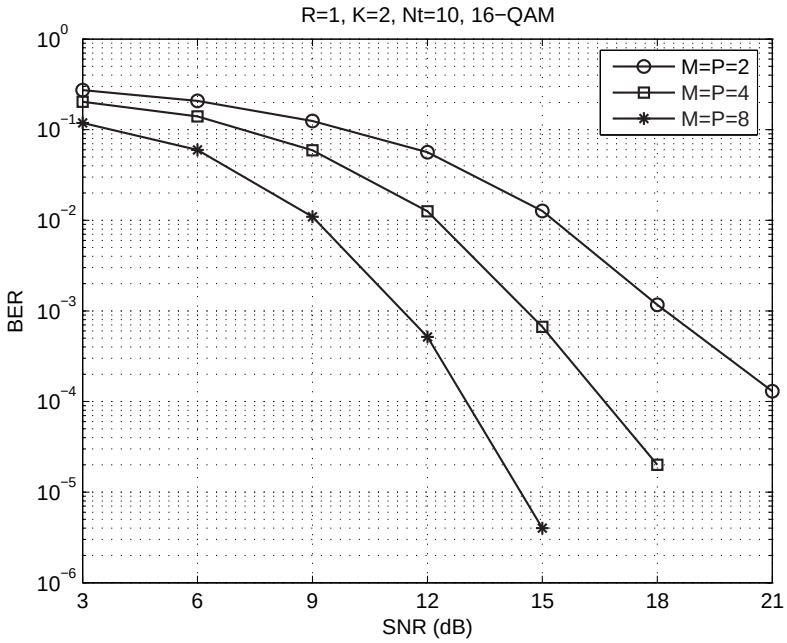

Figure 5.5: Performance as P and M are jointly increased.

5.6.1 Performance of different T-STFS configurations

The performance behavior of T-STFS with blind detection is shown in Fig. 5.5 for $M = P = 2$, 4, 8, and considering $R = 1$ and $F = L = 1$ (no frequency-domain spreading). This figure shows that performance is improved as the space- and time- spreading factors are jointly increased. In Fig. 5.6, T-STFS performance is evaluated for two different multiplexing factors $R = 1$ and $R = 2$. The spatial spreading factor (number of transmit antennas) is also varied. In each case, the temporal spreading factor P is set to the minimum value satisfying (5.21) and (5.27). Note that improved performance is obtained when $R = 1$ but this comes with a rate reduction by a factor of two (c.f. (5.22)). This result illustrates the existing trade-off between the multiplexing factor R and the spatial spreading factor M. It is to be noted that configurations $(R, P) = (2, 8)$ and $(R, P) = (1, 4)$ have the same spectral efficiency (c.f. 5.22). Both configurations also have the same spreading/multiplexing ratio since we have $M = P/2$.

Now, we evaluate the influence of the temporal spreading factor P. The spatial and frequency spreading factors are set to $M = 4$ and $F = L = 2$, respectively. The chosen multiplexing factor is $R = 1$ (single data stream transmission). We consider $P = 2$, 3 or 4. Figure 5.7 shows that performance improves (due to higher

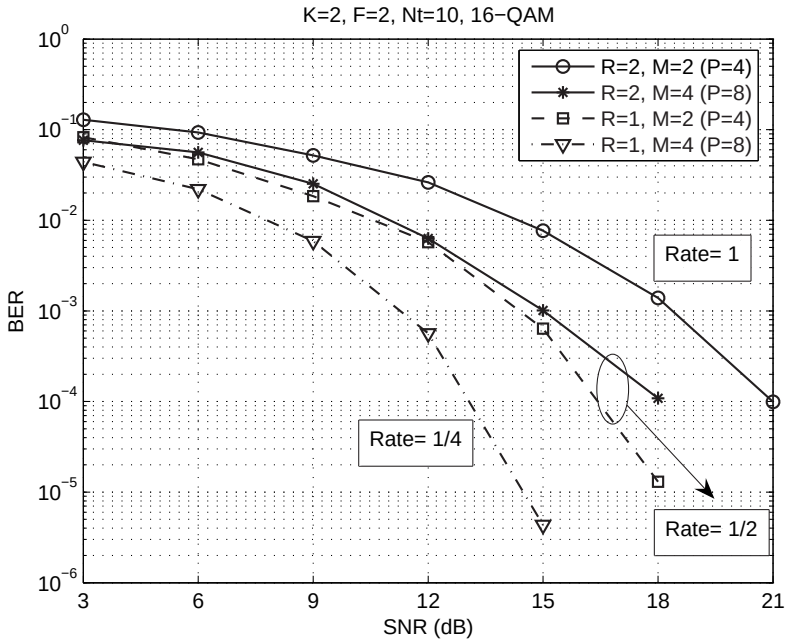

Figure 5.6: Performance for different combinations of multiplexing factors ($R = 1, 2$) and spatial spreading factors ($M = 2, 4$).

diversity gain) when P is increased at the expense of a rate reduction. Therefore, a diversity-rate trade off takes place when the value of P is adjusted. In Fig. 5.8, the influence of the number L of resolvable multipaths is evaluated. The number F of spreading subcarriers is assumed to be equal to L. We consider $K = 1$ and 2 receive antennas. It can be noted that the BER is improved as L is increased from 2 to 4, indicating that T-STFS efficiently exploits frequency (multipath) diversity. Note that such a performance is achieved even with a single receive antenna.

5.6.2 Comparison with the nonblind ZF receiver

As a reference for comparison, we simulated the performance of the nonblind Zero Forcing (ZF) receiver. Contrarily to the proposed blind receiver, the ZF one assumes perfect channel knowledge. The ZF solution is given by:

$$\widehat{\mathbf{S}}^{(n_f)T} = \left[\mathbf{V} \diamond \mathbf{G}^{(n_f)}\right]^{\dagger} \tilde{\mathbf{Y}}_2^{(n_f)},$$

where $\mathbf{G}^{(n_f)}$ is defined in (5.14)-(5.15), with $\mathbf{H}_{..f}^{(n_f)}$ assumed to be known, $f = 1, \ldots, F$. In this experiment, we assume $R = M = P = F = 2$, $K = 1$ and

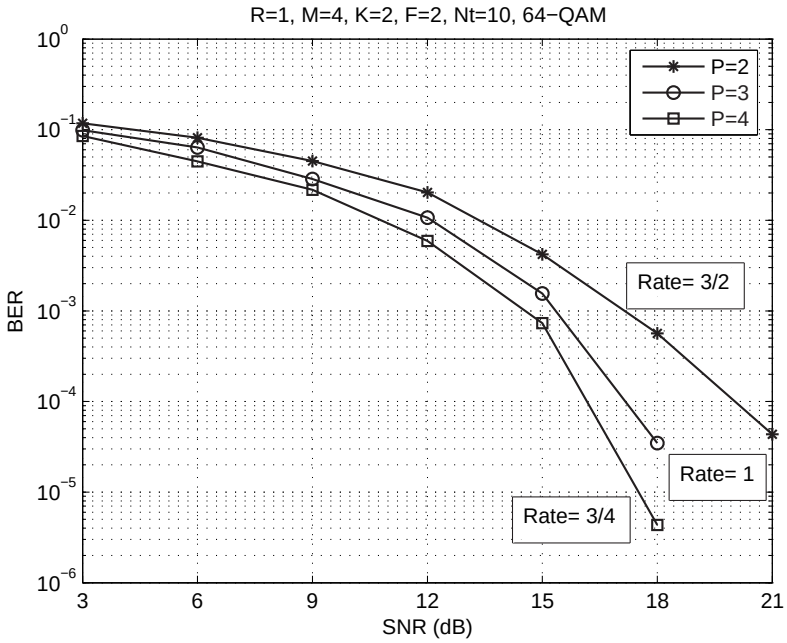

Figure 5.7: Influence of the temporal spreading factor P.

4-QAM. We can observe from Fig. 5.9 that the ZF receiver outperforms the blind receiver as expected. Note that the performance gap between both receivers is nearly 4dB for BER=10^{-3}.

5.6.3 Comparison with a STS scheme [78]

In [78], a Space-Time Spreading (STS) scheme based on spacetime codes was proposed to achieve transmit diversity in the forward link of DS-CDMA systems. For two transmit antennas and one receive antenna, the STS scheme achieves the same spatial diversity gain as the Alamouti code [2] with the advantage that no extra spreading codes are required. Here, we compare STS with T-STFS (with $F = 1$), for $R = 2$ data streams, $M = K = 2$ transmit/rceive antennas and spreading factor $P = 2$. The STS scheme uses orthogonal Walsh-Hadamard codes for spreading both data streams. Both schemes use 4-QAM to achieve a rate of 2 bits per channel use. Perfect channel knowledge is assumed for the STS scheme, which leads to the best performance this scheme can achieve. The proposed T-STFS scheme uses blind detection. The results are depicted in Figure 5.10. Note that the gap between both schemes is around 5dB for BER=10^{-3}. From the slope of the BER curves, we can see that both schemes have the same diversity gain.

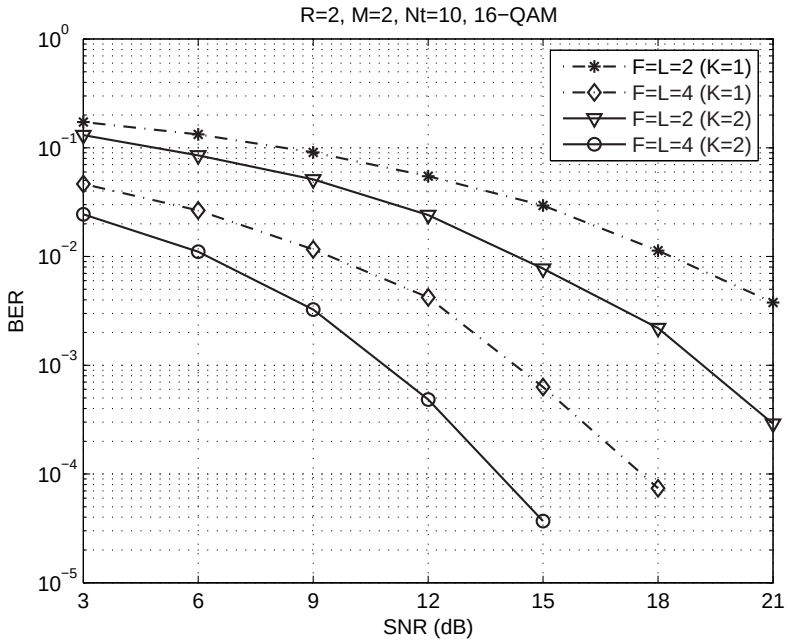

Figure 5.8: Influence of the number L of resolvable multipaths and frequency spreading factor F.

5.6.4 Comparison with the SSSMA model of [104]

In [104], a multicarrier based Spread-Space Spectrum Multiple-Access (SSSMA) model was proposed to provide space and frequency diversities in the forward link of a MIMO wireless system. The STF spreading model proposed therein, is a generalization of [105, 106] to frequency-selective channels. In the multicarrier SSSMA model, each transmitted data stream is modulated with a distinct space-time "diagonal" spreading sequence (its structure is detailed in [106]) at each subcarrier. Frequency-domain spreading is achieved by extending the space-time spread signal across multiple orthogonal subcarriers. The multicarrier SSSMA model is similar to the T-STFS one in the sense that space-, time- and frequency-domain spreading is performed. Both models differ, however, in the construction of the STF spreading codes. In Figure 5.11, the performances of SSSMA and T-STFS are compared. We assume $M = 2$ transmit antennas, $K = 1$ or 2 receive antennas, and $F = 2$ subcarriers. For a fair comparison, we adjust the transmit parameters and the modulation to keep the same data-rate for both approaches. The SSSMA scheme assumes $R = 8$, $P = 2$ and BPSK. For the T-STFS scheme, we have $R = 4$, $P = 4$ and 16-QAM. In this case, both schemes have a rate of 2 bits per channel use. Moreover, the SSSMA scheme uses a ZF receiver, and perfect channel knowledge

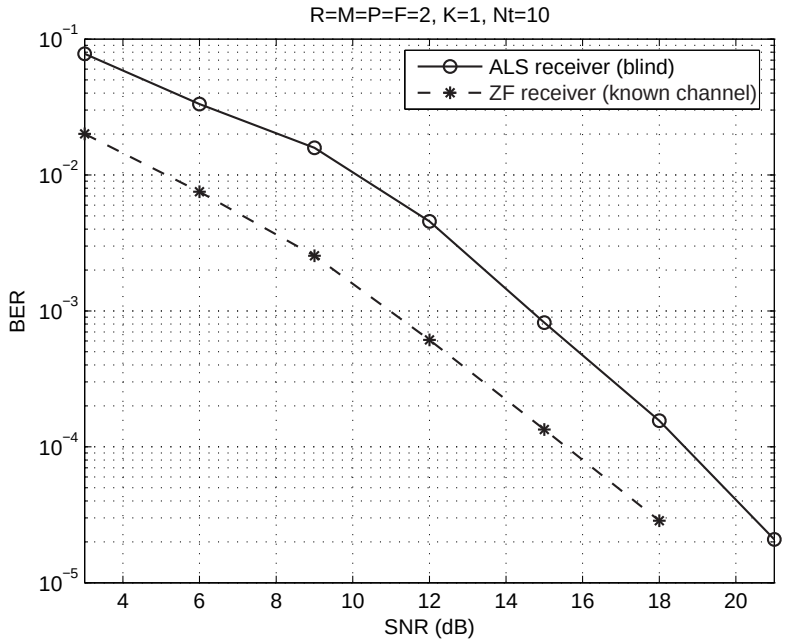

Figure 5.9: T-STFS: Comparison between blind ALS and nonblind ZF receivers.

is assumed. The results are displayed in Figure 5.11. For $K = 1$, the SSSMA scheme exhibits a poor performance. Indeed, this scheme only works for $K \geq M$. The proposed approach has a considerably better performance in this case. The performance gap between both approaches is due to the fact that T-STFS makes an efficient use of the frequency diversity to separate the transmitted data streams when spatial diversity is not available at the receiver. This is in accordance with the identifiability results of Section 5.5.1, which illustrate the trade-off between F and K (see (5.27) and Corollary 3). For $K = 2$, SSSMA outperforms T-STFS over the low-to-medium SNR range. For higher SNR values, T-STFS has superior performance. The slope of the BER curves indicate that the T-STFS scheme has a higher diversity gain.

5.6.5 Channel estimation performance

As detailed in Section 5.5.2, the second stage of the proposed blind receiver consists in estimating the MIMO channel on a per-subcarrier basis by exploiting the known T-STFS structure. The estimation accuracy of the proposed algorithm is evaluated from a Root Mean Square Error (RMSE) measure obtained from 100 independent

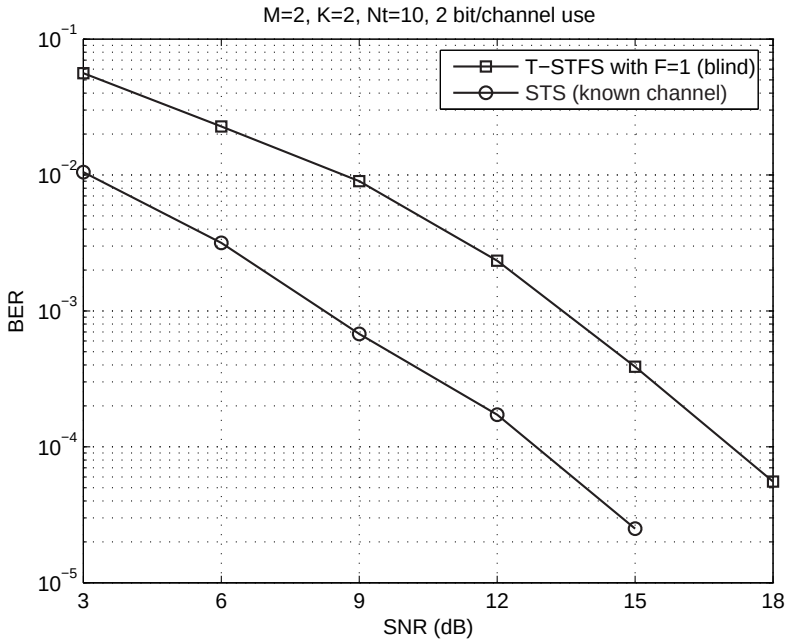

Figure 5.10: Comparison between T-STFS (with blind detection) and a STS scheme (with perfect channel knowledge).

runs. The overall RMSE is calculated using the following formula:

$$\text{RMSE} = \sqrt{\frac{1}{100KMN_f}\sum_{i=1}^{100}\sum_{n_f=1}^{N_f}\left\|\widehat{\mathbf{H}}_{(i)}^{(n_f)} - \mathbf{H}^{(n_f)}\right\|_F^2}$$

The following system configuration is considered: $R = 4$, $M = P = F = 2$ ($N_f = N_c/F = 32$), $N_t = 10$, and $K = 1$ or 2. We can observe from Figure 5.12 that the RMSE has a linear decrease as a function of the SNR in both cases. Using $K = 2$ antennas provides a performance gain of 3dB over the single receive antenna case. Such a gain comes from the increased spatial diversity that helps the separation/resolution of the data streams, despite the larger number of parameters to estimate.

5.7 Summary

We have presented a new space-time-frequency multiple-access transmission model for MIMO wireless systems. The proposed Trilinear (T)-STFS model can be

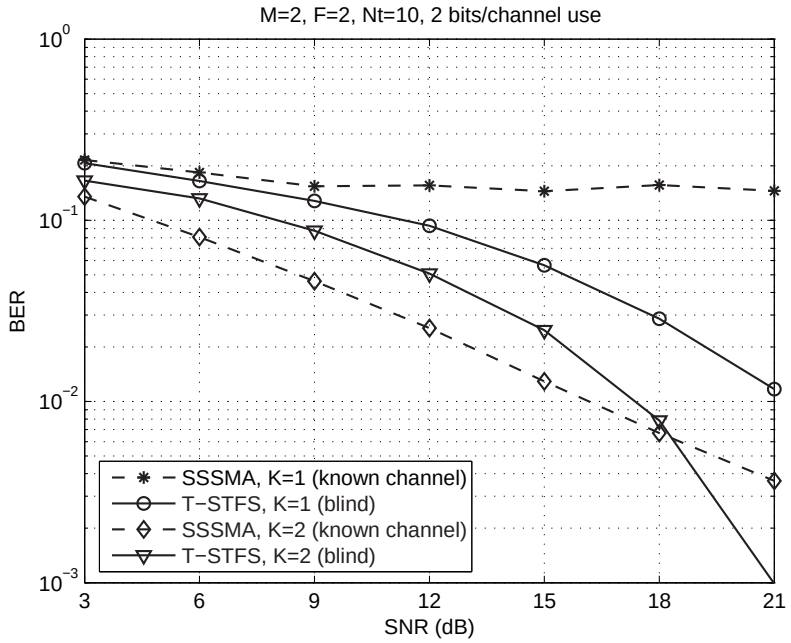

Figure 5.11: T-STFS (with blind detection) *versus* SSSMA (with perfect channel knowledge).

viewed as a 3-D spreading code tensor decomposed into the outer product of the space-, time- and frequency-domain spreading codes. These codes allow multiple data streams to simultaneously access the same set of transmit antennas, chips and subcarriers. We have investigated the diversity gain and rate of the proposed T-STFS model along with a necessary condition for maximum diversity gain in a frequency-selective MIMO channel. The T-STFS structure affords a variable degree of diversity across each one of the three spreading dimensions. It also accommodates an arbitrary number of multiplexed data streams.

We have shown that T-STFS allows blind detection without a priori channel estimation or training sequences. This is achieved thanks to the uniqueness property of the PARAFAC decomposition. An identifiability condition has been presented. This condition gives an upper-bound on the number of transmitted data streams that can be detected/separated for a given system configuration. Some practical corollaries that result from this identifiability condition have also been discussed.

In a multi-user scenario, a generalization of the T-STFS model would consist in reusing the same spreading code in *space*, *time* and/or *frequency* for data streams of the same user, while employing orthogonal spreading codes between users. We conjecture that different reuse patterns of the spreading codes can be incorporated

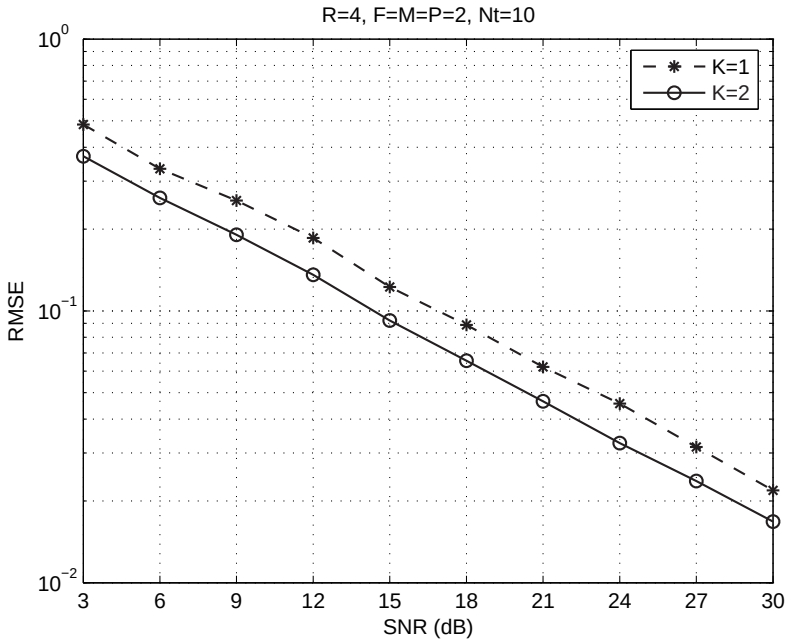

Figure 5.12: RMSE of the estimated channel.

into the T-STFS model using constraint matrices, or alternatively, resorting to the CONFAC decomposition. This idea would generalize the modeling approach of [37, 35].

CHAPTER 6

PARAFAC Methods for Modeling/Estimation of Time-Varying Multipath Channels

In this chapter, we address the problem of multipath parameter estimation of time-varying space-time wireless channels based on PARAFAC modeling. We exploit the different varying rates in the structure of the multipath channel over multiple data-blocks to build a 3D tensor from the received signal. The proposed estimation methods make use of a training sequence that is periodically extended over multiple data-blocks, across which the fading amplitudes are assumed to vary. In the case of SIMO channels, a PARAFAC-based estimator using the ALS algorithm is proposed for joint recovering of the directions of arrival, time delays and complex amplitudes of the multipaths. We also extend this joint modeling/estimation approach to MIMO channels. Simulation results are provided to demonstrate the accuracy of the proposed approach under different channel conditions.

6.1 Motivation and previous work

The issue of parametric multipath channel estimation has been exploited in several works [153, 151, 154]. Most of approaches are based on subspace methods, which exploit shift-invariance properties and/or the knowledge of the pulse shape function. Simultaneous estimation of angles of arrival and delays benefits from the fact that path amplitudes are fast-varying while angles and delays are slowly-varying over multiple transmission blocks or data-blocks. In [153, 151, 154], the angles and delays are blindly-estimated using a collection of previous estimates of the space-time channel impulse response. As in [151, 154], the linear-phase variation property of the frequency domain transformed version of the known pulse shape function is exploited.

Training-sequence-based space-time channel estimation methods exploiting the multiblock invariance of angles and delays have been proposed recently in [134]. In [107, 134], unstructured methods are proposed which are based on the invariance properties of the spatial and temporal subspaces. In [115], a multiblock approach is proposed for multipath parameter estimation in the context of Time Division-Code Division Multiple Access (TD-CDMA) systems. In [108], multiblock processing is also considered for unstructured estimation of the low-rank space-time channels.

In the context of MIMO channels, channel estimation typically uses training/pilot symbols. An accurate channel estimation is important in coherent MIMO communication systems as well as it allows the design of efficient space-time signaling techniques that better exploit the MIMO channel. Parametric channel estimation techniques relying on a physical description of the MIMO channel (i.e. multipath angles, delays and fading amplitudes) are of great interest in wireless position-location systems and future wireless intelligent networks.

Different approaches for channel estimation have been proposed in several works [13, 92, 72]. [13] proposes a modal analysis/filtering concept which exploits the different varying rates of the multipath parameters for estimating time-varying (block-fading) frequency-selective MIMO channels. The authors show that more accurate channel estimates with respect to the standard LS estimation method can be obtained. The approach proposed in [72] is based on spectral factorizations of the specular channel into stationary (space) and non-stationary (fading amplitudes) signature subspaces, and uses linear prediction for estimating/tracking the time-varying channel. In [92], a subspace method is proposed for the parametric estimation of physical MIMO channels. This approach works on a previous unstructured channel estimate, and performs a subspace decomposition of the channel covariance matrix to determine DOAs, DODs and delays.

6.2 Parametric estimation of SIMO channels

In this section, we use the fact that the variation of multipath amplitudes over multiple data-blocks is faster than that of angles and delays for showing that the received signal can be modeled as a third-order (3D) tensor [31]. A PARAFAC model arises thanks to the use of a training sequence which is periodically extended over multiple data-blocks, which are jointly processed at the receiver. By tapping on the powerful identifiability properties of the PARAFAC decomposition, the proposed method performs joint estimation of the angles of arrival, the time-delays and the fading amplitudes of the multipaths without any ambiguity.

Contrarily to other parametric channel estimation approaches such as [153, 151, 154], in which multipath parameters are extracted from unstructured estimations of the space-time channels, the proposed PARAFAC modeling approach directly works on the received signal, thus avoiding error propagation in cases where the unstructured space-time channel is not accurately estimated. Numerical results from computer simulations show that the PARAFAC-based estimator is capable of estimating the triplet angle-delay-amplitude for each multipath with good accuracy even for short training sequences, provided that the number of processed data-blocks is enough. The proposed estimator also performs well with fewer receiver antennas than multipaths.

6.2.1 Signal and channel models

Let us consider a wireless communication system in which a digital signal is transmitted in a specular multipath environment. The receiver is equipped with an array of K antennas spaced half wavelength or closer. We focus on the case of a single-user transmission. The transmitted information symbols are organized into N_b data-blocks. We adopt a block-fading model for the space-time channel, which is based on the fact that, angles and delays (*long-term* parameters) usually experience a much slower rate of variation than the fading amplitudes (*short-term* parameters). We assume that the data-blocks are sufficiently short so that the channel fading can be regarded as stationary over a time-interval necessary for the transmission of a whole data-block and it varies independently from block to block. This is typically the case of Time Division Multiple Access (TDMA)-based systems. In such type of system, different data-blocks are allocated to different mobile users [134].

Figure 6.1 illustrates the idea of a block-transmission. A time-frame is defined as a concatenation of a given number of data-blocks with equal duration. In practice,

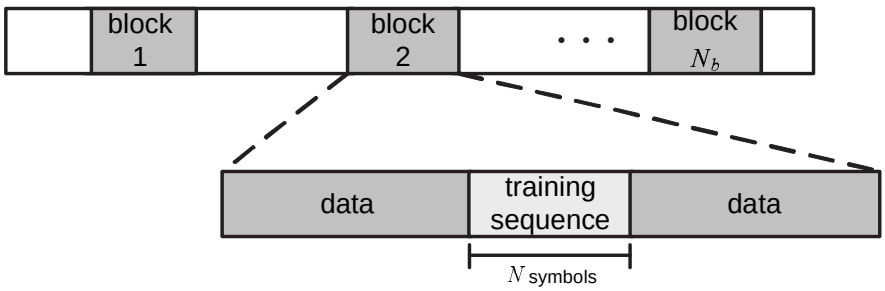

Figure 6.1: Multiblock transmission

each data-block is allocated to a given user, so that the time interval between two data-blocks of a given user is equal to the frame duration.

We assume that the considered system is training-sequence based, with the particular characteristic that consists in reusing the training sequence: A known training sequence of N symbols is periodically extended over multiple data-blocks that are jointly processed at the receiver. The idea of processing multiple data-blocks, based on training sequence reuse is also known as *multiblock processing*. As will be shown, thanks to such a multiblock processing, the problem of multipath parameter estimation can be addressed using PARAFAC analysis.

Let $\{s(n)\}_{n=1}^{N}$ be the training sequence known at the receiver. The temporal support of the channel impulse response is $(0, IT]$. The oversampling factor at the receiver is equal to P. During the n_b-th training block, the received baseband discrete-time signal impinging the k-th receive antenna at the n-th symbol period, can be written, in absence of noise, as:

$$x_{n_b,k,n,p} = \sum_{i=1}^{I} h_{n_b,k,i,p} s_{n,i}, \tag{6.1}$$

where $s_{n,i}$ is the (n,i)-th element of a Toeplitz symbol matrix $\mathbf{S} \in \mathbb{C}^{N \times I}$ constructed from the training sequence $\{s(n)\}_{n=1}^{N}$, with $s_{n,i} \doteq [\mathbf{S}]_{n,i} \doteq s(n-i+1)$. Note that both the received signal and the propagation channel are fourth-order tensors. Comparing (6.1) with (2.19), we can see that the first is a generalization of the later in the sense that a fourth dimension is added in order to model the variation of the fading amplitudes across blocks. It is to be noted, however, that (6.1) is a single-user model (i.e. $Q = 1$) as opposed to (2.19). However, the extension to the multiuser case is straightforward.

We are interested in writing the received signal as an equivalent third-order PA-

RAFAC model by concatenating the third and fourth dimensions into a single dimension. In order to write (6.1) in matrix form, we define $\mathbf{H}_{n_b \cdot i \cdot} \in \mathbb{C}^{K \times P}$ and $\mathbf{X}_{n_b \cdot n \cdot} \in \mathbb{C}^{K \times P}$ as slices of the fourth-order channel and received signal tensors $\mathcal{H} \in \mathbb{C}^{N_b \times K \times I \times P}$ and $\mathcal{X} \in \mathbb{C}^{N_b \times K \times N \times P}$, respectively, in the following manner:

$$[\mathbf{H}_{n_b \cdot i \cdot}]_{k,p} \doteq h_{n_b,k,i,p}, \quad [\mathbf{X}_{n_b \cdot n \cdot}]_{k,p} \doteq x_{n_b,k,n,p}$$

Using these definitions, the (n_b, n)-th slice $\mathbf{X}_{n_b \cdot n \cdot}$ for the received signal tensor can be written as:

$$\mathbf{X}_{n_b \cdot n \cdot} = \sum_{i=1}^{I} \mathbf{H}_{n_b \cdot i \cdot} \, s_{n,i} \tag{6.2}$$

Concatenating the I slices of $\mathbf{H}_{n_b \cdot i \cdot}$ and N slices of $\mathbf{X}_{n_b \cdot n \cdot}$ in the following matrices

$$\begin{aligned} \mathbf{H}_{n_b \cdot \cdot} &= [\mathbf{H}_{n_b \cdot 1 \cdot} \cdots \mathbf{H}_{n_b \cdot I \cdot}] \in \mathbb{C}^{K \times IP}, \\ \mathbf{X}_{n_b \cdot \cdot} &= [\mathbf{X}_{n_b \cdot 1 \cdot} \cdots \mathbf{X}_{n_b \cdot N \cdot}] \in \mathbb{C}^{K \times NP}, \end{aligned}$$

we can express $\mathbf{X}_{n_b \cdot \cdot}$ as:

$$\begin{aligned} \mathbf{X}_{n_b \cdot \cdot} &= \left[\, \mathbf{H}_{n_b \cdot 1 \cdot} \cdots \mathbf{H}_{n_b \cdot I \cdot} \, \right] \begin{bmatrix} s_{1,1}\mathbf{I}_P & \cdots & s_{N,1}\mathbf{I}_P \\ \vdots & & \vdots \\ s_{1,I}\mathbf{I}_P & \cdots & s_{N,I}\mathbf{I}_P \end{bmatrix} \\ &= \mathbf{H}_{n_b \cdot \cdot} \overline{\mathbf{S}}^T, \end{aligned} \tag{6.3}$$

where

$$\overline{\mathbf{S}} = \mathbf{S} \otimes \mathbf{I}_P \in \mathbb{C}^{NP \times IP}.$$

6.2.2 Third-order PARAFAC model

Now, we write the propagation channel $h_{n_b,k,i,p}$ in parametric form by means of a third-order PARAFAC model. The multipath channel within the N_b blocks can be modeled as a combination of L paths, each one of them being characterized by an angle of arrival θ_l, a relative propagation delay τ_l and a complex valued amplitude (fading coefficient) $\beta_{n_b,l}$ that accounts for the channel variations over the N_b blocks. The variations of angles and delays of the paths over the N_b blocks are assumed to be negligible so that the set of parameters $\{\theta_l, \tau_l\}_{l=1}^{L}$ can be assumed constant, i.e., block-independent. In mobile communication systems, this assumption is reasonable if the number of blocks N_b is chosen according to the mobile speed and multipath geometry.

The block-varying propagation channel can be written, in a scalar form, as follows (c.f. (2.20)):

$$h_{n_b,k,i'} = \sum_{l=1}^{L} \beta_{n_b,l} a_{k,l} g_{l,i'}. \tag{6.4}$$

$h_{n_b,k,i'}$ is interpreted as the (n_b, k, i')-th element of an equivalent third-order tensor $\mathcal{H} \in \mathbb{C}^{N_b \times K \times IP}$, and $i' = (i-1)P + p - 1$. Note that:

$$\beta_{n_b,l} = [\mathbf{B}]_{n_b,l}, \quad a_{k,l} = [\mathbf{A}(\boldsymbol{\theta})]_{k,l},$$

$$g_{l,i'} \doteq g(i'/P - \tau_l) = [\mathbf{G}(\boldsymbol{\tau})]_{l,i'},$$

$\mathbf{B} \in \mathbb{C}^{N_b \times L}$ collects the fading gains during the N_b blocks, and $\mathbf{A}(\boldsymbol{\theta}) \in \mathbb{C}^{K \times L}$ concatenates L array responses, and $\mathbf{G}(\boldsymbol{\tau}) \in \mathbb{C}^{L \times IP}$ concatenates L pulse shape responses. Its l-th row $\mathbf{G}_{l\cdot}(\boldsymbol{\tau})$ is given by:

$$\mathbf{G}_{l\cdot}(\boldsymbol{\tau}) = [g(-\tau_l), g(1-\tau_l), \ldots, g(IP-1-\tau_l)] \quad (1 \times IP).$$

$\mathbf{A}(\boldsymbol{\theta})$ and $\mathbf{G}(\boldsymbol{\tau})$ are parameterized by the set of angles and delays $\boldsymbol{\tau} = [\tau_1, \ldots, \tau_L]$ and $\boldsymbol{\theta} = [\theta_1, \ldots, \theta_L]$. We assume that the envelope of the fading amplitudes $\{\beta_{n_b,l}\}_{l=1}^{L}$ follows a Rayleigh distribution while the associated phase is uniformly distributed. They are assumed to be uncorrelated from block to block, although this is not a necessary assumption in our context.

The channel model (6.4) is as an L-factor PARAFAC decomposition of the equivalent third-order channel tensor $\mathcal{H} \in \mathbb{C}^{N_b \times K \times IP}$. The difference between (2.21) and (6.4) are the following. As opposed to (2.21), the block-dependent index n_b is present in (6.4). Another difference is on the definition of the pulse shape response. In (2.21), the oversampling index p is associated with the third dimension of the pulse shape response $g_{l,i,p}$, while in (6.4), p and i are concatenated in $g_{l,i'}$. Moreover, (6.4) is a single-user model, while in (2.21) a multiuser model is considered.

The n_b-th first-mode matrix slice of $\mathcal{H} \in \mathbb{C}^{N_b \times K \times IP}$ is given by:

$$\mathbf{H}_{n_b\cdot\cdot} = \mathbf{A}(\boldsymbol{\theta}) D_{n_b}(\mathbf{B}) \mathbf{G}(\boldsymbol{\tau}), \quad n_b = 1, \ldots, N_b. \tag{6.5}$$

Collecting the N_b slices of the channel response, we arrive at the following unfolded matrix representation for the channel tensor:

$$\mathbf{H} = \begin{bmatrix} \mathbf{H}_{1\cdot\cdot} \\ \vdots \\ \mathbf{H}_{N_b\cdot\cdot} \end{bmatrix} = \begin{bmatrix} \mathbf{A}(\boldsymbol{\theta}) D_1(\mathbf{B}) \\ \vdots \\ \mathbf{A}(\boldsymbol{\theta}) D_{N_b}(\mathbf{B}) \end{bmatrix} \mathbf{G}(\boldsymbol{\tau}) = \big(\mathbf{B} \diamond \mathbf{A}(\boldsymbol{\theta})\big)\mathbf{G}(\boldsymbol{\tau}). \tag{6.6}$$

Now, let us go back to model (6.3), which expresses the received signal for the n_b-th block. Stacking column-wise the N_b slices of the received signal $\mathbf{X}_{1\cdot\cdot}, \ldots, \mathbf{X}_{N_b\cdot\cdot}$, we get:

$$\mathbf{X}_2 = \begin{bmatrix} \mathbf{X}_{1\cdot\cdot} \\ \vdots \\ \mathbf{X}_{N_b\cdot\cdot} \end{bmatrix} = \begin{bmatrix} \mathbf{H}_{1\cdot\cdot} \\ \vdots \\ \mathbf{H}_{N_b\cdot\cdot} \end{bmatrix} \overline{\mathbf{S}}^T = \big(\mathbf{B} \diamond \mathbf{A}(\boldsymbol{\theta})\big)\mathbf{G}(\boldsymbol{\tau})\overline{\mathbf{S}}^T. \tag{6.7}$$

We make use of the fact that a Fourier transform maps a delay to a certain phase shift. This fact will be exploited for an unambiguous multipath parameter estimation. If the pulse shape function is bandlimited and sampled at or above the Nyquist rate, the Discrete Fourier Transform (DFT) of $\big(\mathbf{G}_{l\cdot}(\boldsymbol{\tau})\big)^T$ can be expressed as [151]:

$$\tilde{\mathbf{g}}_l \doteq \mathrm{DFT}\Big[\big(\mathbf{G}_{l\cdot}(\boldsymbol{\tau})\big)^T\Big] = \mathrm{diag}\big(\tilde{\mathbf{g}}_0\big) \cdot \underbrace{\begin{bmatrix} 1 \\ \phi^{\tau_l P} \\ (\phi^{\tau_l P})^2 \\ \vdots \\ (\phi^{\tau_l P})^{IP-1} \end{bmatrix}}_{\mathbf{f}(\tau_l,\phi)} = \mathrm{diag}\big(\tilde{\mathbf{g}}_0\big) \cdot \mathbf{f}(\tau_l, \phi),$$

where

$$\phi = e^{-j(2\pi/IP)}, \quad \tilde{\mathbf{g}}_0 = \boldsymbol{\Gamma}\mathbf{g}_0$$

$\mathbf{g}_0$ is the pulse shaping function at the zero delay, $\tilde{\mathbf{g}}_0$ its associated DFT, $\mathbf{f}(\tau_l, \phi)$ is the phase shift of the frequency response at delay τ_l, and

$$\boldsymbol{\Gamma} = \begin{bmatrix} 1 & 1 & \cdots & 1 \\ 1 & \phi & \cdots & \phi^{IP-1} \\ \vdots & \vdots & & \vdots \\ 1 & \phi^{IP-1} & \cdots & \phi^{(IP-1)^2} \end{bmatrix} \in \mathbb{C}^{IP \times IP}$$

is a DFT matrix. Therefore, by taking the Fourier transform of the signal at each receive antenna, we effectively perform a Fourier transform on every row $\mathbf{G}_{l\cdot}(\boldsymbol{\tau})$ of $\mathbf{G}(\boldsymbol{\tau})$, and we can rewrite (6.7) as:

$$\breve{\mathbf{X}}_2 = \begin{bmatrix} \breve{\mathbf{X}}_{1\cdot\cdot} \\ \vdots \\ \breve{\mathbf{X}}_{N_b\cdot\cdot} \end{bmatrix} = \mathbf{H}_2\overline{\mathbf{S}}^T = \big(\mathbf{B} \diamond \mathbf{A}(\boldsymbol{\theta})\big)\big(\overline{\mathbf{S}}\breve{\mathbf{F}}(\boldsymbol{\tau}, \boldsymbol{\phi})\big)^T, \tag{6.8}$$

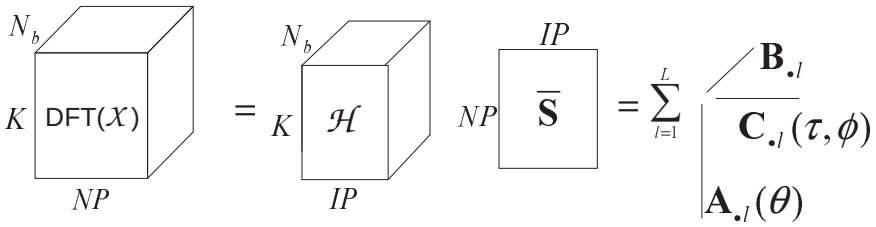

Figure 6.2: Decomposition of the (multi-block) received signal tensor.

where

$$\breve{\mathbf{F}}(\boldsymbol{\tau}, \boldsymbol{\phi}) = \mathrm{diag}\big(\tilde{\mathbf{g}}_0\big) \cdot \mathbf{F}(\boldsymbol{\tau}, \boldsymbol{\phi}) \in \mathbb{C}^{IP \times L}, \tag{6.9}$$

and $\mathbf{F}$ is a Vandermonde matrix:

$$\mathbf{F}(\boldsymbol{\tau}, \boldsymbol{\phi}) = \begin{bmatrix} 1 & \cdots & 1 \\ \phi^{\tau_1 P} & \cdots & \phi^{\tau_L P} \\ \vdots & & \vdots \\ (\phi^{\tau_1 P})^{IP-1} & \cdots & (\phi^{\tau_L P})^{IP-1} \end{bmatrix} = \big[\mathbf{f}(\tau_1, \phi) \cdots \mathbf{f}(\tau_L, \phi)\big] \tag{6.10}$$

Defining

$$\mathbf{C}(\boldsymbol{\tau}, \boldsymbol{\phi}) = \overline{\mathbf{S}}\breve{\mathbf{F}}(\boldsymbol{\tau}, \boldsymbol{\phi}) \in \mathbb{C}^{NP \times L}, \tag{6.11}$$

and using (1.26) with the correspondences $\big(\mathbf{A}, \mathbf{B}, \mathbf{C}\big) \rightarrow \big(\mathbf{B}, \mathbf{A}(\boldsymbol{\theta}), \mathbf{C}(\boldsymbol{\tau}, \boldsymbol{\phi})\big)$, we obtain the three following unfolded representations for the DFT-transformed received signal tensor:

$$\begin{aligned} \breve{\mathbf{X}}_2 &= \big(\mathbf{B} \diamond \mathbf{A}(\boldsymbol{\theta})\big)\mathbf{C}^T(\boldsymbol{\tau}, \boldsymbol{\phi}) \in \mathbb{C}^{KN_b \times NP}, \\ \breve{\mathbf{X}}_3 &= \big(\mathbf{A}(\boldsymbol{\theta}) \diamond \mathbf{C}(\boldsymbol{\tau}, \boldsymbol{\phi})\big)\mathbf{B}^T \in \mathbb{C}^{NPK \times N_b}, \\ \breve{\mathbf{X}}_1 &= \big(\mathbf{C}(\boldsymbol{\tau}, \boldsymbol{\phi}) \diamond \mathbf{B}\big)\mathbf{A}^T(\boldsymbol{\theta}) \in \mathbb{C}^{N_b NP \times K}, \end{aligned} \tag{6.12}$$

Figure 6.2 depicts the PARAFAC decomposition of the received signal tensor into the component matrices characterizing the time-varying SIMO channel.

6.2.3 Identifiability

At this point, we focus on the identifiability conditions of model (6.12) and discuss its link to the problem of multipath parameter estimation. Using Kruskal's

identifiability condition given in Theorem 1.1 (Chapter 1, Section 1.2.2), if

$$k_{\mathbf{A}(\boldsymbol{\theta})} + k_{\mathbf{B}} + k_{\mathbf{C}(\boldsymbol{\tau},\boldsymbol{\phi})} \geq 2(L+1), \tag{6.13}$$

the matrices $\mathbf{A}(\boldsymbol{\theta})$, $\mathbf{B}$ and $\mathbf{C}(\boldsymbol{\tau},\boldsymbol{\phi})$ are unique up to permutation and scaling of columns.

It is worth mentioning that the permutation ambiguity does not need to be solved in the context of the multipath parameter estimation problem, since the ordering of multipath spatial and temporal responses is not important. Concerning the scaling ambiguity, it can be eliminated from our model by exploiting the Vandermonde structure of $\mathbf{A}(\boldsymbol{\theta})$ and $\mathbf{F}(\boldsymbol{\tau},\boldsymbol{\phi})$.

In the present context, we make the following assumptions concerning the multipath channel structure:

- The array manifold is known and the multipath signals arrive at the array at distinct angles and delays;
- The multipaths undergo independent fading and vary independently from block to block.

Under these assumptions, the identifiability condition (6.13) can be further simplified if some additional structure of the model is taken into account. Let us first state the following Lemmas:

Lemma 7.1 (Vandermonde k-rank Lemma [133]): *A Vandermonde matrix* $\mathbf{V} \in \mathbb{C}^{m\times n}$ *with distinct nonzero generators* $\phi_1, \phi_2, \ldots, \phi_n \in \mathbb{C}$ *is full k-rank, i.e.,* $k_{\mathbf{V}} = r_{\mathbf{V}} = min(m,n)$.

Lemma 7.2: *Let* $\mathbf{A} \in \mathbb{C}^{p\times m}$ *and* $\mathbf{B} \in \mathbb{C}^{m\times n}$ *be two matrices. If* $\mathbf{A}$ *is full column rank, then* $r_{\mathbf{AB}} = r_{\mathbf{B}}$. *If* $\mathbf{B}$ *is a Vandermonde matrix with distinct nonzero generators* $\phi_1, \phi_2, \ldots, \phi_n \in \mathbb{C}$, *then the full column rank condition of* $\mathbf{A}$ *implies that* $r_{\mathbf{AB}} = min(m,n)$.

Note that the matrix of spatial array responses $\mathbf{A}$ is Vandermonde, for which Lemma 7.1 applies, i.e., $k_{\mathbf{A}(\boldsymbol{\theta})} = \min(K,L)$. Let us study the structure of matrix $\mathbf{C}(\boldsymbol{\tau},\boldsymbol{\phi})$ in (6.11). This matrix is factored as a function of $\overline{\mathbf{S}}$ and $\breve{\mathbf{F}}(\boldsymbol{\tau},\boldsymbol{\phi})$. Without loss of generality, let us assume that $IP \geq L$. Under the condition of "persistence of excitation" of the training symbols, matrix $\overline{\mathbf{S}}$ is full column-rank (also full k-rank). Thus, Lemma 7.2 can be directly applied to $\mathbf{C}(\boldsymbol{\tau},\boldsymbol{\phi}) = \overline{\mathbf{S}}\breve{\mathbf{F}}(\boldsymbol{\tau},\boldsymbol{\phi})$, which

means that $k_{\mathbf{C}(\boldsymbol{\tau},\boldsymbol{\phi})} = \min(IP, L) = L$. Finally, the matrix of fading amplitudes $\mathbf{B}$ is also full k-rank with probability one, under the condition of independent multipath fading variation [131]. Thus, the identifiability condition (6.13) can be equivalently stated as

$$\min(K, L) + \min(N_b, L) \geq L + 2. \tag{6.14}$$

By studying condition (6.14), we can distinguish two cases:

1. For $N_b \geq L$, $K \geq 2$ antennas are enough for estimating the L multipath parameters;

2. For $K \geq L$, $N_b \geq 2$ training blocks are enough for estimating the L multipath parameters.

6.2.4 PARAFAC-based estimator

The receiver algorithm for the joint estimation of angles, delays and amplitudes of the multipaths fully exploits the trilinear structure of the multipath channel model, and is based on the classical ALS algorithm. As usual, the matrices $\mathbf{A}(\boldsymbol{\theta})$, $\mathbf{B}$ and $\mathbf{C}(\boldsymbol{\tau}, \boldsymbol{\phi})$ are estimated by optimizing the three following least squares criteria:

$$\underset{\mathbf{B}}{\operatorname{argmin}} \left\| \breve{\tilde{\mathbf{X}}}_3 - \big(\mathbf{A}(\boldsymbol{\theta}) \diamond \mathbf{C}(\boldsymbol{\tau}, \boldsymbol{\phi})\big)\mathbf{B}^T \right\|_F^2, \quad \underset{\mathbf{A}(\boldsymbol{\theta})}{\operatorname{argmin}} \left\| \breve{\tilde{\mathbf{X}}}_1 - \big(\mathbf{C}(\boldsymbol{\tau}, \boldsymbol{\phi}) \diamond \mathbf{B}\big)\mathbf{A}^T(\boldsymbol{\theta}) \right\|_F^2,$$
$$\underset{\mathbf{C}(\boldsymbol{\tau},\boldsymbol{\phi})}{\operatorname{argmin}} \left\| \breve{\tilde{\mathbf{X}}}_2 - \big(\mathbf{B} \diamond \mathbf{A}(\boldsymbol{\theta})\big)\mathbf{C}^T(\boldsymbol{\tau}, \boldsymbol{\phi}) \right\|_F^2, \tag{6.15}$$

where $\breve{\tilde{\mathbf{X}}}_{i=1,2,3}$ are the noisy versions of $\breve{\mathbf{X}}_{i=1,2,3}$.

Elimination of the scaling ambiguities

At this point, we show how the scaling ambiguities are eliminated. As previously mentioned, permutation ambiguity is not important in the present context and we do not take it into account. However, we must take care of the scaling ambiguity in order to obtain the final estimates of the channel parameters. At the end of the ALS-based estimation stage, an estimate of the DFT-transformed pulse shape response is obtained from (6.11) as $\widehat{\mathbf{F}}(\boldsymbol{\tau}, \boldsymbol{\phi}) = \big(\overline{\mathbf{S}}\big)^{\dagger} \widehat{\mathbf{C}}(\boldsymbol{\tau}, \boldsymbol{\phi})$. The final (unambiguous) estimate of $\mathbf{A}(\boldsymbol{\theta})$ (array responses), $\mathbf{B}$ (fading amplitudes) and

$\mathbf{F}(\boldsymbol{\tau}, \boldsymbol{\phi})$ (delay responses), denoted by $\widehat{\widehat{\mathbf{A}}}(\boldsymbol{\theta})$, $\widehat{\widehat{\mathbf{B}}}$ and $\widehat{\widehat{\mathbf{F}}}(\boldsymbol{\tau}, \boldsymbol{\phi})$, are linked to the ALS-based estimates by:

$$\widehat{\widehat{\mathbf{A}}}(\boldsymbol{\theta}) = \widehat{\mathbf{A}}(\boldsymbol{\theta})\boldsymbol{\Delta}_1^{-1}, \quad \widehat{\widehat{\mathbf{B}}} = \widehat{\mathbf{B}}\boldsymbol{\Delta}_2^{-1}, \quad \widehat{\widehat{\mathbf{F}}}(\boldsymbol{\tau}, \boldsymbol{\phi}) = \widehat{\mathbf{F}}(\boldsymbol{\tau}, \boldsymbol{\phi})\boldsymbol{\Delta}_3^{-1}, \tag{6.16}$$

The *a priori* knowledge of the Vandermonde structure of $\mathbf{A}(\boldsymbol{\theta})$ and $\mathbf{F}(\boldsymbol{\tau}, \boldsymbol{\phi})$ means that the first row of both matrices have all-ones entries, i.e.:

$$\mathbf{A}_{1\cdot}(\boldsymbol{\theta}) = [1, \ldots, 1], \quad \mathbf{F}_{1\cdot}(\boldsymbol{\tau}, \boldsymbol{\phi}) = [1, \ldots, 1].$$

This allows a unique determination of the scaling ambiguity matrices $\boldsymbol{\Delta}_{i=1,2,3}$ as:

$$\boldsymbol{\Delta}_1 = D_1(\widehat{\mathbf{A}}(\boldsymbol{\theta})), \quad \boldsymbol{\Delta}_3 = D_1(\widehat{\mathbf{F}}(\boldsymbol{\tau}, \boldsymbol{\phi})), \quad \boldsymbol{\Delta}_2 = (\boldsymbol{\Delta}_1\boldsymbol{\Delta}_3)^{-1}, \tag{6.17}$$

from which the final estimates $\widehat{\widehat{\mathbf{A}}}(\boldsymbol{\theta})$, $\widehat{\widehat{\mathbf{B}}}$ and $\widehat{\widehat{\mathbf{F}}}(\boldsymbol{\tau}, \boldsymbol{\phi})$ are obtained.

6.2.5 Simulation results

In this section, the performance of the PARAFAC-based multipath parameter estimator is evaluated through computer simulations. The training sequence to be used over the N_b blocks is randomly generated at each run, following a normal distribution with unity variance. The pulse shape function is a raised cosine with roll-off factor 0.35. The L paths are assumed to have the same average power. The results are averaged over 100 Monte Carlo runs. For each run, multipath fading amplitudes for the N_b data-blocks are drawn from an i.i.d. Rayleigh generator. For the ALS algorithm, random initialization is used. If convergence is not achieved within 100 iterations, we re-start the algorithm from a different initialization point. The Root Mean Square Error (RMSE) between the estimated and true matrices is used here as the evaluation metric of the estimator performance.

Figure 6.3 depicts the RMSE versus SNR for the estimation of the array (angle) and pulse shape (delay) responses, considering a multipath scenario with $L = 3$ paths. The angles of arrival and time delays are $\{\theta_1, \theta_2, \theta_3\} = \{-10^\circ, 0, 20^\circ\}$ and $\{\tau_1, \tau_2, \tau_3\} = \{0, 1.1T, 2T\}$. considering $K = 2$ antennas and $N = 8$ training symbols and an oversampling factor $P = 4$. The temporal support of the channel is $I = 5$. The results are shown for $N_b = 5$ and $N_b = 10$ data-blocks. It is seen that the proposed estimator exhibits a linear decrease in its RMSE as SNR increases. This is valid for both angle and delay RMSE. The performance gap between angle and delay estimation is due to the fact that the raised cosine pulse shape function is not bandlimited, which leads to some delay estimation bias. As expected, the

estimator performance improves as the number of data-blocks increases. Although not displayed in the figure, the RMSE results for the fading amplitudes are very close to those for the delay responses. Note that these performance results are achieved with fewer antennas than multipaths and with a short training sequence, which is interesting characteristic of the proposed PARAFAC-based estimator.

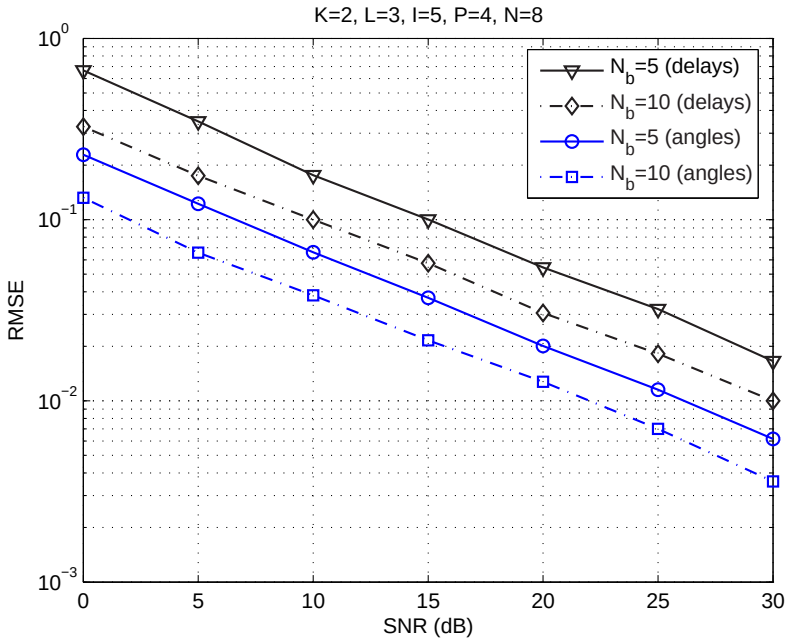

Figure 6.3: RMSE performance (angles and delays).

In Fig. 6.4, we evaluate the impact of the number of training symbols N on the accuracy of the PAFAFAC-based estimator. We assume $L = 3$ with $\{\theta_1, \theta_2, \theta_3\} = \{-10°, 0, 20°\}$ and $\{\tau_1, \tau_2, \tau_3\} = \{0, 0.25T, 2T\}$. The other parameters are $I = 3$, $N_b = 8$, $P = 4$ and $K = 2$. We consider three different training sequence lengths: $N = 5$, 10 and 20. In this figure, we plot the RMSE of the overall estimated channel by averaging over the N_b data blocks. The RMSE is calculated according to the following formula:

$$\text{RMSE}_{overall} = \sqrt{\frac{1}{100KIP}\sum_{r=1}^{100}\left\|\widehat{\widehat{\mathbf{H}}}_2(r) - \mathbf{H}_2\right\|_F^2}, \tag{6.18}$$

where $\mathbf{H}_2 = (\mathbf{B} \diamond \mathbf{A}(\boldsymbol{\theta}))\breve{\mathbf{F}}^T(\boldsymbol{\tau}, \boldsymbol{\phi})$ is defined in (6.8), and $\widehat{\widehat{\mathbf{H}}}_2(r)$ is its reconstructed version at the r-th run. It can be seen from this figure that the performance

improves as N increases, as expected. The gain is more pronounced when N is increased from 5 to 10.

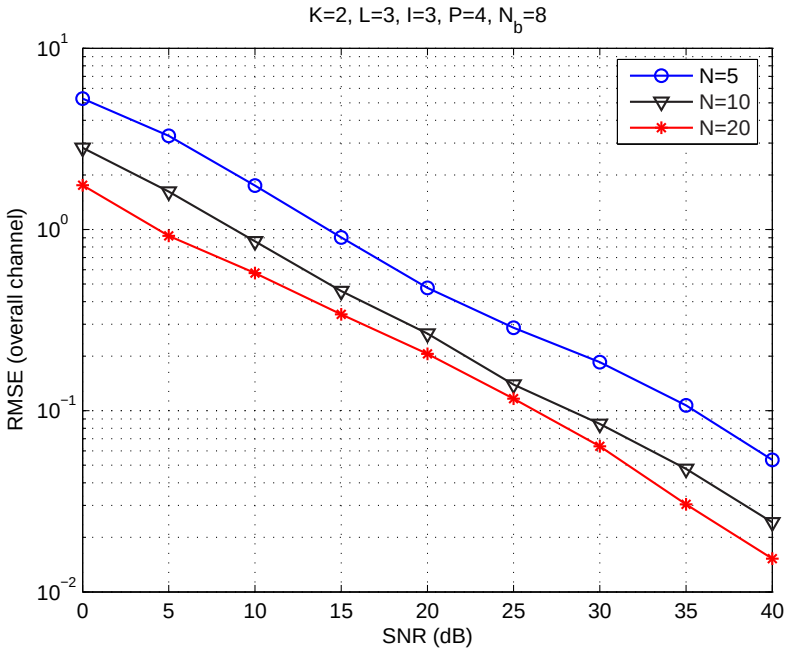

Figure 6.4: RMSE performance for different values of N.

Now, we evaluate the influence of the angular separation of the multipaths on the performance of the proposed estimator. We assume $\{\tau_1, \tau_2, \tau_3\} = \{0, 0.25T, 2T\}$, and the two angular distributions are i) $\{0°, 3°, 5°\}$ (small angular separation) and ii) $\{0°, 15°, 30°\}$ (large angular separation). The other parameters are $I = 3$, $N_b = 5$, $N = 8$, $P = 4$ and $K = 2$. The results are displayed in Fig. 6.5, where the RMSE of the overall channel calculated using (6.18) is plotted. We can see that the performance of estimator is degraded as the angular separation becomes smaller. Such a degradation becomes more important at higher SNR values. For small to medium SNR values (e.g. between 0 and 20dB), there is no significant difference between the two scenarii.

In the next experiment, we evaluate the RMSE for each set of estimated multipath parameters, i.e. angles ($\widehat{\widehat{\mathbf{A}}}(\boldsymbol{\theta})$), delays ($\widehat{\widehat{\mathbf{F}}}(\boldsymbol{\tau}, \boldsymbol{\phi})$), and fading amplitudes ($\widehat{\widehat{\mathbf{B}}}$). The multipath channel is characterized by $L = 2$ dominant paths with associated angles and delays equal to $\{\theta_1, \theta_2\} = \{-10°, 0\}$ and $\{\tau_1, \tau_2, \} = \{0, T\}$. The other parameters are $I = 3$, $N = 8$, $P = 8$ and $K = 2$. We consider $N_b = 2$ and 10 blocks. Figure 6.6 depicts the results. For a fixed value of N_b, we can observe

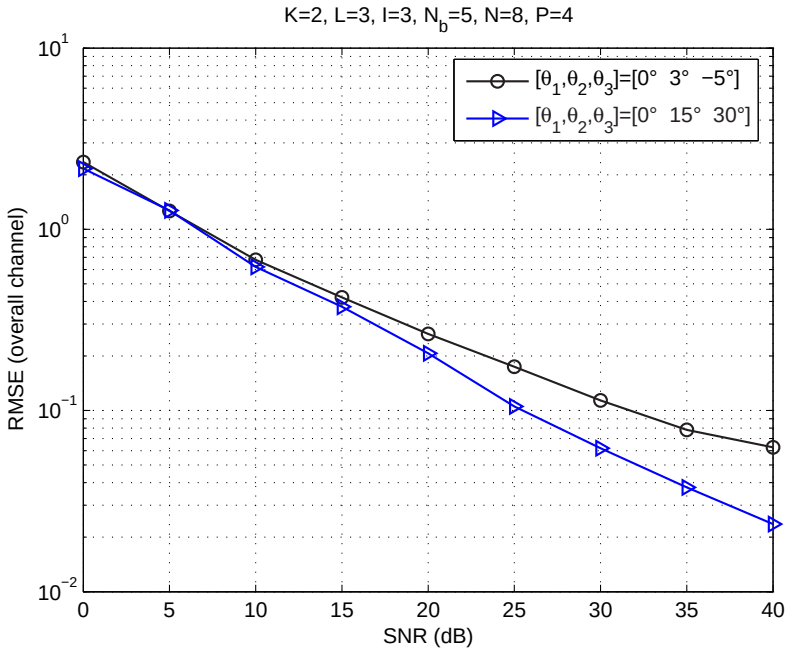

Figure 6.5: RMSE performance for two angular distributions.

that the estimation accuracy of the array responses $\mathbf{A}(\boldsymbol{\theta})$ is better than that of the delays and fading amplitudes. As previously mentioned, the estimation of the delays is biased due to bandlimited pulse shaping. Since the final unambiguous estimate of the fading amplitudes $\widehat{\widehat{\mathbf{B}}}$ directly depends on the scaling factor of the estimated matrix $\widehat{\widehat{\mathbf{F}}}(\boldsymbol{\tau}, \boldsymbol{\phi})$ (c.f. (6.17)), the estimator performance is also limited for the fading amplitudes. A performance gain is obtained when N_b is increased. Such a gain is significant w.r.t the estimation of the angles and delays while becoming less important for the estimation of the fading amplitudes. The RMSE of the overall estimated channel is also shown in Fig.6.6.

6.3 Parametric estimation of MIMO channels

Here, we present a parametric approach for estimating frequency-selective block-fading MIMO channels, which can be viewed as an extension of the tensor modeling approach of the previous section [25]. It is based on the observation that the considered MIMO channel model also has a tensor structure and follows a PARAFAC model. This model is exploited for estimating the complete set of MIMO mul-

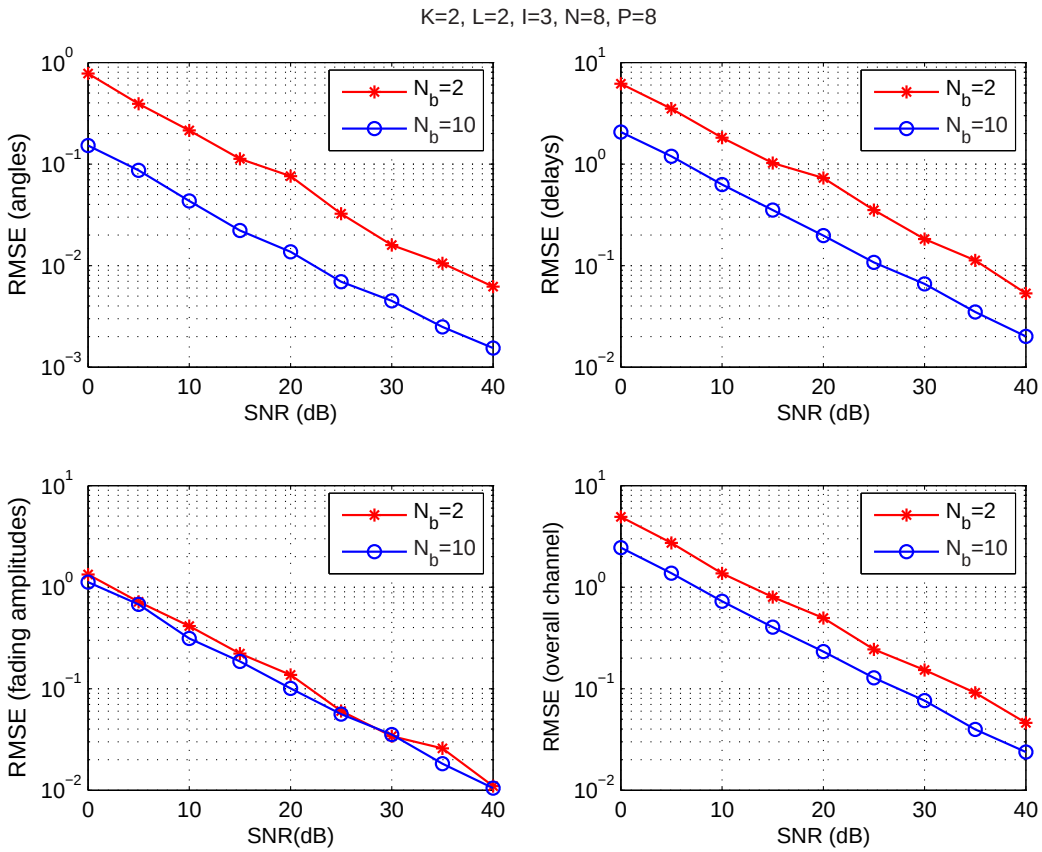

Figure 6.6: RMSE of the estimated channel parameters.

tipath parameters: Directions Of Arrival/Departure (DOAs/DODs), delays and fading amplitudes. The estimation method consists in using the ALS algorithm, followed by a final estimation stage that relies on the knowledge of the training sequence.

6.3.1 System model and assumptions

Let us consider a MIMO antenna system with M transmit and K receive antennas. The spacing between any two antennas at both the transmit and receive arrays is assumed to be half-wavelength, so that we can apply the far-field approximation by assuming a locally plane wave. In this case, the MIMO channel can be characterized by specular multipath propagation, i.e., the channel between each transmit

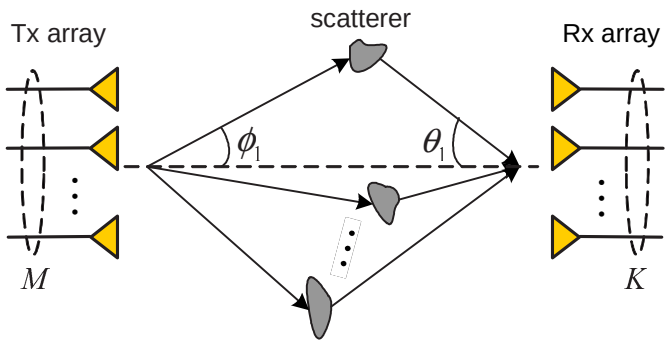

Figure 6.7: MIMO multipath propagation scenario

and receive antenna can be parameterized as the superposition of L paths. This model is widely used for outdoor scenarii and has been adopted for MIMO systems [13].

Figure 6.7 illustrates the considered MIMO propagation scenario. Each path is associated with a different scatterer located between the transmitter and the receiver. The location of the l-th scatterer determines a DOD ϕ_l and a DOA θ_l (with respect to the transmit/receive array broadside) and a relative propagation delay τ_l for the l-th path [122]. As in the SIMO case, it is also assumed that the maximum path delay exceeds the inverse of the coherence bandwidth so that the channel is frequency-selective. The finite support of the channel impulse response is equal to I symbol periods and the oversampling factor at the receiver is equal to P times the symbol rate. Let us define the following matrices collecting the transmitter and the receiver array responses and as well as the combined transmitter/receiver pulse shape responses:

$$\begin{aligned}
\mathbf{A}_{tx}(\boldsymbol{\phi}) &= [\mathbf{a}_{tx}(\phi_1) \cdots \mathbf{a}_{tx}(\phi_L)] \in \mathbb{C}^{M \times L} \\
\mathbf{A}(\boldsymbol{\theta}) &= [\mathbf{a}(\theta_1) \cdots \mathbf{a}(\theta_L)] \in \mathbb{C}^{K \times L} \\
\mathbf{G}(\boldsymbol{\tau}) &= [\mathbf{g}(\tau_1) \cdots \mathbf{g}(\tau_L)] \in \mathbb{C}^{L \times IP}.
\end{aligned}$$

6.3.2 Block-fading MIMO channel model

As considered in the previous section, we also adopt a block-fading model for the time-varying propagation channel. Recall that the fading amplitudes of the multipaths are considered constant over an entire data transmission block, but

vary between two blocks. On the other hand, ϕ_l, θ_l and τ_l are assumed to be constant over an interval of stationarity spanning N_b blocks. This block-fading channel model is reasonable in most of mobile communication systems with block-transmission, and has been exploited in [13, 72], for purposes of MIMO channel estimation.

6.3.3 Multi-block training sequence

At the transmitter, each transmission block is organized in M data streams that are transmitted by the M transmit antennas. The structure of these data streams depend on the considered particular scheme (e.g., spatial multiplexing, space-time coding, etc). Each one of the M data streams has a training sequence of N symbols known at the receiver.

The length-N training sequence at the m-th transmit antenna for the n_b-th transmission block is represented by:

$$\mathbf{s}_m(n_b) = [s_m(n_b, 1) \cdots s_m(n_b, N)]^T \in \mathbb{C}^N.$$

We make the following assumptions concerning the design of the training sequences:

A.1 The M training sequence vectors $\mathbf{s}_1, \ldots, \mathbf{s}_M$ are linearly independent;

A.2 The training sequence length N satisfies $N \geq MI$;

A.3 The training sequence $\mathbf{s}_m$, $m = 1, \ldots, M$, is reused across N_b successive transmission blocks, and we have $\mathbf{s}_m(n_b) = \mathbf{s}_m, \quad \forall n_b \in [1, N_b]$.

We remark that the "independence" assumption does not lead to an optimal training sequence set for estimating the MIMO channel. An optimal design should ensure that the training sequences have perfect periodic autocorrelations and cross-correlations within $I - 1$ temporal shifts [96], where I is the temporal span of the channel impulse response. Here, we are not concerned with optimal training sequence design, and we simply assume independent training sequences. As will be shown later in our simulation results, the independency assumption is enough to guarantee accurate estimates of the MIMO channel using the proposed approach.

Figure 6.8 outlines the multiblock MIMO transmission structure with training sequence reuse across transmission blocks. It is to be noted that one transmission block comprises M parallel data blocks, each one of which having its own training

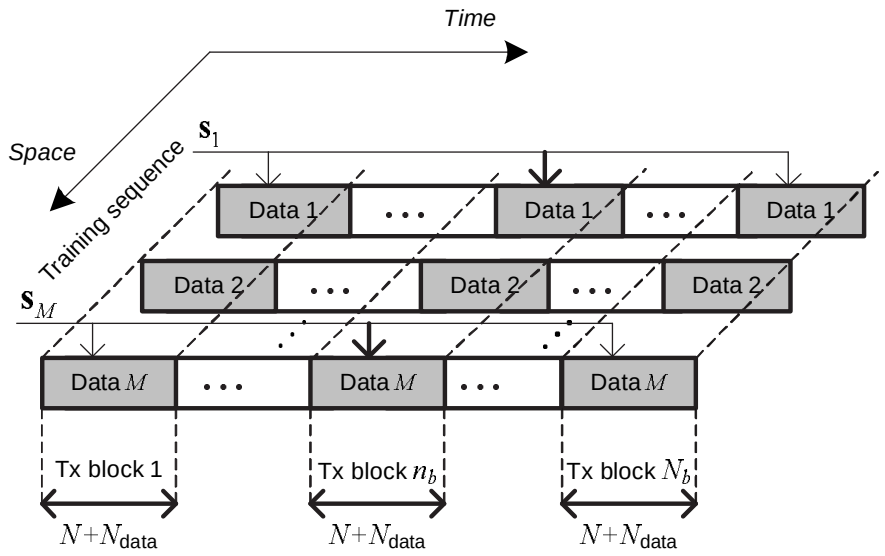

Figure 6.8: Multiblock MIMO transmission with training sequence reuse

sequence. Note also that the figure indicates that the same set of training sequences is inserted into N_b transmission blocks. Each data block has $N_{\text{block}} = N + N_{\text{data}}$ symbols, N_{data} denotes the number of "useful" data symbols of each data block. For signal modeling and channel estimation purposes, we focus only on the training sequence portion of each data block. After having estimated the channel, the useful data portion can be processed/recovered in a subsequent step by means of space-time processing.

6.3.4 Third-order PARAFAC model

The block-fading MIMO channel can be viewed as a fourth-order tensor $\mathcal{H} \in \mathbb{C}^{N_b \times K \times M \times IP}$. Let us define $h_{n_b,k,m,i'}$ as a scalar component of the MIMO channel tensor $\mathcal{H}$, which represents the impulse response of the i'-th tap of the channel between the m-th transmit and k-th receive antenna for the n_b-th fading block, and $i' = (i-1)P + p - 1$. Similarly to the SIMO case of Section 6.2.2, here we also propose a third-order PARAFAC model for the block-fading MIMO channel. In PARAFAC form, the scalar component $h_{n_b,k,m,i'}$ of the L-path block-fading MIMO channel is a direct generalization of (6.4), and can be written as:

$$h_{n_b,k,m,i'} = \sum_{l=1}^{L} \beta_{n_b,l} a_{k,l} \overline{a}_{m,l} g_{l,i'}, \tag{6.19}$$

where $\beta_{n_b,l} = [\mathbf{B}]_{n_b,l}$, $a_{k,l} = [\mathbf{A}(\boldsymbol{\theta})]_{k,l}$, $\overline{a}_{m,l} = [\mathbf{A}_{tx}(\boldsymbol{\phi})]_{m,l}$, $g_{l,i'} = [\mathbf{G}(\boldsymbol{\tau})]_{l,i'}$.

After baseband conversion and oversampling at each receive antenna, we collect NP received samples at each receive antenna. Let us define $x_{n_b,k,n'}$ as a scalar component of the received signal tensor $\mathcal{X} \in \mathbb{C}^{N_b \times K \times NP}$, representing the n'-th received signal sample at the k-th antenna for the n_b-th transmission block, and $n' = (n-1)P + p - 1$. In absence of noise, $x_{n_b,k,n'}$ can be written as:

$$x_{n_b,k,n'} = \sum_{m=1}^{M} \sum_{i'=1}^{IP} h_{n_b,k,m,i'}\, s_{n',m,i'}, \tag{6.20}$$

where

$$s_{n',m,i'} = [\overline{\mathbf{S}}]_{n',(i'-1)M+m},$$

is an element of $\overline{\mathbf{S}} = \mathbf{S} \otimes \mathbf{I}_P \in \mathbb{C}^{NP \times MIP}$, and

$$\mathbf{S} = \text{blocktoeplitz}(\mathbf{s}_1, \cdots, \mathbf{s}_M) \in \mathbb{C}^{N \times MI} \tag{6.21}$$

is a block-Toeplitz training sequence matrix. The n_b-th first-mode matrix-slice $\mathbf{H}_{n_b\cdot\cdot} \in \mathbb{C}^{K \times MIP}$ of the MIMO fourth-order tensor $\mathcal{H}$, defined as $[\mathbf{H}_{n_b\cdot\cdot}]_{k,(m-1)IP+i'} \doteq h_{n_b,k,m,i'}$, can be expressed as a function of the MIMO multi-path parameters as:

$$\mathbf{H}_{n_b\cdot\cdot} = \mathbf{A}(\boldsymbol{\theta}) D_{n_b}(\mathbf{B}) \mathbf{U}^T(\boldsymbol{\tau}, \boldsymbol{\phi}), \quad n_b = 1, \ldots, N_b, \tag{6.22}$$

where $\mathbf{U}(\boldsymbol{\tau}, \boldsymbol{\phi}) \in \mathbb{C}^{L \times MIP}$ is defined as:

$$\mathbf{U}(\boldsymbol{\tau}, \boldsymbol{\phi}) = \mathbf{A}_{tx}(\boldsymbol{\phi}) \diamond \mathbf{G}^T(\boldsymbol{\tau}) \in \mathbb{C}^{MIP \times L}. \tag{6.23}$$

The n_b-th matrix-slice of the received signal, denoted by $\mathbf{X}_{n_b\cdot\cdot} \in \mathbb{C}^{K \times NP}$, can be written as:

$$\mathbf{X}_{n_b\cdot\cdot} = \mathbf{H}_{n_b\cdot\cdot} \overline{\mathbf{S}}^T = \mathbf{A}(\boldsymbol{\theta}) D_{n_b}(\mathbf{B}) \mathbf{C}^T(\boldsymbol{\tau}, \boldsymbol{\phi}), \quad n_b = 1, \ldots, N_b,$$

where

$$\mathbf{C}(\boldsymbol{\tau}, \boldsymbol{\phi}) = \overline{\mathbf{S}} \mathbf{U}(\boldsymbol{\tau}, \boldsymbol{\phi}) \in \mathbb{C}^{NP \times L} \tag{6.24}$$

is a combined space-time channel response at the receiver side, i.e., a convolution between the receiver space-time signatures and the training symbols.

Let us stack N_b slices $\mathbf{X}_{1\cdot\cdot}, \ldots, \mathbf{X}_{N_b\cdot\cdot}$ in a matrix $\mathbf{X}_2 \in \mathbb{C}^{KN_b \times NP}$, and N_b slices

$\mathbf{H}_{1..}, \ldots, \mathbf{H}_{N_b..}$ in a matrix $\mathbf{H}_2 \in \mathbb{C}^{KN_b \times MIP}$:

$$\mathbf{X}_2 = \begin{bmatrix} \mathbf{X}_{1..} \\ \vdots \\ \mathbf{X}_{N_b..} \end{bmatrix}, \quad \mathbf{H}_2 = \begin{bmatrix} \mathbf{H}_{1..} \\ \vdots \\ \mathbf{H}_{N_b..} \end{bmatrix}.$$

$\mathbf{X}_2$ and $\mathbf{H}_2$ are unfolded representations of the tensors $\mathcal{X}$ and $\mathcal{H}$, respectively. Using (6.22)-(6.23), we obtain the following input-output relation:

$$\mathbf{X}_2 = \mathbf{H}_2 \overline{\mathbf{S}}^T = \big(\mathbf{B} \diamond \mathbf{A}(\boldsymbol{\theta})\big)\mathbf{C}^T(\boldsymbol{\tau}, \boldsymbol{\phi}), \tag{6.25}$$

where

$$\mathbf{H}_2 = \big(\mathbf{B} \diamond \mathbf{A}(\boldsymbol{\theta})\big)\mathbf{U}^T(\boldsymbol{\tau}, \boldsymbol{\phi}).$$

The two other unfolded matrix representations are:

$$\begin{aligned} \mathbf{X}_3 &= \big(\mathbf{A}(\boldsymbol{\theta}) \diamond \mathbf{C}(\boldsymbol{\tau}, \boldsymbol{\phi})\big)\mathbf{B}^T \in \mathbb{C}^{NPK \times N_b}, \\ \mathbf{X}_1 &= \big(\mathbf{C}(\boldsymbol{\tau}, \boldsymbol{\phi}) \diamond \mathbf{B}\big)\mathbf{A}^T(\boldsymbol{\theta}) \in \mathbb{C}^{N_b NP \times K}. \end{aligned}$$

6.3.5 Identifiability

Identifiability of (6.25) allows one to uniquely determine (up to trivial ambiguities) the parameters of the L multipaths from the observed received signal tensor $\mathcal{X} \in \mathbb{C}^{N_b \times K \times NP}$. According to the identifiability results of the PARAFAC model, the identifiability of $\mathbf{A}(\boldsymbol{\theta})$, $\mathbf{B}$, and $\mathbf{C}(\boldsymbol{\tau}, \boldsymbol{\phi})$ is linked to the concept of k-rank of these matrices. In our context, a sufficient condition for identifying the MIMO multipath parameters can be obtained by recalling useful results on the k-rank of a matrix having Khatri-Rao product structure as well as on the k-rank of a Vandermonde matrix. These results are derived in [133] (c.f. Lemmas 7.1 and 7.2, respectively). A sufficient identifiability condition for our model can be obtained by applying the identifiability theorem of [133] to our context:

Theorem 7.1 : *Suppose that the L multipaths have statistically independent propagation (i.e. distinct DODs, DOAs and delays). A sufficient condition for identifiability is:*

$$\min(N_b, L) + \min(K, L) + \min(M + IP - 1, L) \geq 2(L + 1)$$

Proof: Use assumptions **A.1**-**A.2** to conclude that $\mathbf{S}$ is full rank (and full k-rank) to deduce $r_{\mathbf{C}(\boldsymbol{\tau},\boldsymbol{\phi})} = r_{\mathbf{U}(\boldsymbol{\tau},\boldsymbol{\phi})}$. Apply Lemma 7.1 in [133] by making the

following correspondences: $\mathbf{A} \rightarrow \mathbf{G}(\boldsymbol{\tau})$, $\mathbf{B} \rightarrow \mathbf{A}_{tx}(\boldsymbol{\phi})$, to verify that $r_{\mathbf{U}(\boldsymbol{\tau},\boldsymbol{\phi})} \geq \min(k_{\mathbf{G}(\boldsymbol{\tau})} + k_{\mathbf{A}_{tx}(\boldsymbol{\phi})} - 1, L)$. Finally, use the fact that the k-rank of a matrix is equal to its rank with probability one whenever its columns are drawn independently from an absolutely continuous distribution. Thus, we have $k_{\mathbf{A}(\boldsymbol{\theta})} = \min(K, L)$, $k_{\mathbf{B}} = \min(N_b, L)$, $k_{\mathbf{C}(\boldsymbol{\tau},\boldsymbol{\phi})} = k_{\mathbf{U}(\boldsymbol{\tau},\boldsymbol{\phi})} = \min(M + IP - 1, L)$. ■

Remarks:

1) The identifiability condition established in the Theorem 7.1 is sufficient but not necessary. Assuming $M > 1$ and $N > 1$ (irrespective of the oversampling factor P), a necessary condition is $k_{\mathbf{B}} \geq 2$ [74]. In practice, this means that at least $N_b \geq 2$ transmission blocks must be collected at the receiver to ensure uniqueness of model (6.25).

2) Column permutation is unremovable although not relevant in our context, since the ordering of the multipath responses is unimportant for channel estimation purposes. Scaling ambiguity can be eliminated by exploiting prior knowledge of the space-time manifold structure i.e., the array geometry and the pulse shape function.

6.3.6 Estimation of the MIMO channel parameters

The estimation of the MIMO multipath parameters is done in two-stages. The first one is blind, and consists in using the trilinear ALS algorithm for fitting a third-order PARAFAC model to the received signal tensor $\mathcal{X} \in \mathbb{C}^{N_b \times K \times NP}$. At the end of the ALS algorithm, we will have the estimates $\widehat{\mathbf{A}}(\boldsymbol{\theta})$, $\widehat{\mathbf{B}}$, and $\widehat{\mathbf{C}}(\boldsymbol{\tau}, \boldsymbol{\phi})$.

The second stage consists in using the training sequence matrix $\overline{\mathbf{S}}$ to find an LS estimate of $\mathbf{U}(\boldsymbol{\tau}, \boldsymbol{\phi}) = \mathbf{A}_{tx}(\boldsymbol{\phi}) \diamond \mathbf{G}^T(\boldsymbol{\tau})$ as:

$$\widehat{\mathbf{U}}(\boldsymbol{\tau}, \boldsymbol{\phi}) = \overline{\mathbf{S}}^{\dagger} \widehat{\mathbf{C}}^{(conv)}(\boldsymbol{\tau}, \boldsymbol{\phi}).$$

It is worth noting that separated estimations of $\widehat{\mathbf{A}}_{tx}(\boldsymbol{\phi})$ and $\widehat{\mathbf{G}}(\boldsymbol{\tau})$ as well as the elimination of the scaling factors can be carried out by exploiting the Vandermonde structures of $\mathbf{A}(\boldsymbol{\theta})$ and $\mathbf{A}_{tx}(\boldsymbol{\phi})$. Note that $\mathbf{U}(\boldsymbol{\tau}, \boldsymbol{\phi})$ has a Khatri-Rao factorization structure. Since the first row of $\mathbf{A}_{tx}(\boldsymbol{\phi})$ and $\mathbf{A}(\boldsymbol{\theta})$ only have unitary entries, i.e. $(\mathbf{A}_{1\cdot})_{tx}(\boldsymbol{\phi}) = [1, \ldots, 1]$ and $\mathbf{A}_{1\cdot}(\boldsymbol{\theta}) = [1, \ldots, 1]$, an estimate of $\mathbf{G}(\boldsymbol{\tau})$ can be extracted from the first matrix block of $\widehat{\mathbf{U}}(\boldsymbol{\tau}, \boldsymbol{\phi})$ of dimension $L \times IP$ (c.f. (6.23)).

6.3.7 Simulation results

In this section, some simulation results are shown to illustrate the performance of the proposed parametric MIMO channel estimator. We assume $N = 10$ training symbols per transmit antenna. The training symbols are modulated using Binary Phase Shift Keying (BPSK). The oversampling factor is assumed to be $P = 2$. The pulse shape function is a raised cosine with roll-off 0.35. We consider $L = 3$ specular multipaths with equal average power. The vector containing the DODs, DOAs and delays of the multipaths are respectively $\boldsymbol{\phi} = [-10^o, 30^o, 50^o]$, $\boldsymbol{\theta} = [-18^o, 20^o, 35^o]$ and $\boldsymbol{\tau} = [0, T, 2T]$, where T denotes the symbol period (I=3 is assumed). The fading amplitudes are modeled as complex Gaussian random variables and assumed to be uncorrelated between two successive blocks.

In order to evaluate the accuracy of the proposed method in estimating the spatial signatures, Fig. 6.9 depicts the normalized MUSIC spectrum for the DODs and DOAs. We have assumed $M = K = 4$, $N_b = 10$ and a SNR of 20dB. We can see that accurate estimates of the transmitter and receiver spatial signatures are obtained. Figure 6.10 shows the RMSE between estimated $\widehat{\mathbf{H}}$ and true $\mathbf{H}$ channel matrices as a function of the SNR. These results are an average over 1000 independent realizations assuming $M = K = 2$ and $N_b = 3$, 10 or 30. In this simulation, 95% of the runs were retained for plotting the results. The 5% worst (ill-convergent) runs were discarded. Convergent runs have converged within 30 iterations in average. Note that the estimation performance improves as the number of transmission blocks is increased. In fact, fading amplitudes variation across the blocks is converted into temporal diversity for resolving the multipath signals.

6.4 Summary

In this chapter, we have presented a new method for estimating space-time wireless channels based on PARAFAC modeling. The proposed estimator relies on a parametric channel model for a time-varying multipath channel. In other words, we have used the fact that the variation of the multipath amplitudes over multiple data-blocks is faster than that of angles and delays in order to build a third-order PARAFAC model for the channel. We have shown that the received signal can also be viewed as a third-order PARAFAC model thanks to the use of a training sequence which is periodically extended over multiple data-blocks to be jointly processed at the receiver. Using the alternating least squares algorithm, the multipath parameters are estimated directly from the received signal tensor. The PARAFAC-based estimator provides a good estimation accuracy even for short

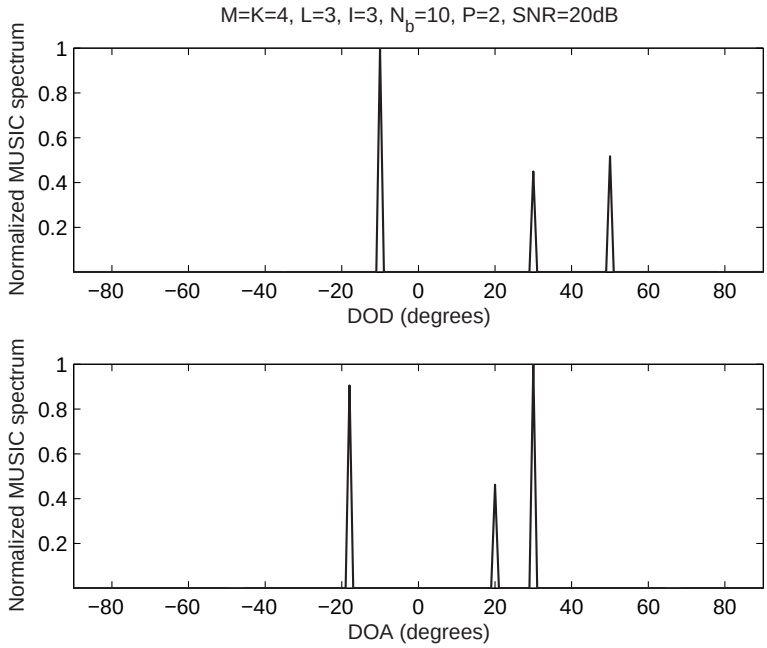

Figure 6.9: The normalized MUSIC spectrum for estimated DODs and DOAs.

training sequences, provided that the number of processed data-blocks is large enough. Due to the identifiability properties of the PARAFAC decomposition, the proposed estimator performs well with fewer receiver antennas than multipaths. We have also generalized the PARAFAC modeling/estimation approach to the case of MIMO channels.

In a future work, we should compare the proposed modeling/estimation technique with classical ones that determine the multipath parameters using previous unstructured channel estimate [153, 151, 154, 92]. Although we have used a third-order PARAFAC approach for channel modeling/estimation, which have allowed the use of classical PARAFAC identifiability results, a fourth-order tensor modeling approach is also possible by means of the block-constrained PARAFAC model.

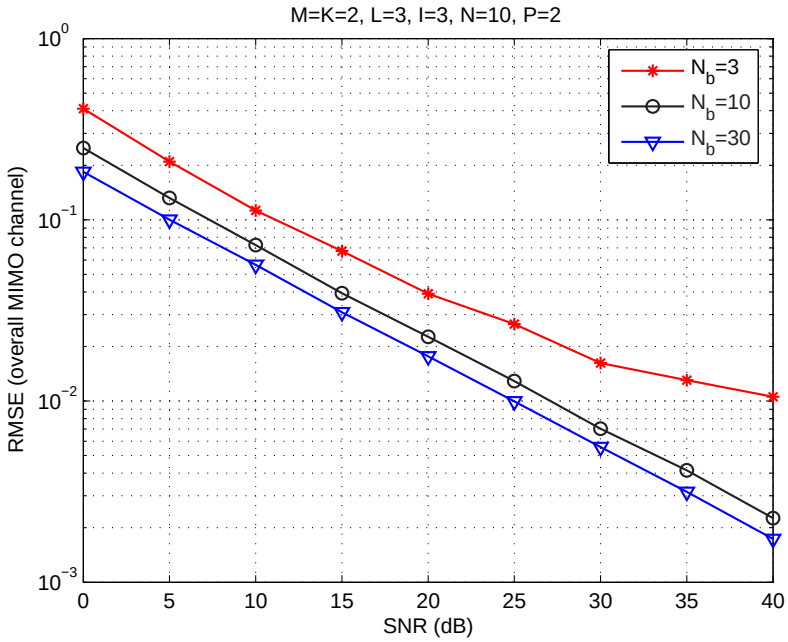

Figure 6.10: RMSE versus SNR performance (PARAFAC-MIMO estimator).

Conclusion and perspectives

This thesis has dealt with the study of generalized tensor decompositions with applications in signal processing for wireless communications. Our contributions have addressed the following main research axes by means of tensor modeling:

– Multiuser signal separation/equalization/detection;
– Multiple-antenna transmission structures;
– Channel modeling and estimation.

The original contributions of this work are based on two new tensor decompositions: the block-constrained PARAFAC and the CONstrained FACtor (CONFAC) decompositions (Chapter 1). These decompositions combine properties of the PARAFAC and the Tucker-3 decompositions by allowing interactions between factors associated with different modes of the tensor. It turns out that he CONFAC decomposition is more general than the block-constrained PARAFAC one, in the sense that arbitrary interaction patterns across all the modes of the decomposed tensor is permitted. The partial uniqueness of the CONFAC decomposition has also been studied and sufficient conditions for the essential uniqueness in one or two modes have been derived.

Different applications of the block-constrained PARAFAC decomposition have been presented in Chapters 2 and 3. In Chapter 2, the block-constrained PARAFAC decomposition has been used for a unified tensor modeling of oversampled, DS-CDMA and OFDM systems under the assumption of specular multipath propagation with multiple paths per user. A generalization of this unified model has been presented by considering that the number of paths of each user can be different. The generalized model was formulated by means of a constrained Tucker-3 modeling. A blind receiver based on the proposed tensor model has been pre-

sented for multiuser signal separation/equalization. The IPSP receiver iteratively combines the ALS algorithm with a subspace method, and makes use of the FA property of the transmitted symbols. The proposed receiver is deterministic and does not require the use of training sequences, nor the knowledge of the channel impulse responses and antenna array responses. The block-constrained PARAFAC decomposition has also been exploited in Chapter 3 to formulate a new multiuser downlink system with block space-time spreading. We have shown that the proposed system allows multiuser space-time transmission with different spatial spreading factors (diversity gains) as well as different multiplexing factors (code rates) for the users. At the same time, the proposed tensor modeling approach generalizes previous work on tensor-based multiple-antenna systems by allowing full spatial spreading of the transmitted data streams across fixed transmit antennas.

Concerning the CONFAC decomposition, we have presented a new modeling approach for MIMO-CDMA systems with space-time spreading/precoding and blind detection (Chapter 4). We have shown that the constrained structure of the CONFAC decomposition has a meaningful physical interpretation. The constraint matrices can be exploited for designing several multiple-antenna schemes with varying degree of spatial spreading, spatial multiplexing and spreading code reuse. Compared with the block space-time spreading model of Chapter 3, the CONFAC-based MIMO-CDMA model of Chapter 4 copes with multiple transmit antennas and spreading codes per user or per data-stream. We have first presented a transmission model based on the type-3 CONFAC decomposition with two constraint matrices only. A design procedure for deriving sets of transmit schemes with guaranteed blind symbol recovery was presented. Then, we have derived a more general CONFAC-based transmission model, where a precoder tensor fully exploiting the decomposition structure defines the allocation of the data streams and spreading codes to transmit antennas. Blind symbol/code/channel recovery has also been studied from the partial uniqueness properties of this decomposition.

This thesis has also studied new applications of the third-order PARAFAC decomposition. In Chapter 5, a Trilinear Space-Time-Frequency Spreading (T-STFS) multiple-access model for MIMO wireless systems was proposed. T-STFS is based on a 3-D spreading code tensor decomposed into the outer product of the space-, time- and frequency-domain spreading codes. These codes allow multiple data streams to simultaneously access the same set of transmit antennas, chips and subcarriers. At the receiver, blind detection without a priori channel estimation or training sequences is possible thanks to PARAFAC uniqueness. The PARAFAC decomposition was also exploited in Chapter 6 for modeling/estimation of SIMO and MIMO multipath wireless channels with time-varying structure. The proposed PARAFAC-based estimator relies on the ALS algorithm to jointly estimate

the angles of arrival, the time-delays and the fading amplitudes of the multipaths. The estimator is deterministic and works directly on the received signal without the need of a previous unstructured channel estimate.

Some perspectives of this thesis work can be drawn. We give hereafter some research topics to be pursued:

- The development of efficient algorithms for estimating the factors of the CONFAC decomposition is an interesting topic for future research. The convergence properties of these algorithms when the number F of factor combinations is large, or when the constraint matrices of the decomposition are unknown should be better understood. Moreover, the identifiability properties of this decomposition deserves further investigation. The influence of the number F of factor combinations on the uniqueness properties is to be studied.

- With respect to CONFAC-based MIMO-CDMA systems, we call attention that the design of the precoder constraint matrices has only focused on uniqueness aspects and has not considered performance optimization at the receiver. We conjecture, however, that limited feedback precoding principles [77, 95] can be used to properly select the canonical precoding matrices from the finite-set of feasible choices by taking practical requirements into account such as diversity and data-rate. Cross-layer optimization can also be taken into account to implement antenna selection and rate adaptation on top of the proposed modeling framework. This would introduce more degrees of freedom in the structure of the canonical precoding matrices.

- In the context of the T-STFS model presented in Chapter 5, an interesting generalization would consist in introducing spreading code reuse in *space*, *time* and/or *frequency*. This can achieved by introducing space-, time- and frequency-domain constraint matrices into the T-STFS model, by means of a CONFAC-based STF model. These constraint matrices would determine the allocation/reuse of the spreading codes by the different transmitted data streams.

- Perspectives of the PARAFAC-based approach for channel modeling/estimation proposed in Chapter 6 include a performance comparison with classical methods that rely on previous unstructured channel estimate [153, 151, 154, 92]. Although we have used a third-order PARAFAC approach for channel modeling/estimation, which allows the use of the classical PARAFAC model, a fourth-order tensor modeling approach is also possible by means of the block-constrained PARAFAC decomposition.

APPENDIX A

Expansion of the block-constrained PARAFAC decomposition using canonical vectors

In the following, we provide a demonstration of the block-constrained PARAFAC decomposition given by (1.55) in Chapter 1. For this sake, we expand the tensor x_{i_1,i_2,i_3} in (1.48) in the form of multiple summations involving tensor products of canonical vectors [62].

Let us recall (1.48):

$$x_{i_1,i_2,i_3} = \sum_{q=1}^{Q} \sum_{r_1=1}^{R_1} \sum_{r_2=1}^{R_2} a_{i_1,r_1}^{(q)} \, b_{i_2,r_2}^{(q)} \, c_{r_1,r_2,i_3}^{(q)}. \tag{1.1}$$

Consider the canonical bases $\mathrm{E}^{(I_1)} = \{\mathbf{e}_1^{(I_1)}, \mathbf{e}_2^{(I_1)}, \ldots, \mathbf{e}_{I_1}^{(I_1)}\}$, $\mathrm{E}^{(I_2)} = \{\mathbf{e}_1^{(I_2)}, \mathbf{e}_2^{(I_2)}, \ldots, \mathbf{e}_{I_2}^{(I_2)}\}$ and $\mathrm{E}^{(I_3)} = \{\mathbf{e}_1^{(I_3)}, \mathbf{e}_2^{(I_3)}, \ldots, \mathbf{e}_{I_3}^{(I_3)}\}$ associated with vector spaces $\mathbb{R}^{I_1}$, $\mathbb{R}^{I_2}$, $\mathbb{R}^{I_3}$, respectively.

The unfolded matrix $\mathbf{X}_2 \in \mathbb{C}^{I_1 I_2 \times I_3}$, defined as $x_{i_1,i_2,i_3} = [\mathbf{X}_2]_{(i_1-1)I_2+i_2,i_3}$, can be expanded in terms of these canonical vectors in the following manner:

$$\mathbf{X}_2 = \sum_{i_1=1}^{I_1} \sum_{i_2=1}^{I_2} \sum_{i_3=1}^{I_3} x_{i_1,i_2,i_3} (\mathbf{e}_{i_1}^{(I_1)} \otimes \mathbf{e}_{i_2}^{(I_2)}) \mathbf{e}_{i_3}^{(I_3)T}. \tag{1.2}$$

Substituting (1.1) into (1.2) we have:

$$\begin{aligned}\mathbf{X}_2 &= \sum_{i_1=1}^{I_1}\sum_{i_2=1}^{I_2}\sum_{i_3=1}^{I_3}\sum_{q=1}^{Q}\sum_{r_1=1}^{R_1}\sum_{r_2=1}^{R_2} a_{i_1,r_1}^{(q)} b_{i_2,r_2}^{(q)} c_{r_1,r_2,i_3}^{(q)} (\mathbf{e}_{i_1}^{(I_1)} \otimes \mathbf{e}_{i_2}^{(I_2)})\mathbf{e}_{i_3}^{(I_3)T} \\ &= \sum_{q=1}^{Q}\sum_{r_1=1}^{R_1}\sum_{r_2=1}^{R_2} \left(\sum_{i_1=1}^{I_1} \mathbf{e}_{i_1}^{(I_1)} a_{i_1,r_1}^{(q)}\right) \otimes \left(\sum_{i_2=1}^{I_2} \mathbf{e}_{i_2}^{(I_2)} b_{i_2,r_2}^{(q)}\right) \left(\sum_{i_3=1}^{I_3} \mathbf{e}_{i_3}^{(I_3)} c_{r_1,r_2,i_3}^{(q)}\right)^T.\end{aligned}$$

Define $\mathbf{a}_{r_1}^{(q)}$ as the r_1-th column of $\mathbf{A}^{(q)} \in \mathbb{C}^{I_1 \times R_1}$, $\mathbf{b}_{r_2}^{(q)}$ as the r_2-th column of $\mathbf{B}^{(q)} \in \mathbb{C}^{I_2 \times R_2}$ and $\mathbf{c}_{r_1,r_2}^{(q)}$ as the $[(r_1-1)R_2 + r_2]$-th column of $\mathbf{C}^{(q)} \in \mathbb{C}^{I_3 \times R_1 R_2}$, and observe that:

$$\sum_{i_1=1}^{I_1} \mathbf{e}_{i_1}^{(I_1)} a_{i_1,r_1}^{(q)} = \mathbf{a}_{r_1}^{(q)}, \quad \sum_{i_2=1}^{I_2} \mathbf{e}_{i_2}^{(I_2)} b_{i_2,r_2}^{(q)} = \mathbf{b}_{r_2}^{(q)}, \quad \sum_{i_3=1}^{I_3} \mathbf{e}_{i_3}^{(I_3)} c_{r_1,r_2,i_3}^{(q)} = \mathbf{c}_{r_1,r_2}^{(q)},$$

we have:

$$\mathbf{X}_2 = \sum_{q=1}^{Q}\sum_{r_1=1}^{R_1}\sum_{r_2=1}^{R_2} (\mathbf{a}_{r_1}^{(q)} \otimes \mathbf{b}_{r_2}^{(q)})\mathbf{c}_{r_1,r_2}^{(q)T}. \tag{1.3}$$

Define the set of canonical vectors $\mathbf{e}_{r_2}^{(R_2)}$, $r_2 = 1, \ldots, R_2$. Inserting $(\mathbf{e}_{r_2}^{(R_2)})^T \mathbf{e}_{r_2}^{(R_2)} = 1$ into (1.3) gives:

$$\mathbf{X}_2 = \sum_{q=1}^{Q}\sum_{r_1=1}^{R_1}\sum_{r_2=1}^{R_2} \left[(\mathbf{a}_{r_1}^{(q)} \otimes \mathbf{b}_{r_2}^{(q)})\mathbf{e}_{r_2}^{(R_2)T}\right] \left[\mathbf{e}_{r_2}^{(R_2)}\mathbf{c}_{r_1,r_2}^{(q)T}\right]. \tag{1.4}$$

As $\mathbf{e}_{r_2}^{(R_2)T} = \mathbf{e}_{r_2}^{(R_2)T} \diamond \mathbf{e}_{r_2}^{(R_2)T}$, the use of property (1.57) allows to rewrite (1.4) as:

$$\mathbf{X}_2 = \sum_{q=1}^{Q}\sum_{r_1=1}^{R_1}\sum_{r_2=1}^{R_2} \left[\mathbf{a}_{r_1}^{(q)}\mathbf{e}_{r_2}^{(R_2)T} \diamond \mathbf{b}_{r_2}^{(q)}\mathbf{e}_{r_2}^{(R_2)T}\right] \left[\mathbf{e}_{r_2}^{(R_2)}\mathbf{c}_{r_1,r_2}^{(q)T}\right]. \tag{1.5}$$

Due to the presence of the unit vector $\mathbf{e}_{r_2}^{(R_2)}$, we can rewrite (1.5) as:

$$\begin{aligned}\mathbf{X}_2 &= \sum_{q=1}^{Q}\sum_{r_1=1}^{R_1} \left[\sum_{r_2=1}^{R_2} \mathbf{a}_{r_1}^{(q)}\mathbf{e}_{r_2}^{(R_2)T} \diamond \sum_{r_2=1}^{R_2} \mathbf{b}_{r_2}^{(q)}\mathbf{e}_{r_2}^{(R_2)T}\right] \left[\sum_{r_2=1}^{R_2} \mathbf{e}_{r_2}^{(R_2)}\mathbf{c}_{r_1,r_2}^{(q)T}\right] \\ &= \sum_{q=1}^{Q}\sum_{r_1=1}^{R_1} \left[(\mathbf{a}_{r_1}^{(q)} \otimes \mathbf{1}_{R_2}^T) \diamond \mathbf{B}^{(q)}\right] \mathbf{C}_{r_1}^{(q)T},\end{aligned} \tag{1.6}$$

with $\mathbf{C}_{r_1}^{(q)} = \sum_{r_2=1}^{R_2} \mathbf{c}_{r_1,r_2}^{(q)} \mathbf{e}_{r_2}^{(R_2)T} \in \mathbb{C}^{I_3 \times R_2}$.

Inserting $\mathbf{e}_{r_1}^{(R_1)T} \mathbf{e}_{r_1}^{(R_1)} = 1$ into (1.6) and using property (1.21), it follows that:

$$\begin{aligned} \mathbf{X}_2 &= \sum_{q=1}^{Q} \sum_{r_1=1}^{R_1} \mathbf{e}_{r_1}^{(R_1)T} \mathbf{e}_{r_1}^{(R_1)} \otimes \left[(\mathbf{a}_{r_1}^{(q)} \otimes \mathbf{1}_{R_2}^T) \diamond \mathbf{B}^{(q)} \right] \mathbf{C}_{r_1}^{(q)T} \\ &= \sum_{q=1}^{Q} \sum_{r_1=1}^{R_1} \left[\mathbf{e}_{r_1}^{(R_1)T} \otimes \left[(\mathbf{a}_{r_1}^{(q)} \otimes \mathbf{1}_{R_2}^T) \diamond \mathbf{B}^{(q)} \right] \right] \cdot \left[\mathbf{e}_{r_1}^{(R_1)} \otimes \mathbf{C}_{r_1}^{(q)T} \right]. \end{aligned} \tag{1.7}$$

Note that:

$$\mathbf{e}_{r_1}^{(R_1)T} \otimes \left[(\mathbf{a}_{r_1}^{(q)} \otimes \mathbf{1}_{R_2}^T) \diamond \mathbf{B}^{(q)} \right] = \left[\mathbf{e}_{r_1}^{(R_1)T} \otimes (\mathbf{a}_{r_1}^{(q)} \otimes \mathbf{1}_{R_2}^T) \right] \diamond \left[\mathbf{e}_{r_1}^{(R_1)T} \otimes \mathbf{B}^{(q)} \right],$$

which allows us to express (1.7) in the following form:

$$\mathbf{X}_2 = \sum_{q=1}^{Q} \sum_{r_1=1}^{R_1} \left[\left[\mathbf{e}_{r_1}^{(R_1)T} \otimes (\mathbf{a}_{r_1}^{(q)} \otimes \mathbf{1}_{R_2}^T) \right] \diamond \left[\mathbf{e}_{r_1}^{(R_1)T} \otimes \mathbf{B}^{(q)} \right] \right] \cdot \left[\mathbf{e}_{r_1}^{(R_1)} \otimes \mathbf{C}_{r_1}^{(q)T} \right]. \tag{1.8}$$

Due to the block structure with zeros introduced by the factor $\mathbf{e}_{r_1}^{(R_1)}$, we can rewrite (1.8) as:

$$\mathbf{X}_2 = \sum_{q=1}^{Q} \left\{ \left[\sum_{r_1=1}^{R_1} \mathbf{e}_{r_1}^{(R_1)T} \otimes (\mathbf{a}_{r_1}^{(q)} \otimes \mathbf{1}_{R_2}^T) \right] \diamond \left[\sum_{r_1=1}^{R_1} \mathbf{e}_{r_1}^{(R_1)T} \otimes \mathbf{B}^{(q)} \right] \right\} \cdot \left[\sum_{r_1=1}^{R_1} \mathbf{e}_{r_1}^{(R_1)} \otimes \mathbf{C}_{r_1}^{(q)T} \right] \tag{1.9}$$

which leads to:

$$\mathbf{X}_2 = \sum_{q=1}^{Q} \left[(\mathbf{A}^{(q)} \otimes \mathbf{1}_{R_2}^T) \diamond (\mathbf{1}_{R_1}^T \otimes \mathbf{B}^{(q)}) \right] \cdot \mathbf{C}^{(q)T}. \tag{1.10}$$

Now, using again property (1.21), we have:

$$\mathbf{A}^{(q)} \otimes \mathbf{1}_{R_2}^T = (\mathbf{A}^{(q)} \otimes 1)(\mathbf{I}_{R_1} \otimes \mathbf{1}_{R_2}^T) = \mathbf{A}^{(q)} \underbrace{(\mathbf{I}_{R_1} \otimes \mathbf{1}_{R_2}^T)}_{\mathbf{\Psi}} = \mathbf{A}^{(q)} \mathbf{\Psi},$$

and

$$\mathbf{1}_{R_1}^T \otimes \mathbf{B}^{(q)} = (1 \otimes \mathbf{B}^{(q)})(\mathbf{1}_{R_1}^T \otimes \mathbf{I}_{R_2}) = \mathbf{B}^{(q)} \underbrace{(\mathbf{1}_{R_1}^T \otimes \mathbf{I}_{R_2})}_{\mathbf{\Phi}} = \mathbf{B}^{(q)} \mathbf{\Phi},$$

and (1.10) can be expressed as:

$$\mathbf{X}_2 = \sum_{q=1}^{Q} (\mathbf{A}^{(q)}\boldsymbol{\Psi} \diamond \mathbf{B}^{(q)}\boldsymbol{\Phi})\mathbf{C}^{(q)T}. \tag{1.11}$$

Defining $\mathbf{A} = [\mathbf{A}^{(1)} \cdots \mathbf{A}^{(Q)}] \in \mathbb{C}^{I_1 \times QR_1}$, $\mathbf{B} = [\mathbf{B}^{(1)} \cdots \mathbf{B}^{(Q)}] \in \mathbb{C}^{I_2 \times QR_2}$ and $\mathbf{C} = [\mathbf{C}^{(1)} \cdots \mathbf{C}^{(Q)}] \in \mathbb{C}^{I_3 \times QR_1R_2}$, and $\boldsymbol{\Psi} = \mathbf{I}_Q \otimes \boldsymbol{\Psi}$ and $\boldsymbol{\Phi} = \mathbf{I}_Q \otimes \boldsymbol{\Phi}$, we can equivalently write (1.11) as:

$$\mathbf{X}_2 = (\mathbf{A}\boldsymbol{\Psi} \diamond \mathbf{B}\boldsymbol{\Phi})\mathbf{C}^T,$$

and the demonstration is finished.

APPENDIX B

Uniqueness of the design criterion (4.12)

We demonstrate that the design criterion (4.12), which results in a partitioned structure for the canonical allocation matrices according to (4.13)-(4.14), leads to the uniqueness of $\mathbf{S}$ up to column permutation and scaling while the uniqueness of $\mathbf{C}$ exists up to multiplication by a non-singular block-diagonal matrix and a block-diagonal permutation matrix.

Let us define $\mathbf{C} \doteq [\mathbf{C}_1 \cdots \mathbf{C}_R] \in \mathbb{C}^{P \times J}$ and $\mathbf{C}_r \doteq [\mathbf{C}_{r,1} \cdots \mathbf{C}_{r,J_r}] \in \mathbb{C}^{P \times \alpha_r}$ with $\mathbf{C}_{r,j_r} \in \mathbb{C}^{P \times \beta_{r,j_r}}$, $j_r = 1, \ldots, J_r$, as the partitioned spreading code matrix. Let us also define $\mathbf{H} = [\mathbf{H}_1 \cdots \mathbf{H}_R] \in \mathbb{C}^{K \times M}$ as the partitioned channel matrix. Based on these definitions, we can rewrite the k-th third-mode slice $\mathbf{X}_{..k} \in \mathbb{C}^{N \times P}$ of the received signal in terms of this partitioning as:

$$\begin{aligned} \mathbf{X}_{..k} &= \mathbf{S} \underbrace{\left(\sum_{r=1}^{R} \mathbf{\Psi}_r D_k\left(\mathbf{H}_r\right) \mathbf{\Phi}_r^T \right)}_{\overline{\mathbf{H}}_k} \mathbf{C}^T \\ &= \mathbf{S}\overline{\mathbf{H}}_k\mathbf{C}^T. \end{aligned} \tag{2.1}$$

Due to the canonical structure of $\mathbf{\Psi}_r$ and $\mathbf{\Phi}_r$ defined in (4.13)-(4.14), it follows that $\overline{\mathbf{H}}_k$ is a row-wise block-diagonal matrix (it has only a single non-zero element

per column), the blocks of which are row-vectors:

$$\overline{\mathbf{H}}_k = \begin{bmatrix} \overline{h}_k^{(1,1)} & \cdots & \overline{h}_k^{(1,J_1)} & & \mathbf{0} & \\ & & & \ddots & & \\ & \mathbf{0} & & & \overline{h}_k^{(R,1)} & \cdots & \overline{h}_k^{(R,J_R)} \end{bmatrix},$$

where

$$\overline{h}_k^{(r,j_r)} = \sum_{i=1}^{\beta_{r,j_r}} h_{k,\overline{\beta}_{r,j_{r-1}}+i},$$

with $\overline{\beta}_{r,j} = \sum_{i=1}^{j} \beta_{r,i}$. Let $\mathbf{T} \in \mathbb{C}^{R\times R}$, $\mathbf{U} \in \mathbb{C}^{J\times J}$ be non-singular transformation matrices. Inserting $\mathbf{T}\mathbf{T}^{-1}$ and $\mathbf{U}\mathbf{U}^{-1}$ in (2.1) yields:

$$\mathbf{X}_{..k} = (\mathbf{S}\mathbf{T}) \left(\mathbf{T}^{-1}\overline{\mathbf{H}}_k\mathbf{U}^{-T}\right) (\mathbf{C}\mathbf{U})^T. \tag{2.2}$$

First, note that $\mathbf{T}^{-1}$ acts over the rows of $\overline{\mathbf{H}}_k$, while $\mathbf{U}^{-T}$ acts over the columns of $\overline{\mathbf{H}}_k$, respectively. It can be easily checked that $\mathbf{T}^{-1}$ only preserves the row-wise diagonal structure of $\overline{\mathbf{H}}_k$ if it is a diagonal matrix or a row-permutation of it, which leads to the form (4.15) of $\mathbf{T}$. On the other hand, any non-singular matrix $\mathbf{U}^{-T}$ having a block-diagonal structure with blocks $\mathbf{U}_1 \in \mathbb{C}^{J_1\times J_1}, \ldots, \mathbf{U}_R \in \mathbb{C}^{J_R\times J_R}$, preserves the structure of $\overline{\mathbf{H}}_k$ which implies a transformational ambiguity over the sets of $J_1, \ldots, J_R$ columns of $\mathbf{C}_1, \ldots, \mathbf{C}_R$. Note also that the blocks $\mathbf{U}_1, \ldots \mathbf{U}_R$ can be arbitrarily permuted without changing the pattern of zeros of $\overline{\mathbf{H}}_k$, which leads to the form (4.15) of $\mathbf{U}$.

The transformational ambiguity matrix $\mathbf{U} = \text{blockdiag}(\mathbf{U}_1, \ldots, \mathbf{U}_R)$ exists when $J > R$ (more spreading codes than data streams). In the particular case $J = R$ (one-to-one correspondence between spreading codes and data streams) with $\alpha_r = \beta_r$, $r = 1, \ldots, R$, $\overline{\mathbf{H}}_k$ is reduced to a diagonal matrix and the joint uniqueness of $\mathbf{S}$ and $\mathbf{C}$ is achieved.

Bibliography

[1] D. Agrawal, V. Tarokh, A. Naguib, and N. Seshadri. Space-time coded OFDM for high data-rate wireless communications over wideband channels. In *Proc. of Vehic. Tech. Conf.*, pages 2232–2236, Ottawa, Canada, 1998.

[2] S. Alamouti. A simple transmit diversity technique for wireless communications. *IEEE J. Sel. Areas Commun.*, 16(8):1451–1458, Oct. 1998.

[3] C. A. Andersson and R. Bro. Improving the speed of multi-way algorithms Part I: Tucker3. *Chemometrics Intell. Lab. Syst.*, 42:93–103, 1998.

[4] G. E. Andrews. *The Theory of Partitions*. Cambridge University Press, Cambridge, England, 1998.

[5] I. Barhumi, G. Leus, and M. Moonen. Optimal training design for MIMO OFDM systems in mobile wireless channels. *IEEE Trans. Signal Processing*, 51(6):1615–1624, 2003.

[6] H. Bolcskei and A. Paulraj. Space-frequency coded broadband OFDM systems. In *Proc. of Wirel. Comm. Networking Conf.*, pages 1–6, Chicago, IL, September 23-28 2000.

[7] R. Bro. PARAFAC: Tutorial and applications. *Chemometrics Intell. Lab. Syst.*, 38:149–171, 1997.

[8] R. Bro. *Multi-way analysis in the food industry: Models, algorithms and applications*. PhD thesis, University of Amsterdam, Amsterdam, 1998.

[9] R. Bro and C. A. Andersson. Improving the speed of multi-way algorithms Part II: Compression. *Chemometrics Intell. Lab. Syst.*, 42:105–113, 1998.

[10] R. Bro, R. A. Harshman, and N. D. Sidiropoulos. Modeling multi-way data with linearly dependent loadings. *KVL tech. report 176*, 2005.

[11] J.-F. Cardoso. Blind signal separation: statistical principles. In *Proceedings of the IEEE*, volume 9, pages 2009–2025, 1998.

[12] J. D. Carroll and J. Chang. Analysis of individual differences in multidimensional scaling via an N-way generalization of "Eckart-Young" decomposition. *Psychometrika*, 35(3):283–319, 1970.

[13] M. Cicerone, O. Simeone, N. Geng, and U. Spagnolini. Modal analysis/filtering to estimate time-varying MIMO-OFDM channels. In *Proc. Works. Smart Ant.*, pages 35–40, Munich, Germany, March 2004.

[14] P. Comon. Independent component analysis, a new concept? *Signal Processing*, 36:287314, 1994.

[15] P. Comon. Tensor decompositions: State of the art and applications. In *IMA Conf. Mathematics in Signal Process.*, Warwick, UK, Dec. 18-20 2000.

[16] P. Comon. Tensor decompositions. In J. G. McWhirter and I. K. Proudler, editors, *Mathematics in Signal Processing V*, pages 1–24. Clarendon Press, Oxford, UK, 2002.

[17] P. Comon. Blind identification and source separation in 2x3 underdetermined mixtures. *IEEE Trans. Sig. Process.*, 52(1):11–22, 2004.

[18] P. Comon. *Canonical Tensor Decompositions.* ARCC Workshop on Tensor Decompositions, Palo Alto, CA, July 18–24 2004. cf. I3S report, June 2004.

[19] P. Comon and B. Mourrain. Decomposition of quantics in sums of powers of linear forms. *Signal Processing, Elsevier*, 53(2):93–107, September 1996. special issue on High-Order Statistics.

[20] P. Comon, B. Mourrain, L.-H. Lim, and G. Golub. Genericity and rank deficiency of high order symmetric tensors. In *ICASSP'06*, Toulouse, May 14-19 2006.

[21] M. O. Damen, K. Abed-Meraim, and J-.C. Belfiore. Diagonal algebraic space-time codes. *IEEE Trans. Inf. Theory*, 48(3):628–636, 2002.

[22] M. O. Damen, K. Abed-Meraim, and A. Safavi. On CDMA with space-time codes over multi-path fading channels. *IEEE Trans. Wireless Commun.*, 2(1):11–19, 2003.

[23] P. Dayal and M. Varanasi. Algebraic space-time codes with full diversity and low peak-to-mean power ratio. In *Proc. of IEEE GLOBECOM*, San Francisco, USA, Dec. 2003.

[24] A. L. F. de Almeida, G. Favier, and Cavalcante C. C. Mota, J. C. M. PARAFAC models for hybrid MIMO: Joint channel estimation and detection. In *Wireless World Research Forum (WWRF)*, Paris, France, November 2005.

[25] A. L. F. de Almeida, G. Favier, and de Lacerda R. L. Mota, J. C. M. Estimation of frequency-selective block-fading MIMO channels using PARAFAC modeling and alternating least squares. In *Asilomar Conference Sig. Syst. Comp.*, Pacific Grove, CA, October 29 - November 1 2006.

[26] A. L. F. de Almeida, G. Favier, and J. C. M. Mota. Blind multiuser equalization using a PARAFAC-subspace approach. In *GRETSI Symposium on Signal and Image Processing*, Louvain-la-Neuve, Belgium, September 2005.

[27] A. L. F. de Almeida, G. Favier, and J. C. M. Mota. Generalized PARAFAC model for multidimensional wireless communications with application to blind multiuser equalization. In *Asilomar Conference Sig. Syst. Comp.*, Pacific Grove, CA, October 31 - November 2 2005.

[28] A. L. F. de Almeida, G. Favier, and J. C. M. Mota. PARAFAC models for wireless communication systems. In *Int. Conf. on Physics in Signal and Image processing (PSIP)*, Toulouse, France, Jan. 31 - Feb. 2 2005.

[29] A. L. F. de Almeida, G. Favier, and J. C. M. Mota. PARAFAC receiver for blind multiuser equalization in wireless communication systems with temporal oversampling. In *European Signal Processing Conference (EUSIPCO)*, Antalya, Turkey, September 4-8 2005.

[30] A. L. F. de Almeida, G. Favier, and J. C. M. Mota. *The constrained block-PARAFAC decomposition.* Three-way methods in Chemistry and Psychology (TRICAP), Chania, Crete, Greece, June 2006.

[31] A. L. F. de Almeida, G. Favier, and J. C. M. Mota. Multipath parameter estimation of time-varying space-time communication channels using parallel factor analysis. In *IEEE Int. Conf. Acoustics, Speech and Sig. Proc. (ICASSP)*, Toulouse, France, May 14-18 2006.

[32] A. L. F. de Almeida, G. Favier, and J. C. M. Mota. Space-time multiplexing codes: A tensor modeling approach. In *IEEE 7th Workshop on Sig. Proc. Advances in Wireless Commun. (SPAWC)*, Cannes, France, July 2006.

[33] A. L. F. de Almeida, G. Favier, and J. C. M. Mota. Tensor-based space-time multiplexing codes for MIMO-OFDM systems with blind detection. In *Proc. IEEE Symp. Pers. Ind. Mob. Radio Commun. (PIMRC)*, Helsinki, Finland, September 2006.

[34] A. L. F. de Almeida, G. Favier, and J. C. M. Mota. Trilinear space-time-frequency codes for broadband MIMO-OFDM systems. In *International Telecom Symposium (ITS)*, Fortaleza, Ceara, September 2006.

[35] A. L. F. de Almeida, G. Favier, and J. C. M. Mota. A constrained factor decomposition with application to mimo antenna systems. *IEEE Trans. Signal Process., accepted for publication*, 2007.

[36] A. L. F. de Almeida, G. Favier, and J. C. M. Mota. Constrained space-time spreading for MIMO-CDMA systems: Tensor modeling and blind detection. In *European Signal Processing Conference (EUSIPCO)*, Poznan, Poland, September 2007.

[37] A. L. F. de Almeida, G. Favier, and J. C. M. Mota. Constrained tensor modeling approach to blind multiple-antenna CDMA schemes. *IEEE Trans. Signal Process., accepted for publication*, 2007.

[38] A. L. F. de Almeida, G. Favier, and J. C. M. Mota. Constrained tucker-3 model for blind beamforming. *Elsevier Signal Processing, submitted*, 2007.

[39] A. L. F. de Almeida, G. Favier, and J. C. M. Mota. Multiuser MIMO system using block space-time spreading and tensor modeling. *Elsevier Signal Processing, accepted for publication*, 2007.

[40] A. L. F. de Almeida, G. Favier, and J. C. M. Mota. PARAFAC-based unified tensor modeling for wireless communication systems with application to blind multiuser equalization. *Signal Processing*, 87(2):337–351, Feb. 2007.

[41] A. L. F. de Almeida, G. Favier, and J. C. M. Mota. Space-time spreading MIMO-CDMA downlink system using constrained tensor modeling. *Elsevier Signal Processing, submitted*, 2007.

[42] A. L. F. de Almeida, G. Favier, and J. C. M. Mota. Space-time spreading MIMO system using canonical precoding tensor model. In *Asilomar Conference Sig. Syst. Comp.*, Pacific Grove, CA, November 4-7 2007.

[43] A. L. F. de Almeida, G. Favier, and J. C. M. Mota. A trilinear decomposition approach to space-time-frequency multiple-access wireless systems. In *IEEE Int. Workshop on Sig. Proc. Advances in Wireless Commun. (SPAWC)*, Helsinki, Finland, June 2007.

[44] A. L. F. de Almeida, G. Favier, and J. C. M. Mota. The trilinear decomposition with constraints: Application in multiple-antenna wireless communication systems. In *GRETSI Symposium on Signal and Image Processing*, Troyes, France, September 2007.

[45] A. L. F. de Almeida, G. Favier, and J. C. M. Mota. Trilinear space-time-frequency spreading for mimo wireless systems with blind detection. *IEEE Trans. Signal Process., submitted*, 2007.

[46] A.L.F. de Almeida, G. Favier, and J.C.M. Mota. Generalized parafac model for multidimensional wireless communications with application to blind multiuser equalization. In *Signals, Systems and Computers, 2005. Conference Record of the Thirty-Ninth Asilomar Conference on*, pages 1429–1433, October 28 - November 1, 2005.

[47] A. de Baynast and L. De Lathauwer. Détection autodidacte pour des systèmes à accès multiple basée sur l'analyse PARAFAC. In *Proc. of XIX GRETSI Symp. Sig. Image Proc.*, Paris, France, Sep. 2003.

[48] A. de Baynast, L. De Lathauwer, and B. Aazhang. Blind PARAFAC receivers for multiple access-multiple antenna systems. In *Proc. VTC Fall*, Orlando, USA, Oct. 2003.

[49] L. De Lathauwer. *Signal processing based on multilinear algebra*. PhD thesis, Katholieke Univ. Leuven, Leuven, Belgium, 1997.

[50] L. De Lathauwer. The decomposition of a tensor in a sum of rank-(R_1, R_2, R_3) terms. In *Workshop on Tensor Decompositions and Applications*, Marseille, France, 2005.

[51] L. De Lathauwer. The decomposition in block terms. In *ThRee-way methods In Chemistry and Psychology (TRICAP 2006)*, Chania, Crete, Greece, June 2006.

[52] L. De Lathauwer. A link between the Canonical Decomposition in multilinear algebra and simultaneous matrix diagonalization. *SIAM J. Matrix Anal. Appl.*, to appear, 2007.

[53] L. De Lathauwer and J. Castaing. Tensor-based techniques for the blind separation of DS-CDMA signals. *Signal Processing*, 87(2):322–336, 2007.

[54] L. De Lathauwer, B. De Moor, and J. Vandewalle. An introduction to independent component analysis. *J. Chemometrics*, 14:123149, 2000.

[55] T. S. Dharma, A. S. Madhukumar, and A. B. Premkumar. Layered space-time architecture for MIMO block spread CDMA systems. *IEEE Commun. Letters*, 10(2):70–72, Feb. 2006.

[56] R. Doostnejad, T. J. Lim, and E. Sousa. Space-time spreading codes for a multiuser MIMO system. In *Proc. of 36th Asilomar Conf. Signals, Syst. Comp.*, pages 1374–1378, Pacific Grove, USA, Nov. 2002.

[57] R. Doostnejad, T. J. Lim, and E. Sousa. Space-time multiplexing for MIMO multiuser downlink channels. *IEEE Trans. Wireless Commun.*, 5(7):1726–1734, 2006.

[58] R. Doostnejad, T. J. Lim, and E. S. Sousa. On spreading codes for the down-link in a multiuser MIMO-OFDM system. In *Proc. of IEEE Vehic. Tech. Conf.*, volume 1, pages 498–502, Orlando, FL, October 2003.

[59] H. El Gamal and M. O. Damen. Universal space-time coding. *IEEE Trans. Inf. Theory*, 49(5):1097–1119, 2003.

[60] R. B. Ertel, P. Cardieri, K. W. Sowerby, T. S. Rappaport, and J. H. Reed. Overview of spatial channel models for antenna array communication systems. *IEEE Personal Commun.*, 5(1):10–22, February 1998.

[61] N. M. Faber, R. Bro, and P. K. Hopke. Recent developments in CANDECOMP/PARAFAC algorithms: a critical review. *Chemometrics Intell. Lab. Syst.*, 65:119–137, 2003.

[62] G. Favier. Calcul matriciel et tensoriel avec applications à l'automatique et au traitement du signal. *under preparation*, 2007.

[63] C. A. R. Fernandes, G. Favier, and J. C. M. Mota. Blind tensor-based identification of memoryless multiuser volterra channels using SOS and modulation codes. In *European Signal Processing Conference (EUSIPCO)*, Poznan, Poland, September 2007.

[64] C. E. R. Fernandes, G. Favier, and J. C. M. Mota. Blind channel identification algorithms based on the Parafac decomposition of cumulant tensors: the single and multiuser cases. *Elsevier Signal Processing, accepted for publication*, 2007.

[65] C. E. R. Fernandes, G. Favier, and J. C. M. Mota. Tensor-based blind channel identification. In *IEEE International Conference on Communications (ICC)*, Glasgow, UK, June 2007.

[66] G. J. Foschini. Layered space-time architecture for wireless communications in a fading environment when using multiple antennas. *Bell Labs Tech. J.*, 1(2):41–59, 1996.

[67] G. J. Foschini and M. J. Gans. On limits of wireless communications when using multiple antennas. *Wireless Pers. Commun.*, 6(3):311–335, 1998.

[68] X. Giraud, E. Boutillon, and J.-C. Belfiore. Algebraic tools to build modulation schemes for fading channels. *IEEE Trans. Inf. Theory*, 43(3):938–952, 1997.

[69] G.D. Golden, G.J. Foschini, R.A. Valenzuela, and P.W. Wolniansky. Detection algorithm and initial laboratory results using the V-BLAST space-time communications architecture. *IEE Electronics Letters*, 35(7):14–15, 1999.

[70] A. Goldsmith, S. A. Jafar, N. Jindal, and S. Vishwanath. Capacity limits of MIMO channels. *IEEE J. Sel. Areas Commun.*, 21(5):684–702, Jun. 2003.

[71] D. A. Gore, R. W. Heath Jr., and A. J. Paulraj. Transmit selection in spatial multiplexing systems. *IEEE Commun. Letters*, 6(11):491–493, 2002.

[72] M. Guillaud and D. T. M. Slock. Pathwise MIMO channel modeling and estimation. In *Proc. IEEE SPAWC'05*, pages 685–689, New York, USA, June 2005.

[73] R. A. Harshman. Foundations of the PARAFAC procedure: Model and conditions for an "explanatory" multi-mode factor analysis. *UCLA Working Papers in Phonetics*, 16:1–84, Dec. 1970.

[74] R. A. Harshman. Determination and proof of minimum uniqueness conditions for PARAFAC1. *UCLA Working Papers in Phonetics*, (22):111–117, 1972.

[75] R. A. Harshman and M. E. Lundy. *The PARAFAC model for three-way factor analysis and multidimensional scaling.* H. G. Law, C. W. Snyder Jr., J. Hattie, and R. P. McDonald Eds., New York: Praeger, 1984.

[76] B. Hassibi and B. M. Hochwald. High-rate codes that are linear in space and time. *IEEE Trans. Inf. Theory*, 48(7):1804–1824, July 2002.

[77] R. W. Heath and D. J. Love. Multimode antenna selection for spatial multiplexing systems with linear receivers. *IEEE Trans. Signal Process.*, 53(8):3042–3056, Aug. 2005.

[78] B. Hochwald, T. L. Marzetta, and C. B. Papadias. A transmitter diversity scheme for wideband CDMA systems based on space-time spreading. *IEEE J. Selec. Areas Commun.*, 19(1):48–60, 2001.

[79] H. Huang, H. Viswanathan, and G. J. Foschini. Multiple antennas in cellular CDMA systems: transmission, detection, and spectral efficiency. *IEEE Trans. Wireless Commun.*, 1(3):383–392, 2002.

[80] A. Hyvarinen, J. Karhunen, and E. Oja. *Independent Component Analysis*. John Wiley and Sons, 2001.

[81] T. Jiang and N. D. Sidiropoulos. A direct semi-blind receiver for SIMO and MIMO OFDM systems subject to frequency offset. In *Proc. SPAWC*, Rome, Italy, June 2003.

[82] T. Jiang and N. D. Sidiropoulos. Kruskal's permutation lemma and the identification of CANDECOMP/PARAFAC and bilinear models with constant modulus constraints. *IEEE Trans. Signal Process.*, 52:2625–2636, Sep. 2004.

[83] A. Khouaja and G. Favier. Identification of PARAFAC-Volterra cubic models using an alternating recursive least squares algorithm. In *European Signal Processing Conference (EUSIPCO)*, Vienna, Austria, September 2004.

[84] A. Khouaja, A. Y. Kibangou, and G. Favier. Third-order volterra kernels complexity reduction using PARAFAC. In *First International Symposium on Control, Communications and Signal Processing (ISCCSP)*, pages 857–860, March 2004.

[85] A. Kibangou and G. Favier. Identification aveugle de canaux de communication non linaires base sur la dcomposition PARAFAC. In *GRETSI Symposium on Signal and Image Processing*, Troyes, France, September 2007.

[86] A. Kibangou, G. Favier, and M. M. Hassani. Récepteur aveugle basé sur la décomposition parafac pour des canaux de communication non-linéaires. In *Proc. GRETSI*, pages 177–180, Louvain-la-neuve, Belgium., September 2005.

[87] H. A. Kiers and A. K. Smilde. Constrained three-mode factor analysis as a tool for parameter estimation with second-order instrumental data. *J. Chemometrics*, 12(2):125–147, Dec. 1998.

[88] T. Kolda. Orthogonal tensor decompositions. *SIAM J. Matrix Anal. Appl.*, 23(1):243255, July 2001.

[89] P. M. Kroonenberg. *Three mode principal component analysis: Theory and applications*. Leiden: DSWO press, 1983.

[90] J. B. Kruskal. Three-way arrays: Rank and uniqueness or trilinear decompositions, with applications to arithmetic complexity and statistics. *Linear Algebra Appl.*, 18:95–138, 1977.

[91] S. E. Leurgans, R. T. Ross, and R. B. Abel. A decomposition for three-way arrays. *SIAM J. Matrix Anal. Appl.*, 14:1064–1083, 1993.

[92] J. Li, .J Conan, and S. Pierre. Joint estimation of channel parameters for MIMO communication systems. In *Proc. ISWCS'05*, pages 22–26, Siena, Italy, Sep. 2005.

[93] Y. Li. Simplified channel estimation for ofdm systems with multiple transmit antennas. *IEEE Trans. Wireless Communications*, 1(1):67–75, 2002.

[94] Z. Liu and G. B. Giannakis. Space-time block-coded multiple access through frequency-selective fading channels. *IEEE Trans. Commun.*, 49(6):1033–1044, 2001.

[95] D. J. Love and R. W. Heath. Multimode precoding for MIMO wireless systems. *IEEE Trans. Signal Process.*, 53(10):3674–3687, Oct. 2005.

[96] X. Ma, L. Yang, and G. B. Giannakis. Optimal training for MIMO frequency-selective fading channels. *IEEE Trans. Wirel. Commun.*, 4:453–466, Mar. 2005.

[97] L. Mailaender. Linear MIMO equalization for CDMA downlink signals with code reuse. *IEEE Trans. Wireless Commun.*, 4(5):2423–2434, Sep. 2005.

[98] P. McCullagh. *Tensor methods in statistics*. Monographs on Statistics and Applied Probability. Chapman and Hall, 1987.

[99] A. Medles and D. T. M Slock. Linear convolutive space-time precoding for spatial multiplexing MIMO systems. In *39th Annual Allerton Conf. Commun., Control and Comput.*, Monticello, USA, Oct. 2001.

[100] A. Medles and D. T. M Slock. Multistream space-time coding by spatial spreading, scrambling and delay diversity. In *Int. Conf. Acoust., Speech and Sig. Proc.*, Orlando, USA, May 2002.

[101] E. Moulines, P. Duhamel, J.-F. Cardoso, and S. Mayrargue. Subspace methods for blind identification of multichannel FIR filters. *IEEE Trans. Signal Process.*, 43(2):516–525, Feb 1995.

[102] S. Mudulodu and A. J. Paulraj. A simple multiplexing scheme for MIMO systems using multiple spreading codes. In *Proc. 34th ASILOMAR Conf. on Signals, Systems and Computers*, volume 1, pages 769–774, Pacific Grove, USA, 29 Oct- Nov 1 2000.

[103] B. K. Ng and E. Sousa. Space-time spreading multilayered CDMA system. In *Proc. of GLOBECOM*, volume 3, pages 1854–1858, Dec. 2000.

[104] B. K. Ng and E. S. Sousa. Multicarrier spread space-spectrum multiple access for the MIMO forward link transmission. In *Proc. IEEE Int. Symp. Pers. Ind. Mob. Radio Commun. (PIMRC)*, Lisbon, Portugal, September 15-18 2002.

[105] B. K. Ng and E. S. Sousa. A novel spread space-spectrum multiple access scheme for the forward link. In *Proc. IEEE WCNC'02*, Orlando, FL, USA, March 2002.

[106] B. K. Ng and E. S. Sousa. SSSMA for multiuser MIMO systems. *IEEE Microwave Magazine*, pages 1527–3342, June 2004.

[107] M. Nicoli, O. Simeone, and U. Spagnolini. Multislot estimation of fast-varying space-time communication channels. *IEEE Trans. Signal Process.*, 51(5):1184–1195, May 2003.

[108] M. Nicoli and U. Spagnolini. Reduced-rank channel estimation for time-slotted mobile communication systems. *IEEE Trans. Signal Process.*, 53(3):926–944, Mar. 2005.

[109] D. Nion and L. De Lathauwer. A block factor analysis based receiver for blind multi-user access in wireless communications. In *Proc. ICASSP*, Toulouse, France, May 2006.

[110] D. Nion and L. De Lathauwer. Levenberg-Marquadt computation of the block factor model for blind multi-user access in wireless communications. In *European Signal Processing Conference (EUSIPCO)*, Florence, Italy, September 4-8 2006.

[111] D. Nion and L. De Lathauwer. Line search computation of the block factor model for blind multi-user access in wireless communications. In *IEEE 7th Workshop on Sig. Proc. Advances in Wireless Commun. (SPAWC)*, Cannes, France, July 2006.

[112] A. Paulraj, R. Nabar, and D. Gore. *Introduction to Space-Time Wireless Communications*. Cambridge University Press, Cambridge, UK, 2003.

[113] A. J. Paulraj, D. A. Gore, R. U. Nabar, and H. Bolcskei. An overview of MIMO communications: A key to gigabit wireless. *Proc. of IEEE*, 92(2):198–218, Feb. 2004.

[114] A. J. Paulraj and C. B. Papadias. Space-time processing for wireless communications. *IEEE Signal Process. Magazine*, 14(6):49–83, Jan. 1997.

[115] J. Picheral and H. Spagnolini. Angle and delay estimation of spacetime channels for TD-CDMA systems. *IEEE Trans. Wireless Commun.*, 3(3):758–769, May 2004.

[116] J. G. Proakis. *Digital Communications*. McGraw-Hill, New York, 2001.

[117] M. Rajih and P. Comon. Enhanced line search: A novel method to accelerate PARAFAC. In *Proc. EUSIPCO*, Antalya, Turkey, Sep. 2005.

[118] M. Rajih and P. Comon. Alternating least squares identification of underdetermined mixtures based on the characteristic function. In *ICASSP'06*, Toulouse, May 14-19 2006.

[119] Y. Rong, S. A. Vorobyov, A. D. Gershman, and N. D. Sidiropoulos. Blind spatial signature estimation via time-varying user power loading and parallel factor analysis. *IEEE Trans. Signal Process.*, 53(5):1697–1710, May 2005.

[120] R. Roy and T. Kailath. ESPRIT: Estimation of signal parameters via rotational invriance techniques. *IEEE Trans. Acoustics, Speech and Signal Process.*, 37(7):984–995, July 1989.

[121] E. Sanchez, , and B. R. Kowalski. Tensorial resolution: a direct trilinear decomposition. *J. Chemometrics*, 4:29–45, 1990.

[122] A. M. Sayeed. Deconstructing multiantenna fading channels. *IEEE Trans. Signal Process.*, 50(10):2563–2579, Oct. 2002.

[123] S. Sfar, R. D. Murch, and K. B. Letaief. Layered spacetime multiuser detection over wireless uplink systems. *IEEE Trans. Wireless Commun.*, 2(4):653–668, July 2003.

[124] L. Shao and S. Roy. Rate-one space-frequency block codes with maximum diversity for MIMO-OFDM. *IEEE Trans. Wireless Commun.*, 4(4):1674–1686, July 2005.

[125] D. Shiu, G. J. Foschini, M. J. Gans, and J. M. Kahn. Fading correlation and its effect on the capacity of multi-element antenna systems. *IEEE Trans. Commun.*, 48(3):502–513, 2000.

[126] N. D. Sidiropoulos. Low-rank decomposition of multi-way arrays: A signal processing perspective. In *Invited plenary lecture at IEEE SAM*, Barcelona, Spain, July 2004.

[127] N. D. Sidiropoulos and R. Bro. On the uniqueness of multilinear decomposition of N-way arrays. *J. Chemometrics*, 14:229–239, 2000.

[128] N. D. Sidiropoulos, R. Bro, and G. B. Giannakis. Parallel factor analysis in sensor array processing. *IEEE Trans. Signal Process.*, 48(8):2377–2388, Aug. 2000.

[129] N. D. Sidiropoulos and R. Budampati. Khatri-Rao space-time codes. *IEEE Trans. Signal Process.*, 50(10):2377–2388, 2002.

[130] N. D. Sidiropoulos and G. Z. Dimic. Blind multiuser detection in WCDMA systems with large delay spread. *IEEE Signal Process. Lett.*, 8(3):87–89, Mar. 2001.

[131] N. D. Sidiropoulos, G. B. Giannakis, and R. Bro. Blind PARAFAC receivers for DS-CDMA systems. *IEEE Trans. Signal Process.*, 48(3):810–822, March 2000.

[132] N. D. Sidiropoulos and X. Liu. Cramer-Rao bounds for low-rank decomposition of multidimensional arrays. *IEEE Trans. Signal Process.*, 49(9):2074–2086, 2001.

[133] N. D. Sidiropoulos and X. Liu. Identifiability results for blind beamforming in incoherent multipath with small delay spread. *IEEE Trans. Signal Process.*, 49(1):228–236, Jan. 2001.

[134] O. Simeone and U. Spagnolini. Multi-slot estimation of space-time channels. In *Proc. IEEE Int. Conf. Commun. ICC*, New York City, USA, Apr. 2002.

[135] A. Smilde, R. Bro, and P. Geladi. *Multi-way Analysis. Applications in the Chemical Sciences*. John Wiley and Sons, Chichester, U.K., 2004.

[136] A. Stegeman and N. D. Sidiropoulos. On Kruskal's uniqueness condition for the Candecomp/Parafac decomposition. *Lin. Alg. Appl.*, 420:540–552, 2007.

[137] G. R Stuber, J. R. Barry, S. W Mclaughlin, Y. Li, M. A. Ingram, and T. G. Pratt. Broadband MIMO-OFDM wireless communications. *Proc. of the IEEE*, 92(2):271–294, Feb. 2004.

[138] W. Su, Z. Safar, and K. J. R. Liu. Full-rate full-diversity space-frequency codes with optimum coding advantage. *IEEE Trans. Inf. Theory*, 51:229–249, Jan. 2005.

[139] W. Su, Z. Safar, and K. J. R. Liu. Towards maximum achievable diversity in space, time and frequency: Performance analysis and code design. *IEEE Trans. Commun.*, 4(4):1847–1857, July 2005.

[140] K. Tachikawa. *W-CDMA Mobile Communications System*. John Wiley and Sons, West Sussex, England, 2002.

[141] S. Talwar, M. Viberg, and A. J. Paulraj. Blind separation of synchronous co-channel digital signals using an antenna array–Part I: Algorithms. *IEEE Trans. Signal Process.*, 44(5):1184–1197, May 1996.

[142] V. Tarokh, N. Seshadri, and A. R. Calderbank. Space-time codes for high data rate wireless communications: performance criterion and code construction. *IEEE Trans. Inf. Theory*, 44(2):744–765, Mar. 1998.

[143] I. E. Telatar. Capacity of multi-antenna gaussian channels. *European Trans. Telecomm.*, 10(6):585–595, Nov. 1999.

[144] J. M. F. ten Berge. Non-triviality and identification of a constrained Tucker3 analysis. *J. Chemometrics*, 16:609–612, 2002.

[145] J. M. F. ten Berge. Partial uniqueness in CANDECOMP/PARAFAC. *J. Chemometrics*, 18(1):12–16, 2004.

[146] J. M. F. ten Berge. Simplicity and typical rank of three-way arrays, with applications to Tucker3 analysis with simple cores. *J. Chemometrics*, 18:17–21, 2004.

[147] J. M. F. ten Berge and N. D. Sidiropoulos. On uniqueness in CANDECOMP/PARAFAC. *Psychometrika*, 67:399–409, 2002.

[148] L. R. Tucker. Some mathematical notes on three-mode factor analysis. *Psychometrika*, 31:279–311, 1966.

[149] A-.J. van der Veen. Algebraic methods for deterministic blind beamforming. *Proceedings of the IEEE*, 86(10):1987–2008, Oct. 1998.

[150] A-.J. van der Veen, S. Talwar, and A. J. Paulraj. A subspace approach for blind space-time signal processing. *IEEE Trans. Signal Process.*, 45(1):173–190, Jan 1997.

[151] A-.J. van der Veen, M. C. Vanderveen, and A. Paulraj. Joint angle and delay estimation using shift invariance techniques. *IEEE Trans. Signal Process.*, 46(2):405–418, Feb. 1998.

[152] R. D. van Nee and R. Prasad. *OFDM for wireless multimedia communications*. Artech House, 2000.

[153] M. C. Vanderveen, C. B. Papadias, and A. Paulraj. Joint angle and delay estimation (JADE) for multipath signals arriving at an antenna array. *IEEE Commun. Lett.*, 1(1):12–14, Jan. 1997.

[154] M. C. Vanderveen, A-.J. van der Veen, and A. Paulraj. Estimation of multipath parameters in wireless communications. *IEEE Trans. Signal Process.*, 46(3):682–690, Mar. 1998.

[155] Y. Xin, Z. Wang, and G. B. Giannakis. Space-time diversity systems based on linear constellation precoding. *IEEE Trans. Wireless Commun.*, 2(2):294–309, 2003.

[156] Z. Xu, P. Liu, and X. Wang. Blind multiuser detection: From MOE to subspace methods. *IEEE Trans. Sig. Proc.*, 52(2):91–103, Feb. 2004.

[157] L-.L. Yang and L. Hanzo. Broadband MC DS-CDMA using space-time and frequency-domain spreading. In *Proc. IEEE Vehic. Tech. Conf. (VTC Fall)*, pages 1632–1636, Vancouver, Canada, September 24-29 2002.

[158] L-.L. Yang, W. Hua, and L. Hanzo. Multiuser detection assisted time- and frequency-domain spread multicarrier code-division multiple-access. *IEEE Trans. Vehic. Techn.*, 55(1):397–405, 2006.